CHEMICAL SYNTHESIS, MODIFICATIONS AND CHARACTERIZATION OF HARD AND SOFT FERRITES

A THESIS SUBMITTED TO THE
UNIVERSITY OF POONA
FOR THE DEGREE OF
DOCTOR OF PHILOSOPHY
IN CHEMISTRY

BY
ATUL GOVIND BAGUL
M.Sc.

PHYSICAL CHEMISTRY DIVISION
IATIONAL CHEMICAL LABORATORY
PUNE 411 008 (INDIA)

SEPTEMBER 1995

CERTIFICATE

This is to certify that the thesis entitled **'Chemical synthesis, modifications and characterization of hard & soft ferrites'** *describes the research work done by Mr. Atul Govind Bagul under my supervision for the Degree of Doctor of Philosophy in Chemistry of the University of Poona. Such material as has been obtained from other sources has been duly acknolwledged in the thesis.*

N.C.L.
Pune 8

(Dr. S. K. Date)
Research Guide

INDEX

CHAPTER 4 : NICKEL ZINC FERRITE

Chapter 1

General Introduction

1.1 INTRODUCTION

1.1.1 Advanced Ceramics

Ceramics represent one of the oldest materials used by human race, both as objects of utility and beauty. Ceramics by definition are nonmetallic inorganic materials processed at high temperatures [1]. They are broadly divided into two classes viz., (a) Traditional ceramics and (b) Advanced ceramics. Traditional ceramics are useful to fulfill the basic human needs by providing materials for shelter and pots for cooking and storage. Ceramics are made from inexpensive materials which occur abundantly in nature and hence are widely used. Ceramics used to meet newer and engineering applications are termed as advanced ceramics [2]. The advanced ceramics differ from the traditional ceramics by virtue of their novelty of preparation and superior mechanical, electrical/electronic, magnetic and optical properties useful for high technological applications. Beauty of advanced ceramics revealed the requirements i.e. high temperature resistance, electrical resistivity, dielectric strength, corrosion resistance, low weight and fracture toughness. These materials are basically pure and/or mixed oxides, nitrides or carbides of Si, Al, Zr, Ti, Fe, etc.

The emergence of the new area of advanced ceramics has created a great deal of interest amongst the scientific as well as engineering communities. Day by day, advanced ceramics are replacing traditionally used materials in the areas like sensors, membranes, superconductors, catalysts, etc. This indicates that as we approach the twenty first century, three technologies i.e. (i) biotechnology, (ii) electronics and (iii) advanced ceramics have moved to the centre of stage of the second industrial revolution.

1.1.2 Classification of Advanced Ceramics

Advanced ceramics are generally classified into two broad areas, viz. (a) Structural ceramics and (b) Electronic ceramics. A more detailed classification of high performance ceramics by their function, properties and application is provided in Table 1 [3].

(a) Structural ceramics: This is a class of advanced ceramics where properties like creep strength, thermal shock resistance, fracture toughness are important for their applications. Advanced ceramics exhibit quantum jumps in properties. Improved fracture toughness of structural ceramics makes them suitable for stringent engineering application. Structural components derived from engineering ceramics are used as monoliths, coatings and composites in conjunction with or as replacement for metals when

2

Table-1 : Classification of High Tech Ceramics by Function

Electronic/Electric Functions	Insulation materials (alumina, beryllium oxide, magnesium oxide)	IC circuit substrate, package, wiring substrates, resistor substrate, electronics interconnection substrate
	Ferroelectrics materials (Barium titanate, Strontium titanate)	Ceramic capacitor
	Piezoelectric materials	Vibrator, oscillator, filter etc. transducer, ultrasonic humidifier, piezoelectric spark generator, etc.
	Semiconductor materials (Barium titanate, silicon carbide, zinc oxide- bismuth oxide, vanadium oxide and other transition metal oxides)	NTC thermistor : Temperature sensor, temperature compensation, etc.
		PTC thermistor : Heater element, switch, temperature compensation, etc.
		CTR thermistor : Heat sensor element
		Thick film thermistor : Infrared sensor
		Varistor : Noise elemination, surge current absorber, lighting arrestor, etc.
		Sintered cadmium sulfide material : Solar cell
		Silicon carbide heater : Electric furnace heater, miniature heater, etc.
	Ion conducting materials (beta-alumina, zirconium dioxide)	Solid electrolyte for sodium battery
		Zirconia ceramics : Oxygen sensor, pH meter, fuel cells
Magnetic Functions	Soft ferrite	Magnetic recording head, temperature sensor, etc.
	Hard ferrite	Ferrite magnet, fractional horse power motors, etc.
Optical Functions	Translucent alumina	High pressure sodium vapor lamp
	Translucent magnesium, mullite etc.	For a lighting tube, special purpose lamp, infrared Transmission window materials
	Translucent yttria-thoria ceramics	Laser material
	PLZT ceramics	Light memory element, video display and storage system, light modulation element, light shutter, light valve
Chemical Functions	Gas sensor (zinc oxide, ferric oxide, tin oxide)	Gas leakage alarm, automatic ventilation fan, hydrocarbon flurocarbon detectors, etc.
	Humidity sensor (magnesium chromate-titanium dioxide)	Cooking control element in microwave oven, etc.
	Catalyst carrier (cordierite)	Catalyst carrier for emission control
	Organic catalyst	Enzyme carrier, zeolites
	Electrodes (titanates, sulfides, borides)	Electrowinning aluminium, photochemical processes, chlorine production
Thermal Functions	Refractoriness/insulation, heat collection (zirconium dioxide, titanium dioxide ceramics)	Infrared radiator, high temperature industrial furnace lining, heat sink for electronic parts

3

```
┌─────────────────────┐        ┌ Cutting tools (alumina, titanium     Ceramic tool, sintered SiN
│ Mechanical Functions │───────┤  carbide, titanium nitride,          Cermet tool, artificial diamond
└─────────────────────┘        │  others)                             Nitride tool
                               │
                               ├─ Wear resistant materials            Mechanical seal, ceramic liner, bearings, thread guide,
                               │  (alumina, zirconia)                 pressure sensors
                               │
                               └─ Heat resistant materials (silicon   Ceramic engine, turbine blade, heat exchangers, welding burner
                                  carbide, alumina, silicon nitride,  nozzle, high frequency combustion crucibles
                                  others)

┌─────────────────────┐        ┌ Alumina ceramics implantation  ┐
│ Biological Functions │───────┤                                 ├─ Artificial tooth root, bone and joint, drug administration
└─────────────────────┘        └ Hydroxyapatite bioglass        ┘

┌─────────────────────┐        ┌ Nuclear fuels
│  Nuclear Functions   │───────┤
└─────────────────────┘        ├─ Cladding material (silicon carbide
                               │  boron carbide, graphite)
                               │
                               └─ Shielding material (alumina,
                                  silicon/boron carbide, graphite)
```

application rely on mechanical behaviour of ceramics. Compared with metals, ceramics are generally more resistant to oxidation, corrosion, creep and are better thermal insulators. They have higher melting point and higher strength than super-alloys at elevated temperatures. Due to these special characteristic properties, ceramic like silicon nitride is therefore used in gas turbine and reciprocating engines where operating temperatures are higher than attainable with metals. Many times structural (engineering) ceramics are used as cutting tools.

(b) Electronic ceramics: Electroceramics or electronic ceramics are materials whose uses rely primarily on their electrical or magnetic behaviour rather than mechanical behaviour. The electroceramics industry dates back to 1940 when Al_2O_3 was used in spark plugs due to its insulating property. Nowadays electroceramics is rapidly expanding area of advanced ceramics and constitute a major share of the advanced ceramic market. Some of the examples of this class are, zinc oxide for varistors, lead zirconium titanate (PZT) for piezoelectrics, barium titanate in capacitors, tin oxide as gas sensors, lead lanthanum zirconium titanate (PLZT) and lithium niobate for electrooptic devices, etc. The electroceramics can be further classified into the following areas - (a) Magnetic ceramics, (b) Ferroelectric and piezoelectric ceramics, (c) Conducting ceramics and (d) Optical ceramics.

1.1.3 Present Status & Scope of the Present Work

In the year 1985 advanced ceramic markets were worth $ 1825 million, out of which about $ 1700 million is for electronic ceramics. The predicted figure in 2000 A.D. is $ 3485 million for electronic ceramics out of a total of $ 5895 million for advanced ceramics. The demand for electronic ceramics in India in 1985 was Rs.240 million which is expected to grow to about Rs.1700 million by end of the century. Amongst electronic ceramics, ferrite constitutes the major share of the Indian market (about 42%), followed by ceramic capacitors (24%). The Indian market is about 0.5% of the world market [4]. The Fig.1 shows enormous size of market potential for these high technological materials in 1980, 1990 and 1995 [5]. Although there is a fair amount of R&D activity in many of the areas of electronic ceramics in our country, cost effective production techniques leading to competitive position in the market place are yet to be significantly evolved. More emphasis therefore has to be placed on technology development aspects in order to fill this gap [4].

Ferrites are electronic ceramics and are generally defined as magnetic materials composed of oxides containing ferric ion as the main constituent. Technologically, the ferrites form an important class of electronic ceramics as

Worldwide sales of high-tech ceramics expected to exceed $12 billion in 1990

Estimated sales, $ billions

	U.S.
	Japan
	Others
	Total

1980   1990   1995

Note: Sales do not include those in communist countries.
Source: H. Kent Bowen and George B. Kenney of MIT
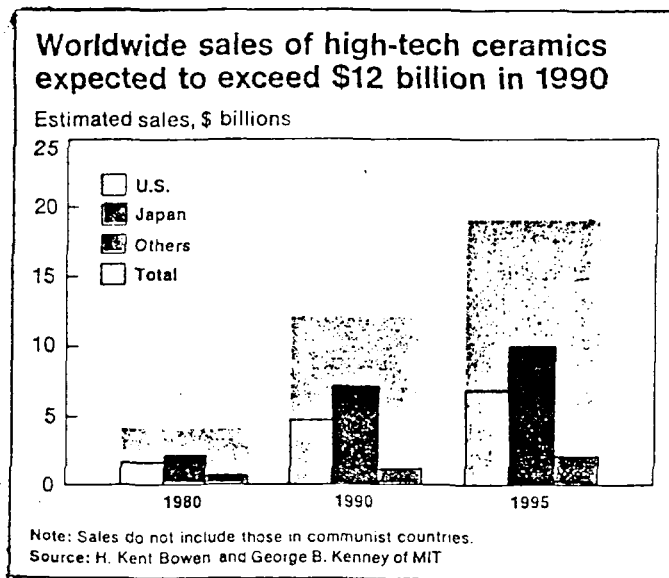
FIG. I : World wide sale of high - tech ceramics.

they find wide applications in the field of electrical and electronics industries. In our modern civilization, vast sum of money are spent for magnetic materials. These are utilized in transformer, generators, motors, television sets, computers and countless other electronic equipments. A representation of the growing application of the ferrites has been elucidated in Fig.2 in the form of a tree [6]. In the world of ceramic magnets, the problem is production of reliable and reproducible products of desired quality at low cost. The key to success lies in the synthesis of highly pure, uniform, submicronic powder with processing under optimised conditions. Thus, for successful processing, first and foremost requirement is availability of desired quality of powders. Conventional solid state method has limitations to synthesize these powders. Various solution techniques are being perfected to obtain highly pure, uniform, submicron size powder of ceramic magnets.

Considering the challenges and opportunities that the field of electronic ceramic magnets has offered, we have undertaken an extensive research in hard and soft ferrites. For the in-depth study of (i) chemical synthesis, (ii) processing and (iii) structure property correlationship, strontium-hexaferrite $(SrFe_{12}O_{19})$ and nickel-zinc ferrite $(Ni_{0.8}Zn_{0.2}Fe_2O_4)$ are selected to establish processing-structure-property correlations.

Chapter-I introduces the electronic ceramics and
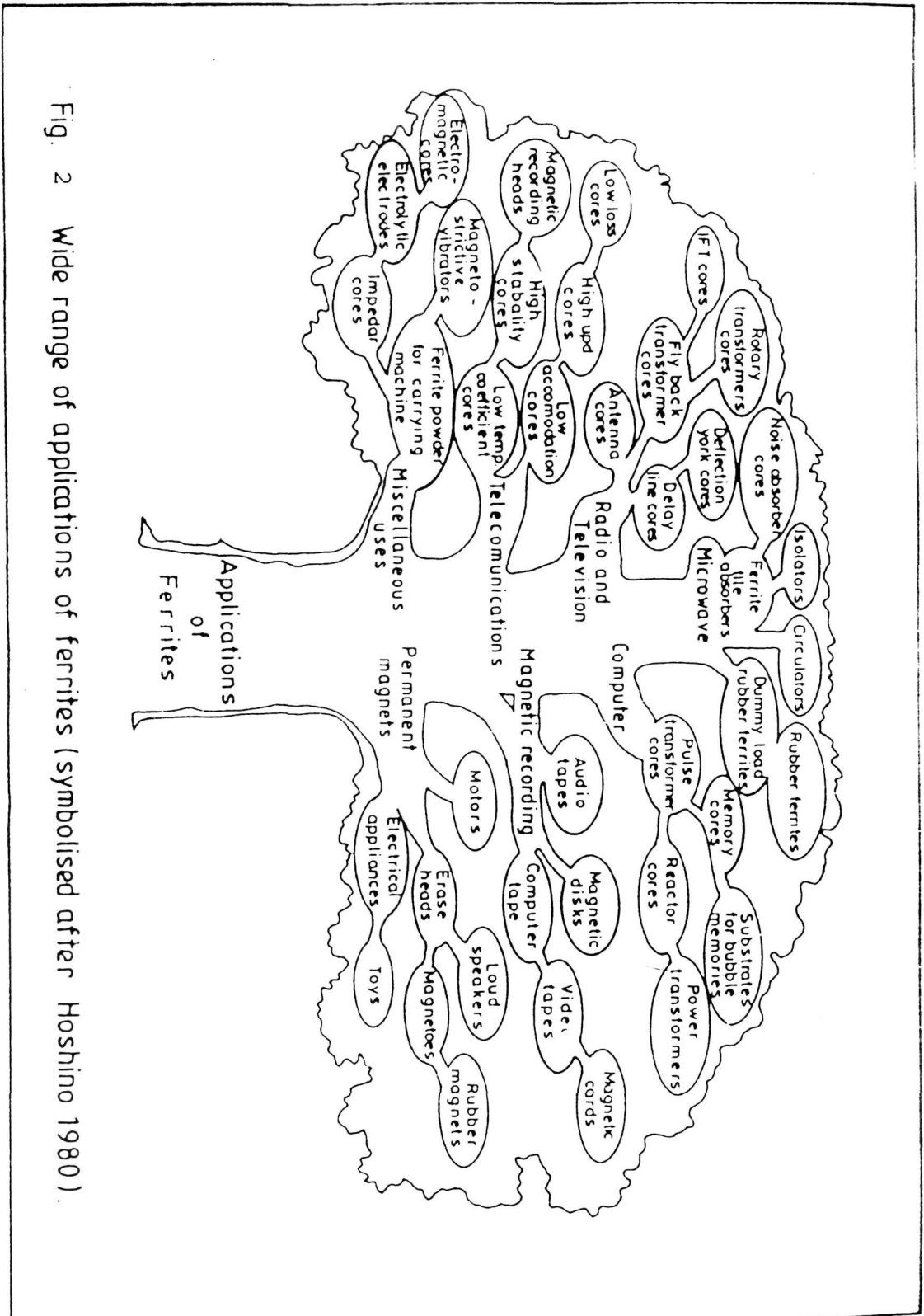
Fig. 2   Wide range of applications of ferrites (symbolised after Hoshino 1980).

presents the general introduction to magnetism and magnetic interactions. Highlighting the applications of the ferrites in today's world, the chapter converges on the developments of new approaches to ferrite processing which·are developed to satisfy the current technological needs of ferrite applications. The processing is discussed under five subtitles namely, (a) powder preparation, (b) additives, (c) compactions, (d) sintering, (e) microstructure and grain boundary analysis.

Chapter-II deals with experimental procedures which include:

i) Method of synthesis of strontium ferrite and Ni-Zn ferrite in our laboratory.

ii) The method of sample preparation with different concentration of dopants/additives.

iii) Physico-chemical characterization techniques used to study different properties.

In Chapter-III fascinating experimental results on strontium ferrite are described. A brief account of the crystal and magnetic structure of $SrFe_{12}O_{19}$ is given in the beginning which is followed by a discussion on magnetic performance parameters and factors governing them. Magnetic properties are governed by various processing parameters. Hence the experimental results of some important parameters like (a) effect of mode of washing or filtration, (b) effect

of crystallinity and (c) effect of additive are discussed in details.

Chapter-IV elaborates synthesis and characterization of $Ni_{0.8}Zn_{0.2}Fe_2O_4$. After a brief introduction of crystal and magnetic structure of spinel ferrite, the important magnetic performance parameters such as permeability (u), magnetisation (M_S) and losses are elaborated along with the factors governing these parameters. The magnetic properties of sintered toroids were measured with the help of Q-meter and VSM. The effect of different dopants such as, BaO and $BaO.B_2O_3$ on the magnetic properties of sintered samples have also been discussed.

1.2   THEORY OF MAGNETISM

Magnetism is one of the basic phenomenon in nature. The historical background of magnetism dates back to a permanent magnet called lodestone which was nothing but Fe_3O_4 found in natural state. Though the properties of magnets were known from ancient times, William Gilbert described magnet as a science in 1600 A.D. for the first time. The electromagnets were discovered by Oersted in 1820. Ewing was the first who considered magnet, made up of a regular framework of elementary magnets. The magnetic phenomenon was understood in more classical way when important laws on magnetism was established by Pierre Currie. The modern magnetism based on quantum mechanics was

9

developed by Van Vleck in 1932. Many significant contributions were made by Neél (ferrimagnetism), Kittle $e\ell$ (ferromagnetism and antiferromagnetism), Anderson (exchange interactions), etc. In addition to the interest in understanding the origin and basis of magnetism in solids, researchers were also interested in applications of magnetic materials in various areas. The magnetism is usually described at two levels, viz. microscopic and macroscopic. Some of the important concepts are presented below [7-18].

Magnetism at microscopic level is related to the atomic currents. This type of magnetism is also known as intrinsic magnetism. The magnetism at macroscopic level is mainly concerned with the properties of magnetic domain and related phenomenon. Of course, there is quite a lot of cross coupling between the two groups.

To understand the basic concepts underlying the term magnetism, one has to analyse the nature of interactions taking place at atomic and/or electronic levels. Truly speaking, every material is magnetic in nature, as it possesses charged particles within the atoms. Since the spin magnetic moment of nucleus is smaller by a factor of 10^3 than that of the electrons, it may be neglected. So the major contribution of magnetism at atomic level is mainly due to spin and orbital motion of electrons.

Motion of electron both spinning as well as orbital, results in the nonzero magnetic moment given by following expressions:

Orbital magnetic moment $= \mu_1 = \dfrac{- eW_o r^2}{2c}$

$$= \dfrac{- e}{2mc} P_1$$

where e = electronic charge, W_o = angular velocity of electron, r = radius of circular orbit, c = velocity of light, P_1 = orbital angular momentum of electron.

Similarly, spin magnetic moment is given by:

$$\mu_s = (-e/2mc).2.P_s$$

where P_s = spin angular momentum of electron. The minus sign indicates that the magnetic dipole moment points in the direction opposite to the vector representing the angular momentum.

Before describing details of magnetism, we would like to define important terms used in the study of magnetism. Any solid when placed in the magnetic field H, develops certain amount of magnetization M. It is defined as the magnetic moment per unit volume and is given by M $= \chi$ H where χ is known as magnetic susceptibility. Due to the magnetization, magnetic induction is defined as:

$$B = H + 4\pi M$$

Thus the amount of magnetization and magnetic induction developed in the solid is intrinsic property of solid.

11

How easily a material can be magnetized is found out from the permeability of the material and is defined as,

$$u = \frac{B}{H} = 1 + 4\pi\chi$$

Magnetic behaviour in solids is broadly categorised into two types, namely, non-cooperative phenomenon and cooperative phenomenon.

Non-cooperative & cooperative phenomena

A)   *Non-cooperative phenomenon*: It is one where individual magnetic dipoles do not interact with each other e.g., (i) diamagnetic solids and (ii) paramagnetic solids.

B)   In *cooperative phenomenon*, the magnetic dipoles interact with each other giving rise to three main kinds of behaviour namely, (i) ferromagnetism, (ii) antiferromagnetism and (iii) ferrimagnetism.

1.2.1   Non-cooperative Phenomenon

A)   *Diamagnetism*: If a sample is placed in magnetic field H, the field within it will generally differ from free space value. If the density of lines of force within sample is less than that of free space, the sample is said to be diamagnetic (Fig.3a). Such a material, when placed in an inhomogenous magnetic field will tend to move towards the region of the lowest field.

Dimagnetism is a property associated with completely field shells in an atom and arises from the interactions of paired electrons with the magnetic field. The paired electrons have the tendency to shield the interior of a body from an applied magnetic field. According to Lenz's law, when the flux through electrical circuit is changed, an induced current is set up in such a direction as to oppose the flux change. When a dimagnetic substance is placed in magnetic field, induced currents are set up due to the changed flux. The currents persist as long as field is present. The magnetic field of induced current is opposite to the applied field. So the total microscopic magnetic field is less than applied macroscopic field H, i.e. the magnetic induction is less than H, making the material dimagnetic. The dimagnetic contribution is in opposite direction to external magnetic field and hence values of dimagnetic magnetisation and susceptibility are negative.

The classical expression for dimagnetic susceptibility given by Langevin is as follows:

$$X_d = \frac{- N\, e^2}{6m\, C^2} \; \underset{i}{\Sigma}\; r_i^{\,2}$$

Where, $r_i^{\,2}$ = mean square distance between the electron and nucleus.

N = ions/atoms per unit volume.

m = mass of electron.
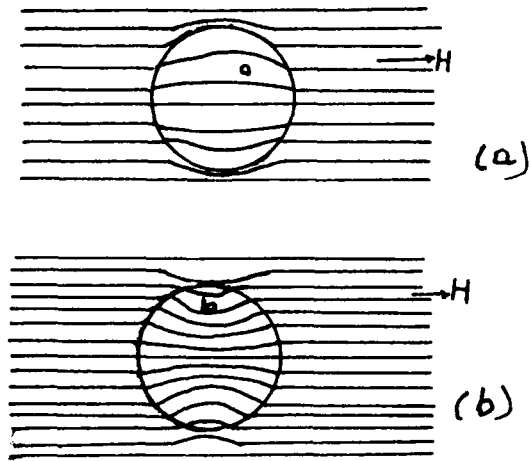
Fig. 3 : Behavior of (a) diamagnetic
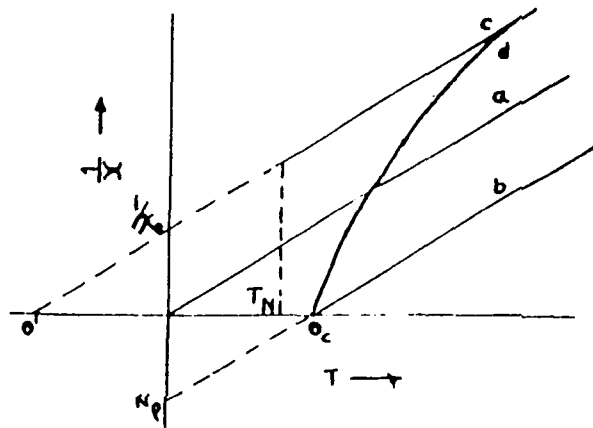and (b) paramagnetic substances
in magnetic fild.

Fig. 4 : Variation of $1/\chi$ as a function of temperature in the
paramagnetic region
a) no interaction, paramagnetic down to $0°K$
b) positive interaction, ferromagnetic below $\theta = \theta_C$
c) negative interaction, antiferromagnetic below T_N
d) negative interaction, ferrimagnetic below θ_C

e = charge on electron.

c = velocity of light.

Paramagnetism: Substances with positive susceptibility are called paramagnetic substances. In absence of externally applied magnetic field, the magnetic moments of individual atoms or ions will point in random direction due to thermal agitation. When an external field is applied, magnetic dipoles tend to align themselves parallel to the field giving rise to a net magnetisation of system of individual dipoles with an external magnetic field is called paramagnetism. This property is exhibited by substances containing unpaired electrons. The paramagnetic contribution to magnetization is due to spin and orbital angular momentum of unpaired electron/electrons. The paramagnetic contribution is in the same direction as the applied field. Following are some examples of paramagnetic substances, viz., oxygen molecule, nitric oxide, large number of organic free radicals, transition elements, rare earth and actinide elements and the compound of these elements.

When paramagnetic substance is placed in magnetic field, the number of lines of force passing through it is greater than those would pass through vacuum (Fig.3b). Consequently, paramagnetic substances are attracted by a magnetic field. Paramagnetic susceptibility is independent of applied field but it is temperature dependent. The

14

relation between susceptibility χ of a paramagnetic substance and its temperature is given by Curie's law and is mathematically expressed as follows:

$$\chi = \frac{C}{T}$$

Where, C = Curie constant

and   T = absolute temperature.

Curie law is obeyed by most of tne paramagnetic substances especially at high temperature. However, a better fit to the experimental data is provided by Curie-Weiss law,

$$\chi = \frac{C}{T + \Theta}$$

Where, Θ = Weiss constant.

These two types of behaviours are illustrated in Fig.4 in which χ^{-1} is plotted against T.   .

The classical theory of paramagnetism was first given by Langevin. For cases of the iron group ions in crystals, where $H_{CF} > H_{LS}$, χ_p is given as follows:

$$p = \frac{N \mu_B^2}{3KT} g^2 s' \ (s'H)$$

Where, N = number of magnetic atoms or ions/unit volume.

μ_B = Bohr magneton.

K = Boltzman constant.

g = Landes splitting factor.

T = Absolute temperature.

s' = Ground state value of the spin quantum number.

1.2.2 Cooperative Phenomenon

Materials belonging to a class of compounds in which cooperative phenomenon is observed have their elementary magnets, spontaneously oriented by some kind of mutual interactions. The spontaneous ordering can be inferred from the observations viz.,

i) existence of remanent magnetisation;

ii) characteristic discontinuities in variation of specific heat with temperature;

iii) the diffraction patterns formed by the scattering of slow thermal neutrons from single crystal samples. Three main types of ordering namely, A) ferromagnetism, B) antiferromagnetism and C) ferrimagnetism will be discussed in details. Various kinds of ordering along with the above three have been shown in Fig.5.

Ferromagnetism: The intense response to an applied magnetic field is known as ferromagnetism. A ferromagnet has a spontaneous magnetisation even in absence of external magnetic field. The presence of spontaneous magnetisation suggests that electron spins and magnetic moments are arranged in regular manner. The magnetism in ferromagnet is described at two levels:
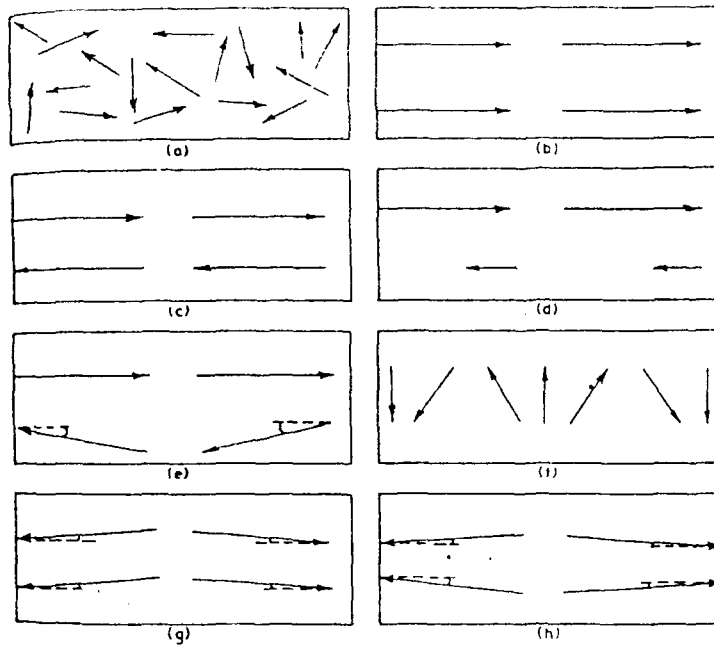
a) Microscopic or atomic level, and

Fig. 5 : Schematic representation of spin arrangements :
    a) disordered paramagnetic state
    b) parallel spins : ferromagnetism
    c) antiparallel spins : Neel type antiferromagnetism
    d) uncompensated antiparallel spins : Neel type
       ferrimagnetism
    e) triangular antiparallel spins : Yafet-Kittel
       type ferrimagnetism
    f) helical spiral structures : compensated anti-
       ferromagnetic or uncompensated ferrimagnetic
    g) canted spin Dzialoshinskii type weak
       ferromagnets.
    h) canted spins compensated antiferromagnets :
       hidden canting

b)   Macroscopic or domain level.

Ferromagnetism at microscopic level: In case of paramagnetic material, the magnetic dipoles of neighbouring magnetic atoms are separated by a large distance. So the interactions between unpaired spins of the neighbouring atoms are negligible. On the other hand, in a ferromagnetic substance, the atoms or ions having permanent magnetic moments are sufficiently near each other due to which neighbouring ion interact with one another. The strong magnetic interaction between nearest magnetic neighbouring ions tend to align the magnetic dipoles. These neighbouring ions, in turn, influence next neighbour and so on. The internal interactions tend to line up the magnetic moments parallel to each other. As a consequence of parallel arrangement of unpaired spins, domains of ferromagnetic material have spontaneous magnetization. This particular aspect tells us why ferromagnetism is observed in certain materials only. Thus regions in which all unpaired spins are oriented parallel to each other are developed and these are known as domains. The existence of such domains was first suggested by Weiss; which is further confirmed experimentally. The domains are separated by domain walls. In unmagnetised state, each domain is in fully magnetised state due to exchange interaction but magnetisation vectors of different domains are randomly oriented with respect to each other. The resultant magnetization of material is given

by the vector sum of the magnetization of all the domains which is found to be zero for unmagnetized sample. Magnetization of material under applied field takes place by the growth of domains of parallel orientation at the expense of the remaining domains through the shifting of domain walls. In ferromagnetic domain, the internal interactions tend to align magnetic moment, the ordering effect of exchange interactions is opposed by thermal agitation and at elevated temperature the spin order is disturbed. There exists a critical temperature called the Curie temperature above which magnetic interactions are not sufficiently strong ($J \leq KT_c$). Above this temperature, substance obeys Curie-Weiss law.

Weiss molecular field theory [14]: The credit in developing the theory of magnetism of ferromagnetic material goes to Weiss. In 1907 he proposed the first model for ferromagnetism. The model is based on two assumptions namely, (i) each ferromagnetic material is composed of small regions called domains, within which the spins are ordered in parallel below T_c, but the direction of magnetisation of different domains need not necessarily be parallel and (ii) a strong internal molecular field H_m called as Weiss field is responsible for the parallel alignment of the individual atomic moments within the domain [10].

When an external magnetic field H_{ext} is applied to unmagnetised ferromagnetic sample, it would align the

18

individual domains within the crystal and yield its full magnetic moment i.e. M_{sat}. The total magnetic field (H_T) experienced by each magnetic dipole may be written in the following form:

$$H_T = Hext + H_m$$

Internal molecular field H_m is proportional to magnetisation, $H_m = \lambda\ M$, where λ is called molecular field constant or Weiss field constant.

The spontaneous magnetization and its variation with temperature was explained by Weiss on the hypothetical molecular field basis. However, he could not suggest any mechanism for the origin of the molecular field. The explanation pertaining to the alignment of the elementary moments was given by Heisenberg [15] based on quantum mechanical approach in terms of exchange interaction between the uncompensated electron spins in the partially filled 3d shells. The interaction energy E_{ex} between two atoms having spins S_i and S_j is given by equation,

$$E_{ex} = -\ Z\ J_e\ S_i.S_j$$

where J_e is exchange integral and is a measure of overlap of the electronic charge distribution of the two atoms. The value of J_e (i.e. magnitude of exchange interaction)
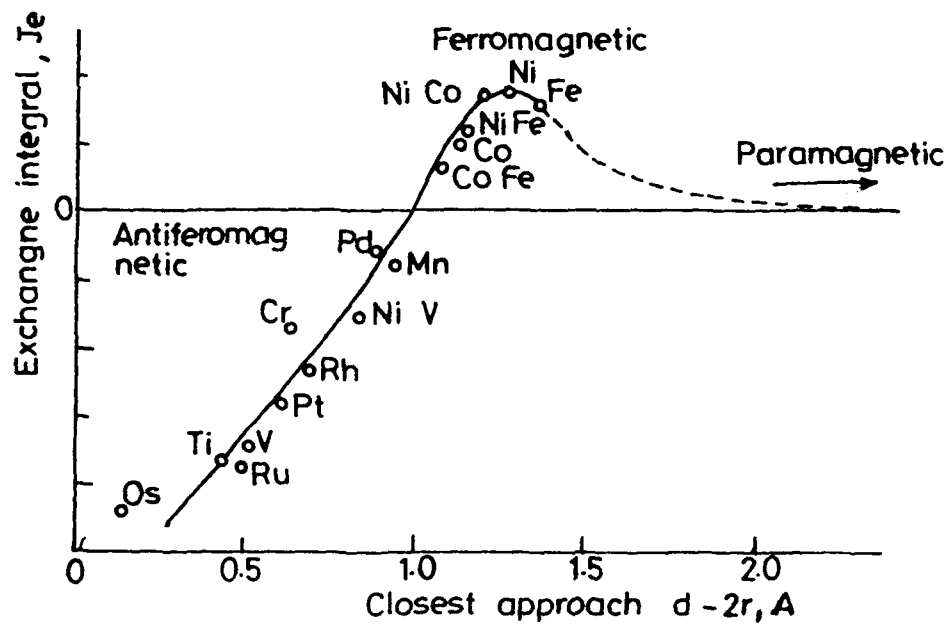
Fig 6 : The relative value of the exchange integral as a function of the distance of closest approach of electrons of neighbouring atoms

strongly depends on unfilled shells of neighbouring magnetic ions. Fig.6 gives a plot of magnitude of exchange integral Vs separation between atoms. When separation is large, the exchange integral is very small and the substance is paramagnetic. For a smaller separation, magnitude of J_e increases. The positive exchange interactions give rise to parallel alignment of magnetic dipoles i.e. ferromagnetism. At a still smaller separation J_e becomes negative making the neighbouring magnetic moments antiparallel resulting into antiferromagnetism.

Ferrimagnetism: The qualitative behaviour of inverse spinel ferrite or hexagonal ferrite is similar to ferromagnetic compounds. For a ferromagnetic compound, the magnetic moment per formula unit is expected to be the sum of ionic moments; thus on the basis of this calculations the magnetic moment for magnetite $Fe^{II}Fe_2^{III}O_4$ should be 14 $\mu\text{ß}$. Weiss & Forrer

in 1929 have found it to be 4.08 $\mu\text{ß}$. From the earlier work it was known that (normal) spinel ferrites $ZnFe_2O_4$ and $CdFe_2O_4$ are paramagnetic and the inverse spinel ferrites of Mn, Co, Ni, Cu and Mg are ferromagnetic like $Fe[Fe^{II}Fe]O_4$. Also it was known that above the Curie temperature several ferrites showed a curvature of the $1/\chi$ Vs T curve concave towards the T axis. Using these data Neel [17] in 1948 put forward a theory of ferrimagnetism to explain the magnetisation in inverse spinel ferrite like Fe_3O_4, $NiFe_2O_4$ etc. Neel's theory is basically an extension of the Weiss molecular field theory and is dealt with spin-spin

interactions in these materials. In this theory, he proposed the presence of two sublattices which are formed due to location of magnetic ions at crystallographically different sites. The computation of magnetization and susceptibility in terms of molecular field coefficient can be done with the help of Néel's theory. Further, the theory also introduces A-A, B-B and A-B interactions. Neel put forward the concept of negative interactions between the ions on A and B sites to promote an antiparallel alignment of moments. Besides A-B interaction, A-A and B-B interactions are also taken into account. The net magnetic moment is obtained from vector sum of these interactions. Néel's model could .satisfactorily explain experimentally observed low value of magnetic moment for Fe_3O_4.

1.3 PROCESSING OF FERRITES

1.3.1 Introduction

The study of ferrite processing dates back to more than forty years. In spite of this background, scientists working on the ferrite magnets are taking a lot of efforts to improve magnetic and electrical properties of ferrites. Recently, new approaches of processing have been developed to satisfy current technological needs of ferrite applications.

It is evident from the preceding section that the ferrites find applications in a wide range of fields and each application warrants some specific characteristic properties. However, it is generally not possible to obtain the best combination of all required properties for any specific applications. The control of most of the required properties for any particular application is possible by varying the composition or preparation technique of the ferrite materials [19]. The variation in the "preparative method" can bring about a large change in some of their extrinsic properties. In addition to chemical composition, magnetic properties are also governed by its microstructure. It is much more fruitful to correlate the magnetic properties with chemical and microstructural characteristics. Understanding of microstructure and study of grain boundary chemistry with the help of modern microanalytical methods is very useful in this respect. The controlling of microstructure is required in order to obtain final product with desired properties. The incorporation of additives and optimisation of sintering conditions play significant role in microstructure control. Optimisation of magnetic properties of sintered product depends upon type of applications. Tailor-making plays a vital role to serve the purpose. Improvement in the properties of ferrites have been made through close control of processing and innovations in processing.

In the light of these points mentioned above,

processing is divided in five major areas viz.,

A)   Powder preparation

B)   Additive

C)   Compaction

D)   Sintering

E)   Microstructure and grain boundary analysis

1.3.2   A)   Powder preparation

The powder preparation is the initial step in processing of ferrite. Naturally, the success of processing is based on quality of powders. With the development of the ultrafine material technology, there is growing demand for developing tailor-made materials of desired morphology (i.e. particle size and their distribution), microscopic homogeneity, texture, and chemical purity. On this background, the synthesis aspects of powder sample are being increasingly recognized as the vital component of materials research. The consideration of affordability and versatility in the development of new synthesis routes for the preparation of fine-grained powders of various mixed-oxide system pose a challenge to all materials scientists. Methods of powder preparation can be divided into two categories, (I) Conventional (ceramic) method and (II) Non-conventional (chemical) method. In the light of above requirements, various conventional and nonconventional methods will be reviewed.

Ceramic method [1]

Numerous methods are known for preparation of mixed oxide materials. Ceramic method is the most commonly used and widely accepted commercial method for preparation of ferrite powder. In this process, appropriate metal oxide (MO & Fe_2O_3) or metal salts (carbonates, oxalates, nitrates or sulphates), which decompose to give reactive metal oxides are accurately weighed and mixed thoroughly in desired proportion. The mixing is carried out in steel ball mills using liquid suspension (water, alcohol). The slurry is dried, the dried powder mixture is transferred to a ceramic crucible and heated in air or oxygen atmosphere. The rate of solid state reactions are generally slow because of large diffusion distance (~ 1000 nm). This difficulty is overcome by carrying out reaction under extreme condition i.e. calcination at high temperature (T > 1000°C). The high temperature calcination results in the increase in particle size. To reduce the particle size, milling and grinding is employed. Therefore in this step, calcined powder is ground in steel (or ceramic) ball mills. This results in better homogenization of the product. It also reduces grain size of the product as well as gives uniform grain distribution.

Though ceramic method of preparation is simple, cheap, well established and industrially adopted process, it has some inherent drawbacks viz.

1) Long heating schedules and high calcination

temperature, the requisites of this route, result in excessive grain growth and agglomeration.

2) The ball milling becomes essential to lower the particle size and to break the agglomerates, but this creates stresses, strains and lattice defects.

3) The process has a poor control of particle size, morphology and microscopic homogeneity.

4) The impurities are inserted in material during grinding.

All these factors are responsible to lower down the performance parameters of the sintered product [20-22].

To overcome these drawbacks of ceramic method, various investigators have tried different nonconventional methods. The nonconventional methods can be broadly classified under the following two headings:

1) Precursor method and 2) Wet chemical method.

1) *Precursor method*: The precursor method involves preparing a precursor - a solid solution or a mixture or gel containing all metal ions M^{2+} and Fe^{3+} in the desired ratio and decomposing the precursor to yield ferrite. If compounds of the two metals are isomorphous (i.e. have identical crystal structure), precursor will be a solid solution containing both metal ions in the same lattice. These solid solutions when decomposed thermally at moderate temperatures yield ferrites.

Of the various methods used to synthesize ferrites, the precursor technique is more advantageous because the precursors achieve excellent stoichiometry, low trace impurity content and homogeneity. The principal advantage of the precursor method is that two metals are mixed on an atomic scale so that greater reactivity and more homogeneous product results. This method not only allows mixing of the different metal species on an atomic scale but also reduces the diffusion distance to ~ 1 nm. In the classical ceramic method, the reactions are generally slow because of large diffusional distance (~ 1000 nm) [23].

Coprecipitation: This technique is most widely used for synthesis of fine grained oxide powders. This is mainly due to the simplicity of the processing route and also due to the fact that the chemistry involved is relatively straightforward. The method was first tried by Economos [24] for precipitation of mixed hydroxides from their chlorides by alkali or ammonium hydroxide. In coprecipitation technique, the solutions of desired ions are mixed together in required proportion and precipitated simultaneously with a suitable precipitating agent. Generally, it is done by dropwise addition of a mixture of cation solution into excess of precipitating solution. The separation of solid phase (the precipitated product) of various ionic species linked with each other by a chemical bond, from liquid phase is called coprecipitation. The coprecipitate thus formed is

washed to remove unwanted ions. It is then dried to get reactive powder which is further calcined to obtain ferrite powder. The precursor of mixed metal oxide can be prepared by coprecipitating mixture of metal ions as hydroxides or carbonates or oxalates etc. using proper precipitating agent. For obtaining the coprecipitate of the well defined stoichiometry of metal ions, the precipitating agent should satisfy the following conditions:

i) the compound should be insoluble in the mother liquor;

ii) the precipitation kinetics should be fast.

Several parameters such as solubility product of various metal ion compounds (e.g. hydroxides, carbonates, oxalates etc.), pH, concentration, rate of mixing, temperature of precipitation, washing mode and temperature of drying and calcination have to be controlled to produce satisfactory results through the coprecipitation route. Haneda [25] reported formation of Ba-ferrite by coprecipitation method. Krieger et al. [26] coprecipitated Ni and Fe carbonates. The carbonate precursor decomposes into spinel ferrite at 900° C.

Liquid-mix technique: This technique was first used by M.P. Pechini [27] to prepare dielectric and piezoelectric composition. It involves following steps:

1) Formation of separate solutions of carbonate/nitrates/ ammonium salts of required metal ions and organic polyfunctional acid possessing at least one hydroxy and one

27

carboxylic functional group such as citric, maleic, tartaric, glycolic or lactic acid (among these, citric acid is more widely used).

2) In second step, mixture of solution is slowly heated to remove the solvent. After the solvent is removed, the dried product is glassy in nature, homogeneous and mixed at atomic level. Such mixture is referred to as a precursor of the mixed oxide.

3) The glass is then calcined at relatively low temperature to get the required compound giving the powder of particle size 30-5000°A depending upon processing conditions. Thus, reactive ceramic powders can be obtained by the decomposition of the precursor salts. The main advantages are as follows: (i) Relatively simple method requiring no special apparatus; (ii) Stoichiometry, purity and composition can be accurately controlled since process involves no washing.

A number of mixed-oxide systems have been prepared by the citrate or modified citrate method by various workers [28,29]. Srivastava et al. reported formation of Ba-ferrite using citrate method [30].

Organometallic precursor method: For many years, inorganic and organic precursors of metals have been utilized for preparation of simple and complex metal oxide and other related systems. According to Yoldas [31], the term metal organic includes the compounds having organic group along

with the metal (or metals) and in which organic groups are bonded to a metal via oxygen etc. When these metal-organic precursors decomposed in air, it may directly lead to the formation of mixed oxides or solid solution in certain cases. At the time of decomposition of these precursors, strong reducing atmosphere is present (e.g., $CO-CO_2$) due to which lowering of oxidation state can take place. When oxygen reappears over reactive solid phase which increases oxidation state of metal ions. This method lowers the preparation temperature and reduces treatment time. Chandrashekhar et al. [32] synthesized Ba-ferrite by the organometallic precursor method. The examples of the ferrite obtained by these methods below 500°C are well known [33,34].

Sol-gel method: The method involves the conversion of a sol (a fluid colloidal suspension of a solid in a liquid) to a gel (a semirigid colloidal dispersion of a solid in a liquid). In a typical procedure, a metal is reacted with an alcohol to form a metal alkoxide, which is then dissolved in appropriate alcohol. Then water is added to hydrolyse the alkoxide. After the adjustment of pH, it polymerises to form a gel. The gel is then dried by heating in the temperature range 200-500°C to remove the liquid, thus converting it into finely divided metal oxide powder with particle size in the range of 0.003-0.1 μm. Rustum Roy [35] pioneered the use of this technique to make finely divided and exceptionally homogeneous glasses of silica and the oxides of Al, Mg, Ti,

Zr, Ge etc. Luchinni et al. [36] adopted lyophilized gel method for preparation of barium hexaferrite.

Wet chemical methods: Preparation of ferrites from solutions of water-soluble salts of the corresponding metals fall under this category. These methods are reported to yield ferrite powders having molecular level homogeneity, smaller grain size, low porosity and large .surface area. These methods include, 1) Spray reactions, 2) Freeze drying and 3) hydrothermal oxidation.

1) *Spray Reactions*: These are classified into (1) Flame spraying, (2) Spray roasting and (3) Spray drying. Flame spraying was developed by Wenckus [37]. In this technique a solution of nitrates salt are dissolved in alcohol with the right ratio of ions, and solution is sprayed in a burner to decompose the salt. Malinofsky & Babbit [38] were able to prepare nickel ferrite by this method with a.grain size of 0.8 μm. Zneimer et al. [39] prepared Ni-Al-Ga spinel ferrite by putting the nitrates salt of the desired metallic ions in solution with methanol, atomizing the solution with oxygen and burning the atomized spray. Spray roasting is a single-step process for the production of ferrite powders from the salt-solution. The method involves dissolving the desired metallic components in a small excess of HNO_3 aqueous solution and spraying the sample with a centrifugal atomizer into a roasting chamber. Hot air is introduced into the chamber at 350°-400°C. The solution is dried and decomposed before leaving the hot zone. The spray-roasting powder

exhibits a remarkable reactivity with high purity. Ruthner et.al. [40] have utilized this method for the production of very reactive Fe_2O_3 suitable for preparing ferrites. In spray-drying method, mixed aqueous solutions of soluble salts of the appropriate metals are atomized into fine droplets (10-20 μm). When they come into contact with hot stream of gas, water evaporates rapidly, giving hollow spheres of mixed salt. Compounds prepared by this technique have great purity and homogeneity [41].

Freeze drying: In this method, an aqueous salt solution is first prepared with the exact requirement of ions. This solution is then subjected to quick freezing by spraying it into a low-temperature bath (e.g. liquid nitrogen or hexane bath chilled with dry ice and acetone). This solidifies the solution as fine beads of salts and ice. The frozen material is transferred to a freeze dryer and dewatered in vacuum at -70°C by sublimation of ice. The resulting product of anhydrous salt is homogeneous on the molecular scale and free from contaminants from the starting material. The salt is converted to oxide by decomposition at an elevated temperature. This method has been applied for preparing a number of ceramic materials. Schnettler & Johnson [42] have claimed that this method can form ferrites with small grains and theoretical density could be prepared. Ni-Zn ferrite prepared by this method gave a density of 5.3 gm/cm^3 (99% of the theoretical density) with a grain size of 5 μm when sintered between 1000-1200°C.

Hydrothermal oxidation: Preparation of ferrite directly from the solution is achieved by this process. In this method, alkaline solution is added to a stoichiometric solution of metallic salts with ion in the divalent state. This results in a suspension of the mixture of hydroxides. The suspension is kept at the optimized temperature. When air is bubbled uniformly into this suspension, it promotes the oxidation reaction, converting the precipitate into ferrite [43].

Takada & Kiyama [44] have prepared manganese zinc ferrite by this method. The hydrothermal method for preparation of barium hexaferrite was tried by Barb et al. [45]. The particles of 1 um diameter of $BaFe_{12}O_{19}$ were obtained by hydrothermal processing of a water suspension of $Ba(OH)_{2.8}H_2$ and aFeOOH at 315 ± 5°C and under vapour pressure 98 to 110 atm.

1.3.3   Additives

The ferrites are technologically important materials. They find applications in varied areas. Depending upon the type of application, optimisation of characteristic properties is needed. Several attempts of improving the properties of ferrite for technological applications have been made using various additives. Additive is an impurity

added to the pure bulk material, usually in small amount, at the stage of processing. The amount of additive and the stage at which it is mixed are found to be important. Recent scientific research continues to probe the effect of additive or dopants on the properties of ferrites.

Depending upon the nature of additive, several effects are possible. Taking into consideration the effect and role of additives in modifying the ferrite properties, additives have been categorised into three types: A) Additive ions that substitute or replace the cation from crystal lattice, B) Additives that act as grain growth inhibitors and C) Additives useful in the process of sintering mechanism known as liquid phase sintering.

A) <u>Additives acting as cation substituents</u>: The ferrite materials, by virtue of their structure, can accommodate a variety of cations at different sites enabling a wide variation in properties. The effect of such additive depends on the nature and site preference of substituting ion. For example, when a diamagnetic cation replaces Fe^{3+} ion, magnetic interactions with neighbouring ions in unit cell are locally disturbed. Such replacement of cation affects the intrinsic properties of ferrites like magnetocrystalline anisotropy, intrinsic coercivity, etc. The properties of ferrites can be tailored as per requirement by controlled incorporation of additives e.g., addition of (Co+Ti) in Ba-ferrite makes it useful for perpendicular magnetic recording

media [46]. Al^{3+} when substitutes Fe^{3+} ion in Ba/Sr ferrite, increase in intrinsic coercivity is observed· [47]. Nickel ferrite or NiZn ferrite used at high frequencies is doped with cobalt. The magnetocrystalline anisotropy (K) is lowered by addition of Co^{2+} [48]. The presence of Fe^{2+} ion in Mn-Zn ferrite is useful to minimise the magnetostriction and to increase the permeability [49].

B) Additive acting as grain growth inhibitors: Second type of additives are designed to segregate at grain boundaries. The additives of this class usually modify sintering behaviour by decreasing sintering temperature and modifying the microstructure. The modified microstructure in turn improves the magnetic properties. The effect of SiO_2 addition on hexaferrite was studied by different coworkers [50,51]. The SiO_2 and excess Ba/Sr oxide from hexaferrites segregates at grain boundary and impedes the grain growth and also helps in densification. H_3BO_3 [52], Bi_2O_3 [53] are other examples of this class used in processing of hexaferrite. The additives from this class when segregated, grain boundaries found to increase resistivity and reduce eddy current losses. This property is very useful for soft ferrites, especially Mn-Zn ferrites. Incorporation of CaO in Mn-Zn ferrite found to reduce eddy current losses [54]. Akashi [55] showed that combination of CaO with judicious amount of SiO_2 increases resistivity and lower the losses. Addition of BaO in Ni-Zn-Co ferrite helps in densification and makes microstructure more uniform [56].

34

C) <u>Additives help in liquid phase sintering</u>: Additives from this class act as a low melting flux. During sintering they wet the particles of the calcined powder, cover the surface of particles and do not allow them to grow. Thus additives from this group form a liquid phase at sintering temperature and can substantially modify the microstructure [57,58]. The Tables 1-a&b enlist some of the important examples from these three different types of additives used for hexaferrite and spinel ferrite respectively.

1.3.4   Compaction

To achieve the requisite microstructure and properties, high quality ferrite powders have to be compacted followed by sintering. Dry calcined ferrite powder is pressed into required shape by compaction. Compact formation is a simple process where a previously prepared homogeneous ferrite powder is compressed to give a body that is 50-60% theoretically dense, eliminating large pores. For effective compaction, the ferrite powder should possess uniform flow characteristics. Generally, coarser particles tend to flow more uniformly than fine ones. Hence, fine ferrite powders are subjected to granulation. In this technique, fine particles of ferrite are converted into granules to increase their flowability.

Table-1a

Additives/Dopants used in $MFe_{12}O_{19}$ (M = Ba/Sr)

Type I	II	III
	SiO_2 [50]	$MO-Al_2O_3-SiO_2$ [57]
La^{3+} [59]	H_3BO_3 [52]	$MO-Al_2O_3-B_2O_3$ [57]
Ru^{3+} [60]	$H_3BO_3+SiO_2$ [52]	
Al^{3+} [47]	Bi_2O_3 [53]	
Cr^{3+} [47]	Na_2O [63]	
$(Co^{2+} + Ti^{4+})$ [46]		
$(Co^{2+} + Sn^{4+})$ [61]		
$(Ni^{2+} + Ti^{4+})$ [62]		

Table-1b

Additives/Dopants used in MFe_2O_4 (M = Mn,Zn,Ni)

Type I	II	III
Fe^{2+} [48]	BaO [56]	MoO_3 [58]
Co^{2+} [49]	$NaOH$ & KOH [66]	
Ti^{4+} [64]	SiO_2 [67]	
Sn^{4+} [65]	V_2O_5 [68]	
	CaO [54]	
	$CaO + SiO_2$ [55]	

36

To obtain better compaction, ferrite powder is usually mixed with suitable binder before pressing. The selection and use of binder is important factor in compaction. The role of binder is to increase the strength of pressed compacts. Polyvinyl alcohol is widely used as the binder for ferrite powders. External lubricant is applied to the surface of die before pressing. Use of lubricants facilitates mold release and interparticulate sliding. It reduces the friction gradient of the powder at the walls of the die and between the particles themselves during sintering. Zinc stearate is also suited for ferrite powders. Plasticizers alter the rheology of the powders, improve flexibility of binder films and allow plastic deformation of granules. Gum arabic is used as plasticizer for ferrite powders. Use of plasticizer such as polyethylene glycol soften the particles. Deflocculants control the pH and particle surface charge and acts as dispersion agent. Powder compaction can be done by two methods: uniaxial pressing (dry pressing) and isostatic or hydrostatic pressing. The hard ferrite powder can be pressed into pellets either in presence or absence of magnetic field. Pressing in presence of magnetic field gives rise to oriented or anisotropic magnets.

Pressing in absence of magnetic field: In this type of pressing, binder mixed ferrite powder is dry pressed or isostatically pressed. Isostatic pressing gives compacts with better green density.

37

Pressing in presence of magnetic field: It is also known as anisotropic pressing. For M-type hexaferrite, c-axis is easy axis of magnetisation. During the pressing of fine ferrite powder in magnetic field, easy axis of crystallites is aligned in the direction of magnetic field. For a random orientation, the remanence value is half of its saturation value. With the pressing of hard ferrite powder in presence of magnetic field by two times and the material becomes anisotropic also on macroscopic scale [69]. By anisotropic pressing, the degree of orientation increases. The degree of orientation is one of the factors governing magnetic parameters like B_r and $(BH)_{max}$ and hence anisotropic pressing causes a distinct increase in B_r and $(BH)_{max}$ by this type of pressing. Technologically, this orientation can be obtained either by (a) dry pressing or (b) wet pressing.

1.3.5   Sintering

The calcined powder compacts obtained by unit processing of compaction is composed of individual grains having an overall porosity of $\sim$ 25-60 vol%, depending on the particular material used and pressing method. To maximise the properties of material, it is desirable to minimise the porosity. Such minimisation is obtained through the process, called densification by sintering. The purposes of the sintering process are:

1)   To complete the interdiffusion of the component metal ions into the desired crystal lattice.

38

2) To establish the appropriate valencies for the multivalent ions by proper oxygen control.

3) To develop the microstructure most appropriate for the application [70].

The sintering is a process by which the fine particles which are in the direct contact with each other, form a solid continuous matrix when heated to a suitable temperature. The driving force for sintering·is the excess surface energy present in a powder compact as compared to a single crystal of the same composition. As the temperature is increased, the atoms acquire sufficient mobility to cause changes that reduce the overall surface energy in the morphology of the particles. The optimum temperature and time condition should be the minimum needed to achieve the required homogeneity and microstructure. Excessive temperature or time degrades the ferrite properties by exaggerated grain growth and increased porosity. Many manufacturers found that sintering time can reduce to half by judicious choice of raw materials, additives, processing techniques and firing parameters [70]. The different factors which have dominant effect on sintering are given by Stuijts [71]. They are particle size, particle size distribution, particle shape, intraparticle porosity, agglomeration, homogeneity in chemical composition, pore size distribution, temperature gradients, activated sintering, gas atmosphere and pressure. Out of these factors mentioned above, particle size plays a vital role in

producing high-density ferrites by sintering. Many recent sintering techniques are developed with the aim of lowering the cost and to improve properties e.g., hot pressing, fast sintering, etc.

Sintering of spinel ferrite

Among the spinel ferrites, nickel ferrite is the least complicated ferrite from processing point of view. The Ni^{2+} oxidation state of nickel is stable, so most of the time air is used as the firing atmosphere. In case of Mn-Zn ferrites, along with the problem of zinc loss, other serious problems encountered are (i) stabilization of the Fe^{2+} content and (ii) the variable valence of the Mn. On this background, for Mn-Zn ferrites, unlike the Ni and NiZn ferrite, control of the atmosphere is the most crucial variable in the sintering process. Many investigators have stressed the importance of maintaining the equilibrium oxygen atmosphere above Mn-Zn ferrites to obtain appropriate Fe^{2+}/Fe^{3+} ratio [71-72]. Thus in order to produce high-quality ferrites, it is therefore most critical that the proper temperature-atmosphere equilibrium be determined and maintained for the specific Mn-Zn ferrite product. 9255

In case of the sintering of hard ferrites, both cations in hard ferrites do not change valencies at their sintering temperature and therefore hard ferrite pellets are often fired in air.

1.3.6 Microstructure & grain boundary chemistry

The properties of ceramic products are determined not only by the composition and structure of phases present, but also by microstructure of final product. According to specific application, optimisation of intrinsic properties is done by choosing proper chemical composition. Similarly, the microstructure of a ferrites can also be designed to optimise the extrinsic parameters that will improve property required for application. The study of ·microstructure property/analysis reveals that in obtaining high quality reproducible ferrites, crucial problem is to get required microstructure. The microstructure depends on initial composition, impurity or dopant levels, powder-particle size, size distribution and sintering conditions. The basic element of structure on which all the magnetic properties depend is the domain structure. The study of soft ferrites reveals that permeability increases linearly with grain size [73]. For Mn-Zn ferite sample permeability upto 40,000 is achieved with grains of 80 μm [74]. Porosity is an important feature limiting permeability. Intragranular porosity is more deleterious than intergranular porosity. Brown & Gravel demonstrated a decrease in permeability with porosity for Ni and NiZn ferrites [75]. Roess found that Mn-Zn ferrite with exaggerated grain growth and much induced porosity has a permeability of 2000. In contrast, the ferrite with the same grain size that grow normally has a permeability of 40,000

[74]. Dorfenik has reported that distance between pores rather than the grain size accounts for variation in permeability [76,77]. Knowles showed that a 6 um grain size is optimum for attaining maximum rotational permeability and minimum hysteresis and residual losses for Mn-Zn ferrite [78].

The most important feature which distinguishes a polycrystalline ceramic from a single crystal is the presence of grain boundaries. The characterization of grain boundaries in ceramics has become more important day by day. The wide variety of techniques developed for surface analysis such as ESCA, EPMA, AES, etc. are used in recent years to analyse grain boundaries exposed by fracture. The use of these techniques in the analysis of boundaries is based on the assumptions that ceramics examined, fracture intergranularly. The use of modern analytical tools has resulted into a better understanding of the effect of small amount of additives (impurities) on the grain boundary chemistry and microstructure. The microstructure and grain boundary chemistry can be modified by incorporation of additives. Akashi showed that addition of CaO and SiO_2 in MnZn ferrite increases resistivity and lowers the losses [44]. This effect is due to increase in grain boundary resistivity. Stijntjes [79] using electron microprobe analysis confirmed that additive such as Ca and Si segregate at grain boundaries. Franken studied composition of Ti substituted MnZn ferrite using Auger electron spectroscopy. He found a

Ti gradient at the grain boundaries which extended for 2 nm thickness, with the Ti extending further into the grain [80]. Ghate reviewed boundary phenomena in soft ferrites [81]. According to him, for a low loss ferrite, the grain boundaries influence properties by, 1)   Creating a high-resistivity intergranular layer.   2) Acting as a sink for impurities that may serve as a sintering aid and as grain growth modifiers. 3) Providing a path for oxygen diffusion which may modify the oxidation state of cations near the boundaries.

In case of hard ferrite permanent magnets, the two important properties are remanence and coercive force. The remanence is function of chemistry, density and orientation. On the other hand, coercive force is governed by microstructure. To obtain maximum values, all particles should be single domain size i.e. about ~ 1 μm. In the sintering of hard ferrites, the problem is to achieve fine grain size and high density simultaneously. The additives like SiO_2 is found to be very useful to achieve this target. Effect of SiO_2 on magnetic properties and microstructure of Ba/Sr ferrite was subject of interest of different investigators [50,51]. The microstructural study and grain boundary composition of sintered $SrFe_{12}O_{19}$ with SiO_2 addition was studied by means of ESCA and the presence of secondary phase, especially at grain boundaries was estimated by TEM. It has been found that· grain growth inhibiting action of SiO_2 is dependent on the molar ratio

x = SiO_2/SrO excess. The AES and ESCA study showed that silicon segregate at grain boundaries in a layer of 2 nm thickness [51].

REFERENCES

1. D. Segal, in Chemical Synthesis of Advanced Ceramic Material (1989), Cambridge University Press, Cambridge.

2. E.C. Subbarao, in Advanced Ceramics, edited by E.C. Subbarao, Indian Academy of Sciences, Bangalore (1988) p.1.

3. R.R. Hirwani, Chemical Business, 1 (1987) 45.

4. V.C.S. Prasad, in Advanced Ceramics, edited by E.C. Subbarao, Indian Academy of Sciences, Bangalore (1988) p.37.

5. H.J. Sanders, Chemical & Engineering News, 62 (1984) 26.

6. Y. Hoshino, Ferrites, Proc. 3rd Int. Conf. on Ferrites, Kyoto (1982).

7. D.H. Martin, Magnetism in Solids (1967); Iliffe Books Ltd., London.

8. A.J. Dekker, Solid State Physics (1952), McMillan & Co. Ltd., London.

9. J. Smit and H.P.J. Wijn, Ferrites (1959), N.V. Philips' Gloeilampenfabricken.

10. M.M. Schieber, Experimental Magnetochemistry (1967), North Holland Publishing Company, Amsterdam.

11. Ing. C. Heck, Magnetic Materials and Their Applications (1974), Butterworth & Co. (Publishers) Ltd.

12. J. Crangle, The Magnetic Properties of Solids (1977), Edward Arnold (Publishers) Ltd., London.

13. Solid State Physics, Kittel.

14. A.H. Morrish, Physical Principles of Magnetism, John Wiley & Sons, New York.

15. L.J. de Jongh and A.R. Miedema, Adv. Phys. 23 (1974) 1.

16. S.Krupicka and P.Navak in Ferromagnetic Materials. Edited by E.P.Wohlfarth. Vol.3 (1982) North Holland Publishing Company.

17. L.Néel, Ann. Phys. (France) 3 (1948) 137.

18. B.Lax, K.J.Button, Microwave Ferrites and Ferrimagnetics (1962) Mc-Graw-Hill Book Company Inc.

19. B.K. Das, in Preparation and Characterization of Materials, edited by J.M. Honlg and C.N.R. Rao (New York Academic Press).

20. A. Srivastava, Ph.D. Thesis, Poona University (1985).

21. R.C. Tenzer, J. Appl. Phys., 34 (1963) 1267.

22. G. Heimke, Z. Angew. Phys. 15 (1963) 271.

23. E.C.Subbaroa in Advanced Ceramics (1988) Edited by E.C. Subbaroa, Ind. Academy of Sciences, Bangalore (Publisher).

24. G. Economos, J. Am. Ceram. Soc. 38 (1955) 241.

25. K. Haneda, C. Miyakawa and H. Kojima, J. Am. Ceram. Soc. 57 (1974) 354.

26. E.M. Krieger, E.A. Nazarova and F.T. Yakushouskaya, Soviet Powder Metallurgy Metal Ceramics 89 (1970) 414.

27. M.P. Pechini, U.S. Patent 3,330,697 (1967).

28. C. Marcily, P. Courty and B. Delmon, J. Am. Ceram. Soc. 53 (1970) 56.

29. D.J. Anderton and F.R. Sale, Powder Metallurgy 1 (1979) 8.

30. A. Srivastava, P. Singh and M.P. Gupta, J. Mat. Sci. 22 (1987) 1489.

31. B.E. Yoldas, J. Mater. Sci. 12 (1977) 1203.

32. R. Chandrashekhar, S.W. Charles, K. O'Grady, S. Marup and J. Van Wonterghem, Adv. Ceram. Mat. 2 (1987) 65.

33. G.A. Sawartzky, F. Van Der Wood and A.H. Morrish, Phys. Rev. 187 (1969) 747.

34. A. Roussest, F. Chassagneux and J. Paris, J. Mat. Sci. 21 (1986) 3111.

35. R. Roy, J. Am. Ceram. Soc. 52 (1969) 344.

36. E. Lucchini, S. Meriani, F. Delben, and S. Padetti, J. Mat. Sci. 19 (1984) 121.

37. J.F. Wenckus and W.Z. Leavitt, in Proc. of Conf. on Mag. Mat., AIEE Special Publication, T-91 (1956) 526.

38. W.W. Malinosfsky and R.W. Babbit, J. Appl. Phys. 32 (1961) 2375.

39. J.E. Zneimer, B. Kaplan, K. Lehman and D.A. Lepore, J. Appl. Phys. 35 (1964) 1020.

40. M.J. Ruthner, Ferrites, 3rd Int. Conf. on Ferrites (1980) 48.

41. P. Reijnen, G.P. Th.A. Aarts, R.M. Van de Heuvel and A.L. Stuijts, Ber. Deut. Keram. Ges. 47 (1970) 669.

42. F.J. Schettler and D.W. Johnson, Ferrites, Proc. of Int. Conf. Japan (1970) 121.

43. T. Utsunomiya, Y. Hoshino and K. Show, Mat. Res. Bull. 20 (1985) 85.

44. T. Takada and M. Kiyama, Ferrites, Proc. Int. Conf.

Japan (1971) 69.

45. D. Barb, L. Diamandescu, A. Rusi, D. Tarbasa, M. Morariu and V. Teodorescu, J. Mater. Sci. 21 (1986) 1118.

46. F. Chow, X. Feng and Y. Liu, J. Appl. Phys. 61 (1987) 3881.

47. K. Haneda and H. Kojma, Jap. J. Appl. Phys. 12 (1973) 355.

48. A.D. Giles and F.F. Westendarp, J. de Phys. 38 (1977) C1-47.

49. C. Guillaud, Proc. IEE 104 (1957) 165.

50. F. Kools, Sci. of Sintering 17 (1985) 49.

51. F.J.A. Der Broeder and P.E.C. Franker, in Adv. in Ceramics 1 (1981) 494.

52. H. Harada, Ferrites: Proc. of the Int. Conf. Japan (1980) 354.

53. K.K. Laroia and A.P.B. Sinha, Ind. J. Pure & Appl. Phys. 2 (1964) 48.

54. C. Guillaud, Proc. IEEE 104B (1957) 165.

55. T. Akashi, Trans. Jap. Inst. Metals 2 (1961) 171.

56. S. Besenicar and D. Hanzel, J. de Phys. 46 (1985) C6-169.

57. R.H. Arendt, J. Appl. Phys. 44 (1973) 3300.

58. C.G. Jain, B.K. Das and N.C. Goel, J. Am. Ceram. Soc. 62 (1979) 79.

59. K. Higuchi, S. Naka and S. Hirano, Adv. Ceram. Mat. 1 (1986) 104.

60. J.Z. Liu, M. Lu, T.Z. Jin, Z.J. Wang and H.R. Zhai, Ferrites: 3rd Int. Conf. on Ferrites, Japan (1980).

61. P.C. Kuo, Y.D. Yao, W.I. Tzang, J. Appl. Phys. 73 (1993) 6292.

62. g. Turilli, F. Licci, A. Paoluzi and T. Besagni, IEEE Trans. Mag 24 (1988) 2146.

63. Y.T. Chien and Y.C. Ko, J. Mat. Sci. 25 (1990) 2835.

64. T.G.W. Stijntjes, Philips Res. Rep. 25 (1970) 95.

65. C.G. Jain, B.K. Das and S. Kumari, IEEE Trans. on Mag., Mag. 12 (1980) 1428.

66. H.M. O'bryan, P.K. Gallagher, F.R. Monforte and F. Schrey, Ceramic Bull. 48 (1969) 203.

67. G.C. Jain, B.K. Das and S. Kumari, J. Appl. Phys. 49 (1978) 2894.

68. R. Narayan, R.B. Tripathi, B.K. Das, G.C. Jain, J. Mat. Sci. 18 (1983) 1583.

69. J.M. Haspers in : Modern Materials 3 (1962) 259; edited by Henrey H. Hausner, Academic Press, New York & London.

70. A. Goldman, in Modern Ferrite Technology (1990), Van Nostrand Reinhold, New York.

71. E.D. Macklen, J. Appl. Phys. 36 (1965) 1072.

72. R. Morineau and M. Paulus, IEEE Trans. Mag. 11 (1975) 1312.

73. D.J. Perduijn and H.P. Peloschek, Proc. Brit. Ceram. Soc. 10 (1968) 2636.

74. E. Ross, Ferrites: Proc. Int. Conf. Ferrites (1971) 187.

75. F. Brown and C.L. Gravel, Phys. Rev. 97 (1955) 55.

76. M. Drofenik, S. Besenicar and M. Limpel, Adv. in Ceram. 16 (1985) 229.

77. M. Drofenik, Am. Ceram. Soc. Bull. 65 (1986) 656.

78. J.E. Knowles, J. Phys. Colloq. C-1 (1977) 27.

79. T.G.W. Stijntjes, A. Broese van Groneou, R.F. Pearson, J.E. Knowles and Ranki, Ferrites (1971) 194.

80. P.E.C. Franken, J. Am. Ceram. Soc. 63 (1980) 315.

81. B.B. Ghate, Adv. in Ceram. 1 (1981) 477.

Chapter 2

Experimental

2.1   SYNTHESIS

The synthesis of fine particles is subject of interest due to their application in preparation of high density ferrite at low temperature and with superior magnetic properties. The conventional ceramic method is not quite useful for the preparation of fine particle ferrite, since it is not possible to grind a material much below a particle size of one micron. Wet chemical methods such as coprecipitation, hydrothermal oxidation, decomposition of organometallic precursor, liquid mix technique etc. are used to synthesize submicron size particles.

The most widely used reaction is coprecipitation and thermal decomposition of hydroxides. The pH has to be monitored in the precipitation of hydroxides. Haneda et. al. [1] used this technique for the preparation of Ba-hexaferrite. The ferrite powder prepared by this method found to give final product with superior magnetic properties. Considering the advantages of this method in the present work, we have selected conventional coprecipitation method for the synthesis of strontium hexaferrite powders. Following are chemicals used for the preparations:

1) $FeCl_3.6H_2O$ - A.R. grade, SD Fine Chemicals, India.

   $Fe(NO_3)_3.9H_2O$ - L.R. grade, Loba Chemicals, India.

2) $SrCl_2.6H_2O$ - G.R. grade, Loba Chemicals, India.

   $Sr(NO_3)_2$ - L.R. grade, Loba Chemicals, India.

3)   NaOH   - A.R. grade, Loba Chemicals, India.

2.1.1   Preparation of Stock Solution

The metal nitrates/chlorides are dissolved in distilled water to prepare respective stock solutions. The solutions are then filtered through sintered glass funnel (G-4) to remove undissolved matter. The concentrations (molarity) of aqueous stock solutions of different chemicals are given below:

$Fe(NO_3)_3$ (L.R.) & $FeCl_3$ (A.R.) - 2.6M

$Sr(NO_3)_2$ (L.R.) & $SrCl_2$ (G.R.) - 1.2M

NaOH (G.R.)   - 5.1M

2.1.2   Preparation of Strontium Hexaferrite: Important Features

To obtain highly uniform, ultrafine, active powders by coprecipitation method, optimisation of processing parameters is necessary. The precursor samples of Sr-ferrite were synthesised for the study of following processing parameters:

1)   Effect of mode of washing/filtration

2)   Effect of crystallinity

3)   Effect of additives

To study the effect of these parameters on Sr-ferrite, we prepared various samples described in the Table 1.

Table 1

Name of Sample	Chemicals used	Precipi-pitating agent	Washing/Filtration method
A	$Fe(NO_3)_3 + Sr(NO_3)_2$	NaOH	Centrifuge
B	$Fe(NO_3)_3 + Sr(NO_3)_2$	NaOH	Decantation
C	$FeCl_3 + SrCl_2$	NaOH	Centrifuge
D	$FeCl_3 + SrCl_2$	NaOH	Decantation
E	$FeCl_3 + SrCl_2$	NaOH	Decantation

For the synthesis of precursor samples by coprecipitation route, we followed the method given by Date et. al. [2] with some suitable modifications. The solutions of chlorides/nitrates of iron and strontium were thoroughly mixed so as to obtain the molar ratio of Fe/Sr = 10.6/1. This atomic ratio was chosen after a series of experiments required for ratio optimisation [3]. The coprecipitate of hydroxides of strontium and iron was obtained by dropwise addition of an aqueous solution of mixed metal ions into sodium hydroxide solution. The dropwise addition was done with the help of separating funnel at the rate of 3-4 ml/min. The solution was continuously stirred with the help of mechanical stirrer to ensure uniform mixing. The temperature and pH at which precipitation was done, also play important role in affecting properties of final

product. We did all the experiments at room temperature between 25°C-35°C and the pH was $\geq$ 13. The high pH is essential for complete and simultaneous precipitation of mixed hydroxides of strontium and iron.

After completion of precipitation reaction the mixture of metal hydroxides was washed with distilled water to remove Na^+, NO^-_3/Cl^- ions and excess of alkali either by centrifugal filtration or decantation method. About 32 litres of water was used to wash 100 gm of precursor sample, in ten successive washings. The amount of water used during washing was optimised by taking into account the solubility of strontium hydroxide in water [3]. The precipitate was dried in air at 100°C in an oven. The dried coprecipitate is used as a starting material for synthesis of Sr-hexaferrite. The experimental procedure involved in the coprecipitation route is shown by a schematic representation in Fig.1.

This is a general outline of synthesis of coprecipitate precursor of Sr-hexaferrite. The modification in synthesis during the study of each processing parameter are given below.

The study of effect of mode of washing/filtration : To study this effect, the coprecipitate was synthesised in two different batches, namely A & B.

Batch A: 435 ml of 2.6M $Fe(NO_3)_3$ solution was mixed with 90 ml 1.2M $Sr(NO_3)_2$ solution. 525 ml of above mixture was added
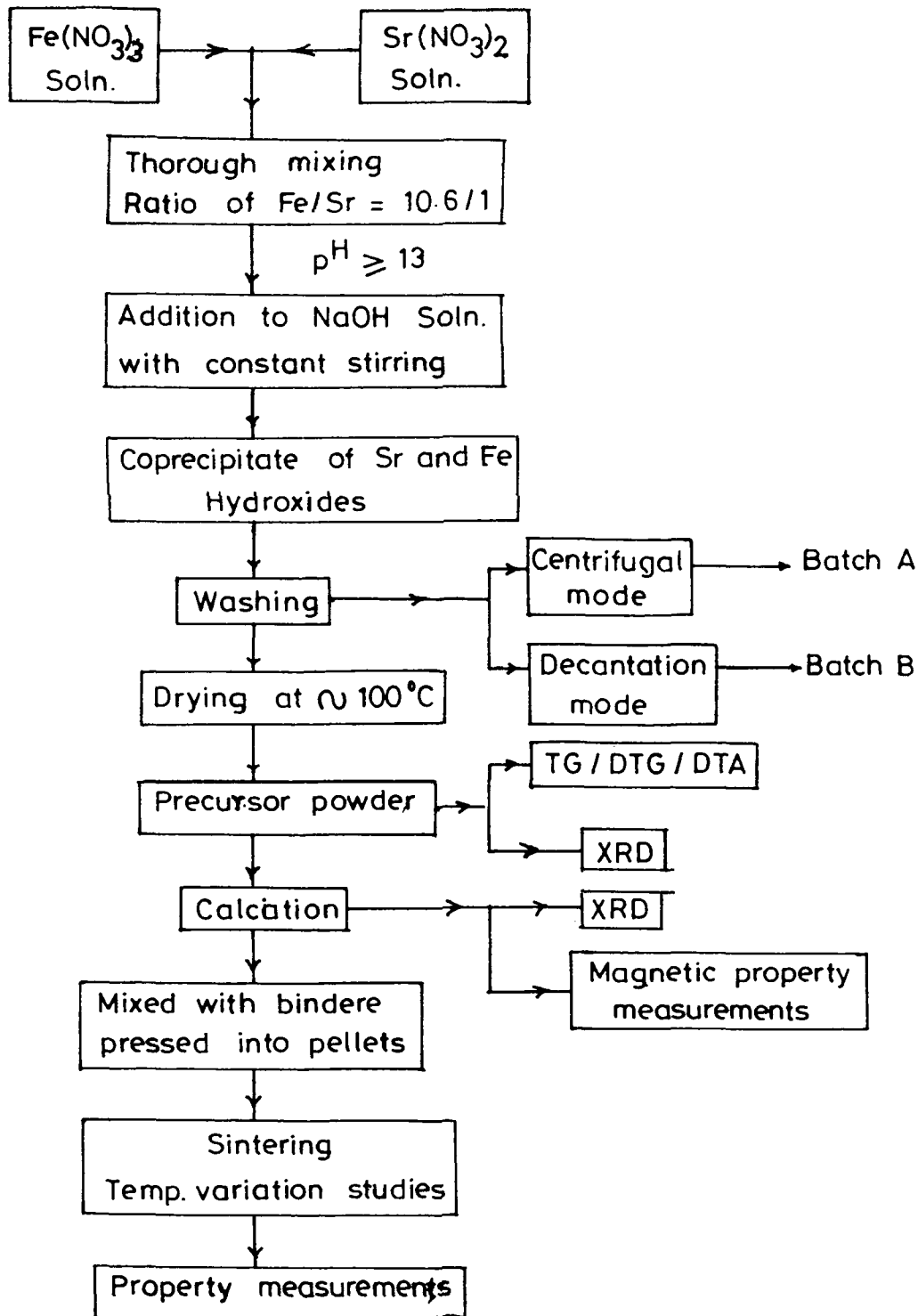
Fig.1 : Flow diagram showing preparation procidure for Sr-ferrite from coprecipitation method.

dropwise to 1415 ml 5.1M sodium hydroxide solution. The precipitate was washed with centrifugal method of filtration. Ten washings were given to coprecipitate to remove Na^+, NO^-_3 ions and excess alkali, using about 32 litres of distilled water. The coprecipitate thus obtained was in the form of lumps and dried in an oven at ~ 100°C. The dried coprecipitate was divided into three parts. They were calcined at 750°C/5 hr, 850°C/5 hr and 925°C/2 hr.

Batch B: 435 ml of $Fe(NO_3)_3$ and 90 ml of $Sr(NO_3)_2$ solutions were mixed. The coprecipitation was carried out under similar conditions as that of batch A, except the mode of washing. The coprecipitate from this batch was washed via decantation mode of filtration. In this type the washing was done simply by allowing the precipitate to settle down for some time and then siphoning out the supernatant liquid. Total ten washes of 3.2 litres each (i.e. 3.2 X 10 = 32 litres) were given. The coprecipitate thus obtained was in the form of slurry. It was dried in oven at 100°C. The dried coprecipitate was divided into three equal parts which were subsequently calcined at 750°C/5 hr, 850°C/5 hr and 925°C/2 hr in air.

Pellet pressing: For preparation of pellets, the powder obtained on calcination was mixed with polyvinyl alcohol binder (about 1 ml of a 1% aqueous solution of polyvinyl alcohol was added to one gram of the powder). The mixture

was dried under an IR lamp. The powder was then pressed into pellets by means of a three-tiered die on a Carver make Laboratory Press at pressure of about 2.2 tons/sq.cm. The pellets were removed from the die by applying a pressure in the reverse direction. Several pellets were prepared in this fashion (denoted as green pellets).

The green pellets were then transferred on a ceramic platform and sintered at various temperatures in the range 1100°C to 1250°C for two hours in an electrically heated OK Furnace fitted with SiC rods. The pellets were furnace cooled to room temperature.

The sintered pellets were weighed on a Mettler balance. The diameter and thickness were measured by using Vernier calipers. The data thus obtained were used to find out the density of the pellets. Table 2 gives pellet number and sintering conditions for the pellets derived from batch A & B.

Effect of crystallinity of coprecipitate: To study this effect of crystallinity the precursors having different crystalline nature were synthesised. The iron and strontium were coprecipitated using NaOH as precipitating agent (batch C). The centrifugal mode of washing was followed to wash the coprecipitate. The washed coprecipitate was in the form of lumps which was divided into two parts - (i) first part was dried in the form of lump and (ii) the second part was mixed

Table 2

Parent Sample	Sample Name	Calcination temp./time °C/hr	Sintering conditions
AI	A-237	750°C/5 hrs	1100°C/2 hrs
	A-238	750°C/5 hrs	1150°C/2 hrs
	A-240	750°C/5 hrs	1200°C/2 hrs
	A-241	750°C/5 hrs	1250°C/2 hrs
AII	A-243	850°C/5 hrs	1100°C/2 hrs
	A-244	850°C/5 hrs	1150°C/2 hrs
	A-246	850°C/5 hrs	1200°C/2 hrs
	A-242	850°C/5 hrs	1250°C/2 hrs
AIII	A-249	925°C/5 hrs	1100°C/2 hrs
	A-250	925°C/5 hrs	1150°C/2 hrs
	A-252	925°C/5 hrs	1200°C/2 hrs
	A-248	925°C/5 hrs	1250°C/2 hrs
BI	B-215	750°C/5 hrs	1100°C/2 hrs
	B-216	750°C/5 hrs	1150°C/2 hrs
	B-217	750°C/5 hrs	1200°C/2 hrs
	B-218	750°C/5 hrs	1250°C/2 hrs
BII	B-221	850°C/5 hrs	1100°C/2 hrs
	B-222	850°C/5 hrs	1150°C/2 hrs
	B-223	850°C/5 hrs	1200°C/2 hrs
	B-226	850°C/5 hrs	1250°C/2 hrs
BIII	B-227	925°C/5 hrs	1100°C/2 hrs
	B-228	925°C/5 hrs	1150°C/2 hrs
	B-229	925°C/5 hrs	1200°C/2 hrs
	B-230	925°C/5 hrs	1250°C/2 hrs

with about 1.5 litres of distilled water and vigorously
stirred with mechanical stirrer for 5-6 hours [Fig.2]. The
stirring helped to disperse the lumps and to obtain
homogeneous slurry. Both the lumps and the slurry were dried
in an oven under the same conditions of temperature and
time. The coprecipitate dried in the form of lumps was
labeled as C-I while another coprecipitate (which was dried
in the form of slurry) was labeled as C-II. Since both the
precursor samples were dried from same batch, problems of
batch to batch variation (i.e. reproducibility), personal
error and uncontrolled parameters were overcome. In short,
preparation history of C-I and C-II is same, except
conversion of part of lumps into slurry. Both the precursor
samples were calcined at 750°C/5 hr. The calcined powder was
pressed into pellets which were sintered at various
temperatures between the range 1100-1220°C. The Table 3
gives the pellet number and sintering conditions of the
pellets.

Effect of additive: In the present study we try to
understand effect of sodium ion as an additive on magnetic
properties of final sintered Sr-ferrite product. This effect
is studied by mixing additive at two different stages viz,
(I) before calcination i.e. mixing of additive in precursor
sample, (II) after calcination i.e. additive is mixed in
calcined powder sample. Polycrystalline strontium ferrite
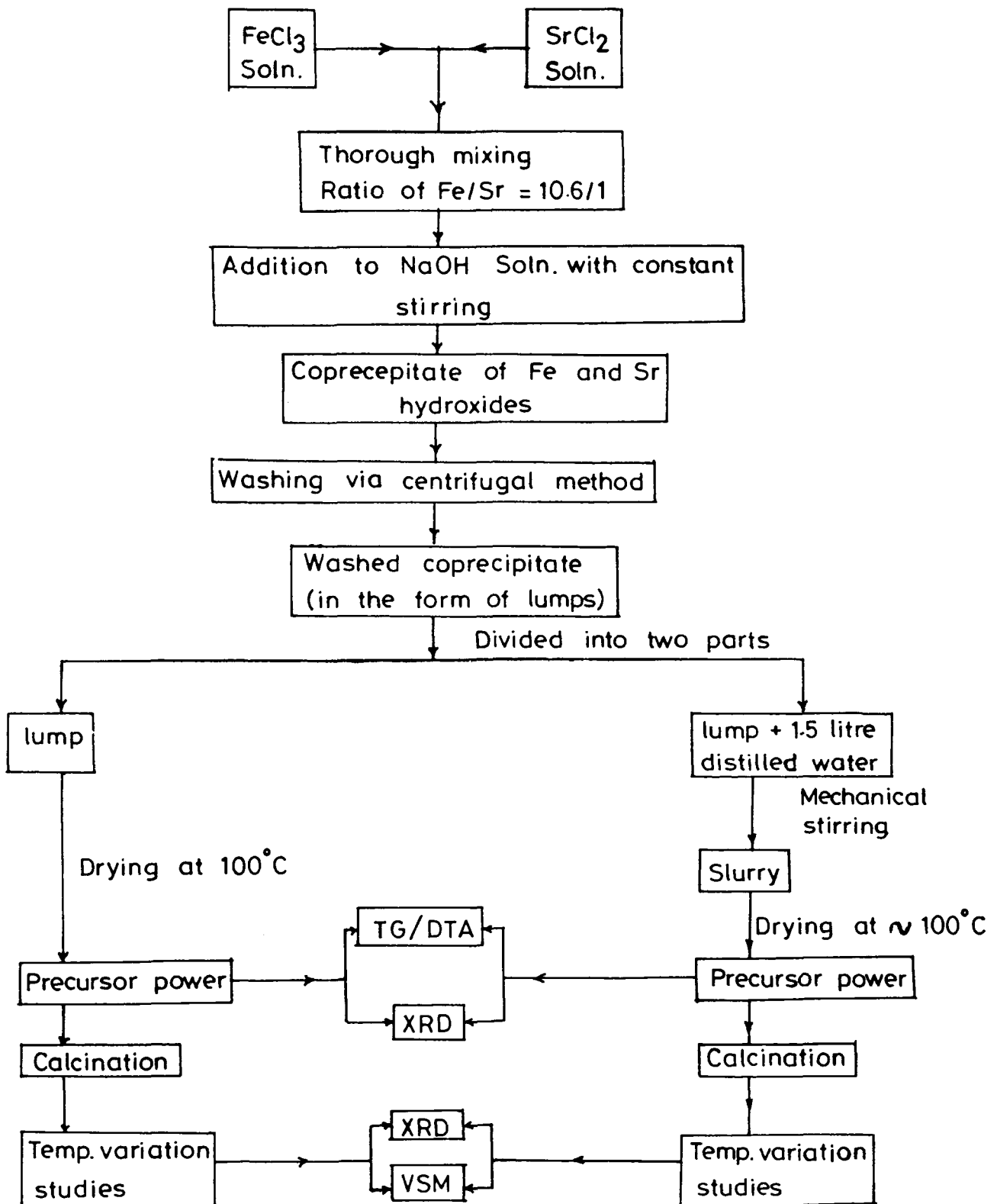was synthesised by following coprecipitation route. The two

Fig. 2 : Flow diagram showing preparation procedure for C-I and C-II samples.

Table-3

Parent Sample	Sample Name	Calcination temp./time	Sintering condition
C-I	C-1	750°C/5 hr	1130°C/2 hr
	C-2	750°C/5 hr	1160°C/2 hr
	C-3	750°C/5 hr	1190°C/2 hr
	C-4	750°C/5 hr	1220°C/2 hr
C-II	C-11	750°C/5 hr	1130°C/2 hr
	C-12	750°C/5 hr	1160°C/2 hr
	C-13	750°C/5 hr	1190°C/2 hr
	C-14	750°C/5 hr	1220°C/2 hr

batches of coprecipitate on 100 gm scale were prepared for the study. The mixture of metal hydroxides obtained by coprecipitation was washed with distilled water by decantation method. The slurry obtained was dried at ~ 100°C in an oven.

I) Addition before calcination: The dried coprecipitate was divided into nine equal parts as shown in flow sheet shown in Fig.3a. The first part was processed without additive. The samples derived from this part are known as virgin sample and used as reference sample during comparative study. The predetermined quantity of sodium ions
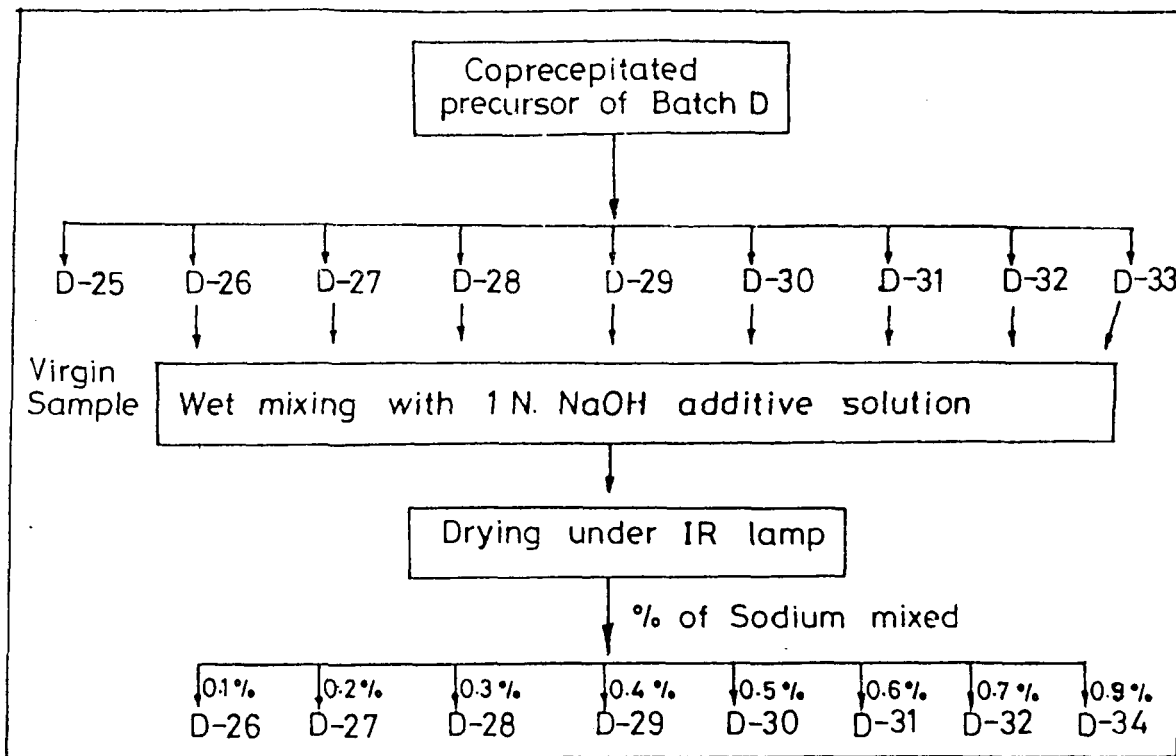
Fig.3a:Flow sheet for the preparation of Sr-Ferrite sample
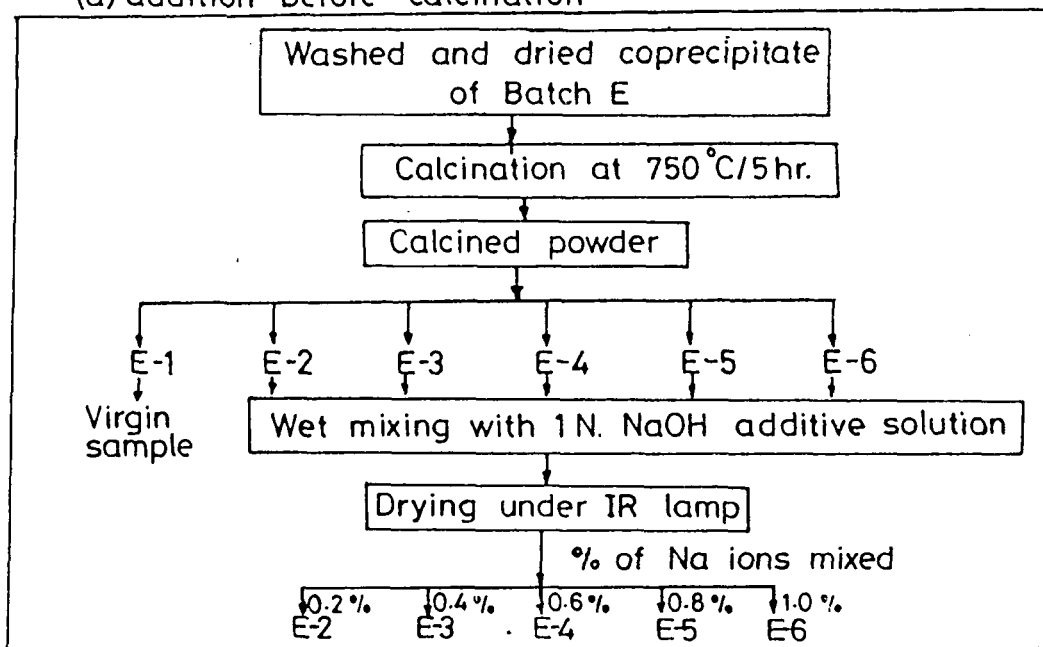(a) addition before calcination

Fig.3 b:Flow sheet for preparation of Sr-Ferrite samples
(b)addition after calcination.

were mixed with remaining eight parts by wet mixing the precursor powder with 1N NaOH solution. The amount of NaOH solution was mixed in such a way that quantity of sodium ions remained in the range of 0.1 to 0.9 wt percent. The wet mixed powders were dried under IR lamp. To initiate the ferritisation reaction, the dried coprecipitates were calcined at 750°C/5 hr in air [2,3].

All the powder samples were mixed with polyvinyl alcohol (1%) binder solution and pressed into pellets at a pressure of 2.2 tons/cm^2. The pellets were sintered at different temperatures in the range 1100-1200°C for 2 hr in air.

Addition after Calcination: The oven dried coprecipitate of batch E was calcined at 750°C/5 hr. Calcined powder was divided into six parts. One part was processed without incorporation of additive. From the remaining five parts, each part was wet mixed with NaOH solution keeping sodium percentage in the range 0.2 to 1.0 wt% of ferrite powder (Fig.3b). The wet mixed samples were dried under IR lamp. The powders were subsequently pressed into pellets after mixing with 1% polyvinyl alcohol binder solution. The green pellets thus obtained were sintered at various temperatures in the range 1100-1200°C for 2 hrs in air.

Tables 4 & 5 describe the details of preparation and processing conditions of various samples from batches D & E.

Table-4

Parent Sample	Pellet Name	Amount of sodium mixed (in wt%)	Calcination temp./time	Sintering conditions
D-25	D-252	0.0	750°C/5 hr	1100°C/2 hr
D-26	D-262	0.1	750°C/5 hr.	1100°C/2 hr
D-27	D-272	0.2	750°C/5 hr	1100°C/2 hr
D-28	D-282	0.3	750°C/5 hr	1100°C/2 hr
D-29	D-292	0.4	750°C/5 hr	1100°C/2 hr
D-30	D-302	0.5	750°C/5 hr	1100°C/2 hr
D-31	D-312	0.6	750°C/5 hr	1100°C/2 hr
D-32	D-322	0.7	750°C/5 hr	1100°C/2 hr
D-34	D-342	0.9	750°C/5 hr	1100°C/2 hr
D-25	D-255	0.0	750°C/5 hr	1130°C/2 hr
D-26	D-266	0.1	750°C/5 hr	1130°C/2 hr
D-27	D-275	0.2	750°C/5 hr	1130°C/2 hr
D-28	D-286	0.3	750°C/5 hr.	1130°C/2 hr
D-29	D-294	0.4	750°C/5 hr	1130°C/2 hr
D-30	D-305	0.5	750°C/5 hr	1130°C/2 hr
D-31	D-314	0.6	750°C/5 hr	1130°C/2 hr
D-32	D-324	0.7	750°C/5 hr	1130°C/2 hr
D-34	D-344	0.9	750°C/5 hr	1130°C/2 hr
D-25	D-256	0.0	750°C/5 hr	1160°C/2 hr
D-26	D-265	0.1	750°C/5 hr	1160°C/2 hr
D-27	D-276	0.2	750°C/5 hr	1160°C/2 hr
D-28	D-285	0.3	750°C/5 hr	1160°C/2 hr
D-29	D-293	0.4	750°C/5 hr	1160°C/2 hr
D-30	D-304	0.5	750°C/5 hr.	1160°C/2 hr
D-31	D-313	0.6	750°C/5 hr	1160°C/2 hr
D-32	D-323	0.7	750°C/5 hr	1160°C/2 hr
D-34	D-346	0.9	750°C/5 hr	1160°C/2 hr

Table 5

Parent Sample	Pellet Name	Amount of sodium mixed (in wt%)	Calcination temp./time	Sintering conditions
E-1	E-11	0.0	750°C/5 hr	1100°C/2 hr
E-2	E-21	0.2	750°C/5 hr	1100°C/2 hr
E-3	E-31	0.4	750°C/5 hr ·	1100°C/2 hr
E-4	E-41	0.6	750°C/5 hr	1100°C/2 hr
E-5	E-51	0.8	750°C/5 hr	1100°C/2 hr
E-6	E-61	1.0	750°C/5 hr	1100°C/2 hr
E-1	E-12	0.0	750°C/5 hr	1130°C/2 hr
E-2	E-22	0.2	750°C/5 hr	1130°C/2 hr
E-3	E-32	0.4	750°C/5 hr	1130°C/2 hr
E-4	E-42	0.6	750°C/5 hr	1130°C/2 hr
E-5	E-52	0.8	750°C/5 hr	1130°C/2 hr
E-6	E-62	1.0	750°C/5 hr	1130°C/2 hr
E-1	E-13	0.0	750°C/5 hr ·	1160°C/2 hr
E-2	E-23	0.2	750°C/5 hr	1160°C/2 hr
E-3	E-33	0.4	750°C/5 hr	1160°C/2 hr
E-4	E-43	0.6	750°C/5 hr	1160°C/2 hr
E-5	E-53	0.8	750°C/5 hr	1160°C/2 hr
E-6	E-63	1.0	750°C/5 hr	1160°C/2 hr

2.1.3. Preparation of Ni-Zn Ferrite
Important Features

The Ni-Zn ferrite ($Ni_{0.8}Zn_{0.2}Fe_2O_4$) was synthesized by two different methods: I) Ceramic method and (II) Liquid mix technique. Chemicals used for both the methods of preparation are as follows:

I) *Ceramic method*

a-Fe_2O_3 - Commercial grade, NMDC, India.

NiO - L.R. grade, S.D. Fine Chemicals, India.

ZnO - L.R. grade, S.D. Fine Chemicals, India.

II) *Liquid mix technique*

$Fe(NO_3)_3 9H_2O$ - L.R. grade, Loba Chemicals, India.

NH_3 (25% solution) - L.R. grade, S.D. Fine Chemicals, India.

Citric acid - L.R. grade, Loba Chemicals, India.

$NiCO_3$ - L.R. grade, S.D. Fine Chemicals, India.

$ZnCO_3$ - L.R. grade, S.D. Fine Chemicals, India.

I) Ceramic method

The reactants namely, nickel oxide, zinc oxide and iron oxide were mixed in the required ratio. The mixture was wet milled for four hours to obtain through mixing and uniform distribution of each species and then dried in the oven at 100°C. The mixture was then calcined at 950°C/3 hr [4]. The reacted oxides are ground with the help of ball mill for 24 hours. The milling and grinding is employed to obtain a
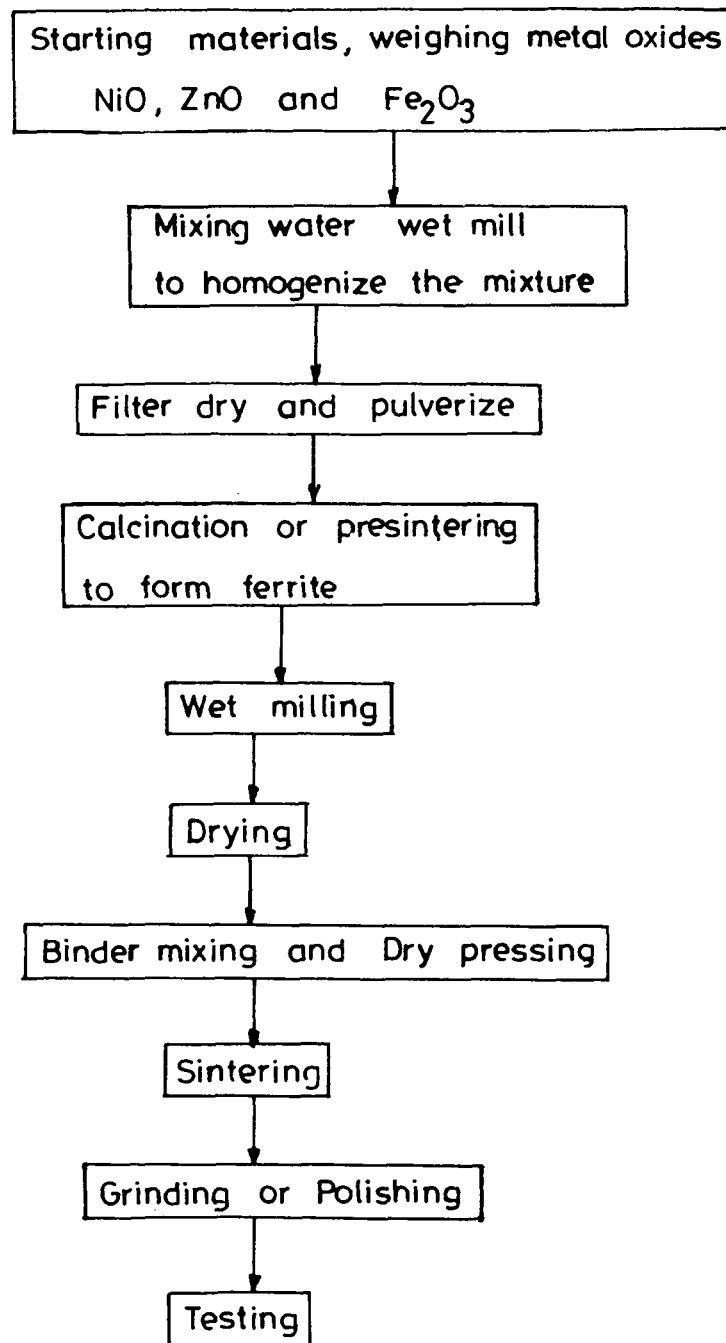
63

Fig.4: Flowchart for ferrite production by ceramic method.

mixture in a fine state of subdivision. The experimental procedure involved in the synthesis is shown by a schematic representation in Fig.4.

Effect of additive: In the present work, we tried to find out effect of two different additives namely, (i) BaO and (ii) BaO-B_2O_3 on performance parameters of Ni-Zn ferrite.

To study the effect of these additives, 500 gm $Ni_{0.8}Zn_{0.2}Fe_2O_4$ powder was synthesized by ceramic method. The calcined powder after milling was divided into three parts A, B & C. The first part (part A) was processed without additive. The samples prepared from this part are known as virgin samples and used as reference samples during comparative study.

i) Addition of BaO: The GR grade barium carbonate is dissolved in acetic acid to obtain barium acetate. The solution is diluted by addition of distilled water to obtain 1M solution of barium acetate. The second part of calcined powder (part B) was divided into four parts. The amount of barium acetate solution was mixed in such a way that quantity of BaO remained in the range of 0.1 to 0.4 wt% (Fig.5). The wet mixed powders were dried under IR lamp and subsequently heated at 500°C so that barium acetate will decompose.
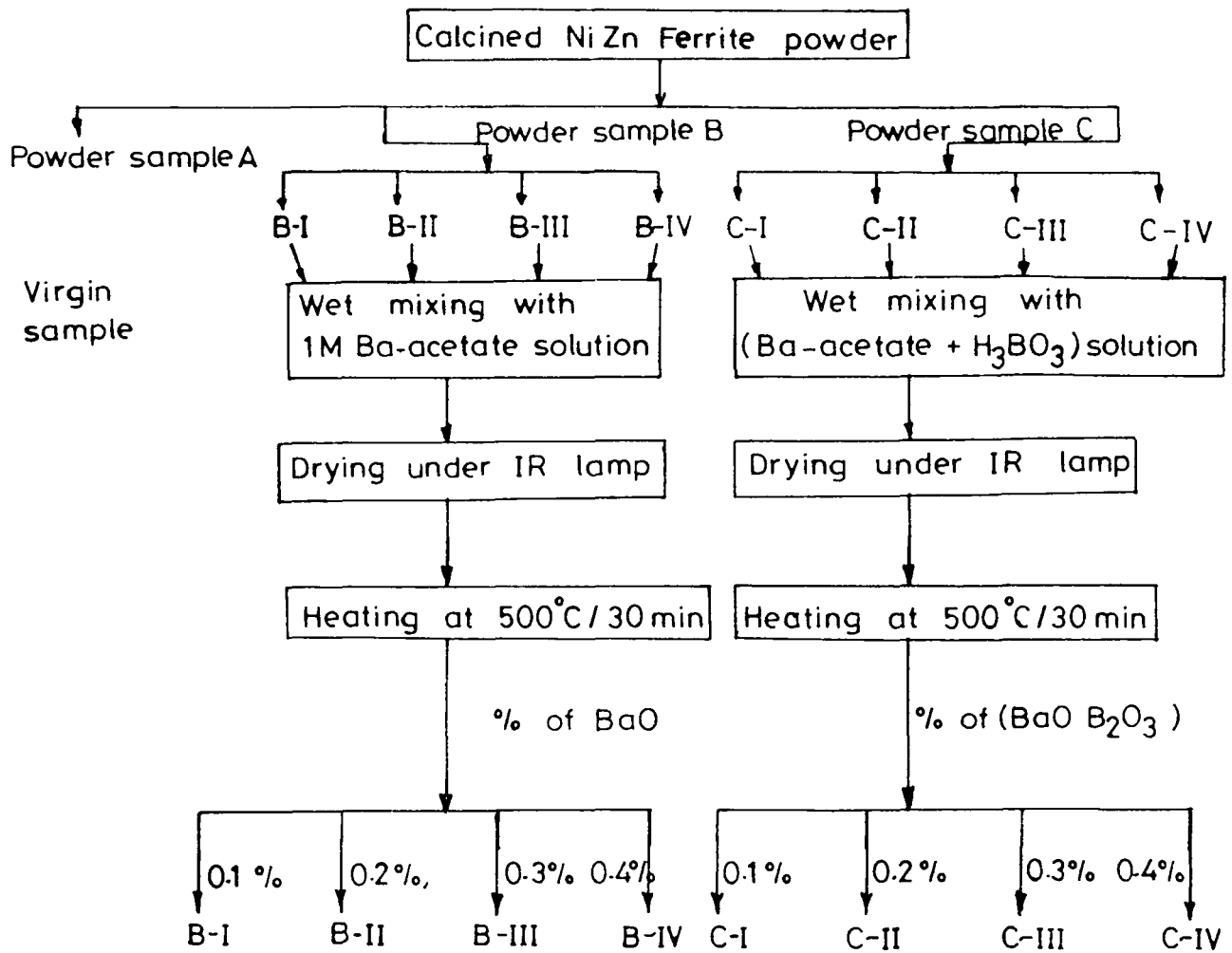
Fig. 5: Flow chart for the preparation of undoped and doped NiZn ferrite sample.

ii) __Addition of (BaO-B$_2$O$_3$)__: The solution of barium acetate was prepared as described earlier. It was mixed with solution of H$_3$BO$_3$ in such a way that molar ratio of BaO : B$_2$O$_3$ will be 1 : 0.66. The mixture of Ba-acetate and H$_3$BO$_3$ was homogenised with four subparts of calcined powder C in such a way that amount of BaO.B$_2$O$_3$ remains in the 0.1 to 0.4 wt% range (Fig.5♦). All the four samples with additive were heated at 500°C so that the organic part will get decomposed.

The doped and undoped powders were then mixed with polyvinyl alcohol (PVA) as a binder and then pressed into toroids at a pressure 2.2 tons/cm^2 using Curver Laboratory Press. The toroids were sintered at different temperatures in the range 1100°C to 1250°C.

II) __Liquid mix technique (LMT)__

The fine particles of NiZn ferrite were prepared by nonconventional Liquid mix technique. This technique is a simple one and preparation by this technique does not require any special apparatus. The technique involves the formation of citrates of metals which on calcination burn off all the organic material giving rise to homogeneous oxides.

For preparation of Ni-Zn ferrite by Liquid mix technique : In the first step precipitate of ferric hydroxide is prepared by dropwise addition of 2.0N Fe(NO$_3$)$_3$

solution in liquor ammonia. During addition the mixture was stirred with the help of mechanical stirrer. To remove the impurity ions, the precipitate was washed using centrifugal method with the help of distilled water. The washed precipitate of ferric hydroxide is then mixed with citric acid in the required proportion. The precipitate reacts with citric acid giving clear solution,

$$Fe(OH)_3 + C_6H_8O_7 \longrightarrow Fe(C_6H_5O_7) + 3H_2O$$
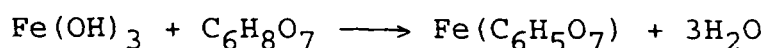
In this clear solution $NiCO_3$ and $ZnCO_3$ were added. The amount of $NiCO_3$ and $ZnCO_3$ was added in such a way that molar ratio of Ni : Zn : Fe would be 20 : 5 : 50. The reaction was observed to commence immediately with a strong effervescence of CO_2 indicating the formation of the metal citrate complex as shown by the following equation:

$$3MCO_3 + 2C_6H_8O_7 \longrightarrow M_3(C_6H_5O_7)_2 + 2H_2O + 3CO_2 \uparrow$$
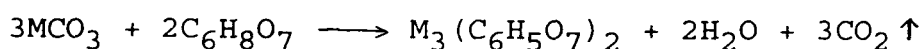
M = Metal (Ni or Zn)

At the end of the reaction, a completely transparent solution was obtained indicating the complete formation of the citrate complex. In the second step the solution was slowly heated to remove the solvent and to form a solution of increasing viscosity. The mixture of metal citrate was evaporated to dryness on a hot plate. The solid mass obtained on drying was brown in colour and had a glassy appearance. The colour of solid was observed to be uniform indicating that citrates were homogeneously mixed. The glassy mass was then broken into small bits in an agate mortar and subjected to calcination at ˙ the desired
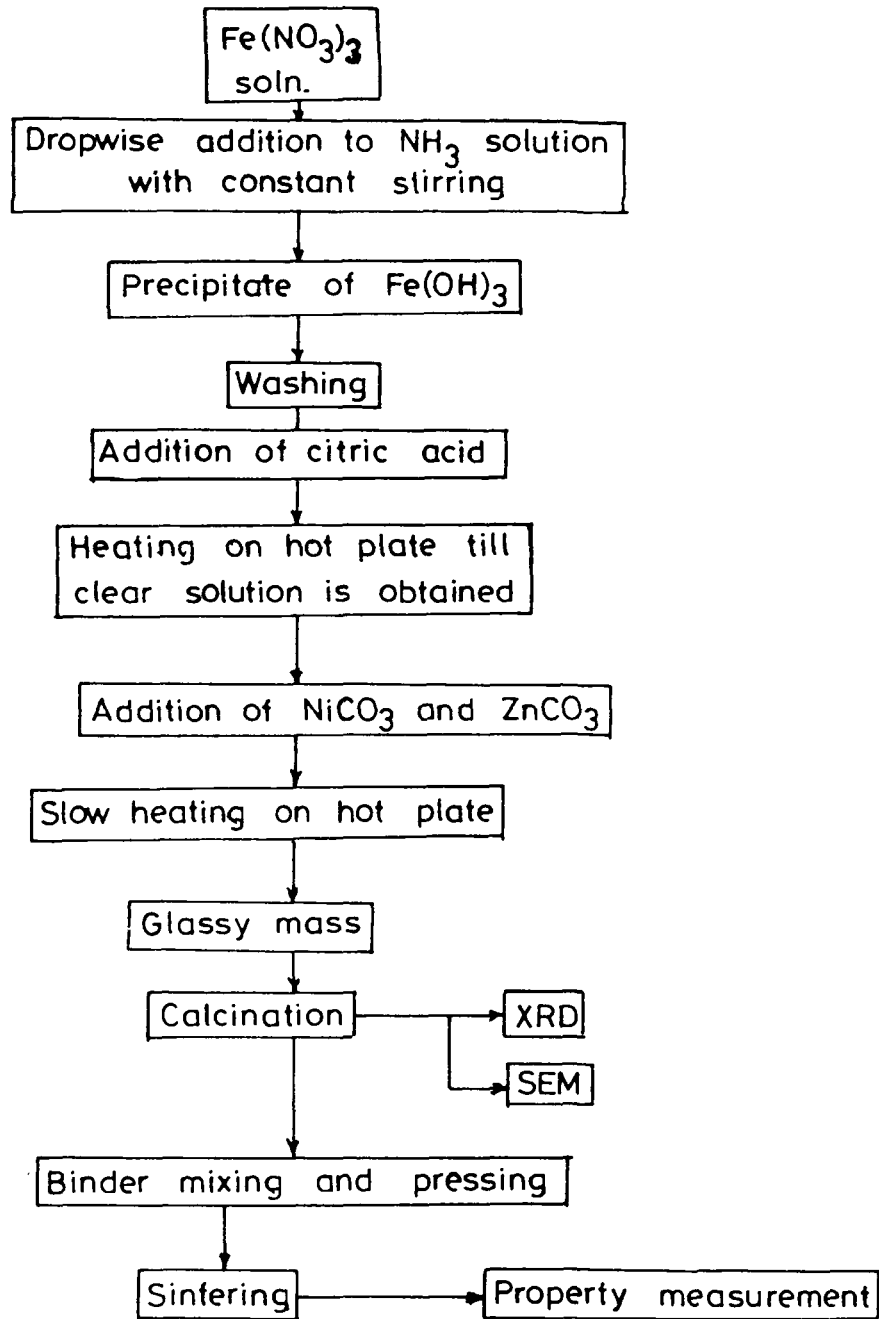
Fig. 6 : Flow diagram showing preparation procedure for Ni-Zn ferrite by liquid mix technique (LMT).

temperature to remove the organic materials and to finally obtain product as homogeneous oxide phase. Table-6 describes the details of processing conditions for doped and undoped NiZn ferrite samples.

Table-6

Parent Sample	Sample Name	Method of preparation	Amount of Additive mixed (in wt%)	Sintering condition
A	C-722	Ceramic	Virgin sample	1140°C/4 hr
B-I	C-741	Ceramic	0	1140°C/4 hr
B-II	C-746	Ceramic	0.2% BaO	1140°C/4 hr
B-III	C-751	Ceramic	0.3% BaO	1140°C/4 hr
B-IV	C-756	Ceramic	0.4% BaO	1140°C/4 hr
C-I	C-726	Ceramic	0.1% $BaO-B_2O_3$	1140°C/4 hr
C-II	C-704	Ceramic	0.2% $BaO-B_2O_3$	1140°C/4 hr
C-III	C-732	Ceramic	0.3% $BaO-B_2O_3$	1140°C/4 hr
C-IV	C-709	Ceramic	0.4% $BaO-B_2O_3$	1140°C/4 hr
A	C-723	Ceramic	Virgin sample	1180°C/4 hr
B-I	C-742	Ceramic	0.1% BaO	1180°C/4 hr
B-II	C-747	Ceramic	0.2% BaO	1180°C/4 hr
B-III	C-752	Ceramic	0.3% BaO	1180°C/4 hr
B-IV	C-757	Ceramic	0.4% BaO	1180°C/4 hr
C-I	C-728	Ceramic	0.1% $BaO-B_2O_3$	1180°C/4 hr
C-II	C-703	Ceramic	0.2% $BaO-B_2O_3$	1180°C/4 hr
C-III	C-733	Ceramic	0.3% $BaO-B_2O_3$	1180°C/4 hr
C-IV	C-708	Ceramic	0.4% $BaO-B_2O_3$	1180°C/4 hr
---	C-901	LMT	----	1140°C/4 hr
---	C-902	LMT	----	1140°C/4 hr

2.2 **CHARACTERIZATION TECHNIQUES**

As described in Figs.1 & 2, the samples were characterized at different stages of synthesis, with the help of following techniques.

1) Thermal analysis, DTA/DTG/TG: A Netzsch STA 409 differential thermal analyser was used to locate the reaction temperature, mechanism of ferrite formation and weight change taking place in the sample during heating. This instrument plots simultaneously the results of differential thermal analysis (DTA), thermogravimetric analysis (TGA) and derivative thermogravimetric analysis (DTG) along with the sample temperature (T). The TG curve gives the weight loss of the compound with increase in temperature. Difference in the temperature of the sample and that in the reference is recorded as a function of temperature in DTA. DTG records the rate of weight of loss sample with temperature. A calibrated Pt/Pt-10 to Rh thermocouple was used for scanning the temperature accurately. The samples were heated in dynamic air, at the heating rate of 10°C/min. and a chart speed of 120 mm/hr. The DTA/DTG/TG were scanned for samples A, B, C-I and C-II.

2) X-Ray Diffraction (XRD) Analysis: The X-ray powder diffraction technique was employed to identify the structure and phases of the samples obtained on calcination or

68

sintering at various temperatures. The X-ray diffraction (XRD) patterns were recorded on powder samples as well as on pellets. The samples were mounted on a sample holder of a Philips PW 1730 X-ray diffractometer. The diffracted X-ray intensities were recorded as a function of 2θ by using copper target (CuK$_a$ radiation with λ = 1.5404 Å). The values of the interplanar spacings 'd' were calculated using the Bragg's relation:

$$n\lambda = 2d \sin\theta$$

where λ is the wavelength of the X-ray used, 'd' is the distance between the two neighbouring atomic planes, θ is the Bragg angle. The 2θ values were obtained from the graph of 2θ Vs intensity. The 'd' values were obtained from these 2θ values using the above equation. Different phases in a sample were identified by comparing a set of 'd' values and the corresponding intensities with the standard from ASTM data file.

3) <u>Magnetic Measurements</u>: The B-H hysteresis curve for the ferrites was recorded using a commercial B-H recorder, M/s. Walker Scientific Incorporation, U.S.A., model No.MH-1020. The samples were placed between the poles of an electromagnet. The required D.C. current was passed through the coils of the electromagnet to apply the necessary field. Using the hard system of the unit the B-H hysteresis curve of the samples was recorded. Various properties such as remanence (B$_r$), coercivity ($_b$H$_c$), intrinsic coercivity

69

$(_iH_c)$, maximum energy product $(BH)_{max}$ etc. have been computed from hysteresis loop. The induction coercivity $_bH_c$ of material was determined from the hysteresis loop,op, whereas the value of intrinsic coercivity $_iH_c$ was determined from the graph of (B-H) versus H.

4) Scanning Electron Microscopic (SEM) Analysis: Microstructural studies were made with a Cambridge Stereoscan 150 Scanning Electron Microscope and the particle size, its distribution, and morphology of the samples prepared by different methods were studied.

5) Electron Probe Microanalysis (EPMA): Electron probe microanalysis is a powerful analytical technique capable of performing elemental analysis. The sample is analysed non-distractively and quantitative analysis can be obtained with a good accuracy. It gives the elemental distribution in the area of interest. Electron probe microanalysis of samples were carried out using Hitachi model no.H-8010 coupled with Kevex analyst 8000 microanalyser. The EPMA analysis of fractured sintered Sr-ferrite samples was carried out at different points and areas mainly for atomic percentage of Na, Sr and Fe.

6) Q-meter: The measurement of initial permeability of all the samples was carried out on sintered ferrite toroids with the help of a Q-meter.

3 to 5 turns of copper wire were wound on the sintered toroid and connected to inductance terminals. The instrument was set at a particular frequency and the resonance was obtained by adjusting the capacitance. The value of Q and capacitance were directly read on the meter, whereas value of μ' and μ'' were calculated mathematically.

REFERENCES

1. K. Haneda, C. Miyakawa and H. Kojima, J. Am. Ceramic Soc., 57 (1974) 354.

2. S.K. Date, C.E. Deshpande, S.D. Kulkarni and J.J. Shrotri, Advances in Ferrites, Proc. 5th Int. Conf. on Ferrites 5 (1989) 55.

3. Ph.D. Thesis, S.D. Kulkarni, Poona University (1990).

4. S. Pyun and J. Baek, Am. Ceram. Soc. Bull., 64 (1985) 602.

Chapter 3

Strontium Hexaferrite

3.1 INTRODUCTION

Ferrites are broadly classified into two groups viz. hard ferrites and soft ferrites. The ferrites which are difficult to magnetise and demagnetise are termed as hard ferrites whereas the ferrites which are easy to magnetise and demagnetise are termed as soft ferrites. In the group of hard ferrites, magnetoplumbite or M-type hexagonal ferrites ($MeFe_{12}O_{19}$, Me = Ba/Sr/Pb) are widely used in many technological applications due to their superior magnetic properties. The present chapter is devoted to the study of M-type hard ferrites. The crystal and magnetic structure of M-type ferrite is discussed in section 1, which is followed by a discussion on the working of permanent magnets and factors governing magnetic properties. In the next section, an extensive literature survey is carried out covering various aspects such as synthesis, physico-chemical characterization and property evaluation. Section 3 deals with the study of effect of various processing parameters on magnetic properties of strontium hexaferrite, synthesised by coprecipitation method. The processing-structure-property correlation of Sr-ferrite is established with the help of various techniques like Thermal analysis, X-ray diffraction, Scanning electron microscopy and Magnetic property measurements. Our experimental results are also presented in the same section of this chapter.

3.1.1 Crystal Structure of M-type Hexagonal Ferrite

A class of ferrites having composition $MeO.6Fe_2O_3$ (Me = $Ba^{2+}/Sr^{2+}/Pb^{2+}$) is isostructural to mineral magnetoplumbite and commonly known as M-type hexagonal ferrites. The term magnetoplumbite was coined by a group of Swedish investigators [1]. Adesköld (1938) determined the crystal structure of barium ferrite, strontium ferrite and lead ferrite [2,3]. Obadors [4,5] furnished an accurate analysis of the crystal structure of barium and strontium ferrites.

Magnetoplumbite structure: The Fig.1(a) is a perspective drawing of $(Ba/Sr)Fe_{12}O_{19}$ unit cell. The O^{2-} ions form a skeleton of hexagonal close packed lattice. Unit cell of magnetoplumbite crystal is made up of ten O^{2-} layers. These layers are perpendicular to (001) direction as shown in Fig.1(a). Generally each layer contains four oxygen ions, but in every fifth layer three oxygen ions and one Me ion are present. Five oxygen layers make one molecule of $MeFe_{12}O_{19}$ and two molecules of $MeFe_{12}O_{19}$ make one unit cell of magnetoplumbite structure. Each molecule shows 180° rotation around the hexagonal c-axis with respect to lower and upper molecule. Thus the unit cell of ferrite comprises of ten oxygen layers with Fe^{3+} ions occupying five different types of interstitial positions. In the crystal structure, Fe^{3+} ions are distributed within three different kinds of octahedral sites, one tetrahedral site and one trigonal
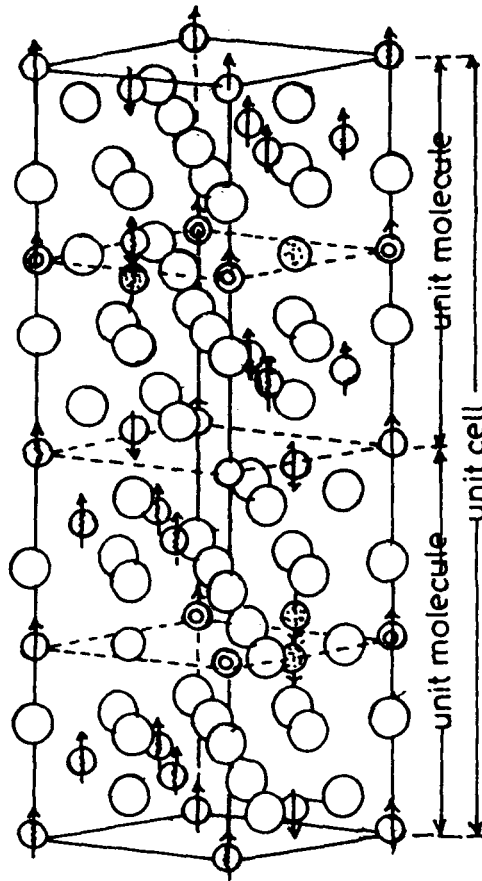
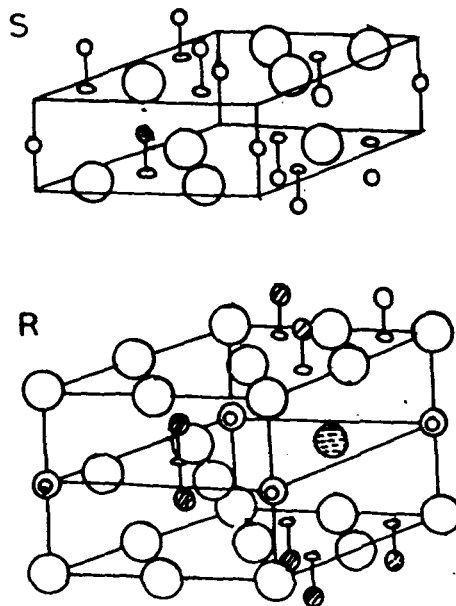Fig. 1(a) : Perspective illustration
of MeO.6Fe$_2$O$_3$
(Me= Ba/Sr/Pb)

Fig. 1(b) : Building blocks in
the hexagonal
compound.
S(Fe$_6$O$_8$) &
R(MeFe$_6$O$_{11}$)

bipyramidal site. Table-1 gives crystallographic and magnetic characteristics of various Fe^{3+} ions in M-type structure. The space group of the compound $MeFe_{12}O_{19}$ is denoted as P6/mmc (D^4_{6h}) using Hermann-Mauguin's (Schönflies') symbols. At room temperature, lattice parameters of Sr-ferrite are a = 5.8844°A and c = 23.050°C [5].

The magnetoplumbite crystal structure can also be described in terms of two blocks, namely S block and R block.

S-Block: Fig.1(b) illustrates the three dimensional structure of S-block. The S-block is normally described as a spinel block having composition $(Fe^{3+}_6O_8)^{2+}$. It comprises of two oxygen layers. Each layer contains four oxygen ions. These two inner layers contain two tetrahedral sites ($4F_1$) and one octahedral site (2a), while in the common layer of two blocks, three octahedral sites (12K) are found. In this way, six Fe^{3+} ions are distributed over these two tetrahedral and four octahedral sites. It is important to note the <111> axis of this spinel block is oriented parallel to the c-axis of hexagonal unit cell.

R-Block: It consists of three oxygen layers with composition $(Me^{2+}Fe_6^{3+}O_{11})^{2-}$ {Fig.1(b)}. The two terminal layers contain four oxygen ions each, while central layer has three oxygen ions and one Me^{2+} ion. This block has mirror symmetry at Z = 1/4. The MeO_3 layer acts as mirror plane. The other two oxygen layers are present at the upper

Table 1

Coordination number and direction of magnetic moment of Fe^{3+} ions in the unit cell of the magnetoplumbite type crystal [3]

Coordination number	Number of positions in unit cell	Wychof's notation	Direction of magnetic moment per mole	Remarks
6 (Octahedral site)	12	k	↑↑↑↑↑	R-S I (a)
	4	f_2	↓↓	R III (d)
	2	a	↑	S V (b)
4 (Tetrahedral site)	4	f_1	↓↓	S II (c)
5 (Trigonal bipyramidal site)	2	b	↑	R IV (e)

and lower sides of mirror plane. The five iron ions, out of six, from R block are distributed over octahedral site ($4F_2$ & 12K) and one iron ion at trigonal bipyramidal site (2b). The complete unit cell is built up of alternate stacking of R and S blocks in the sequence RSR^*S^*. Where * indicates that these blocks are rotated by 180° around the c-axis with respect to the R and S blocks.

These features of the structure play a vital role in determining the magnetic structure and magnetic properties

76

of the M-ferrites.

3.1.2 Magnetic Structure of M-type Hexagonal Ferrite

M-type ferrite compounds have a typical ferrimagnetic structure. In the hexaferrite unit cell, the magnetic moments of the ferric ions are oriented along the c-axis. The theoretical explanation for such an alignment of ferric ions in ferrite crystal was first given by Neel (1948) and Anderson (1950) [6,7]. They predicted that the alignment of magnetic Fe^{3+} ions is due to the exchange interaction through oxygen ions (superexchange interactions). The magnetic structure is evolved due to such an alignment via superexchange interaction. Thus ferrimagnetism observed in ferrite is a result of the cooperative phenomenon amongst the Fe^{3+} ions situated at different sites in the magnetoplumbite structure. This model has been able to explain experimental results of magnetic measurements, neutron diffraction, Mössbauer effect and nuclear magnetic resonance etc.

Grill & Haberey (1974) theoretically calculated exchange integral of Fe^{3+} ions in BaM [8]. The calculations revealed that superexchange interactions for Fe^{3+}-O-Fe^{3+} in magnetoplumbite are strong and negative. It was also observed that value of exchange integral depends on the angle between the Fe^{3+}-O-Fe^{3+}. When this angle approaches

180°, the exchange integral becomes large. On the other hand, when angle is closer to 90°, the exchange integral becomes negligibly small. In Fig.1a, ferric ions are shown by arrows. The orientation of the magnetic moments of each ferric ion is represented by the direction of arrows.

Exchange interactions in S-block: Since S-block is a spinel block, magnetic interactions in it are the same as that of spinel ferrite. Out of the six ferric ions from the S-block, four ferric ions at octahedral sites (2a & 12K) and two ferric ions at tetrahedral sites ($4F_1$) have oppositely oriented magnetic moments.

Exchange interaction in R-block: The superexchange interactions in R block can be explained by considering ferric ion at trigonal bipyramidal site (2b) as a reference point. This ion is in the vicinity of two iron ions occupying $4F_2$ sites. The angle between these two ferric ions $Fe(b)-O_R-Fe(F_2)$ is nearly 140°. The angle between the ferric ions at $4F_2$ sites is ~ 84° [3] {i.e. angle $Fe(F_2)-O_R-Fe(F_2)$}. The superexchange interaction $Fe(b)-O_R-Fe(F_2)$ is strong and negative due to favourable angle while $Fe(F_2)-O_R-Fe(F_2)$ is negligible because of the unfavourable angle between them. Thus, due to exchange interactions, magnetic moments of Fe^{3+} ions at 2b site and $4F_2$ site are oppositely oriented. The coupling of R block with S block is brought about by interaction between magnetic moments of the
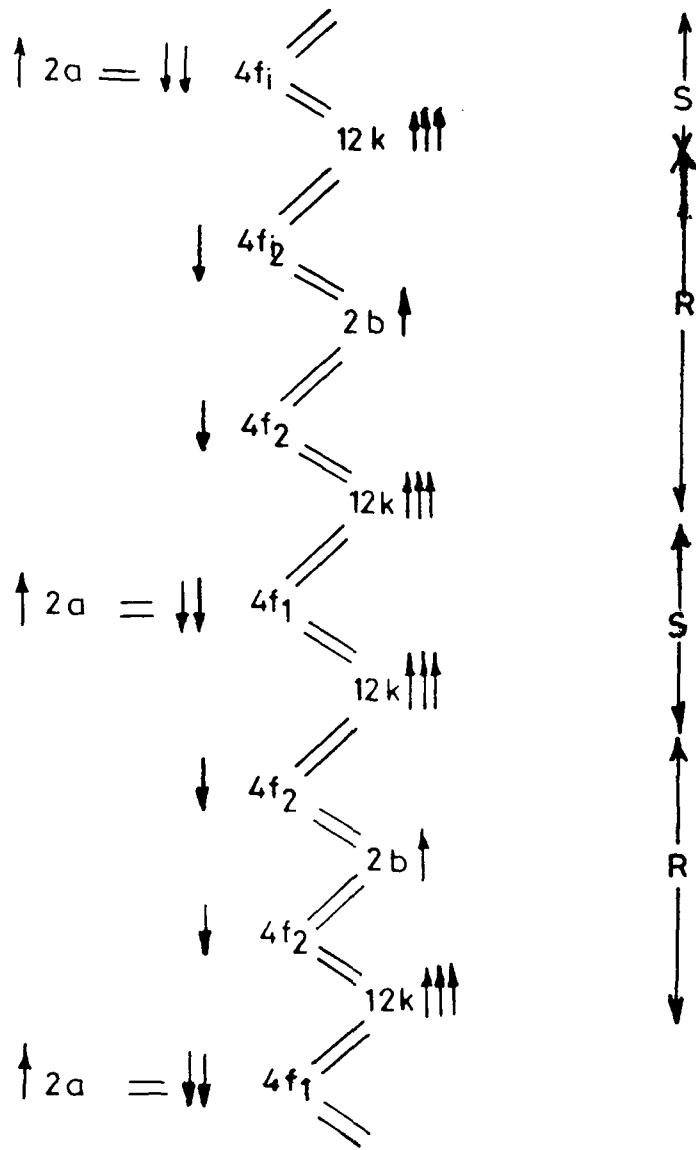
78

Fig. 2 : Exchange interaction scheme in the unit cell
of the magnetoplumbite structure. Each arrow
represent the magnetic momentof a Fe^{+3} ion. [9]

octahedral ions $Fe(4F_2$ and $Fe(12K)$. The superexchange interaction $Fe(F_2)-O_R-Fe(K)$ has an angle of 127° [3]. This angle being a favourable angle, alignment of magnetic moments of $Fe(F_2)$ and $Fe(K)$ is antiparallel. The above interaction is the most important interaction between R and S blocks.

In short, out of the six ferrite ions from R-block, magnetic moment of four ferric ions present at 2b and 12K sites are parallel to each other. While the magnetic moment of two ferric ions occupying $4F_2$ sites are oriented antiparallel to the above four ferric ions. On the basis of Anderson's indirect exchange theory, Gorter (1957) proposed the exchange interaction scheme in the unit cell of magnetoplumbite structure illustrated in Fig.2 [9].

The superexchange interaction in the vicinity of strontium layer accounts for uniaxial anisotropy of magnetoplumbite ferrite along the c-axis. Since, the cubic spinel block does not have strongly preferred axis of alignment, the coupling from strontium layer, has its strong preferential orientation on the spinel block. Due to the magnetocrystalline anisotropy, the magnetic moments of all ferric ions are aligned along the hexagonal c-axis.

Ferric ions at five different crystallographic sites are high spin in nature. Out of the twelve ferric ions in formula unit, the magnetic moments of eight ions (occupying

seven octahedral and one trigonal bipyramidal sites) are parallel to each other. On the other hand, magnetic moments of remaining four ions (situated at two octahedral and two tetrahedral sites) are oppositely oriented to them [3]. The resultant magnetic moment per formula unit of $MeFe_{12}O_{19}$ is therefore equal to the sum of the magnetic moments oriented in upward and downward directions. The magnetic moment of high spin Fe^{3+} ions, is 5 μ_B at OK. Thus, the net magnetic moment is equal to 5 x (8-4) = 20 μ_B. This value agrees well with the experimental results of barium and strontium ferrites [10]. Various properties of Ba and Sr ferrites are listed in Table 2.

The above description of crystal and magnetic structure of M-type ferrites shows that they are important in determining magnetic properties of Ba/Sr ferrites. This discussion refers to the study of single crystal. In a polycrystalline sample, magnetic properties are also governed by factors such as orientation of particles, particle size, sintered density, etc. The details of which are described in the next section.

Table 2

Various properties of Ba/Sr ferrite

	Ionic radius of Ba and Sr A°	Anisotropy constant K_1 at 300K erg/cm^3	Curie Temp. T_C °C	Bohr magnetron number n_B	Spontaneous magnetization at abs. zero $M_S(O)$, G	X-ray densities gm/cm^3	Lattice Parameters C A°	Lattice Parameters a A°	Radius of single domain particle c, μ_m
Ba-ferrite	1.6	3.25×10^6	440	19.3	515	5.28	23.18	5.889	$\simeq 1$
Sr-ferrite	1.44	3.57×10^6	450	19.7	525	5.21	23.03	5.864	$\simeq 1$
References	5	10	10	10	10	10	11	11	11

3.1.3   <u>Working</u> <u>of</u> <u>a</u> <u>Permanent</u> <u>Magnet</u>

The peculiar characteristic of the ferro- and ferri-magnetic materials is its hysteresis loop, which is commonly called as (B-H) curve. The word 'hysteresis' is coined from the greek word hystereo meaning 'lag behind'.

Hysteresis loop is obtained by plotting a graph of variation in magnetic induction B with the externally applied magnetic field H. The change in B lags behind the change in H, resulting in a characteristic curve, which resembles a thick 'S', and is known as hysteresis loop. Fig.3 illustrates the nature of a typical hysteresis curve.

The curve O to D (O-A-B-C-D) is known as virgin curve or initial magnetisation curve, as it represents the magnetization of a virgin sample. This curve can be further divided into four regions which are related to basic magnetic processes, viz, (a) Reversible bloch wall displacement (O to A); (b) Irreversible wall displacement (A to B); (c) Domain rotation (B to C); (d) Saturation (C to D) [12].

After reaching the saturation value of induction (B_s), if the applied magnetic field is reduced to zero, induction or flux density does not return to zero but attains a positive value called the retaintivity or remanence (B_r).

[This is known as demagnetization curve D to B_r]. To make the induction zero, magnetic field is applied.in opposite or negative direction. The field (in negative direction) required to make induction equal to zero is called as coercivity and is denoted by symbol $_bH_c$. Further increase in the field in the same direction, causes the saturation to reach at $-B_s$. If the field is then reduced to zero and is applied once again in the positive direction the induction follows the curve $-B_s$ to $-B_r$ to $+B_s$. Completion of this cycle thus results in the characteristic B-H curve. The area enclosed by the curve is known as hysteresis area. Its magnitude is a measure of the energy (W_h) which is required to take the material through one complete cycle.

Any (BH) curve can be redrawn as a (M-H) curve by referring to the equation $B = M + 4\pi H$ (shown by dotted line in fig.3) [13]. The field required to make magnetization (M) to zero is known as intrinsic coercivity $(_iH_c)$. Thus, there are two different types of coercivities viz. $_bH_c$ & $_iH_c$ of which later is higher $(_iH_c > {_bH_c})$ for highly coercive permanent magnets like ferrites [13]. Each point in the loop represents some value of B times H. The maximum of this value is known as $(BH)_{max}$. It is the index of quality of permanent magnet.

3.1.4   Factors governing magnetic properties of hexagonal ferrites

The magnetic performance parameters like (i) Remanence (B_r), (ii) Coercive force ($_bH_c$ & $_iH_c$), (iii) Energy product $(BH)_{max}$, (iv) Saturation magnetisation (M_s) of sintered and green ferrite samples are measured by plotting hysteresis loop. These parameters are indicators (measures) of the quality of magnets.

The (BH) product measures the energy available from the magnet. Thus $(BH)_{max}$ can be taken as the figure of merit of a given magnetic material. Many applications of hard ferrites demand for a high value of $(BH)_{max}$. To fulfill this need, improvement in the values of B_r and $_bH_c$ is required.

Magnetic properties of permanent magnets depend upon intrinsic parameters such as chemical composition, cation distribution, anisotropic field etc. and extrinsic parameters like sintering temperature, sintering atmosphere, impurity inclusion, microstructure etc. For modification and tailor-making of material, the knowledge about inter-relation between magnetic properties and intrinsic and extrinsic parameters is essential.

Remanence or residual flux density (B_r) :

The residual flux density (B_r) of polycrystalline hard ferrites is given by the equation,

$$(B_r) = K \, M_S \cdot n_C \, (\rho / \rho_o) \quad \ldots\ldots\ldots \quad [14]$$

where, K = constant of proportionality

M_S = saturation flux density

n_C = degree of orientation

ρ = sintered density

ρ_o = theoretical density (i.e. single crystal density)

For random orientation, remanent induction (B_r) is half the saturation value [15]. Increase in the values of B_r is achieved by the following ways:

(a) The degree of orientation (n_C) is increased by pressing hard ferrite powder in strong magnetic field [15]. About 80-90% orientation is obtained by this method.

(b) The saturation flux density (M_S) of bulk is also increased by pressing the hard ferrite powder in magnetic field.

(c) The sintered density nearly equal to single crystal density is also essential to obtain high remanence. The densification is increased by the use of proper additives or by hot pressing [16].

The magnetic properties for (a) isotropic, (b) anisotropic and (c) hot pressed ferrites are given in Table 3.

Table 3

Magnetic properties for isotropic, anisotropic, and
hot pressed samples

	Br (G)	$_bH_c$ (Oe)	$_iH_c$ (Oe)	$(BH)_{max}$ MGOe	Ref.
Isotropic	3000	2200	4000	1.7	17
Anisotropic	4400	4000	4030	4.74	18
Hot pressed	3700	2500	3500	2.3	17

Intrinsic coercivity ($_iH_c$) :

Stonner and Wohlforth proposed the model to calculate the intrinsic coercivity, for an assembly of randomly oriented noninteracting uniaxial single domain particles of M type ferrites (SW model) [19]. The equation for the calculation of theoretical value of intrinsic coercivity is given by,

$$_iH_c = k \, n_s \, (2K/M_s)$$

where, 1) k is a constant

2) n_s is contribution of single domain particles

3) K corresponds to magnetocrystalline anisotropy

4) M_s is saturation magnetization.

To obtain a high intrinsic coercivity for a permanent magnet, particle size should be equal to single domain size i.e. n_s should be high. Table 3 gives $_iH_c$ values for Ba/Sr

ferrite synthesized by different methods. The intrinsic coercivity of a sample prepared by solid state method is found to be the lowest. This low value of $_iH_C$ is because of (a) large grain size, (b) stress and strain on particles which is developed due to ball milling.

Single domain sized particles, free from stress and strain are obtained by using wet chemical methods. The intrinsic coercivity of such samples is in the range 4000 Oe to 6700 Oe [Table 4].

The intrinsic coercivity is also increased when anisotropic constant K is increased e.g., the anisotropic constants for Ba and Sr ferrites are 3.25 x 10^6 erg/cm^3 and 3.57 x 10^6 erg/cm^3 respectively. The higher value of K for Sr-ferrite is reflected in a higher value of $_iH_C$ for Sr-ferrite. The theoretically calculated values of coercivity for Ba and Sr ferrites are 6700 Oe and 7900 Oe respectively [17].

The anisotropic constant K (consequently intrinsic coercivity) is found to be increased by addition of dopant like Al_2O_3 [28].

The relation of coercivity ($_iH_C$) with remanence (B_r) and microstructure was studied by Kools [29]. He proposed following empirical formula on the basis of the concept that

Table 4

Magnetic properties of Ba/Sr ferrite calcined (green)

sample prepared by different methods

| Sr. No.	Method of preparation	Formation temp. °C	Magnetic properties		Particle size	Ref.
			$_iH_c$ Oe	r emu/gm		
1	Ceramic method (Solid state method)	1300	1000	52.0	5-10 μm	20
2	Decomposition of organo-metallic complexes	720	3917	58.0	0.1-0.5 μm	21
3	Aerosol synthesis for $BaFe_{12}O_{19}$ particles	900	4867	70.7	0.3-0.4 μm	22
4	Coprecipitation by using ammonium carbonate	1000	3450	45.9	- - - -	23
5	Coprecipitation by NaOH + Na_2CO_3	925	6000	67.8	~ 0.2 μm	17
6	Sol gel method	1000	2200	54.0	- - - -	24
7	Glass ceramic method	1350/2hr & 875/5hr	5800	60.0	~ 0.3 μm	25
8	Hydrolysis of metal organic complex	925	6700	62.7	0.3-0.8 μm	26
9	Coprecipitation by NaOH	925	6600	46.5	~ 0.2 μm	27
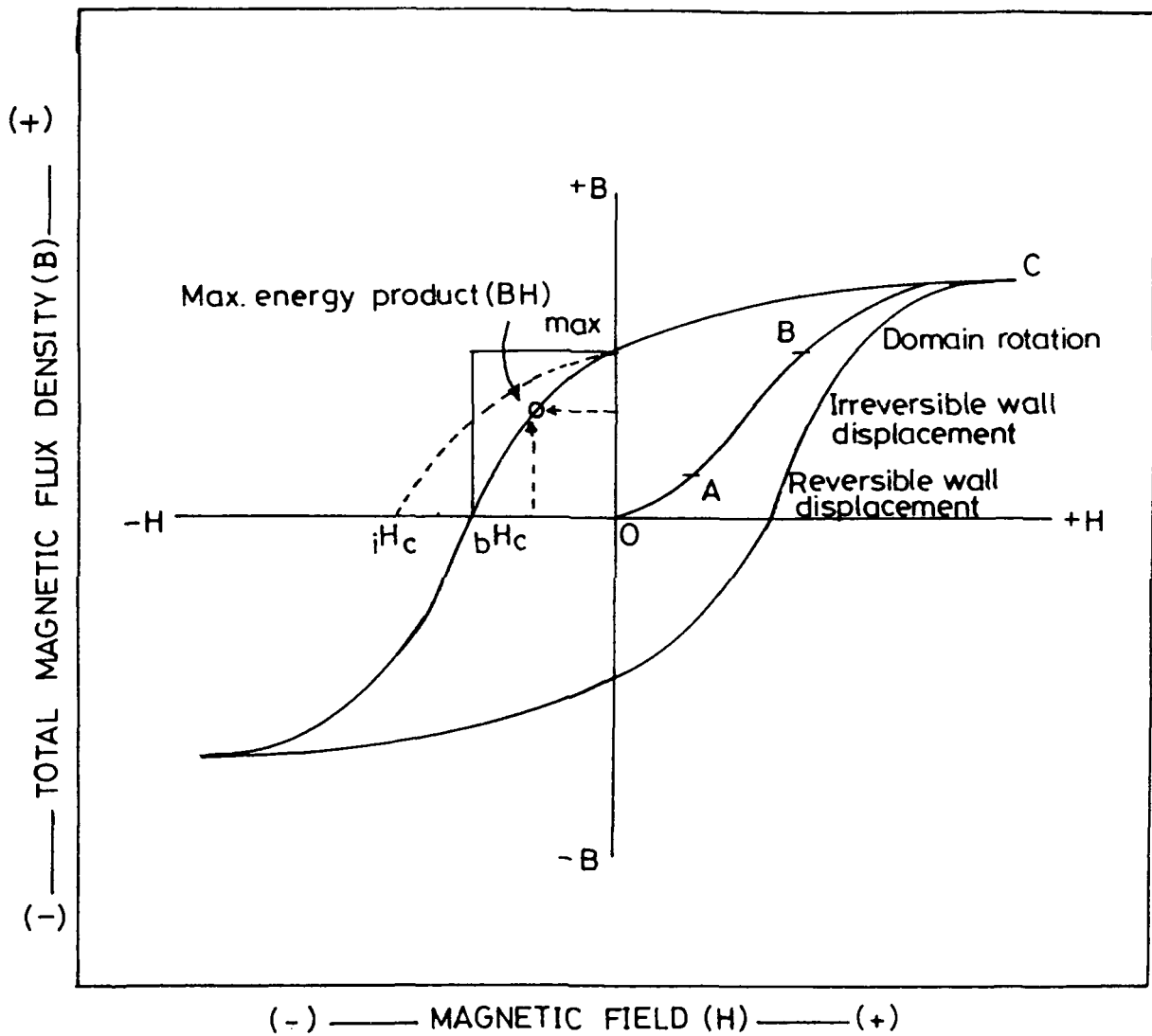
Fig.3 : Hysteresis loss of a permenant magnet. OABC is typical magnetisation curve of a virgin specimen.
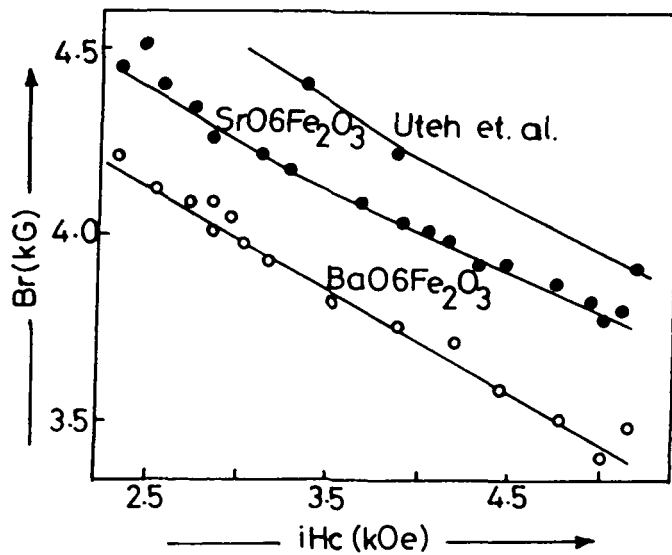

Fig. 4 : Relationship between $_iH_c$ and Br of hard ferrites. [14]

$_i H_C$ is governed by the growth of large multicrystal reversed regions. The resulting expression for the coercivity is,

$$_i H_C = K_1 H_A - N(K_2^{-1} + 1) B_r \mu_o^{-1} \quad \ldots \ldots [29]$$

where, K_1 = a constant depending on grain size

H_A = anisotropic field

N = demagnetization factor (which depends on crystal shape)

B_r = remanence

K_2 = a constant (which depends on density, degree of orientation and amount of nonmagnetic second phase).

Fig.4 shows a graph of B_r Vs $_i H_C$ [14]. This graph and the formula given by Kools indicate that $_i H_C$ decreases with increasing B_r. This implies that, it is not possible to obtain high B_r and high $_i H_C$ at the same time.

Energy product (BH)$_{max}$

The plot of B Vs H is of special technical importance, since B indicates M as well as H and is more directly related to the performance of many devices. Each point on the loop represents some value of the product BH. The maximum of this value is known as 'Energy product' and is denoted by (BH)$_{max}$. The (BH)$_{max}$ is the index of quality of the permanent magnet. It is expressed as,

$$(BH)_{max} = \frac{(4\pi\, M_s)^2\, A^2\, \varsigma^2}{4} \qquad \ldots\ldots \qquad [30]$$

where,

A = Alignment (orientation) factor

ς = Packing density

M_s = Saturation magnetisation.

3.1.5   Literature Survey

A group of ferrimagnetic oxides with hexagonal structure has been developed over past four decades. Table 5 gives various stages in the development of Ba/Sr M-type hexagonal ferrite permanent magnets. Though the use of ferrite as a permanent magnet was first reported by Koto and Takai [40], the ferrites became technically popular only after their $(BH)_{max}$ was improved to 1MGOe. Hexagonal hard ferrite is best known for its cost effective performance in the magnetic industry. The ferrite magnets are important materials for electric motors and for automobile industry. Considering importance of hexaferrite magnets a lot of efforts have been made to improve their properties and productivity. Nowadays the Ba and Sr ferrites are replacing metal magnets in many areas of applications, due to their high resistivity and low cost. Fig.5 gives global permanent magnet market trend [41]. The annual growth rate of demand of ferrite materials in the world is expected to be 10% per

Table 5

Various stages in development of M-type hexagonal ferrite

permanent magnet

Year	Important stages in development	Author	Ref.
1938	Determination of the crystal structure of barium ferrite	Adeskold	[3]
1948	S-W model for calculation of theoretical value of intrinsic coercive	Stoner & Wohl Farth	[19]
1952	Initial development of M-type compounds, use of ferrite as a permanent magnet	Went et. al.	[31]
1954	Production of anisotropic magnet by pressing powder in magnetic field	Fahlenbra-ch et al. Stuijts	[32] [33]
1957	Exchange interaction scheme (Magnetic structure) for Ba ferrite	Gorter	[9]
1959	Collection of comprehensive data of ferrimagnetic compounds	Smit & Wijn	[34, 35]
1960	Phase diagram of BaO-Fe_2O_3 system and SrO-Fe_2O_3 system	Goto et al.	[36, 37]
1962	Replacement of $BaFe_{12}O_{19}$ by $SrFe_{12}O_{19}$ due to superior magnetic properties of SrM.	Cochardt	[38]
1969	Study of temperature dependence of bulk magnetic properties of BaM & SrM	Shirk et al.	[10]
1973	Theoretical calculation of radius of single domain BaM particle	Haneda et al.	[39]
-	Synthesis of Ba/Sr hexaferrite by novel solution techniques.	-----	[21-27]
-	Use of different additive for tailor-making the magnetic properties.	-----	[28, 55-62]
1992	Preparation of high performance ferrite magnets.	Taguchi et.al.	[49]

annum [41]. To meet the market requirements, researchers are putting in continuous efforts to improve the quality of ferrite magnets.

The quality of hard ferrites is governed by different processing parameters such as quality of raw materials, chemical composition, preparation method, additives, temperature and time of sintering etc. Ghate has discussed different aspects of ferrite processing [42].

Preparation of single phase magnetoplumbite material is the first and foremost important step in processing. The solid state method is a widely accepted method of preparation. In this method, formation temperature of ferrites is very high ($\geq$ 1200°C) which causes excessive grain growth. Particle size is then reduced by milling various improved milling techniques are described by Ries [43]. Jey Ho et al. studied the effect of ball milling on sintering behaviour and subsequent magnetic properties of Sr-ferrite system [44]. Haneda & Kojima reported the effect of milling on coercive force of $BaO.6Fe_2O_3$ [45]. It is observed that though milling causes reduction in particle size, it introduces lattice strain and defect. These defects adversely affect magnetic properties. The milling for a longer time is therefore not advisable [46]. To overcome the limitations and drawbacks of solid state method, various nonconventional methods were innovated and developed. Some
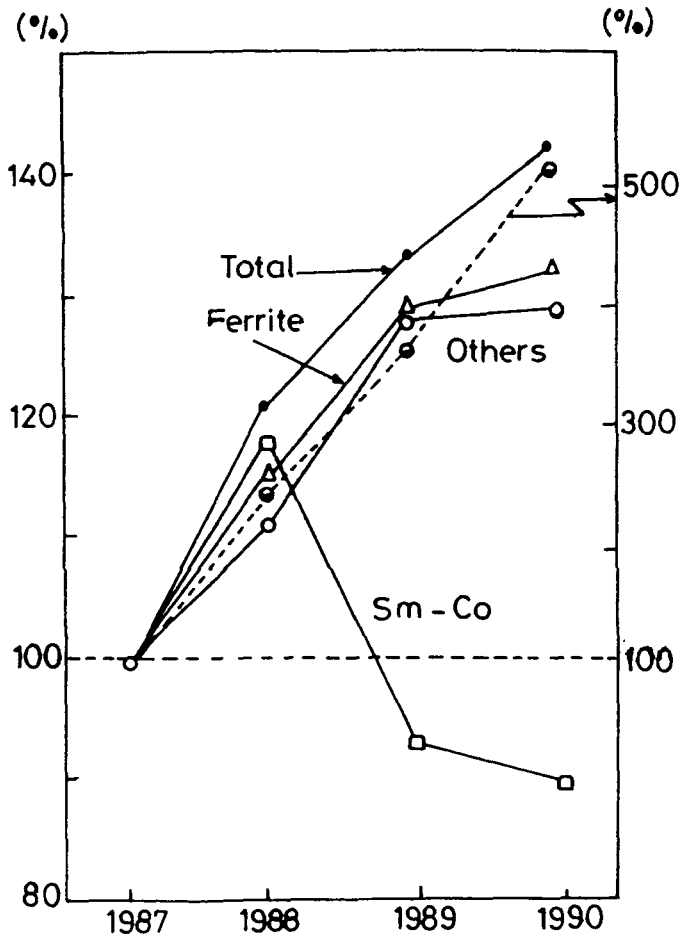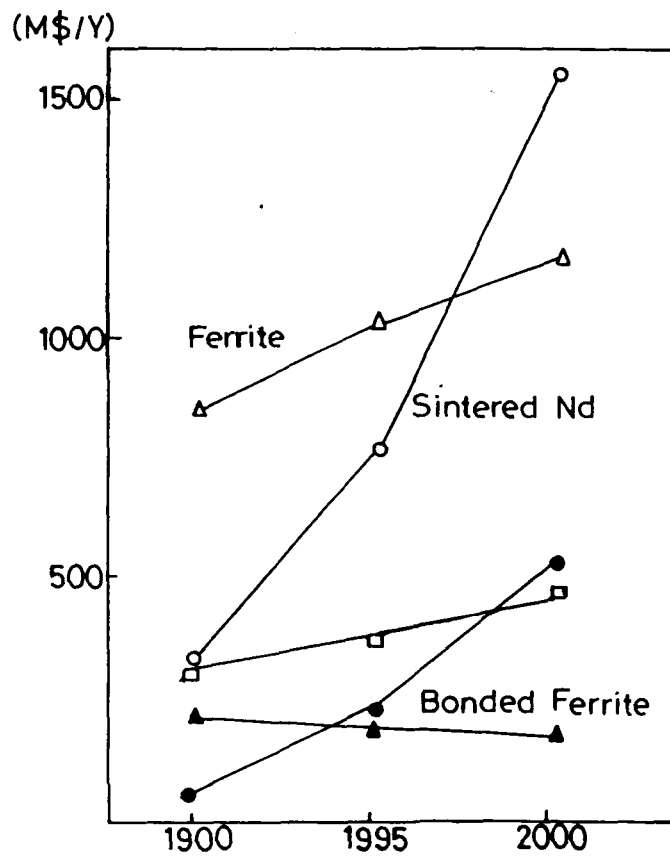
Fig. 5a : Globle permanent magnet market.

Fig. 5b : Globle permanent magnet market.

of these routes are as,

. Coprecipitation [17,27]

. Sol gel [24]

. Liquid mix technique [47]

. Decomposition of organometallic precursor [21]

. Hydrothermal method [48]

. Hydrolysis of metal organic complex [26]

. Glass crystallisation method [25]

The wet chemical methods play an important role in obtaining highly pure, uniform, strain free and fine ferrite particle. The tables 4 & 6 give magnetic properties of calcined and sintered compacts of Ba/Sr ferrites prepared by different methods. The data of magnetic property measurements reveals that ferrites prepared by wet chemical methods are much better than that of ferrites prepared by ceramic method.

Even though the synthesis of hexaferrite with different methods are well known, the controversy in mechanism of hexaferrite formation still persists. Furthermore, the number of papers devoted to kinetics and mechanism of the ferrite formation are comparatively small [50]. The kinetics and mechanism of magnetoplumbite ferrite formation is studied by thermal analysis, X-ray diffractometry, Mössbauer spectroscopy, IR spectroscopy etc. [51,52]. The studies of

Table 6

Magnetic properties of hexagonal ferrites by different methods

Sr. No.	Method	B_r (G)	H_C (Oe)	$_iH_C$ (Oe)	$(BH)_m$ MGOe	D g/cm^3	Ref.
1	Solid state	2300	1650	2500	1.02	4.7	20
2	Chemical } by NaOH coprecipitation }+ Na_2CO_3	3000	2200	4000	1.70	4.8	17
3	Liquid Mix Technique	1800	1600	3750	0.72	4.9	47
4	Hydrothermal method	2600	1998	-	1.5	4.8	48
5	Coprecipitation by NaOH	3000	1800	2550	1.42	4.58	27

formation kinetics evince that the reaction temperature and rate of reaction are low for solid state reaction than that of nonconventional chemical methods. The study of reaction mechanism of hexaferrite formation by solid state reaction between $BaCO_3$ and αFe_2O_3 indicates presence of $BaFe_2O_4$ and $BaFeO_{3-x}$ as intermediate phases [52]. Such intermediate phases were not observed when nonconventional techniques were used for synthesis [53,54].

In the struggle for improvement of the properties of hexaferrites to satisfy the current technological needs, different additives are incorporated. The studies of additive incorporation have evidenced that they are helpful

in alteration and tailormaking the magnetic properties. Depending upon the nature and role, additives are categorised into three types.

Additive acting as substituents: This type of additives affect magnetic structure and intrinsic properties of ferrite which in turn affect performance parameters of hexaferrite. Substitution of Fe^{3+} by elements such as Al^{3+}, Cr^{3+} found to increase $_iH_c$ [28,39]. On the contrary, when $(Co^{2+} + Ti^{4+})$ replace Fe^{3+} ion from Ba-ferrite lattice reduction in intrinsic coercivity without much decrease in saturation magnetisation is observed [55]. This substitution is useful for high density perpendicular magnetic recording media. The substitution of Ba^{2+} ion by La^{3+} ion enhance coercive force [56].

Additive acting as sintering aid: The second type of additives increase the rate of sintering. They segregate at grain boundaries and control the microstructure. SiO_2, H_3BO_3, PbO, Bi_2O_3 are some of the typical examples of this type [57-60].

Additives useful for liquid phase sintering: This type of additives act as low melting flux during sintering. They wet the particles of calcined powder and do not allow them to grow [61,62].

The Ba/Sr ferrite are oxide compounds containing iron as main element. Fe^{57} Mössbauer spectroscopy has been proved as an extremely powerful technique in detecting magnetic hyperfine fields and the population of the various sublattices. Van Wievinger [63] reviewed Mössbauer data of M-compounds. He summarised the results as follows:

1) The iron ions are trivalent in all sublattices.

2) The twelve iron ions are distributed over five lattice sites and all of them contribute to the crystal anisotropy. Evans et al. have reported comparative account of Mössbauer spectra for the $BaFe_{12}O_{19}$ prepared from high purity starting material [64]. The results show significantly smaller isomer shift of ferric ion at 2b site in $BaFe_{12}O_{19}$ than isomer shift ferric ion of 2b site of $SrFe_{12}O_{19}$. The 2b site is closest to the Mn^{2+} ion, hence he attributed significant difference in isomer shift to change in chemical environment of 2b site. The study of dopant cation which substitutes metal ion affects magnetic structure. Preferential occupancy of these ions in crystal lattice is subject of interest to many investigators [65-69].

With partial substitution at a particular site causes decrease in the intensity of corresponding hyperfine sub-spectra. This property is useful to find out locations of dopant ion in crystal lattice sites. Kreber & Gonser [65] studied the Mössbauer spectrum of arsenic and antimony substituted ferrite and found that As/Sb ions occupy the

bipyramidal lattice site preferentially. Pankhurst et al. [66] observed that cobalt and titanium appear to preferentially occupy sites 12K, $4F_2$ and 2b in R block of M type ferrite. In Ba/Sr ferrite Fe^{3+} ions at 12k and 2b sublattice are known to have major contribution to the overall uniaxial anisotropy. The substitution at these sites therefore reduces the coercivity of $BaFe_{12-2x}CO_xTi_xO_{19}$. Turilli [67] confirmed similar effects in the case of Mn-Ti substituted $BaFe_{12}O_{19}$. The Cr^{3+} ions are reported to occupy three different octahedral sites with the preferential hierarchy in the order 2a, 12K, $4F_2$ [68,69].

The magnetic properties of ferrites are temperature dependent. Study of bulk magnetic properties and their temperature dependence was carried out by Shirk & Suessem [10]. From extensive literature survey it is found that magnetic properties are governed by two types of parameters:
I) Intrinsic parameters such as purity of the sample, magnetocrystalline anisotropy (K), or anisotropic field (H_A), saturation magnetization (M_S) etc.
II) Extrinsic parameters such as method of preparation, processing conditions, dopants/additives added to the material, microstructure, sintered density, degree of orientation etc.

Many attempts have been made to obtain magnetic properties close to single crystal value for polycrystalline compacts. In fact, this is the major goal of all researchers

97

in tailormaking of electronic and magnetic materials. The improvement in processing is necessary to obtain magnetic performance parameters close to single crystal value. The controlled microstructure with high sintered density (approximately equal to theoretical density) and high degree of alignment are key factors in processing of ferrites.

3.2 RESULTS & DISCUSSION

For high performance magnet, Sr ferrite particle size should be nearly 1 μm (which is $\sim$ single domain size) with uniform and narrow particle distribution. The solid state method is conventionally used to synthesize ferrite powders, but it has many limitations. These limitations can be overcome by use of nonconventional methods. Nonconventional solution methods are being perfected to obtain highly pure, uniform, submicron size powders of Sr-hexaferrite.

Scope of present chapter:

Considering the advantages of solution methods, we have adopted coprecipitation method to synthesise the fine powders of Sr-ferrite. To obtain active powder with desired properties optimisation of various processing parameters is essential. In our laboratory, extensive research work has been done in identification and optimisation of various processing parameters of coprecipitation method, such as, (a) effect of quality of reactants, (b) effect of concentration of reactants, (c) effect of rate of addition, (d) effect of Fe/Sr ratio, (e) effect of surfactants, (f) effect of binder, (g) effect of dopants, etc.

In this section, we have presented the investigations dealing with (i) effect of mode of washing or filtration, (ii) effect of crystallinity and (iii) effect of

incorporation of additive. The basic framework of chapter 3 is therefore limited to:

1) The study of effect of mode of filteration/washing of coprecipitate on magnetic properties of final product i.e. sintered strontium ferrite magnets.

2) Optimisation of calcination and sintering temperature.

3) Effect of crystallinity on (a) kinetics and mechanism of ferrite formation and (b) magnetic properties, is studied with the help of thermal analysis, XRD studies and magnetic property measurements.

4) Effect of incorporation of sodium ions as an additive on magnetic properties of Sr-ferrites.

5) Optimisation of additive concentration in order to achieve a good microstructure.

6) Physico-chemical characterisation of the samples/ specimens by means of specialized techniques like XRD, SEM, EPMA, etc. for the understanding of probable role of additive and also to establish structure property correlationship.

The details pertaining to above are presented in the next few pages.

3.2.1   Effect of mode of washing/filtration

To study this effect, coprecipitate is synthesised in two separate batches. After completion of precipitation, the coprecipitate from first batch is washed with centrifugal

mode of washing (Batch A). Decantation mode of filtration is followed for washing precipitate from second batch (Batch B). Both the precipitates are dried in an oven at 100°C (Experimental details are given in Chapter 2). The dried coprecipitate from both the batches are analysed at different stages of processing with the help of TG/DTG/DTA, XRD and Magnetic property measurements.

Initially we propose to discuss the results of the effect of mode of washing on coprecipitate using the technique of thermal analysis.

3.2.1.1 Thermal analysis

Thermal analysis of coprecipitate is used to understand (1) chemical changes during heating and (2) temperature of formation of hexagonal strontium ferrite.

For thermal study, 50 mg oven dried co-precipitated precursor sample A was heated in air from room temperature to 1000°C. Rate of heating was 10°C/min. TG/DTG/DTA plots against the temperature were obtained simultaneously. A typical TG/DTG/DTA graph for co-precipitated precursor powder obtained through centrifugal mode of filtration (Sample A) is shown in Fig.6a. The thermogram revealed a two step decomposition of mixed metal hydroxide precursor powder between 30°C to 690°C. The total weight loss associated with the full thermal decomposition is 19.2%. The first step is

initiated at $\sim$ 30°C. In this step sample looses 18% of its weight corresponding to the first step of TG, a broad endothermic peak is observed at 92°C in DTA curve. This endotherm can be assigned to loss of adsorbed water [53]. The second weight loss of 1.2% occurs in the temperature range 660-690°C. With further increase in temperature, a marked exothermic peak occurs on DTA curve at about 710°C without any weight loss effect in TG curve. This peak is assigned to ferrite formation reaction which is further confirmed by XRD studies [20,53,70].

The sample B was also analysed under similar conditions as that of sample A. The thermal decompositon of coprecipitated precursor powder, obtained through decantation mode of washing is observed to be three step process (Fig.6b). The decomposition begins at around 30°C and ends around 710°C. The total weight loss during full thermal decomposition is 26.8%. The first weight loss was found to be in the temperature range 33°C to 215°C with a loss of 24.4% of sample weight. A big endotherm is observed on DTA corresponding to this step. This weight loss is assigned to loss of adsorbed water [53]. The second step in weight loss occurred in the temperature range 280°C to 340°C. This is accompanied with endothermic change. The peak of this endotherm appears near the temperature T $\sim$ 310°C on DTA curve. The TG curve shows a gradual weight loss over wide temperature range from 640°C-710°C. The second weight
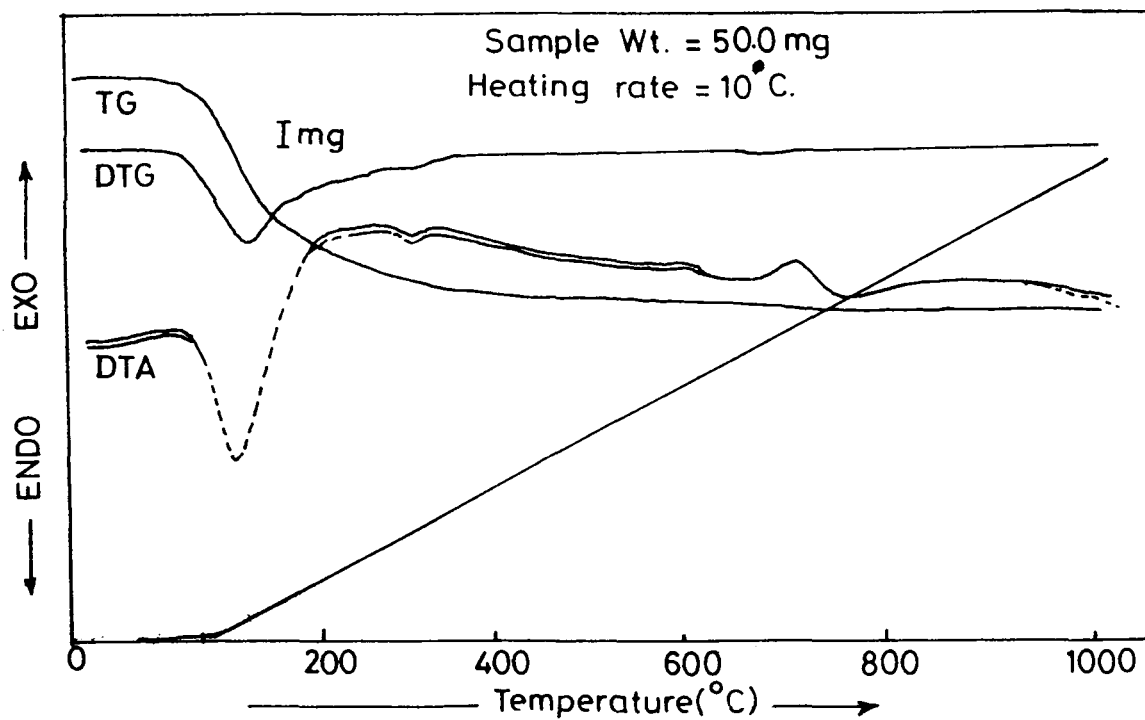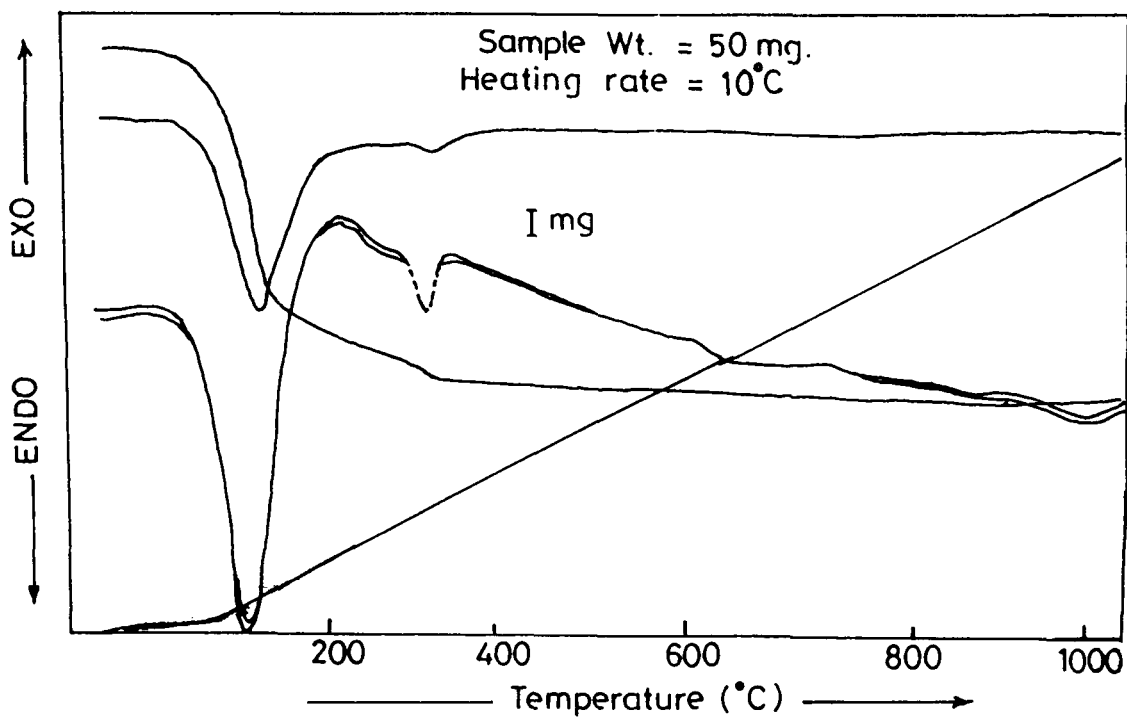
Fig. 6a : Simultaneous TG/DTG/DTA curve (Sample A.)

Fig. 6b : Simultaneous TG DTG DTA curve (Sample - B.)

loss is attributed to the loss of water crystallisation from hydrated iron oxide [71]. No exothermic peak is seen on DTA. The third weight loss may be due to decomposition of strontium carbonate. No exothermic peak is seen on DTA curve here T $\simeq$ 700°C. The details of the TG/DTG/DTA data for the precursor powder A and B is summarised in the Table 7.

Table 7

Summary of thermal decomposition data

Sample name	TG % wt. loss	DTG temp. range °C	DTA peak temp.	Peak characteristics	Associated change
Powder Sample A	18%	30-430	90°C	Endotherm	Loss of adsorbed water.
	1.2%	660-690	---	---	Decomposition of $SrCO_3$.
	-	-	710°C	Exotherm	Ferritisation
Powder Sample B	24.4%	30-215	90°C	Endotherm	Loss of adsorbed water
	1.6%	280-340	310°C	Endotherm	Loss of water of crystallisation
	1.0%	640-710	---	---	$SrCO_3$ decomposition

The study of thermal analysis shows that by changing mode of washing, thermal behaviour of coprecipitate is changed. To find out the reason for this behaviour both the coprecipitates are analysed by powder XRD analysis.

3.2.1.2 Structural analysis by XRD

The nature of coprecipitate and the chemical and structural changes during heating are investigated with the help of powder X-ray diffraction technique. These results are discussed in the present section. On the basis of results of thermal analysis the temperatures for heating the coprecipitate were chosen. The different temperatures chosen for heating coprecipitate were 650°C, 750°C, 850°C and 925°C. The X-ray diffractogram of all the samples were scanned in the range of $2\theta = 20°-60°$. The changes occurring in the XRD pattern during heating of the coprecipitate at various temperatures are shown in Fig.7. Identification of phases present in XRD pattern of coprecipitate and calcined samples was done with the help of ASTM data.

The X-ray diffractogram of coprecipitate A (Fig.7a) shows the presence of lines corresponding to $SrCO_3$ phase ($2\theta = 25.5°$ and $25.9°$) [72]. The presence of $SrCO_3$ phase in coprecipitate is due to conversion of $Sr(OH)_2$ into $SrCO_3$ by reaction with atmospheric carbondioxide. Strontium being an alkaline earth metal, its hydroxide is more susceptible to
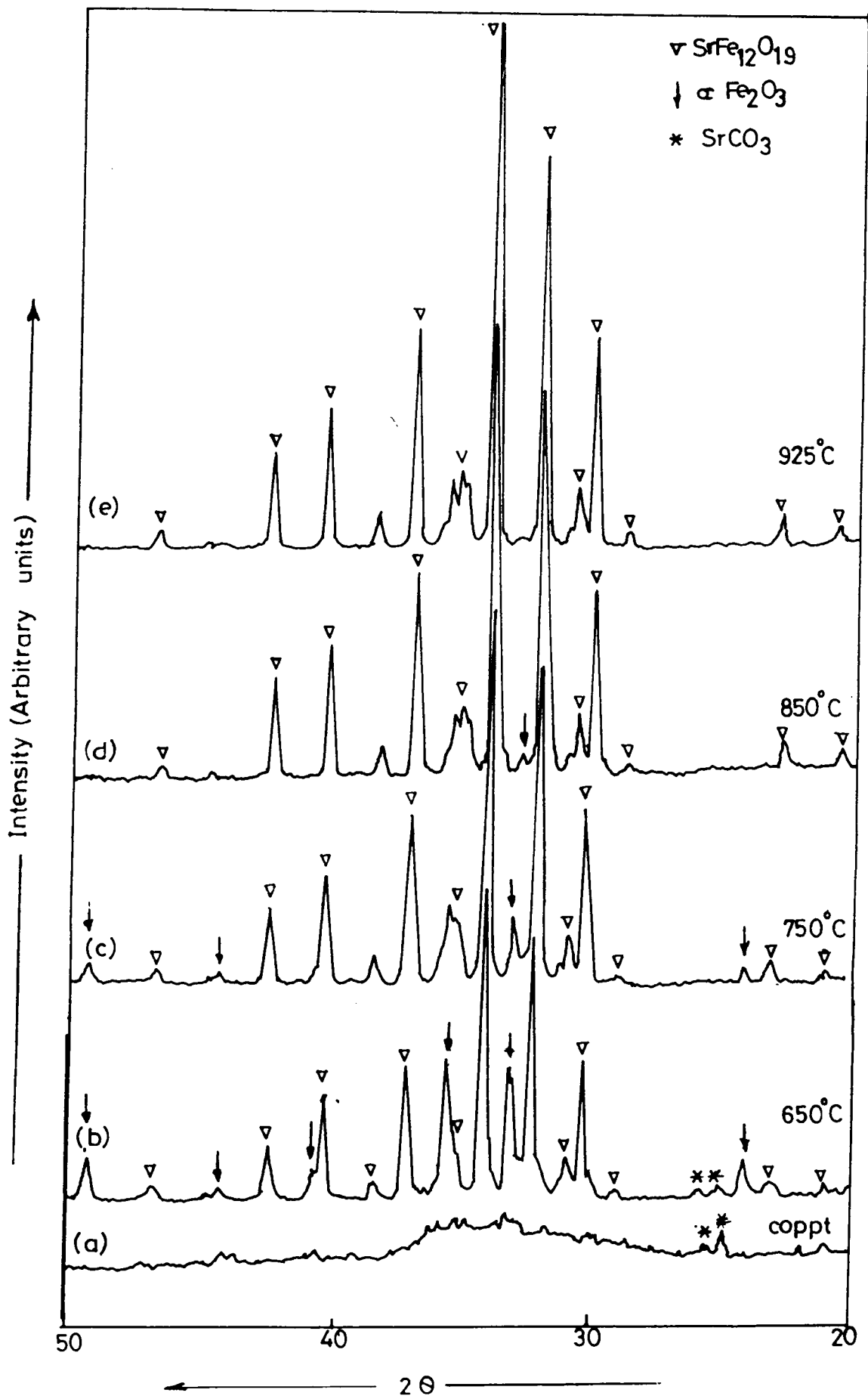
104

Fig. 7 : X-ray diffraction patterns of sample A heated
at various temperatures between 650°C to 925°C.

carbondioxide leading to formation of more stable compound i.e., strontium carbonate [73]. Rest of the pattern does not show any peak indicating X-ray amorphous nature of coprecipitate. Heat treatment of precursor powder at 650°C results in the emergence of the lines corresponding to phases viz, $SrCO_3$, α-Fe_2O_3, and $SrFe_{12}O_{19}$ (Fig.7b) [72,74,75]. With increase in calcination temperature, the intensity of Sr-hexaferrite peak is found to increase while that of α-Fe_2O_3 and $SrCO_3$ phases is found to decrease. On heating the coprecipitate at 925°C, single phase $SrFe_{12}O_{19}$ is formed. The 'd' values of Sr-hexaferrite of our sample matches well with reported data [75].

Alongwith the qualitative analysis of phases present, the XRD pattern is also used for quantitative analysis. The relative percentage of $SrFe_{12}O_{19}$ phase formed at different temperatures is estimated by comparing area under 100% intensity peak of strontium ferrite [114] of single phase with area of [114] peak of powders calcined at different temperatures [76]. The results of the XRD studies are compiled in Tables 8a & 8b. The coprecipitated precursor powder, obtained after following decantation mode of washing shows crystallinity in the virgin sample itself (Fig.8a). The characteristic diffraction lines observed can be assigned to the presence of α-Fe_2O_3, $Fe_2O_3nH_2O$ and $SrCO_3$ phases.
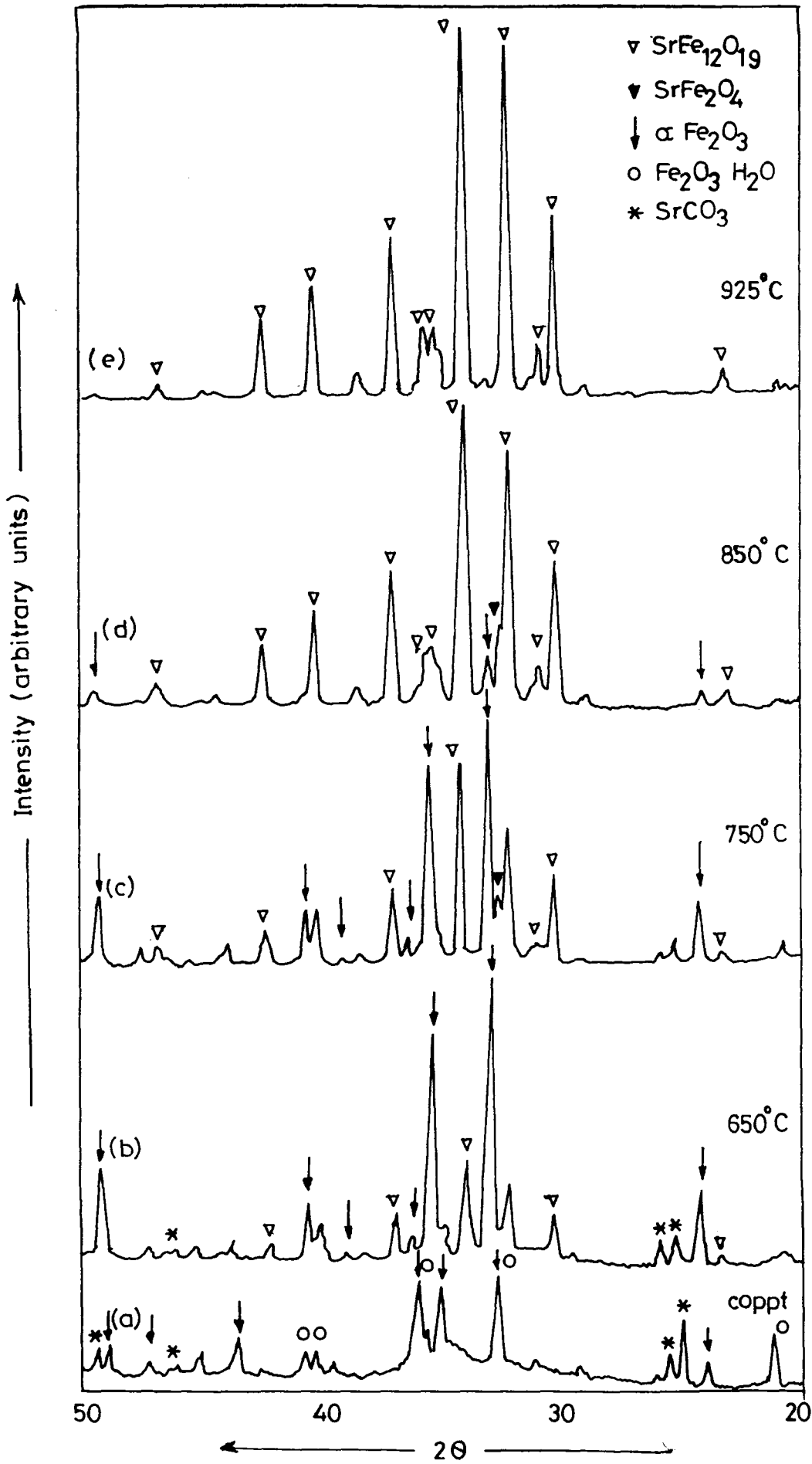
Fig. 8 : X-ray diffraction patterns of sample B heated
at various temperatures between 650°C to 925°C.

Table 8a

XRD and thermal analysis data of coprecipitates A and

calcined samples

Calcination temperature	Phases present	% of $SrFe_{12}O_{19}$	DTA	Remarks
Oven dried precipitate	Two small peaks of $SrCO_3$	-	Endothermic peak in the temperature range 30°C to 430°C.	Loss of adsorbed moisture during heating. No structure change is detected.
650°C/5hr	α-Fe_2O_3, $SrCO_3$, $SrFe_{12}O_{19}$	58%	Exothermic peak in the temperature range 690°C to 735°C with maxima at 712°C.	Initiation of ferrite formation is observed when sample is heated near the temp. range Therefore this peak is assigned to reaction of ferrite formation.
750°C/5hr	α-Fe_2O_3, $SrCO_3$, $SrFe_{12}O_{19}$	68%		
850°C/5hr	α-Fe_2O_3, $SrFe_{12}O_{19}$	85%	-	Percentage of Sr-ferrite phase is increased.
925°C/2hr	$SrFe_{12}O_{19}$	100%	-	Single phase $SrFe_{12}O_{19}$ is formed.

Table 8b

XRD and Thermal analysis of coprecipitates B and

calcined samples

Calcination temperature	Phases present	% of $SrFe_{12}O_{19}$	DTA	Remarks
Oven dried precipitate	$\alpha\text{-}Fe_2O_3$ $Fe_2O_3 \cdot nH_2O$ $SrCO_3$	-	Two endo-thermic peak in the temp. range (1) 33 to 215°C & (2) 283 to 340°C	Loss of absorbed water
650°C/5hr	$\alpha\text{-}Fe_2O_3$, $SrCO_3$, $SrFe_{12}O_{19}$	24%	Endothermic peak in the temperature range 640°C to 707°C	Though exo-thermic peak near temp. ~ 700°C is not observed ferrite for-mation is initiated in the same temp. range. But the per-centage of Sr-ferrite formed is less than that is observed for sample A.
750°C/5hr	$\alpha\text{-}Fe_2O_3$, $SrCO_3$, $SrFe_{12}O_{19}$	48%		
850°C/5hr	$\alpha\text{-}Fe_2O_3$ $SrFe_{12}O_{19}$	74%	-	Formation percentage of Sr-ferrite phase is increased.
925°C/2hr	$\alpha\text{-}Fe_2O_3$ $SrFe_{12}O_{19}$	95%		

Calcination at 650°C or above shows initiation of magnetoplumbite phase (Fig.8c). Alongwith Sr-hexaferrite, α-Fe_2O_3 and $SrCO_3$ peaks a small peak of $SrFe_2O_4$ phase (2Θ = 33.9°) is seen for samples calcined at 750°C (Fig.8c). At 925°C, intensity of Sr-ferrite phase increases and that of other phases disappears. The amount of Sr-ferrite formed is estimated in similar manner as it is described earlier. The results of XRD studies are summarised in Table 8b.

3.2.1.3 Chemical analysis

The samples from both the batches are analysed to find out amount of residual sodium percent of samples from batch A & B with the help of atomic absorption spectroscopy. Table 9 gives percentage of different amount of sodium present in the samples. The analysis shows that along with iron and strontium small quantity of sodium is also present in sample. The amount of sodium is higher for the sample washed by decantation method (sample from batch B).

Table 9

Chemical analysis of amount of sodium

Sample Name	Mode of washing	% of Na
A	Centrifugal method	0.436
B	Decantation method	1.103

3.2.1.4   Optimisation of calcination & sintering temperature

During the study of effect of mode of washing on magnetic properties, the optimisation of calcination and sintering temperature is carried out. Both the coprecipitates A & B are calcined at 750°C, 850°C and 925°C to find the opotimum calcination temperature. The calcined powders thus obtained are pressed into pellets and subsequently sintered at different temperatures in the range 1100-1250°C. The magnetic properties of green as well as sintered samples are determined from B Vs H and (B-H) Vs H hysteresis loop. The optimum calcination and sintering temperatures are decided on the basis of magnetic properties of final sintered product.

a)   Optimisation of calcination and sintering temperature for coprecipitate A:

The coprecipitated precursor is divided into three parts and calcined at temperatures 750°C, 850°C and 925°C respectively. The magnetic property measurements of calcined samples show that the remanence (B_r), coercivity ($_bH_c$) and energy product $(BH)_{max}$ increase with an increase in calcination temperature (Table 10). Among the three green samples, a sample calcined at 750°C shows maximum coercivity and its value is equal to 6500 Oe. The coercive force is

found to decrease with increase in calcination temperature. It is well known from the study of solid state reaction that with increase in calcination temperature, the particle size increases. The coercivity is a function of particle size. Therefore decrease in coercive field with increase in calcination temperature can be ascribed to increase in particle size.

The magnetic properties of sintered compacts from series AI (calcination temperature 750°C), AII (calcination temperature 850°C) and AIII (calcination temperature 925°C) are compiled in Table 10a, b & c respectively. The magnetic properties of sintered samples from the same batch and having same calcination temperature are compared. Systematic changes in magnetic performance parameters are observed with increase in sintering temperature. Following are some important observations of comparative study of samples from AI series (Table 10a).

Important features of the sintered samples from AI series are as follows:

a)   The remanence (B_r) increases with an increase in sintering temperature and then decreases with a maxima at 1200°C (Fig. 9a).

b)   Similar trend is observed for other magnetic properties namely, saturation magnetization (M_s), energy product $(BH)_{max}$ and sintered density (ρ).

TABLE 10

MAGNETIC PROPERTIES OF SINTERED SAMPLES FROM BATCH A
(Centrifugal mode of filteration)

Table 10a

A-I - Cal. temp. 750°C/5 hrs.

Sample No.	Sintering temp.	B_r (G)	bH_c (Oe)	iH_c (Oe)	$(BH)_m$ MGOe	$4\pi M_s$ (G)	D gm/cm^3
A 236	Green	1000	850	6500	0.16	1400	-
A 237	1100/2 hr	2100	1650	3450	0.84	2550	3.96
A 238	1150/2 hr	2300	1200	1600	0.91	2550	4.40
A 240	1200/2 hr	2500	1050	1250	0.97	3100	4.55
A 241	1250/2 hr	2200	1050	1250	0.845	2950	4.11

Table 10b

A-II - Cal. temp. 850°C/5 hrs.

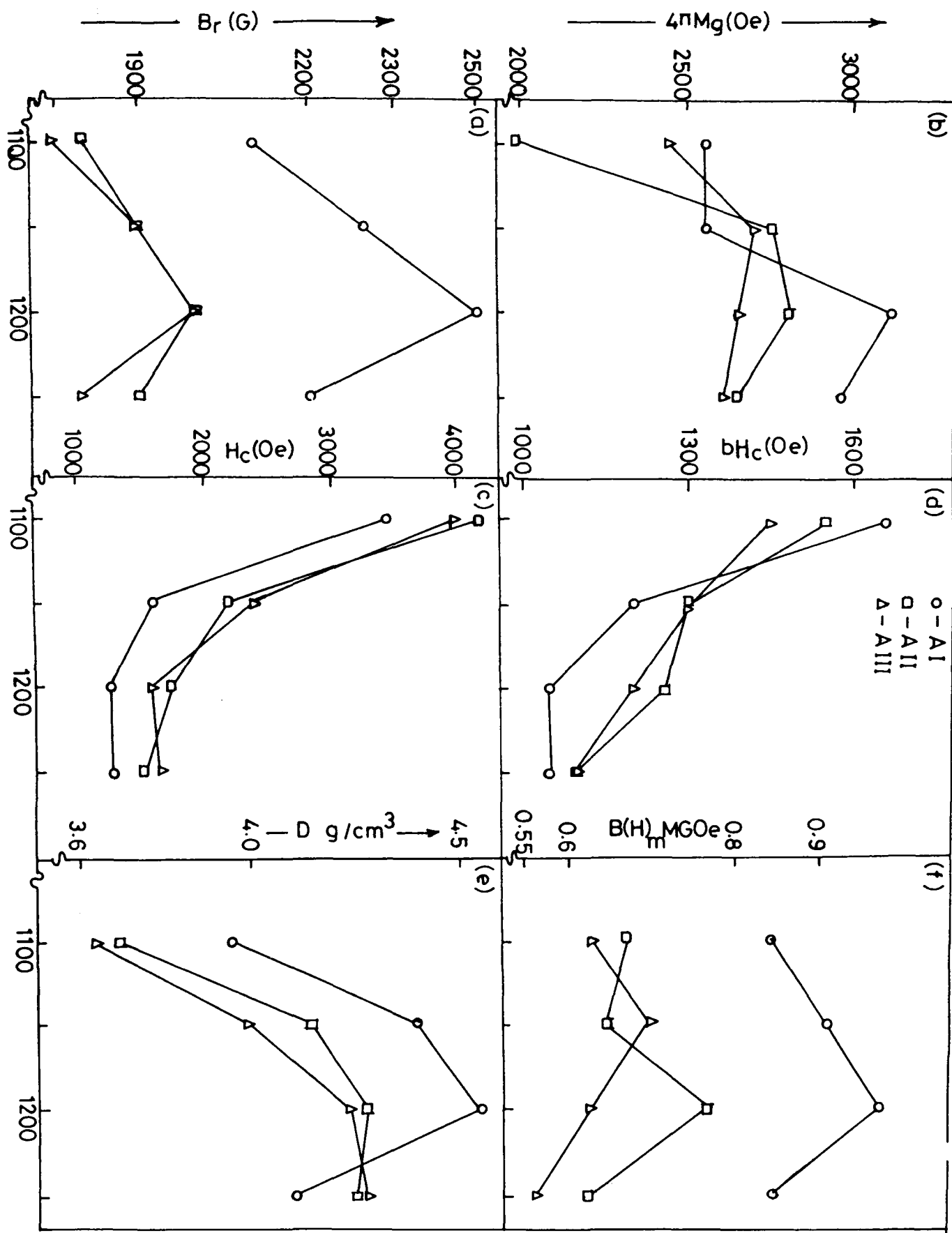| Sample No.	Sintering temp.	B_r (G)	bH_c (Oe)	iH_c (Oe)	$(BH)_m$ MGOe	$4\pi M_s$ (G)	D gm/cm^3
A 242	Green	1250	1100	6150	0.36	1650	-
A 243	1100/2 hr	1800	1550	4200	0.675	2000	3.69
A 244	1150/2 hr	1900	1300	2200	0.65	2750	4.15
A 246	1200/2 hr	2000	1250	1750	0.77	2800	4.28
A 242	1250/2 hr	1900	1100	1550	0.63	2650	4.25

Fig. 9 : Effect of calcination temperature on magnetic
         properties of sintered Sr-ferrite samples
         (Batch A)

Table 10c

A-III - Cal. temp. 925°C/2 hrs.

Sample No.	Sintering temp.	B_r (G)	$_bH_c$ (Oe)	$_iH_c$ (Oe)	$(BH)_m$ MGOe	$4\pi M_s$ (G)	D gm/cm^3
A 248	Green	1300	1100	5750	0.36	1750	-
A 249	1100/2 hr	1750	1450	4000	0.63	2450	3.63
A 250	1150/2 hr	1900	1300	2400	0.70	2700	4.00
A 252	1200/2 hr	2000	1200	1600	0.63	2650	4.23
A 248	1250/2 hr	1800	1100	1650	0.57	2600	4.28

c)   On the other hand, values of $_bH_c$ and $_iH_c$ are found to decrease continuously with increase in sintering temperature from 1100°C to 1250°C (Fig. 9b & c).

Similar trends are also observed for samples from AII and AIII series (Tables 10b & 10c).

The results of magnetic property measurements can be explained as follows:

i)   The remanence value depends upon degree of orientation (n_c),   saturation magnetization (M_s) and   sintered density   (ς) [14]. As all the samples are isotropi- cally pressed, it would be reasonable to presume that the degree of orientation is the same for all the samples. Changes in remanence (B_r) of sintered samples can be related to combined effect of changes in saturation magnetization and sintered density (Table10).

ii) The intrinsic coercivity ($_iH_c$) is proportional to the contribution of single domain particle (n_s), anisotropy constant (K) and inversely proportional to saturation magnetization [19]. Among these three factors anisotropic constant (K) is material's intrinsic property. The second factor n_s is maximum when all particles have size equal to single domain i.e. ~ 1 um. With increase in sintering temperature particle size increases and particles are no more single domain but become multidomain. This results into decrease in n_s value. The saturation magnetization is found to increase with sintering temperature. Therefore decrease in $_iH_c$ is attributed to the combined effect of increase in particle size and saturation magnetization.

The magnetic properties of samples from AI, AII & AIII series are compared by plotting graphs of different magnetic properties with the sintering temperatures (Fig.9). The comparative study shows that the samples from AI series are showing relatively better performance parameters. From the study it is evident that better magnetic properties are obtained when coprecipitate A is calcined at 750°C. In conclusion, it can be said that 750°C is an optimum calcination temperature.

b) <u>Optimisation of calcination and sintering temperature for sample B</u>:

The dried coprecipitate from batch B (labelled as

sample B) is divided into three parts. These parts are calcined at 750°C, 850°C and 925°C. The pellets are pressed from the calcined powders which are subsequently sintered at different temperatures in the range from 1100°C to 1250°C. Magnetic performance parameters of green and sintered samples are measured by plotting B Vs H and (B-H) Vs H hysteresis loops and results obtained are summarised in Table 10. The B_r, $_iH_c$, $4\pi M_s$ and $(BH)_{max}$ of green compacts increase with increasing calcination temperature. It may be noted that observations are comparable to the one obtained for samples from batch A.

The magnetic properties of sintered samples for BI, BII and BIII series are given in Tables 11a,b & c respectively. The effect of sintering temperature on magnetic properties is graphically shown in Fig.10. The graphs show that remanence (B_r), saturation magnetization $(4\pi M_s)$, energy product $(BH)_{max}$ and density (ρ) increase with sintering temperature, upto 1150°C. The sample shows maxima on magnetic property curve at this temperature. On crossing this temperature deterioration magnetic properties are observed and therefore this temperature is selected as optimum sintering temperature. The $_bH_c$ and $_iH_c$ are found to decrease continuously with increase in sintering temperature from 1100°C to 1250°C.

TABLE 11

MAGNETIC PROPERTIES OF SINTERED SAMPLES FROM BATCH B
(Decantation mode of washing)

Table 11a

B-I - Calcination temp. 750°C/5 hrs.

Sample No.	Sintering temp.	B_r (G)	$_bH_c$ (Oe)	$_iH_c$ (Oe)	$(BH)_m$ MGOe	$4\pi M_s$ (G)	D gm/cm^3
B 218	Green	700	700	5450	0.12	950	-
B 215	1100/2 hr	2150	1700	3900	0.935	2900	4.28
B 216	1150/2 hr	2450	1450	2100	1.1	2900	4.54
A 217	1200/2 hr	2400	1300	1750	1.01	2750	4.41
A 218	1250/2 hr	2350	1150	1450	0.11	2800	4.21

Table 11b

B-II - Calcination temp. 850°C/5 hrs.

Sample No.	Sintering temp.	B_r (G)	$_bH_c$ (Oe)	$_iH_c$ (Oe)	$(BH)_m$ MGOe	$4\pi M_s$ (G)	D gm/cm^3
B 224	Green	950	800	5150	0.20	1400	-
B 221	1100/2 hr	2000	1650	4400	0.80	2750	3.61
B 222	1150/2 hr	2200	1550	2900	0.92	2800	4.52
B 223	1200/2 hr	1950	1300	2150	0.74	2550	4.58
B 226	1250/2 hr	1850	1100	1750	0.60	2700	4.44

B-III - Calcination temp. 925°C/2 hrs.

Sample No.	Sintering temp.	B_r (G)	$_bH_c$ (Oe)	$_iH_c$ (Oe)	$(BH)_m$ MGOe	$4\pi\,M_s$ (G)	D gm/cm^3
B 230	Green	950	850	5250	0.18	1350	-
B 227	1100/2 hr	1900	1600	4450	0.76	2550	4.02
B 228	1150/2 hr	2100	1500	3200	0.79	2800	4.68
B 229	1200/2 hr	2150	1300	2200	0.84	2950	4.63
B 230	1250/2 hr	1250	450	600	0.12	2450	4.10

The comparison of magnetic properties of samples from B-I, B-II and B-III series (Fig.10) shows that samples from B-I series have superior magnetic properties. This once again confirms that lower calcination temperature (i.e. 750°C here) is favourable parameter to obtain sintered compacts with better magnetic properties.

The comparative study of magnetic properties of samples from both the batches shows that best magnetic properties are obtained when calcination temperature is 750°C. When coprecipitate is calcined at lower temperature calcined powder is more fine having high surface area. When such powder is processed it gives sintered compacts with better performance. On the other hand, when powder is calcined at higher temperature (here 850°C, 925°C) the particle size increases. Such powder when processed shows deterioration in magnetic properties. The study confirms that better quality
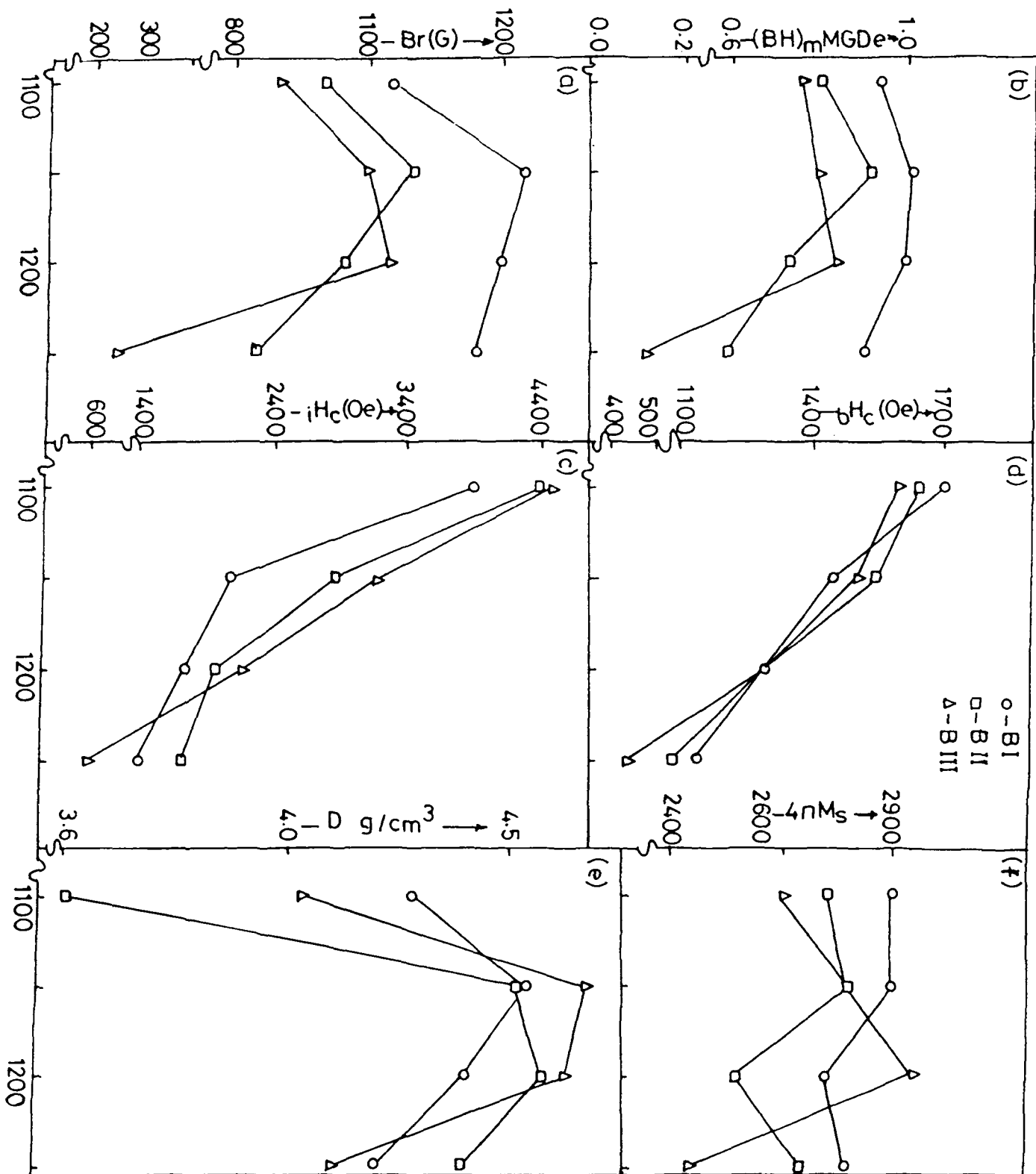
Fig. 10: Effect of calcination temperature on magnetic
properties of sintered Sr-ferrite samples
(Batch B)

of powder is obtained when calcination temperature is low leading to final product with highest energy product i.e. $(BH)_{max}$.

The magnetic properties of samples from A-I and B-I series are found to be the best in the respective batches. Therefore they have been selected for study of effect of mode of washing on magnetic performance parameters of sintered product.

The comparison between A-I and B-I series reveals that optimum sintering temperature is 1150°C for B-I series which is lower by 50°C than that of A-I series. Secondly, the magnetic properties from B-I series are superior to A-I series samples. This indicates that better magnetic properties are obtainable when co-precipitate is washed by using decantation method.

The results of thermal analysis, structural studies, chemical analysis and magnetic property measurements of samples from batch A & B are compared. Following are the important features of comparative study:

a) Thermal analysis shows that ferrite formation takes place exothermically in coprecipitate A while no such exothermic change is observed for sample B (Figs. 6a & 6b).

b) Structural studies reveal that coprecipitate A is X-ray

amorphous while coprecipitate B is X-ray crystalline. Centrifugal mode of washing results in X-ray amorphous precursor while crystalline coprecipitate is obtained when decantation mode of washing is followed (Fig. 7 & Fig. 8).

c)   Percentage of ferrite formed at different calcination temperatures is higher for amorphous precipitate A (Table 8).

d)   When the coprecipitate is amorphous no intermediate phase is formed during Sr-hexaferrite formation. On the other hand, when coprecipitate is crystalline, spinel ferrite is formed as an intermediate phase during Sr-hexaferrite formation.

e)   The chemical analysis shows that both the samples contain small amount of sodium along with iron and strontium. The amount of sodium is higher for the sample washed by decantation mode i.e. for sample B (Table 9).

f)   The comparison between magnetic properties of samples from Batch A & B shows that magnetic properties of samples from Batch B are better. This indicates that better magnetic properties are obtainable when coprecipitate is washed via decantation mode.

From the comparative evaluation we propose that two important parameters derived from mode of washing may be responsible for observed effects. These are: 1) Difference in nature (crystallinity) of coprecipitate, 2) Amount of

residual sodium ion concentration. We will discuss effect of each of them separately in the next section.

3.2.2   Effect of crystallinity of coprecipitate

The systematic experiments were planned and carried out to study the effect of crystallinity of coprecipitate of kinetics, and mechanism of ferrite formation. In these experiments, strontium and iron hydroxides were coprecipitated using sodium hydroxide. The precipitate was washed by centrifugal mode using distilled water. The coprecipitate thus obtained was in the form of lumps. The lumps were divided into two parts. One part of the lumps was mixed with approximately 1.5 lit of distilled water and vigorously stirred with the help of mechanical stirrer for 5-6 hours. The mechanical stirring was done to disperse the lumps and to obtain homogeneous slurry. Both the lumps and slurry were dried in an oven under the same condition of temperature and time. The coprecipitate which was dried in the form of lump was labelled as C-I while another coprecipitate (which was dried in slurry form) was labelled as C-II.

Since the samples C-I and C-II both were derived from the same batch, the preparation conditions are the same for both the samples. Also the problems of batch to batch variation (i.e. reproduciblity, personal error and

uncontrolled parameters were nullified. In short, preparation history of C-I and C-II is the same, except the conversion of part of lumps into slurry. With this background, it is reasonable to assume that residual sodium ion concentration is exactly equal for C-I and C-II samples.

After completion of 48 hrs. drying, precursor C-I and C-II are characterised using TG/DTG/DTA, X-ray diffraction and magnetic measurements.

3.2.2.1 Thermal analysis (of precursor samples C-I & C-II)

The simultaneously recorded TG/DTG/DTA curve for C-I precursor is depicted in Fig.11a. The thermogram shows that weight loss is initiated at ~ 40°C and ends at around 450°C. In this temperature range sample loses its weight in two steps with total weight loss associated with full thermal decomposition is 14.0%. The first step is initiated at temperature 40°C and continues up to 185°C. In this step 9.39% weight loss takes place. Corresponding to first step a broad dip endothermic peak is observed. DTA curve with absorption of heat around ~-170 mcal/mg. This loss is assigned to loss of adsorbed moisture from the precursor powder. The second weight loss takes place in the temperature range 195°C-450°C. This weight loss is also accompanied by endothermic change. The heat absorbed during the process is -4.5 mcal/mg. The precursor C-I is X-ray
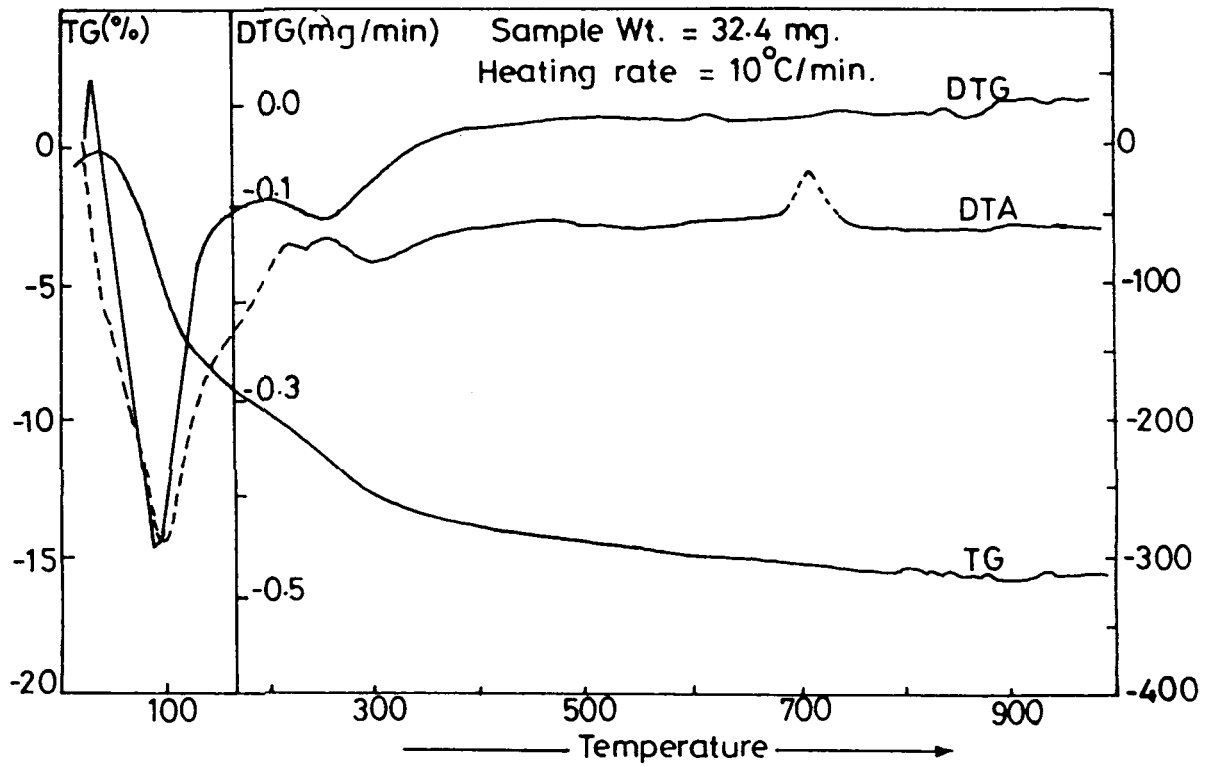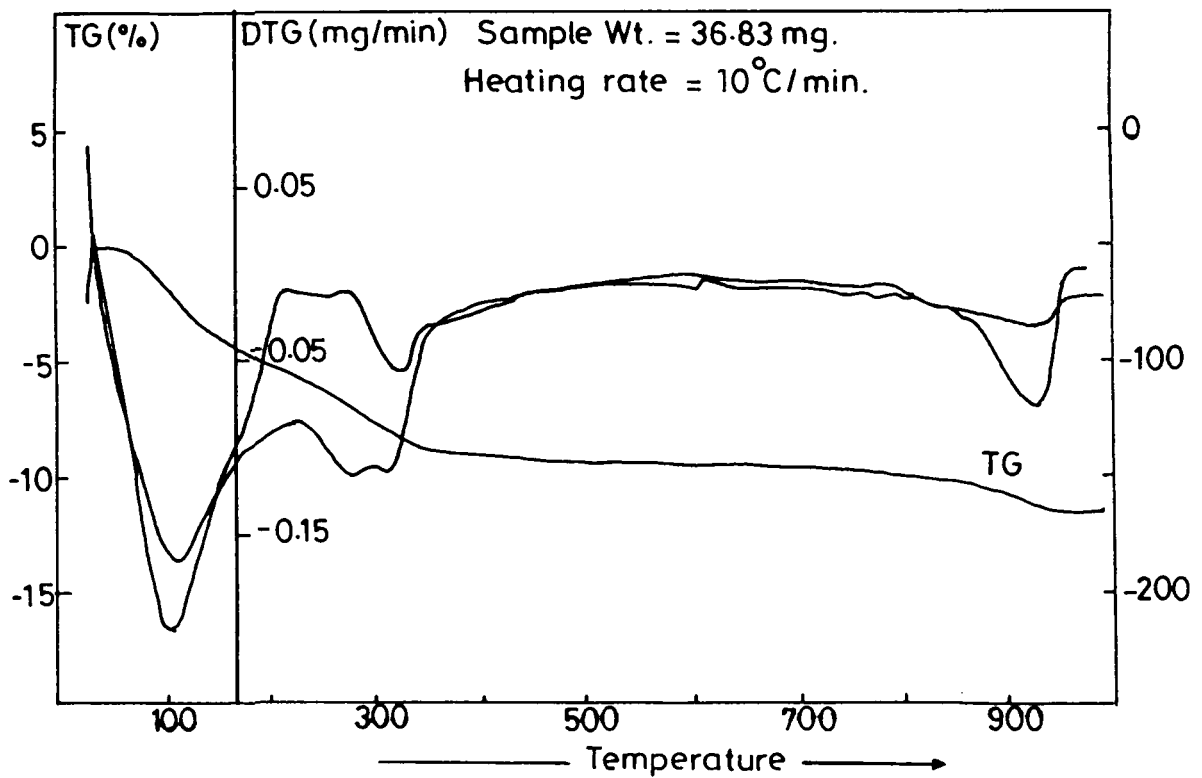
Fig.11a : Simultaneous TG/DTG/DTA curve (Sample C.I)

Fig.11 b :Simultaneous TG/DTG/DTA curve (Sample C.II)

amorphous (Fig.13a) and heat absorbed during second loss is higher than that of first one. Therefore this weight loss can be assigned to loss of tightly bound water [53]. In addition, the DTA curve of precursor powder C-1 shows another peak at 710°C without any weight change effect in the TG curve. The heat liberated during the process is around 15.9 mcal/mg. This exothermic change is ascribed to onset of ferritisation reaction [53,70].

A typical TG/DTG/DTA curve of precursor material C-II is shown in Fig.11b. The precursor powder C-II is observed to decompose between 40°C to 970°C. The thermal decomposition of precursor consists of three steps. The sample loses about 5.57% of its weight in first step (Temperature range 40°C-220°C) with absorption of energy around -218.9 mcal/mg. The endothermic peak in this temperature range signifies a possible loss of moisture from the sample. The second weight loss immediately follows the first one and found to be in the range of 220°C-410°C. In this step, 3.63% loss takes place. DTA shows endothermic peak corresponding to this loss with absorption of about -31.4 mcal/mg energy. The second loss is ascribed to loss of water of crystallisation (which is confirmed from phase analysis studies), (Fig.14b) [70]. TG curve shows gradual weight loss throughout the temperature range 780°C to 970°C with a loss of 1.66% weight. It is associated with endothermic change in DTA. The energy during the decomposition is -19.6 mcal/mg. This loss is ascribed to decomposition of strontium

121

carbonate [77]. The results of thermal analysis are compiled in Table 12.

Table 12(a)

Summary of Thermal analysis of C-I & C-II samples

Sample Name	TG % wt. loss	DTG temp. range	DTA		Peak characteristic	Associated change
			Peak temp. $^{\circ}C$	Temp. range $^{\circ}C$		
C-I	9.39%	40.0°C to 185.0°C	95.3	45-180	Endothermic	Loss of adsorbed water
	4.59%	195.0°C to 450.0°C	252.1	190-290	Endothermic	Loss of tightly bound water
	-	-	711.2	690-740	Exothermic	Ferrite formation reaction

Table 12(b)

C-II	5.57%	40.0°C to 220.0°C	106.4	40-200	Endothermic	Loss of adsorbed water
	3.63%	220.4°C to 410.5°C	325.0	280-400	Endothermic	Loss of water of crystallisation
	1.66%	780.0°C to 970.0°C	934.0	780-960	Endothermic	Decomposition of $SrCO_3$

3.2.2.2 Structural analysis

To find out the temperature of magnetoplumbite phase formation, the coprecipitates C-I & C-II were heated in air at different temperatures from 350°C to .1050°C. After heating for two hours, the samples were removed from the furnace and immediately quenched in the distilled water. These heat treated samples are analysed with the help of Vibrating sample magnetometer (VSM) and powder X-ray diffractogram. Typical values of r_s and $_iH_c$, obtained from VSM measurements, for calcined samples from C-I and C-II series are presented in the Tables 13a and 13b respectively. The Fig.12a & b depict graphs of $_iH_c$ Vs calcination temperature and r_s Vs calcination temperature respectively for these samples. The results of magnetic measurements revealed that up to 600°C calcination temperature r and $_iH_c$ are very small and show little variation with increase in calcination temperature (Fig.12). Both the $_iH_c$ and r_s show sudden and sharp increase in their values when calcination temperature approaches 650°C. The sharp rise in magnetic properties indicated the formation of magnetically ordered phase. With further increase in temperature up to 850°C, there is a small increase in $_iH_c$ and .thereafter it decreases with further increase in calcination temperature. The decrease in $_iH_c$ is due to increase in particle size.
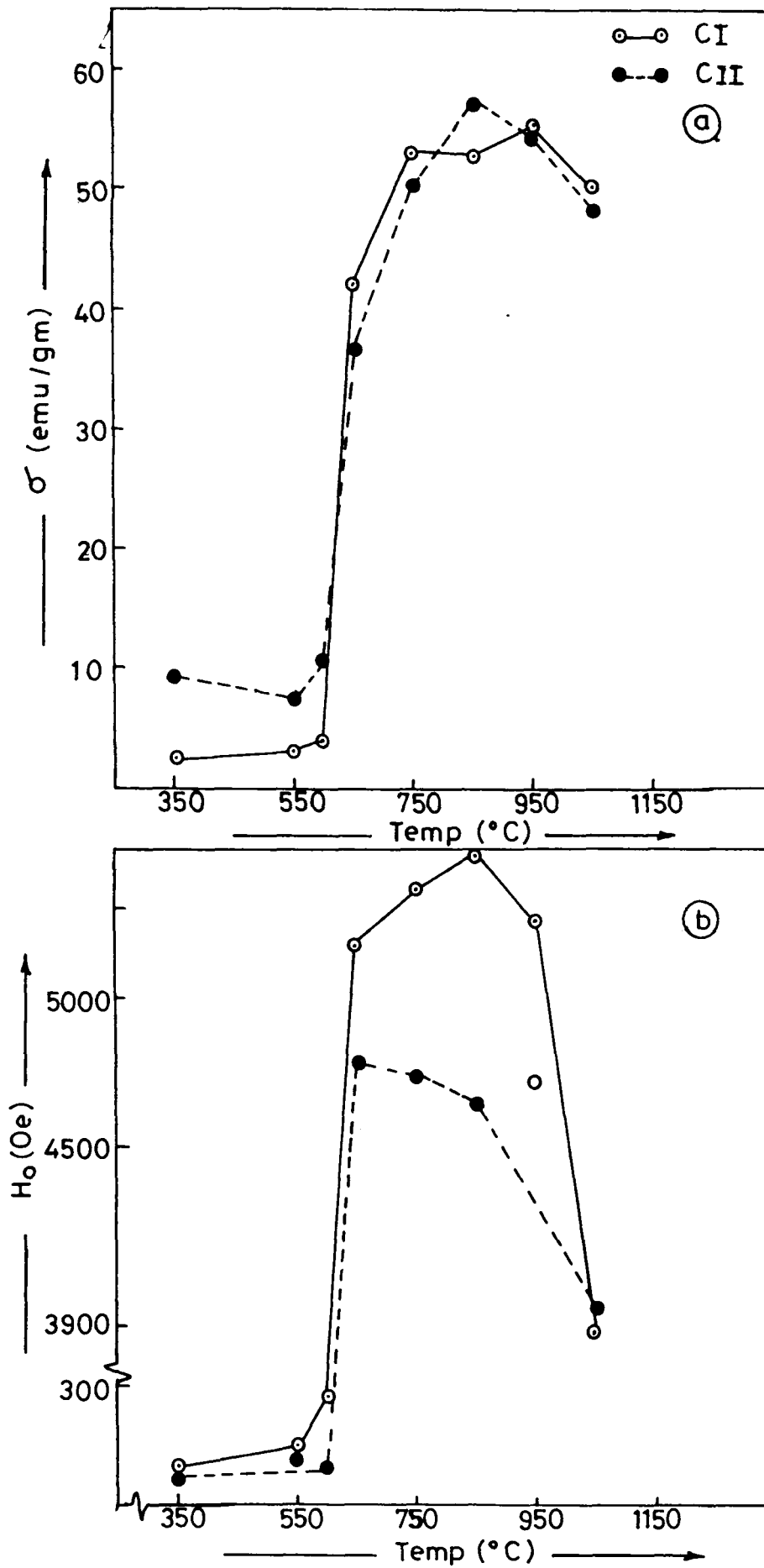
Fig 12 a-b : Manetic properties of calcined powders from C-I & C-II series

Table 13(a)

Magnetic properties of calcined powder

Sample	Cal. temp. °C	σ emu/gm	$_iH_C$ Oe
C-I	350°/2 hrs	2.72	72.3
	550°/2 hrs	3.12	150.8
	600°/2 hrs	3.85	280.1
	650°/2 hrs	42.10	5191.0
	750°/2 hrs	53.01	5358.0
	850°/2 hrs	52.45	5481.0
	950°/2 hrs	55.28	5264.0
	1050°/2 hrs	50.00	3895.0

Table 13(b)

CII	350°/2 hrs	9.32	68.6
	550°/2 hrs	7.05	122.0
	600°/2 hrs	10.38	97.4
	650°/2 hrs	36.62	4788.0
	750°/2 hrs	50.11	4755.0
	850°/2 hrs	57.33	4658.0
	950°/2 hrs	54.81	4710.0
	1050°/2 hrs	48.79	3963.0

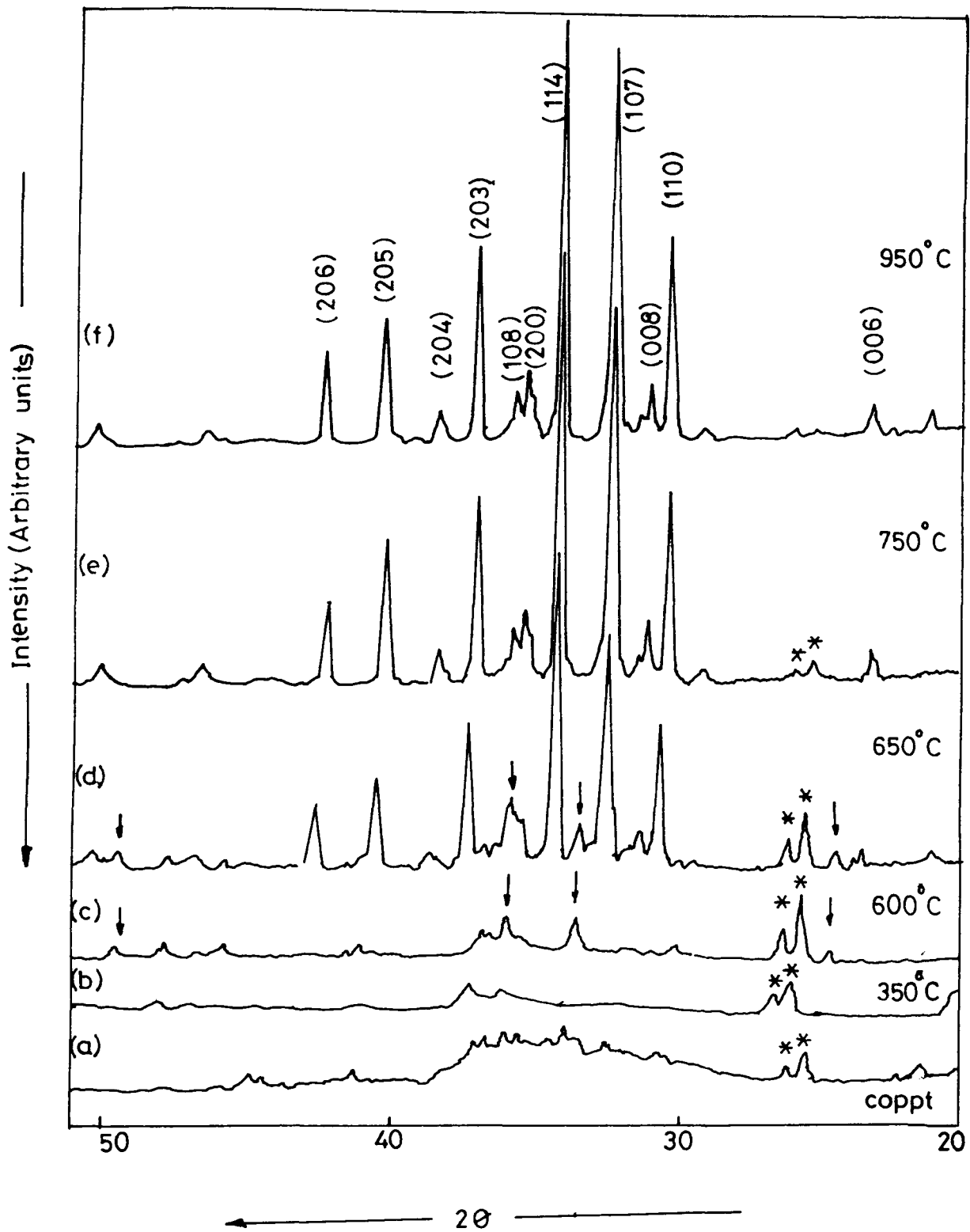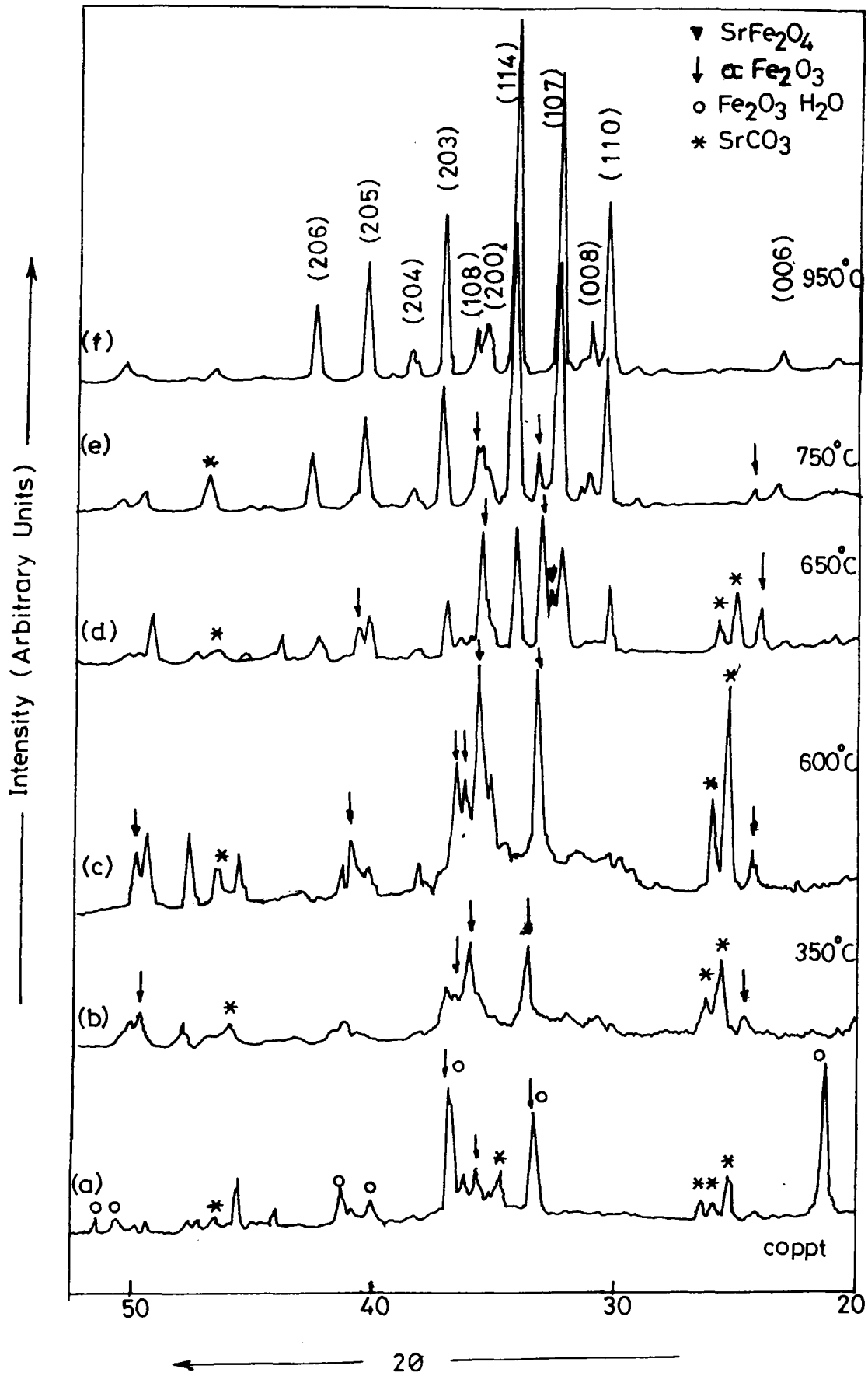Fig. 13 : X-ray diffraction patterns of C-I sample heated between 350°C to 950°C.

Fig. 14 : X-ray diffraction patterns of C-II sample
heated between 350°C to 950°C.

The phase analysis studies of the precursor samples and the heat treated samples are carried out with the help of XRD. The typical plots for samples from C-I and C-II series are shown in Fig. 13 & 14 respectively. The study gives chemical and structural changes occurring in the samples due to heat treatment. From the above figures, it is evident that precursor C-I (dried in the form of lumps) is X-ray amorphous. On the other hand, precursor powder C-II (dried in the form of slurry) is crystalline. The results of this study are tabulated in the Tables 14 & 15. Following are the salient features of the study:

a) The precursor sample C-I and the powders obtained by calcining precursor at 350°C and 600°C were X-ray amorphous. On the other hand, the precursor sample C-2 revealed presence of phases namely α-Fe_2O_3, $Fe_2O_3.nH_2O$ and $SrCO_3$. The same precursor on calcination at 350°C and 600°C indicated the presence of α-Fe_2O_3 and $SrCO_3$ phases and absence of $Fe_2O_3.nH_2O$ phase.

b) Both the precursor samples when calcined at 650°C indicated emergence of peaks corresponding to $SrFe_{12}O_{19}$. Along with these peaks, the peaks belonging to α-Fe_2O_3 and $SrCO_3$ are also found to be present (Fig. 13d & 14d). The result is consistent with results of thermal analysis and magnetic property measurements.

c) Although ferrite formation is initiated at 650°C in case of both the samples, the percentage of ferrite formed is found to be different. The comparison of

125

Table 14

The results of magnetic property measurements and

structural analysis of sample C-I

Calcination temperature	Phases present	% of $SrFe_{12}O_{19}$	$_iH_c$ Oe	σ_r emu/gm	Remarks
Oven dried coprecipitate	Two small peaks of $SrCO_3$	-	-	-	Coprecipitate is X-ray amorphous
350°C/2 hrs	$SrCO_3$	-	72.39	2.72	Amorphous nature of precipitate is not affected
600°C/2 hrs	$SrCO_3$, $\alpha\text{-}Fe_2O_3$	-	280.10	2.85	Initiation of crystallisation of iron oxide
650°C/2 hrs	$\alpha\text{-}Fe_2O_3$, $SrCO_3$, $SrFe_{12}O_{19}$	70%	5191.0	42.10	Ferrite formation has been started
750°C/2 hrs	$\alpha\text{-}Fe_2O_3$, $SrFe_{12}O_{19}$	90%	5358.0	53.01	Percentage of Sr-ferrite phase is increased
950°C/2 hrs	$SrFe_{12}O_{19}$	100%	5264.0	55.28	Single phase Sr-ferrite is formed

Table 15

The results of magnetic property measurements and

structural analysis of sample C-II

Calcination temperature	Phases present	% of $SrFe_{12}O_{19}$	$_iH_c$ Oe	r emu/gm	Remarks
Oven dried coprecipitate	α-Fe_2O_3 $Fe_2O_3.H_2O$ $SrCO_3$	-	-	-	Coprecipitate is crystalline
350°C/2 hrs	$SrCO_3$ & α-Fe_2O_3	-	68.68	9.32	i) Hydrated iron oxide is converted to iron oxide
600°C/2 hrs	$SrCO_3$ & α-Fe_2O_3	-	97.49	10.38	ii) No new phase has been formed
650°C/2 hrs	α-Fe_2O_3, $SrCO_3$, $SrFe_2O_4$ $SrFe_{12}O_{19}$	30%	4788.0	36.62	Initiation of ferrite formation. Spinel ferrite is also formed.
750°C/2 hrs	α-Fe_2O_3, $SrFe_2O_4$ $SrFe_{12}O_{19}$	75%	4755.0	50.11	Percentage of Sr-ferrite phase is increased.
950°C/2 hrs	$SrFe_{12}O_{19}$	100%	4710.0	54.81	Single phase Sr-ferrite is formed.

127

percentage of Sr-hexaferrite formed (Tables 14 & 15) at different temperatures for C-I and C-II series samples. The rate of Sr-ferrite formation is higher when starting precursor is C-I (amorphous) than that of precursor C-II (crystalline precursor).

d) The structural analysis of calcined sample from C-2 series shows presence of $SrFe_2O_4$ (spinel ferrite) as an intermediate phase during formation of $SrFe_{12}O_{19}$ (Fig.14d). No such intermediate phase is observed for calcined samples from C-I series. The trend of chemical and structural changes with heating shown by precursor C-I is similar to precursor A (Please refer to Figs.7 & 13) while structural features of C-II series samples are observed to be similar to that of calcined samples derived from precursor B (Please refer to Figs.8 & 14).

In order to understand the effect of crystallinity on kinetics and mechanism of strontium hexaferrite formation, the results of thermal and XRD analysis for coprecipitates A, B, C-I and C-II are given in the Table 16. All these observations confirm that the crystallinity of coprecipitate affects the kinetics (rate of formation) and mechanism of ferrite formation.

Higher rate of ferrite formation for amorphous coprecipitated precursor can be explained as follows:

<u>Kinetics of reaction</u>: The solid state reaction takes place

Table 16

Name of precursor	Nature	DTA	Intermediate phases present	Relative % of $SrFe_{12}O_{19}$ formed at various temp
				Temp.
A	X-ray amorphous	Exothermic peak of ferritisation at 710 °C	-	650°C - 58% 750°C - 68% 850°C - 85% 925°C - 100%
C-I	X-ray amorphous	Exothermic peak of ferritisation at 711 °C	-	650°C - 70% 750°C - 90% 950°C - 100%
B	Crystalline	No exothermic peak	$SrFe_2O_4$	650°C - 24% 750°C - 48% 850°C - 74% 925°C - 95%
C-II	Crystalline	No exothermic peak	$SrFe_2O_4$	650°C - 30% 750°C - 75% 950°C - 100%

through (1) nucleation and growth, (2) diffusion. The solid state reaction involves atomic movement. The diffusion is defined as mechanism by which matter is transported through matter. During formation of new substance rate of movement of atoms of reacting species i.e. diffusion rate is very important. The rate at which diffusion occurs depends on (a) type of diffusion mechanism, (b) the temperature at which diffusion takes place (as temperature increases diffusivity also increases), (c) type of crystal structure (Rate of diffusion is higher if crystal structure has lower atomic packing factor), (d) The type of crystal imperfection. More open structure allows more rapid diffusion of atoms e.g. diffusion takes place more rapidly along grain boundary than in grain matrix. The concentration of the diffusing species [78]. In solid state reaction rate of formation of product also depends upon diffusion length e.g. rate of formation is lower for conventional ceramic method than the non-conventional precursor method. All these factors govern the rate of solid state reaction i.e. the kinetics of the reaction.

From the above discussion we propose that the higher rate of formation of Sr-hexaferrite is possible when starting precursor is amorphous. It is known that the amorphous structure is more open and having smaller diffusion length as compared to their crystalline form. The difference in rate of formation is also reflected in

differential thermal analysis. Due to higher rate of hexaferrite formation when starting precursor is amorphous, the energy change per unit time is higher and is detected as an exothermic peak on DTA curve in temperature range 690°C-740°C. On the contrary, when precursor is crystalline rate of formation is lower, therefore energy change per unit time is small and hence is not detected by differential thermal analysis (DTA).

Similar results were also reported by Beretka et al. [79]. He studied kinetics of reaction between barium carbonate with two different types of iron oxides. It was observed that the reaction proceeded more readily when iron oxide is poorly crystalline [79].

Mechanism of hexaferrite formation

Even though the synthesis of hexaferrites with different methods is well known, the mechanism of ferritisation reaction is poorly understood and varied and often contradictory observations regarding the nature of reaction have been reported. According to few researchers, in initial stages of formation of $BaFe_{12}O_{19}$ intermediate phases like $BaFe_2O_4$, $BaFeO_{3-x}$ are formed [50,51]. According to others, layers of barium hexaferrite and $BaFe_2O_4$ can form simultaneously [84]. Synthesis of Ba/Sr ferrite by solution techniques like coprecipitation, liquid mix technique, decomposition of organometallic precursor do not

show presence of intermediate phases like $BaFe_2O_4$ or $BaFeO_{3-x}$ etc. [53,54].

In our study of mechanism, we have analysed the precursor samples and calcined samples with the help of powder X-ray diffractogram to find out different phases present. It has been observed that when precursor sample is amorphous (sample A & C-I) during hexaferrite formation presence of intermediate phase is not detected. These results are consistent with results reported by Roos [53]. On the contrary, when precursor sample is crystalline (sample B & C-II) presence of intermediate phase like $SrFe_2O_4$ is detected at lower calcination temperatures (please see Table 16). From above results and the results reported in literature, it can be said that presence of intermediate phase during hexaferrite formation depends upon nature of starting precursor sample.

3.2.2.3 Effect of crystallinity on magnetic properties

In order to examine the effect of nature of coprecipitate (amorphous/crystalline) on magnetic properties of final sintered product coprecipitated precursor C-I and CII are chosen for the study. These samples are chosen on the basis of following considerations:

i) The coprecipitate C-I is amorphous while C-II is crystalline.

132

ii)   Both the coprecipitates are derived from the same batch
      (batch C) and therefore their preparation history
      remains presumably identical.

iii) The residual sodium ion concentration is same for both
the precursor samples.

These considerations imply that precursor samples are
identical in all respects except the crystallinity of
coprecipitate.

During the study of effect of this parameter, the
coprecipitated samples are calcined at optimised temperature
i.e. 750°C. Calcined powders thus obtained are pressed into
pellets which are subsequently sintered in the temperature
range 1100°C-1220°C at an interval of 30°C. The magnetic
properties of sintered pellets are summarised in Table 17.
The Fig.15 manifests the changes in magnetic performance
parameters with sintering temperature graphically. Magnetic
performance parameters of samples (from C-I & C-II series)
sintered under the same conditions are compared. The
comparative account indicates that,

1)   The remanence (B_r) and coercivity $(_bH_c)$ of sintered
      samples from C-II series are greater by about 5-10% and
      10-12% respectively, than the corresponding samples
      from C-I series.

2)   The superiority of C-II series samples in remanence and
      coercivity is obviously reflected in energy product
      value (Fig.15c). The $(BH)_{max}$ value is found to be

133

Table 17(a)

Magnetic properties of sintered samples from C-I series

Sample Name	Sintering temp. °C	B_r G	H_c Oe	$_iH_c$ Oe	$(BH)_{max}$ MGOe	$4\pi M_s$ G	Density gm/cc
C1	1130/2 hr	1750	1500	2550	0.75	2600	4.20
C2	1160/2 hr	2050	1600	2500	0.89	2800	4.67
C3	1190/2 hr	2050	1550	2450	0.84	2850	4.67
C4	1220/2 hr	2100	1300	1750	0.82	2950	4.77

Table 17(b)

Magnetic properties of sintered samples from C-II series

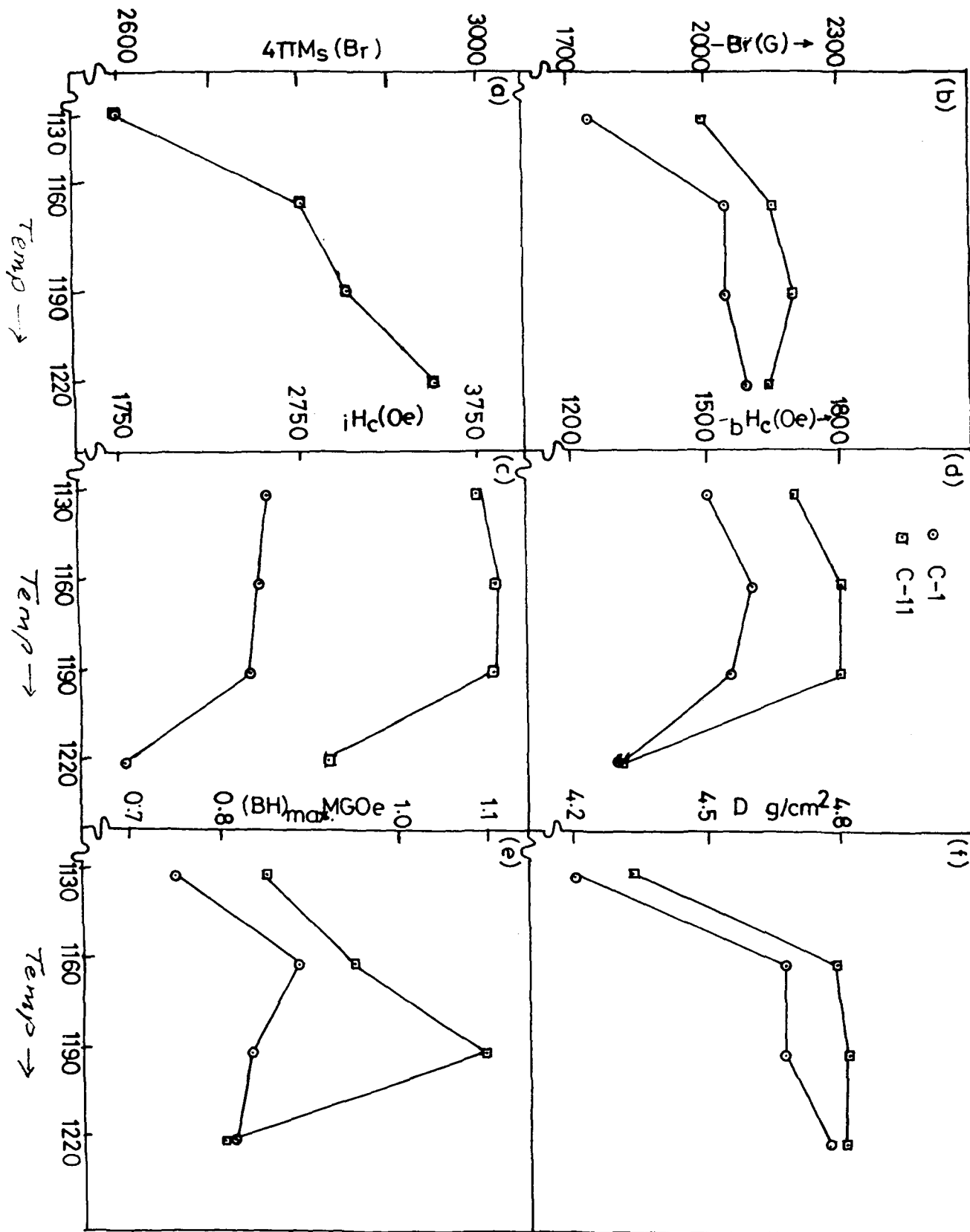| Sample Name	Sintering temp. °C	B_r G	H_c Oe	$_iH_c$ Oe	$(BH)_{max}$ MGOe	$4\pi M_s$ G	Density gm/cc
C11	1130/2 hr	2000	1700	3750	0.85	2600	4.33
C12	1160/2 hr	2150	1800	3850	0.95	2800	4.78
C13	1190/2 hr	2200	1800	3850	1.10	2850	4.81
C14	1220/2 hr	2150	1300	2900	0.80	2950	4.80

Fig. 15 : Effect of nature of coprecipitate on
magnetic properties of Sr-ferrite.

higher by about 7% to 30% for C-II series samples than C-I series samples.

3) The comparison between $_iH_c$ values of the samples from above two series reveals that value of intrinsic coercivity ($_iH_c$) is higher by about 50% for samples from C-II series.

4) It is rather interesting to note that saturation magnetisation is the same for the samples sintered under identical conditions, from both the series (Fig.15d).

3.2.2.4 Microstructural analysis

The particle size of C-I and C-II powders calcined at 750°C and two representative sintered samples namely C-2 & C-12 were examined with the help of scanning electron microscope. The Figs. 16a&b show microstructure of calcined powders C-I and C-II respectively. The calcined powder C-I shows presence of fine particles < 0.5 μm with uniform particle distribution while powder sample C-II shows presence of particles having 0.5 to 1.0 μm size. It is also observed that particles tend to from cluster. Thus submicron size particles can be obtained directly by the coprecipitation method without employing the grinding or milling operation. The difference in particle size and particle distribution of C-I and C-II calcined sample is reflected in their $_iH_c$ value. The powder sample C-II shows comparatively lower $_iH_c$ value.
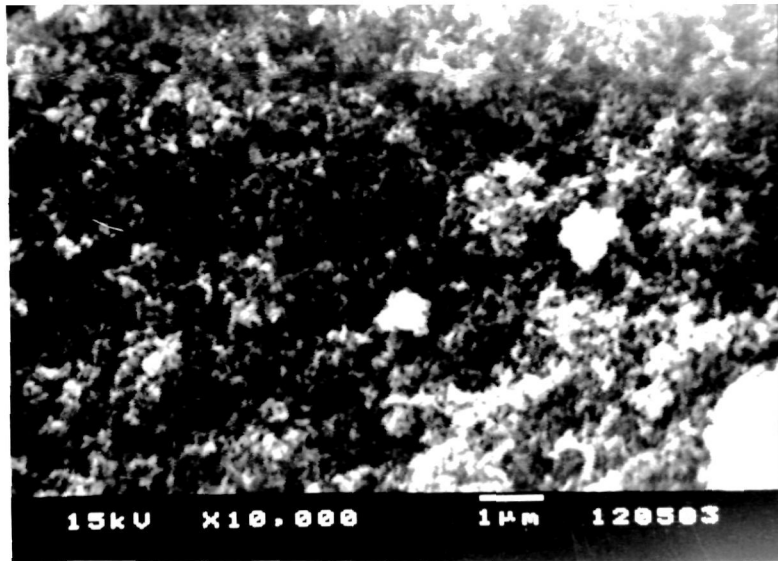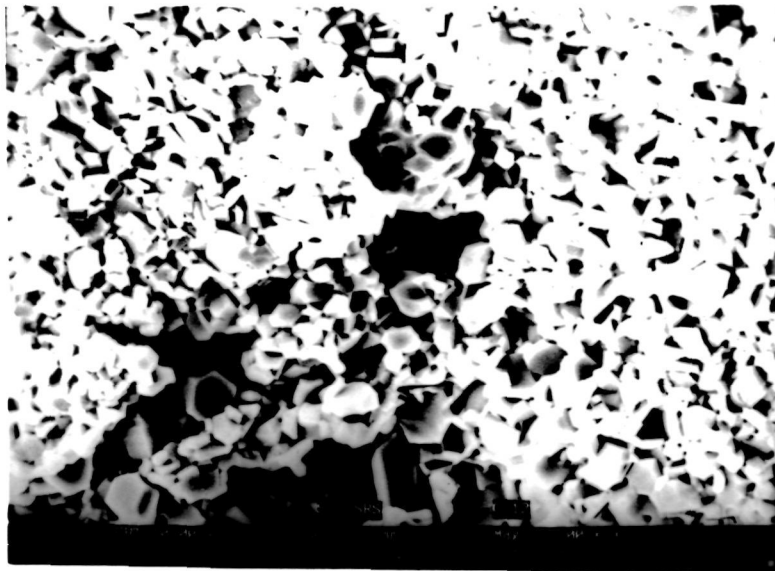
(a)
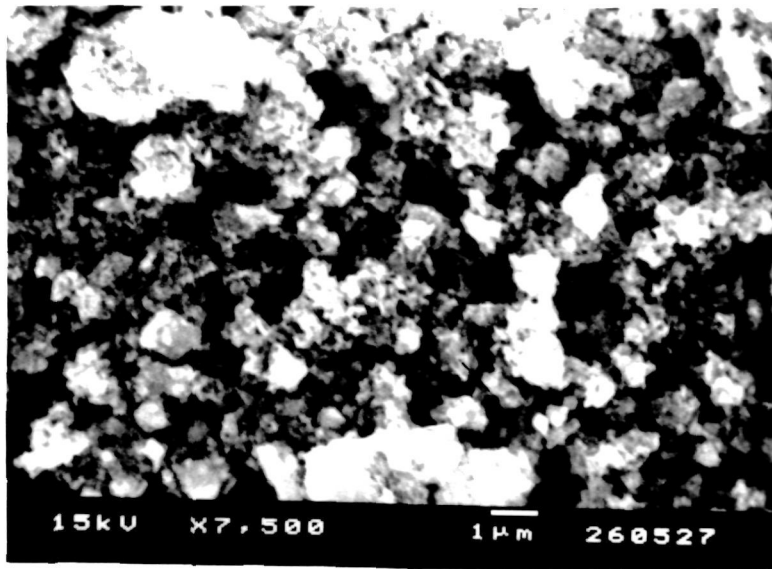
(b)

Fig 16 a-b : Scanning electron micrographs of calcined
powders (a) C-I (b) C-II

(c)

(d)

Fig 16 c-d : Scanning electron micrographs of (a) C-2 (b)
C-12 Sv-ferrite samples sintered at 1160° C

The microphotographs of the strontium ferrite pellets sintered at 1160°C for two hours are shown in Figs. 16c&d. The sintered sample C-2 (sample from C-I series) shows plate-like hexagonal crystals of strontium ferrite of 2-3 um size. The sintered sample C-12 shows grains of 1-2 um size with more uniform distribution. The relatively higher grain size for C-2 sample can be explained as follows. The sample C-2 is derived from calcined powder C-I which is fine and hence more reactive. This results into higher rate of grain growth for the samples derived from C-I calcined powder. Since grain size and $_iH_C$ are interrelated, the difference in average grain size of C-2 and C-12 is reflected in $_iH_C$ value of sintered sample. These results imply that crystallinity of precursor coprecipitate affects the microstructure of calcined and sintered samples which in turn affects magnetic properties.

The difference in magnetic properties can be explained as follows:

i) The remanence is the function of degree of orientation, saturation magnetisation (M_s) and fired density (ϱ). Since all the samples are pressed under identical conditions, we take liberty to presume that degree of orientation is same for all the samples. The samples sintered under identical conditions have same saturation magnetisation. The relatively higher value

of remanence for C-II series samples is therefore attributed to higher degree of densification (Fig.15e).

ii) According to S-W model the particle size is the key factor in determining the $_iH_C$ value. The considerably lower value of $_iH_C$ for C-I series samples is indicating presence of bigger particles than the corresponding samples from C-II series.

The above observations indicated that when precursor sample is crystalline it gives final sintered product with superior magnetic properties.

3.2.3 Effect of sodium ion on magnetic properties of sintered samples

During the extensive study on the optimization of processing parameters in our laboratory, it is found that residual sodium ion concentration affects the magnetic performance parameters of sintered product. In order to investigate the nature of this effect and to obtain the concrete and quantitative picture, systematic experiments were carried out. The additive was mixed at two different stages namely (I) before calcination i.e. in oven dried precursor and (II) after calcination i.e. in calcined powder. The effects of sodium ion on magnetic properties and on microstructure has been studied by various characterization techniques.

3.2.3 (I) Effects of additive :
(mixing before calcination)

A mixture of iron and strontium hydroxides was coprecipitated by using NaOH. The coprecipitate was washed by decantation method, washed precipitate was dried in oven and the oven dried precipitate was divided into nine parts. One part of the same was processed without additive and the green pellets subsequently prepared using this part were labeled as D-251 to D-259. These ten samples (without additive) were used as reference samples during further studies. From remaining eight parts, each part was homogenised with sodium hydroxide solution separately by keeping the sodium percentage in the range of 0.1 to 0.9 weight percentage of the powder. The homogenisation was carried out by wet mixing in pestle and mortar. The wet mixed samples were calcined at optimized temperature and time i.e. 750°C/5 hr. The material was examined at different stages of processing to comprehend the structural, microstructural and magnetic properties of Sr-ferrite.

3.2.3.1 Structural analysis

The examination of XRD pattern of dry coprecipitate of mixed hydroxides showed the presence of α-Fe_2O_3, $Fe_2O_3.H_2O$ and $SrCO_3$ phases (Fig. 17a). The presence of these phases indicated the crystalline nature of coprecipitate XRD pattern of calcined sample D-251 (Fig.
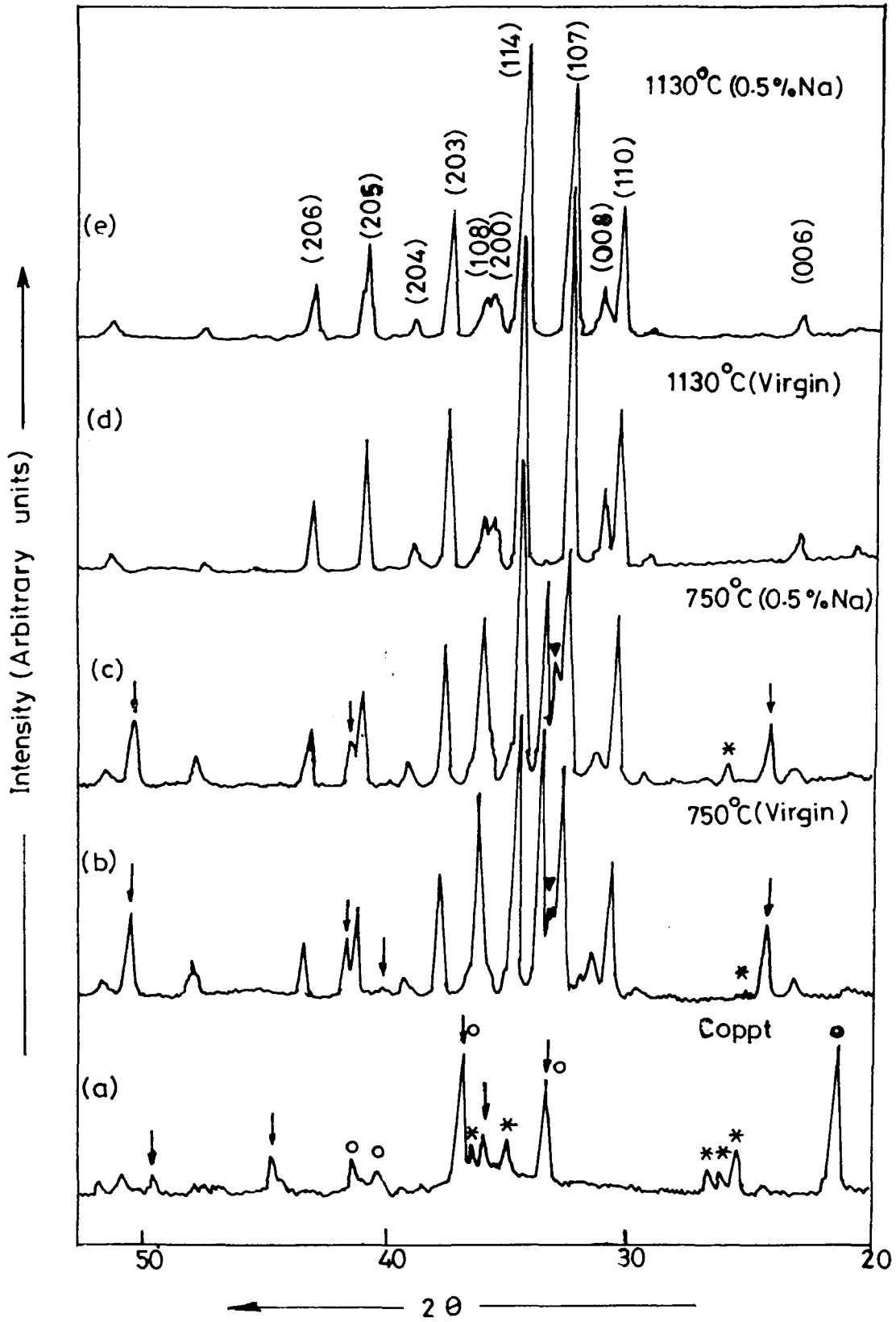
138

Fig. 1.7 : X-ray diffraction patterns of virgin
and doped samples of Sr-ferrite.

17b) showed prominent diffraction peaks ascribable to hexagonal Sr-ferrite ($SrFe_{12}O_{19}$) phase. Peaks corresponding to $\alpha-Fe_2O_3$ and $SrCO_3$ phases are also obtained (Fig. 17c) showed XRD pattern of calcined Sr-ferrite sample with the additive (D-301). It is noticed that the intensities of $SrFe_{12}O_{10}$ peaks are larger while the intensity of $\alpha-Fe_2O_3$ peaks are smaller as compared to that of calcined sample D-251.This is an indication of the increase in the extent of formation of Sr-ferrite phase due to the addition of sodium ions. Single phase Sr-ferrite is obtained on sintering the sample at higher temperature. A representative XRD pattern is given in Fig. 17d. It is important to note that the XRD pattern of samples containing an additive does not show any additional peak attributable to either additive or additive related phases.

Each calcined powder sample was mixed with 1% polyvinyl alcohol (PVA) binder solution. After drying, these powders were pressed into pellets. The pellets were subsequently processed by sintering at different temperatures in the range of 1100°C to 1200°C for 2 hours in air.

3.2.3.2 Magnetic properties

To compute magnetic properties B Vs H and (B-H) Vs H hysteresis graphs were recorded for green and sintered samples. The intrinsic coercivity of reference sample D-251 (sample without additive) is found to be 6000 Oe. The $_iH_C$ is

found to decrease with increase in percentage of additive (mixed in the precursor before calcination) and reaches a value of 4900 Oe when additive concentration becomes 0.9 wt%. The magnetic property measurements are also done on samples fired at 1100°C, 1130°C and 1160°C for 2 hours. The results are tabulated in the Tables 18a,b & c respectively. Figs.18a to f depict changes in magnetic properties as a function of additive percentage graphically, for the samples sintered at 1100°C, 1130°C and 1160°C. The systematic variation in magnetic properties is observed with change in additive concentration at a constant sintering temperature (Figs.18a to f). The magnetic performance parameters of sample sintered at different temperatures are compared to select optimum sintering conditions. Samples sintered at this temperature showed optimum values for remanence (B_r) and coercivity $(_bH_c$ & $_iH_c)$, hence giving rise to the best energy product $(BH)_{max}$. Thus optimum sintering temperature was found to be 1130°C.

The samples sintered at optimum temperature are analysed in more details. The Table 18b gives magnetic properties of samples sintered at 1130°C. Fig. 18 illustrates the variation in magnetic properties as a function of sodium percentage. Variation in magnetic properties is found by comparing magnetic properties of sample without additive i.e. reference sample (D-255). The important features of this study are as follows:
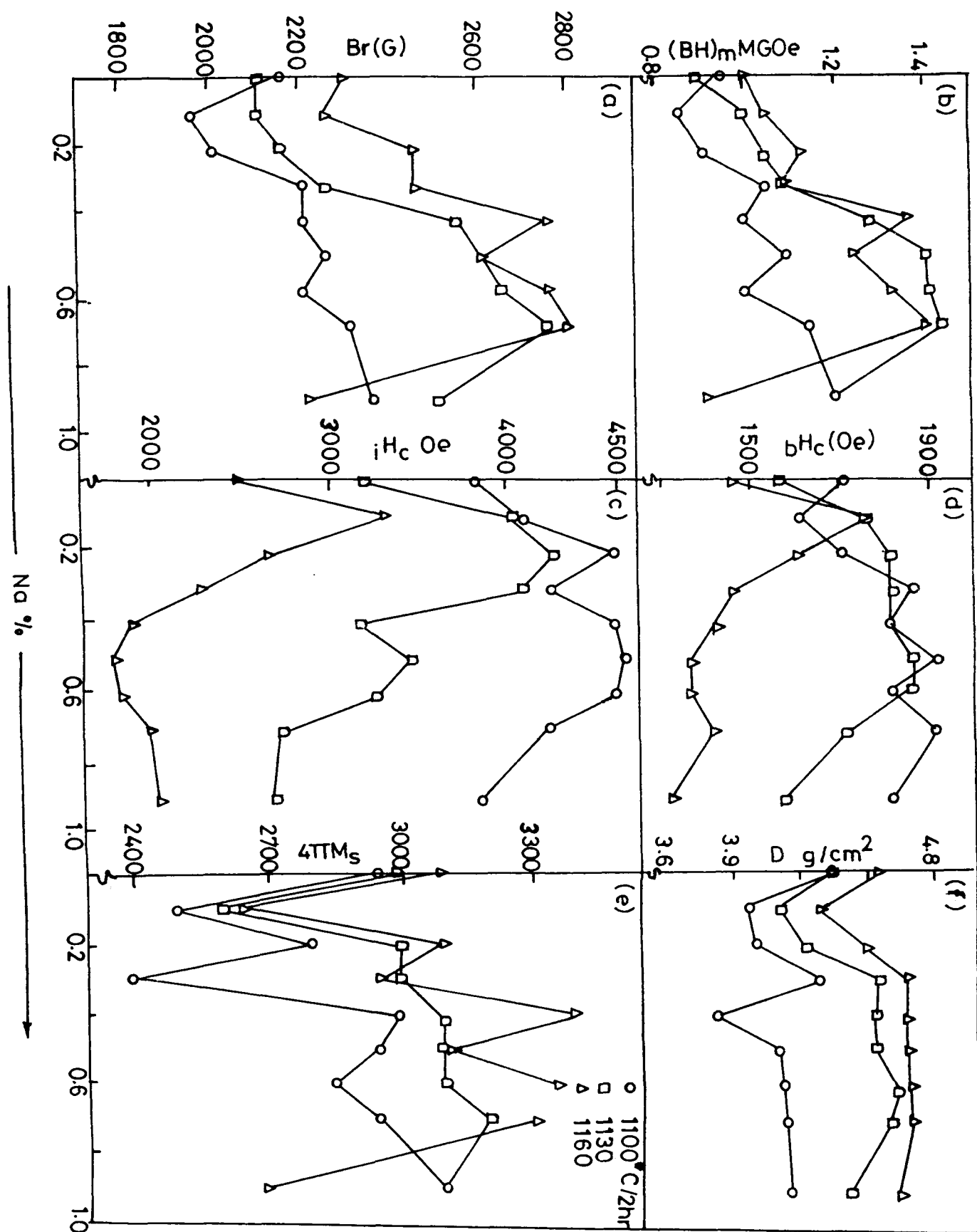
Fig. 18 : Effect of Sodium ion addition on
magnetic properties of Sr-ferrite
(addition before calcination.)

Table 18a

Effect of sodium ion additive on magnetic properties of sintered strontium ferrite

Sintering conditions : 1100°C/2 hrs

Sr. No.	Pellet No.	Sodium %	B_r (G)	H_c (Oe)	iH_c (Oe)	$(BH)_{max}$	$4\pi M_s$	Density gm/cm^3
1	D-252	0.0 Virgin sample	2150	1700	3800	0.935	2950	4.36
2	D-262	0.1	1950	1600	4050	0.85	2500	3.99
3	D-272	0.2	2000	1700	4450	0.90	2800	4.08
4	D-282	0.3	2200	1850	4200	1.04	2400	4.30
5	D-292	0.4	2200	1800	4450	0.99	3000	3.83
6	D-302	0.5	2250	1900	4500	1.09	2950	4.15
7	D-312	0.6	2200	1800	4450	0.99	2850	4.25
8	D-322	0.7	2300	1900	4200	1.145	2950	4.37
9	D-342	0.9	2350	1800	3200	1.195	3100	4.40

Table 18b

Effect of sodium ion additive on magnetic properties of sintered strontium ferrite

Sintering condition: 1130°C/2 hrs

Sr. No.	Pellet No.	Sodium %	B_r (G)	H_c (Oe)	$_iH_c$ (Oe)	$(BH)_{max}$	$4\pi M_s$	Density gm/cm^3
1	D-255	0.0 Virgin sample	2100	1550	3150	0.88	3000	4.43
2	D-266	0.1	2100	1750	4000	0.99	2600	4.10
3	D-275	0.2	2150	1800	4250	1.04	3000	4.24
4	D-286	0.3	2250	1800	3800	1.09	3000	4.55
5	D-294	0.4	2550	1800	3000	1.28	3100	4.53
6	D-305	0.5	2600	1850	3300	1.40	3100	4.58
7	D-314	0.6	2650	1850	3100	1.40	3100	4.67
8	D-324	0.7	2750	1700	2550	1.43	3200	4.59
9	D-344	0.9	2500	1550	2500	1.19	3100	4.42

Table 18c

Effect of sodium ion additive on magnetic properties
of sintered strontium ferrite

(Addition before calcination)

Sintering condition: 1160°C/2 hrs

Sr. No.	Pellet No.	Sodium %	B_r (G)	H_c (Oe)	$_iH_c$ (Oe)	$(BH)_{max}$	$4\pi M_s$	Density gm/cm^3
1	D-256	0.0 Virgin sample	2300	1450	2200	1.00	3100	4.58
2	D-265	0.1	2250	1750	3450	1.04	2650	4.39
3	D-276	0.2	2450	1600	2650	1.12	3100	4.50
4	D-285	0.3	2450	1450	2250	1.08	2950	4.69
5	D-293	0.4	2750	1400	1850	1.36	3400	4.67
6	D-304	0.5	2600	1350	1750	1.24	3100	4.68
7	D-313	0.6	2750	1350	1800	1.32	3350	4.69
8	D-323	0.7	2800	1400	1950	1.40	3300	4.69
9	D-346	0.9	2200	1300	2000	0.90	2700	4.64

a) With increase in sodium concentration B_r increases and attains a maximum value of 2750 G (0.7% of sodium). Further increase in additive concentration decreased the remanent induction.

b) The saturation magnetization ($4\pi M_s$) is found to decrease with incorporation of small amount of additive. But it increases with further increase in additive concentration and attains a maxima of 3200 G at 0.7 wt% of sodium. When this limit is exceeded, its value again decreases.

c) Sintered density shows a similar trend as that of magnetization.

d) The coercivity ($_bH_c$) increases from 1550 Oe to 1800 Oe with addition of 0.2% of sodium. This value remains steady in the range of 0.2% to 0.6% of sodium. When this limit is exceeded, $_bH_c$ is found to decrease and reaches a value of 1550 Oe at sodium ion concentration of 0.9%.

e) The intrinsic coercivity ($_iH_c$) sharply increases by 900 Oe (from 3150 Oe to 4250 Oe) as compared to the reference sample with addition of 0.2 wt% of sodium ions. Its value is found to be continuously decreasing with further incorporation of additive.

f) The energy product, which is a measure of quality of magnet, is 0.88 MGOe for reference sample (D-255). It increases and attains a maxima of 1.43 MGOe for 0.7 wt% of additive concentration. It decreases to 1.19 MGOe

(sample A-344) for additive concentration 0.9 wt%. The
Table 19 gives % increase in magnetic properties with
0.5% additive incorporation.

The variation in magnetic properties of sintered
product with additive incorporation can be explained
as follows:

a)As seen earlier, magnetic properties are functions of
different intrinsic and extrinsic factors. The
remanence is a function of degree of orientation (n_c),
saturation magnetization (M_s) and fired density (ρ)
[14]. To find out the effect of additive on the degree
of orientation, the relative intensity of lines
parallel to the c-axis from XRD patterns of reference
and doped samples are examined. If there is any

Table 19

Percentage increase in magnetic properties

| Magnetic property	Ref. Sample	Sample with 0.5% additive	% increase
B_r	2100 G	2600 G	23.8
$_bH_c$	1500 Oe	1850 Oe	19.3
$(BH)_{max}$	0.88 MGOe	1.40 MGOe	59.0
$4\pi M_s$	3000 G	3100 G	3.33
	4.43 g/cm^3	4.58 gm/cm^3	3.39
$_iH_c$	3150 Oe	3300 Oe	4.76

145

orientation effect, then the lines parallel to the c-axis e.g. [006], [008] etc. of the crystal shows a preferential growth, i.e. their relative intensity increases [80]. But, with additive incorporation, no such change in relative intensity of lines parallel to the c-axis is observed. So results of change in remanence are analysed in the light of change in saturation magnetization and density of sintered sample. The increase or decrease in· remanence is accompanied by increase or decrease in sintered density and saturation magnetization. The maxima and minima of these three properties occur in the same range of additive percentage (Fig. 18). It implies that the change in remanence is a combined effect of change in saturation magnetization and sintered density.

b) As it is suggested from S-W model, the intrinsic coercive force ($_iH_c$) for hard ferrites is directly proportional to magnetocrystalline anisotropy (K), contribution of single domain particles (n_c) and inversely proportional to saturation magnetization (M_s) [19]. The magnetocrystalline anisotropy (K) is material's property. Since all the samples under the study are Sr-ferrite samples, the value of K is the same for all of them. With this background the changes in $_iH_c$ are analysed in the light of microstructural study (which gives idea about grain ·size and its distribution) and variation in magnetization.

146

3.2.3.3 Microstructural analysis

The microstructure of the sintered samples is studied by recording scanning electron micrographs (SEM) of fractured sintered pellets. It is a well established fact that the microstructure is the key factor in governing the bulk magnetic properties of ceramic magnets. The samples D-255, D-275, D-305, D-344 are selected for microscopic analysis. The photographs of microstructure of above samples are shown in Fig.19. The sample D-255 (reference sample) shows nonuniform grain distribution (Fig.19a). The smaller grains are 2-3 um while bigger grains are 8-10 um in size. The nonuniformity in grain size and its distribution is reflected in low value of $_bH_c$ (1550 Oe) and $_iH_c$ (3150 Oe). Uniform grain distribution is observed for sample D-275 (0.2 wt% additive, added before calcination) with average grain size of 1-2 um. The grain distribution becomes narrow with incorporation of small amount of additive, as a consequence of which, contribution of single domain particles increases and hence the intrinsic coercivity increases.

The best magnetic properties amongst above samples were recorded for the sample D-305 (0.5% of sodium). The micrographs of fractured sintered pellet (Fig.19c) shows average grain size 2-3 μm, with narrow grain distribution. Though grain size distribution is narrow, the average grain
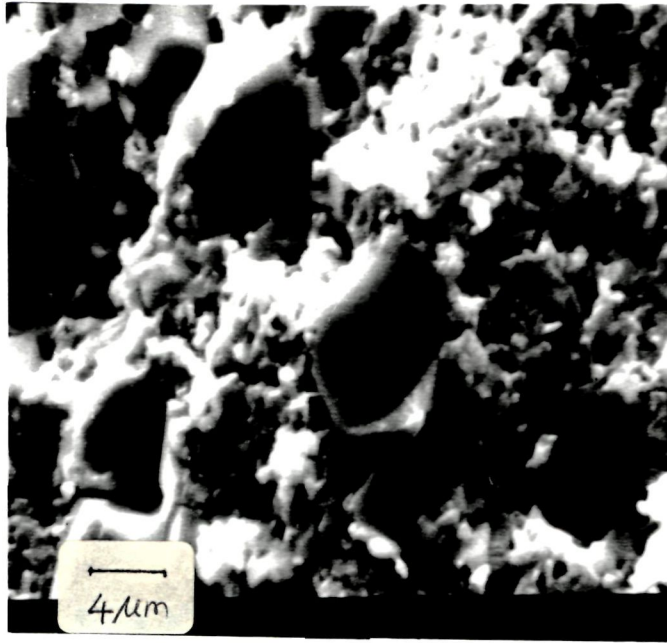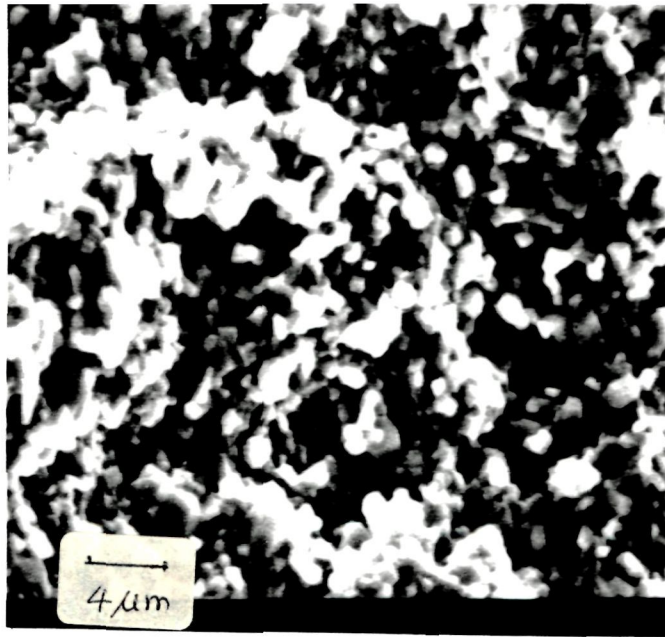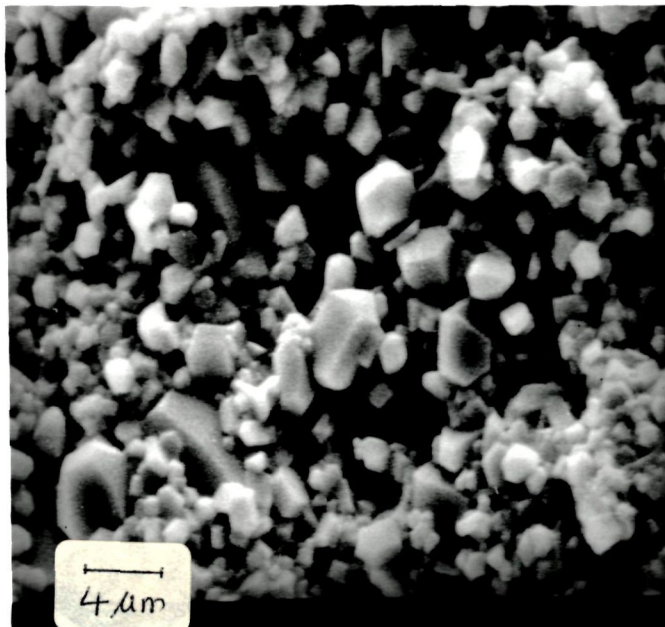
(a)
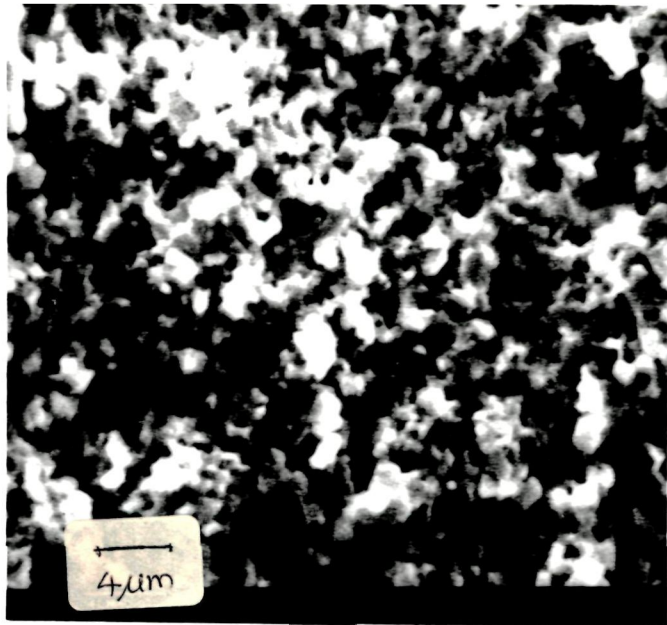
(b)

Fig 19 a-b : Scanning electron micrographs of sintered
samples (a) D-255 (b) D-275

(c)

(d)

Fig 19 c-d : Scanning electron micrographs of sintered
smaples (c) D-305 (d) D-344

size is increased. Due to the increase in grain size, single domain particles become multidomain. So contribution of single domain particles decreases and hence the $_iH_C$ decreases. The microscopic structure of the sample with 0.9 wt% additive (sample D-344, Fig.19d) shows smaller grains with size about 2-4 μm, while bigger grains are 8-10 μm in size. Big voids are also seen. This indicates that grain distribution in sample D-344 is nonuniform. The $_iH_C$ which directly depends on microstructure, is found to decrease up to 2500 Oe. This analysis supports the increase and decrease in intrinsic coercivity ($_iH_C$) value.

Two representative samples, namely D-255 (reference sample) and D-305 (a sample with the best magnetic properties) were analysed with the help of electron probe microanalysis (EPMA). EPMA analysis was carried out at different points and areas, mainly for atomic percentage of Na, Sr and Fe. The results of the analysis are given in Table 19.

The results show that for sample D-255, Fe/Sr ratio has varied from 11.6 to 32.9 as against the expected variation between 11 to 12 (Table 20a). The broad range of this ratio implied chemical inhomogeneity at microstructural level in reference sample D-255.

Fe/Sr ratio for sample D-305 lies between 11.4 and 15.5 (Table 20b), which is an indication of increase in chemical

homogeneity at microscopic level which again may be due to sodium ion incorporation.

The changes in magnetic performance parameters, with variation in additive percentage of samples sintered at other two temperatures (1100°C and 1160°C respectively) can be explained in a similar way.

The above results of magnetic properties of samples with additive shows that with addition of sodium (as sodium hydroxide), the magnetic properties of sintered compacts are increased, reach a maxima for certain additive concentration and then decrease for excess additive concentration. A systematic variation in magnetic properties of Sr-ferrites is observed with additive incorporation at different sintering temperatures. When optimum amount of additive is added, the magnetic properties are found to be considerably improved, as compared to the samples without additive. The optimum amount of additive is found to be in the range of 0.4 to 0.7 wt% of sodium.

During the study of effect of additives on magnetic performance parameters, different samples were derived using the coprecipitate from the same batch. So for the samples, which were sintered at the same temperature and time, preparation and processing parameters are identical, except intensionally incorporated amount of additive. This implies

Table 20a

EPMA analysis of sample $\cancel{D}$-255

Area	I	II	III	IV	V
NaK$_a$	-	0.26	0.88	-	0.16
FeK$_a$	93.69	91.80	94.70	97.05	91.93
SrL$_a$	6.31	7.94	4.42	2.95	7.91
Fe/Sr ratio	14.84	11.56	21.42	32.89	11.62

Table 20b

EPMA analysis of sample $\cancel{D}$-305 .

Area	I	II	III	IV	V	VI
NaK$_a$	-	-	0.79	0.28	0.41	0.99
FeK$_a$	93.7	93.96	92.15	91.68	93.02	91.37
SrL$_a$	6.3	6.04	7.06	8.05	6.57	7.64
Fe/Sr ratio	14.87	15.58	13.05	11.38	14.15	11.96

150

that the change in microstructure and variation in magnetic properties of sintered Sr ferrite samples is only due to the variation in sodium percentage.

3.2.3.4 Role of additive

Additional experiments were performed to understand the role of sodium ions. In these experiments, the coprecipitate of strontium and iron was synthesized in three different batches by following the same procedure as that of batch D. The dry coprecipitate from each batch was mixed with different additive percentages.

Batch I - The coprecipitate was mixed with 0.2 wt% of sodium ion (additive concentration was lower than the optimum concentration).

Batch II - The coprecipitate from the second batch was mixed with 0.4 wt% of sodium ion (optimum concentration of additive).

Batch III - The coprecipitate was mixed with 0.9 wt% of sodium ion (excess additive concentration).

All the three coprecipitates were calcined at 750°C/5 hrs. After calcination, calcined powder from each batch was divided into two parts. In order to remove Na ions from calcined powder, one part (from all the three batches) was washed with hot distilled water. The removal of Na ion was checked by testing the washing with the help of flame photometer. The second part of the calcined powder was

processed without washing. The six powders thus obtained were labelled as follows:

Batch No.	Unwashed calcined powder [Pellet numbers]	Washed calcined powder [Pellet numbers]
I	D-770 to D-779	D-780 to D-789
II	D-730 to D-739	D-740 to D-749
III	D-760 to D-769	D-750 to D-759

Structural and magnetic property measurements of washed and unwashed calcined powder were carried out using powder X-ray diffractogram and VSM. XRD pattern and magnetic properties of washed and unwashed calcined samples from the same batch were found to be identical. This implied that washing after calcination did not affect structural and magnetic properties.

The pellets prepared from these calcined powders were sintered in the temperature range 1100°C-1200°C for two hours. The magnetic properties of sintered samples were computed from hysteresis loop. The magnetic performance parameters of sintered compacts, obtained from washed and unwashed calcined material of the same batch were compared. The comparison gave us idea about (a) role of additive during sintering and (b) effect of removal of additive after calcination on magnetic properties.

Magnetic properties

Magnetic properties of sintered samples from above three batches are compiled in Tables 21a, b & c. The

Table 21(a)

Magnetic properties of sintered Sr-ferrite samples: Batch-I

(Unwashed samples)

(Amount of sodium mixed before calcination = 0.2%)

Pellet No.	Sintering conditions °C	B_r G	$_bH_c$ Oe	$_iH_c$ Oe	$(BH)_{max}$ MGOe	$4\pi M_s$ G	Density gm/cc
D-774	1100/2 hr	1900	1600	4550	0.76	2550	3.96
D-772	1130/2 hr	2100	1750	4000	0.95	2800	4.35
D-776	1150/2 hr	2250	1900	4000	1.1	2800	4.49
D-777	1180/2 hr	2400	1750	2550	1.17	2700	4.56

(Washed samples)

(Additive is removed from calcined powder by washing)

Pellet No.	Sintering conditions °C	B_r G	$_bH_c$ Oe	$_iH_c$ Oe	$(BH)_{max}$ MGOe	$4\pi M_s$ G	Density gm/cc
D-784	1100/2 hr	1700	1450	4450	0.64	2300	3.78
D-782	1130/2 hr	1850	1550	3900	0.72	2400	4.14
D-786	1150/2 hr	1950	1600	4000	0.76	2850	4.14
D-787	1180/2 hr	1950	1000	1950	0.58	3150	4.48

Table 21(b)

Magnetic properties of sintered Sr-ferrite samples: BatchII

(Unwashed samples)

(Amount of additive mixed before calcination = 0.4%)

Pellet No.	Sintering conditions °C	B_r G	$_bH_c$ Oe	$_iH_c$ Oe	$(BH)_{max}$ MGOe	$4\pi M_s$ G	Density gm/cc
A-730	1100/2 hr	1800	1650	4550	0.76	2550	4.35
A-731	1130/2 hr	2150	1800	4300	0.945	2600	4.54
A-733	1150/2 hr	2400	2050	4200	1.26	2650	4.63
A-734	1180/2 hr	2650	1800	3000	1.45	2650	4.66

(Washed samples)   .

(i.e. additive is removed after calcination by washing)

Pellet No.	Sintering conditions °C	B_r G	$_bH_c$ Oe	$_iH_c$ Oe	$(BH)_{max}$ MGOe	$4\pi M_s$ G	Density gm/cc
A-740	1100/2 hr	1850	1550	4450	0.76	2400	3.72
A-741	1130/2 hr	2050	1750	4400	0.900	2300	4.08
A-743	1150/2 hr	2100	1800	4050	0.90	2350	4.21
A-744	1180/2 hr	2200	1600	3350	0.935	2550	4.41

Table 21(c)

Magnetic properties of sintered Sr-ferrite samples:Batch III

(Unwashed samples)

(Amount of Na mixed before calcination = 1.0%)

Pellet No.	Sintering conditions °C	B_r G	$_bH_c$ Oe	$_iH_c$ Oe	$(BH)_{max}$ MGOe	$4\pi M_s$ G	Density gm/cc
D-760	1100/2 hr	2100	1800	4800	0.94	2350	4.56
D-761	1130/2 hr	2050	1800	4800	0.94	2350	4.57
D-763	1150/2 hr	2000	1700	4850	0.90	2600	4.53
D-764	1180/2 hr	1950	900	2600	0.40	2450	4.57

(Washed samples)

(Additive is removed from calcined powder)

Pellet No.	Sintering conditions °C	B_r G	$_bH_c$ Oe	$_iH_c$ Oe	$(BH)_{max}$ MGOe	$4\pi M_s$ G	Density gm/cc
D-750	1100/2 hr	1900	1600	4300	0.76	2200	4.01
D-751	1130/2 hr	2000	1650	4050	0.80	2400	4.16
D-753	1150/2 hr	2150	1800	4200	0.93	2650	4.37
D-754	1180/2 hr	1750	1450	4100	0.64	2000	4.32

155

magnetic performance parameters of sintered samples derived from washed and unwashed calcined powders of the same batch were compared. The salient features of the comparison are as follows:

1) Magnetic properties such as remanence (B_r), energy product (BH)$_{max}$, saturation magnetization ($4\pi M_s$) and sintered density (ϱ) are found to be higher for pellets of unwashed samples than washed samples from the same batch.

2) Sintered samples containing additive (i.e. unwashed samples) show relatively higher $_bH_c$ and $_iH_c$ than the washed sample from the same batch.   .

3) Sintered density is also found to be greater for unwashed samples.

These observations are consistent for all the three batches.

The results of magnetic property measurements from all the three batches can be explained as follows. The washed and unwashed calcined powders from the same batch are found to have identical XRD pattern and magnetic properties. Since washed calcined sample is obtained by simply washing calcined powder with additive by distilled water it is reasonable to assume that particle size and particle size distribution in washed and unwashed calcined samples from the same batch would be identical. The green pellets from these two calcined samples are processed under identical conditions. The only differnece present between them is

presence of additive in unwashed calcined powder. The results of magnetic property measurements of sintered compacts indicate that the presence of sodium, as an additive, during sintering is useful for improvement in saturation magnetization $(4\pi\,M_s)$, magnetic induction (B_r), energy product $(BH)_{max}$, and better densification. The presence of additive is also found to be useful for higher $_bH_c$ and $_iH_c$ values in most of the cases. On the other hand, when additive is mixed before calcination and removed from the material after calcination, deterioration in magnetic performance parameters is observed. This observation is consistent for all the three batches. The comparative study of magnetic properties between three different batches reveals that the best magnetic properties are obtained only when optimum amount of additive is mixed with the comprecipitate (Batch II, series D-730). The addition of excess amount of additive is found to be responsible for deterioration of magnetic properties (Batch III, series D-760).

The above discussion implies that the difference in magnetic performance parameters of sintered compact obtained from washed and unwashed calcined powder of the same batch is only due to the presence of sodium during sintering. It can be concluded that 'presence of additive' plays an important role during sintering.

SEM/EPMA Analysis

The additive incorporated may be present in different regions such as (1) surface of particle, (2) grain boundary and (3) void. To find in which regions additive is segregated and to investigate probable role of additive one of the samples from each batch is analysed with the help of electron probe microanalysis. The samples chosen for analysis are D-786 (sodium is removed after calcination), D-733 (0.4% sodium) and D-763 (0.9% sodium).

The results of EPMA analysis of D-786 are compiled in the Table-22. The point and area analysis of sample A-786 shows that sodium is scarcely present (Table 22a). The ratio of Fe/Sr is in between 11.87 to 15.66. The analysis of sample D-733 (Table 22b) reveals that sodium is absent on surface of particle (Fig.20d). The ratio of Fe/Sr is 15.12 on the particle's surface. The Fe/Sr ratio in general part is nearly equal to ~ 12 (11.92 in Fig.20c and 12.6 in Fig.20e). The percentage of sodium in this area is 0.5 and 0.7 respectively which is nearly equal to amount of sodium externally added as an additive. The iron to strontium ratio is very high in area of black cavity (Fig.20f). The percentage of sodium is 1.0 in cavity. This is higher than amount of sodium added. The results of EPMA analysis of A-763 are summarized in Table 22c. The analysis of general part shows 0.6% of sodium and Fe/Sr ratio 9.69 (Fig.20g). In black cavity percentage of sodium is higher as compared to

Table 22a

EPMA Analysis of sample D-786

Analysis	Area probed	Atomic percent Na	Fe	Sr	Fe/Sr ratio	Fig. No.
Point	1) Specific	0.0	94.0	6.0	15.66	-
	2) Specific	0.0	93.7	6.3	14.87	-
	3) Specific	0.0	92.4	7.6	12.15	-
Area	4) Surface of particle	0.0	94.1	5.9	15.95	20a
	5) General part	0.1	92.1	7.8	11.87	20b

Table 22b

EPMA Analysis of sample D-733

Analysis	Area probed	Atomic percent Na	Fe	Sr	Fe/Sr ratio	Fig. No.
Point	1) Specific	0.0	92.9	7.1	13.08	-
	2) Specific	0.0	93.0	7.0	13.28	-
	3) Specific	0.6	92.7	6.6	14.05	-
Area	1) General part	0.7	92.0	7.3	12.6	20c
	2) General part	1.1	92.1	6.8	13.54	-
	3) General part	1.6	91.7	6.7	13.69	-
	4) Surface of particle	0.0	93.8	6.2	15.12	20d
	5) General part	0.5	92.8	7.7	11.92	20e
	6) Black cavity	1.0	98.4	0.5	197.0	20f

159

Table 22c

EPMA Analysis of sample D-763

Analysis	Area probed	Atomic percent			Fe/Sr ratio	Fig. No.
		Na	Fe	Sr		
Area	1) General part	0.6	90.1	9.3	9.69	20g
	2) Black cavity	4.9	87.4	7.7	11.35	20h
	3) General part	2.8	90.2	7.0	12.88	20i
	4) Black cavity+ white particle	0.8	94.7	4.5	21.04	20j
	5) Black cavity	1.5	94.5	4.0	23.67	20k
	6) General part	2.2	91.0	6.8	13.38	20l

general part. The ratio of Fe/Sr is high in these areas (21.04 in Fig.20j and 23.67 in Fig.20k) due to depletion in percentage of strontium. From EPMA it is evident that sodium is not present on surface of particle but it segregates in voids and in between area of the particles. This helps in controlling particle size during sintering. When additive concentration is ~ 1% its distribution is inhomogeneous (sample D-763).
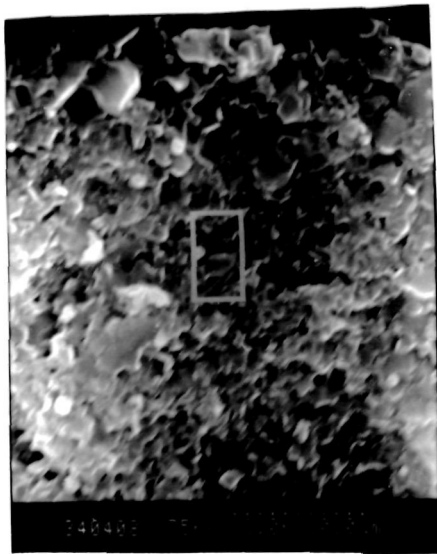
The additive sodium ion is mixed with precursor sample in the form of sodium hydroxide. Since amount of additive is very small ($\leq$ 1% by wt.) it is difficult to find out whether additive reacts with material or it forms a secondary phase etc. with the help of XRD analysis. Separate experiments are
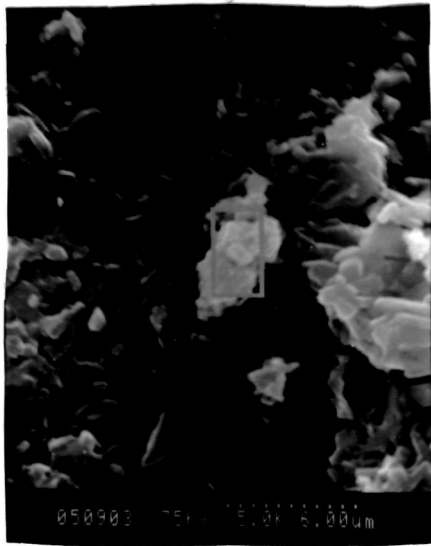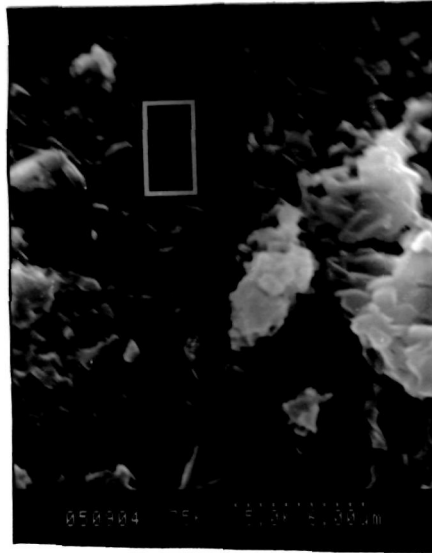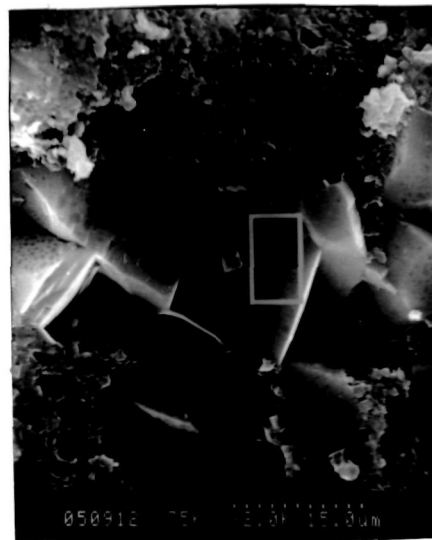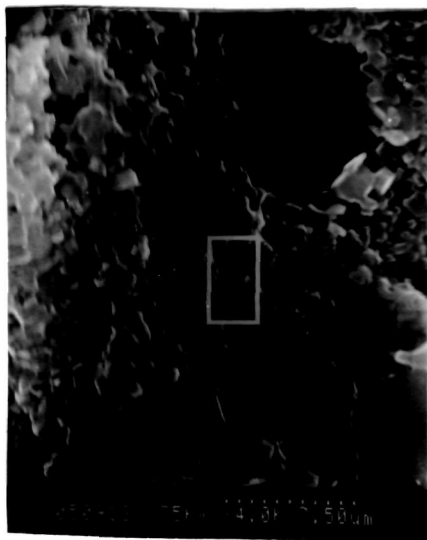
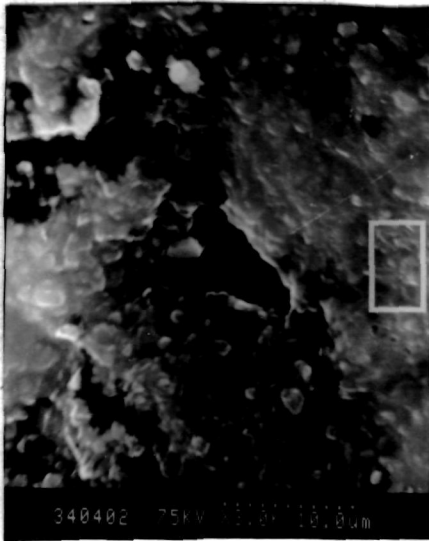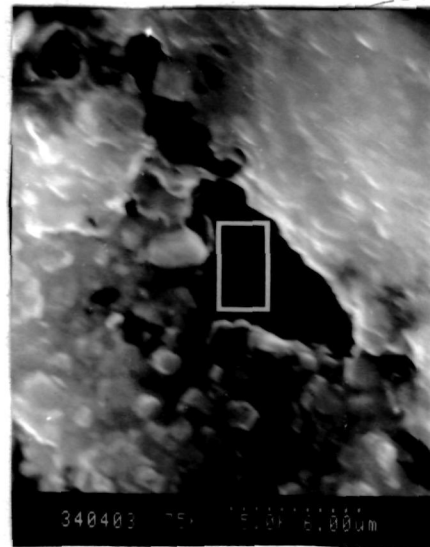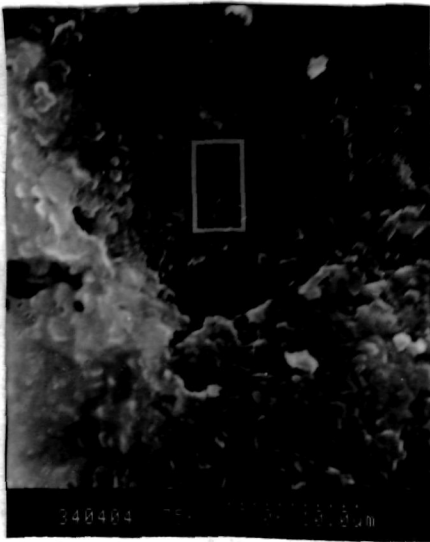Fig 20 **a**-f : Scanning electron micrographs of simtered
samples D-786 (Fig 20 a & b) D-733 (Fig 20 c -20 f

(g)

(h)

(i)
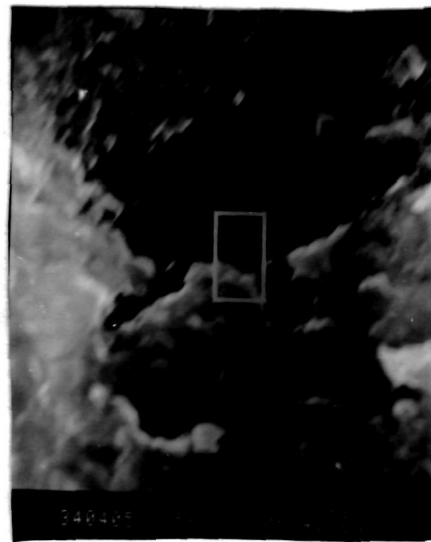
(j)
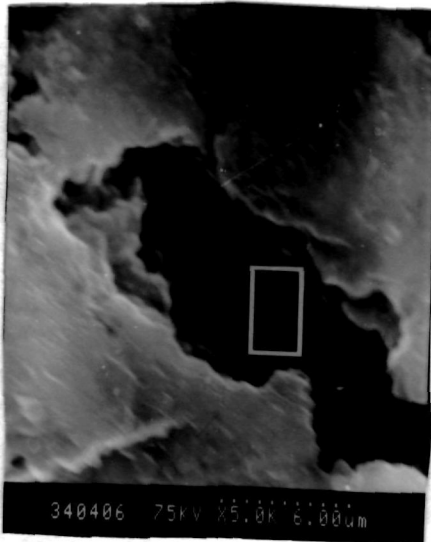
(K)
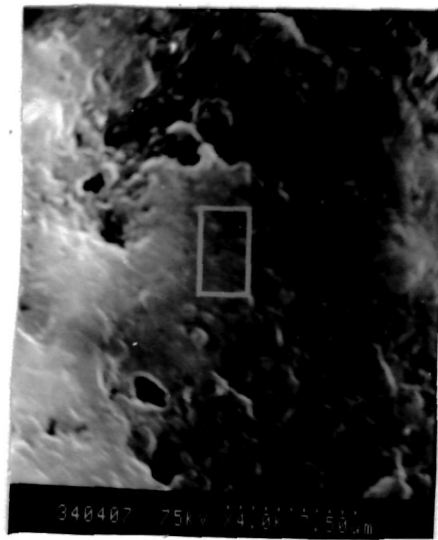
(L)

Fig 20 g-l : Scanning electron micrographs of sintered
sample D-763

carried out to find out the the answer. In first experiment

NaOH and αFe$_2$O$_3$ are mixed together in a molar ratio 1:1. The

mixture is fired at 750°C. The product is analysed with the

help of X-ray diffractogram. The XRD pattern shows presence

of peaks corresponding NaFeO$_2$ [81] along with some peaks of

unknown phase (Fig.21). In another experiment NaOH is added

to dried precursor keeping sodium percentage equal to three.

The coprecipitate is calcined at usual temperature. In

calcined sample along with peaks of SrFe$_{12}$O$_{19}$ very small

peaks corresponding to NaFeO$_2$ are also seen. it implies

that additive is not inert but reactive one.

The results of above study and EPMA indicate that,

1)   When small amount of additive is mixed in precursor, it

       reacts with excess iron oxide which, in turn, helps in

       bringing chemical homogeneity at microscopic level.

2)   Since amount of additive is very small and hence

       detection of compound formed is beyond the limit of

       powder X-ray diffractometry.

3)   This newly formed compound segregates at grain boundary

and controls microstructure during sintering.

3.2.3 (II) Effects of additive: Mixing after
calcination

The mixing of additive in Sr-ferrit precursor (addition

before calcination have distinct effects on magnetic properties and microstructure of sintered compacts. With this background, we try to investigate the effect of an additive when it is mixed after calcination. For this study polycrystalline strontium ferrite was synthesized by following coprecipitation route (Experimental details are given in Chapter 2). After calcination of optimum temperature and time, the calcined powder was divided into six parts. One part was processed without additive. From the remaining five parts, each was wet mixed with predetermined quantity of sodium ion (as NaOH) from 0.2 to 1.0 wt% of ferrite powder. The wet-mixed powders were dried at 100°C in air.

At the various stages of processing, the structural and magnetic properties of material were investigated with the help of powder X-ray diffractogram, B-H loop tracer and scanning electron microscope.

3.2.3.5 **Structural Analysis**

The XRD pattern of dry coprecipitate calcined powder and sintered material are given in Fig.22. The dried precipitate is crystalline (Fig.22a). Calcined powder without additive shows presence of phases such as $SrFe_{12}O_{19}$, $SrCO_3$ and $\alpha\text{-}Fe_2O_3$ (Fig.22b). No additional phase is observed with mixing of additive in the calcined powder which is because the amount of additive is below the detection limit
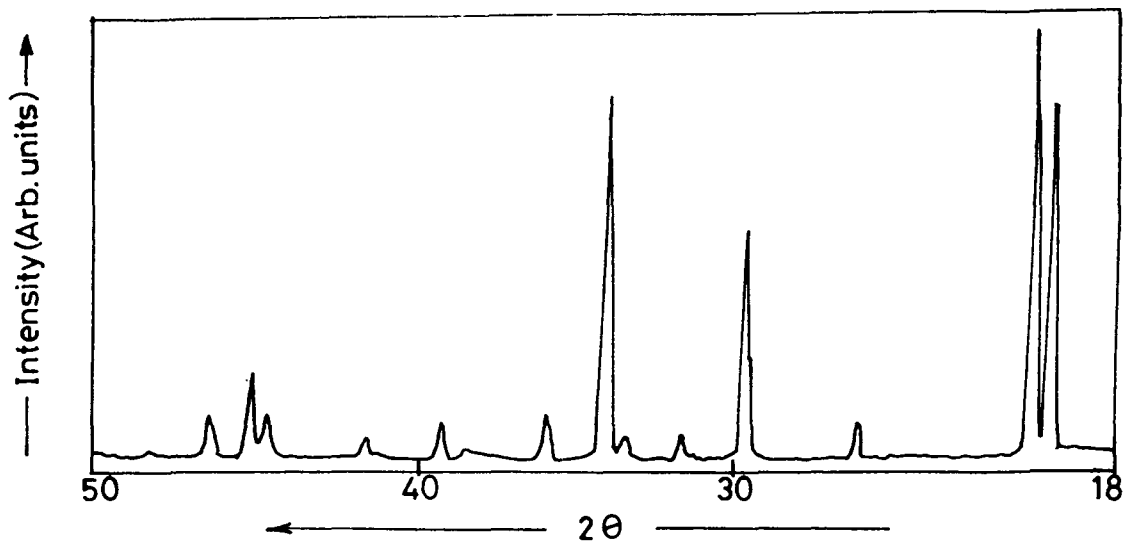
Fig. 21 : X-ray diffraction pattern of NaFeO₂.
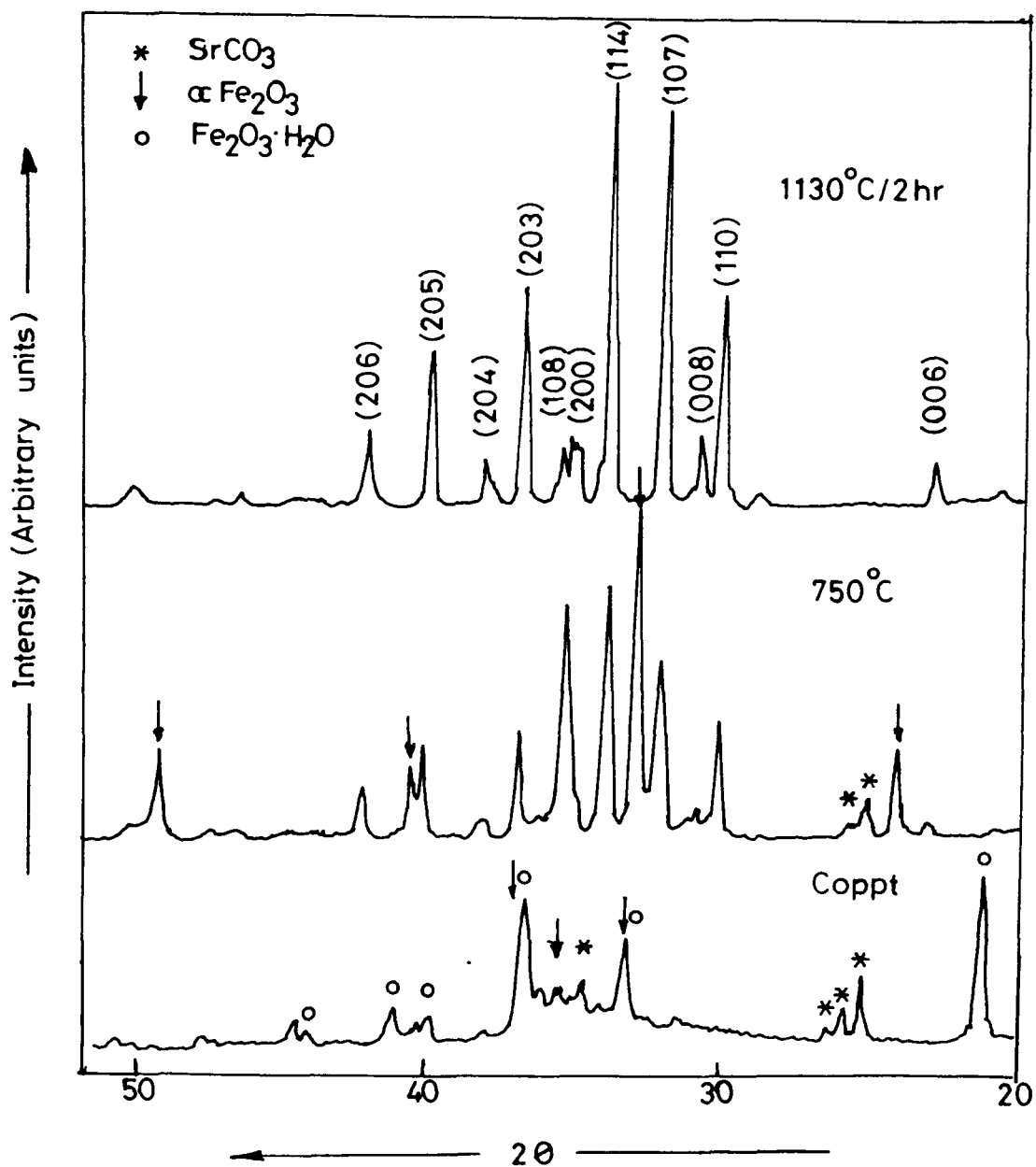
Fig. 22 : X-ray diffraction patterns of Sr-ferrite
samples from batch E.

of the instrument. The single phase formation of $SrFe_{12}O_{19}$ is observed in case of sintered sample (Fig.22c).

3.2.3.6 Magnetic Properties

The plots of B Vs H and (B-H) Vs H hysteresis loops were recorded for calcined samples with and without additive. The magnetic properties of green pellets were computed from these loops. The remanence (B_r) and coercivity ($_bH_c$) are ~ 600 G and 450 Oe respectively for samples with and without additive. The intrinsic coercivity is found to be 4700 Oe for all the samples. Thus the XRD studies and magnetic property measurement of calcined samples reveal that the samples are identical in respect of structure and magnetic properties.

The sintering of green pellets with and without additive was carried out by heating them at 1100°C, 1130°C and 1160°C for two hours. The Tables 23(a), (b) & (c) respectively give magnetic properties of samples sintered at these temperatures. Figs. 23-a to f depict graphical presentation of change in magnetic properties, with incorporation of additive, for samples sintered at 1100°, 1130°C and 1160°C respectively. As seen from Table 23 and Fig.23, usually magnetic properties are found to increase with increase in percentage of additive, reach maxima and

163
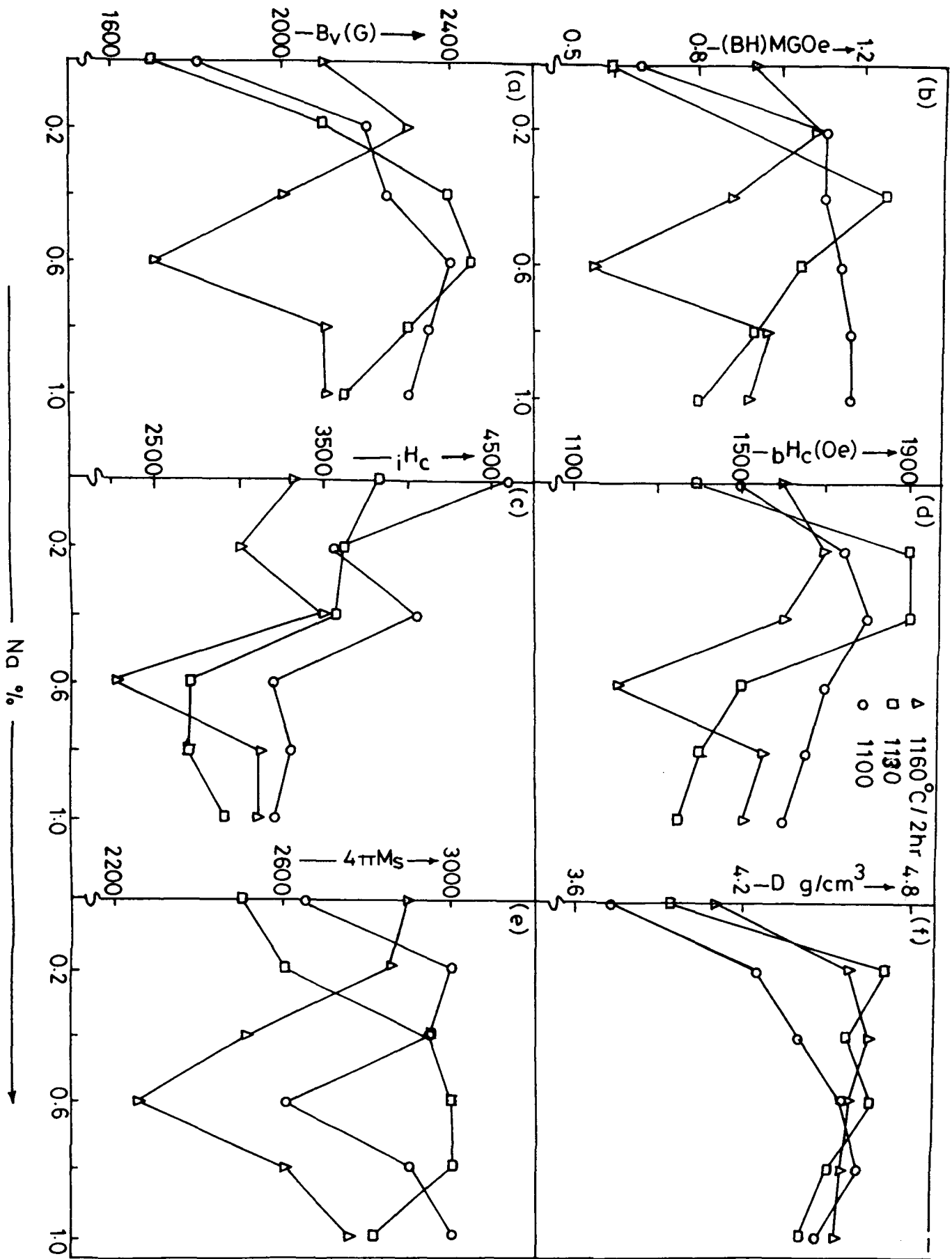
Fig. 23: Effect of Sodium ion addition on
magnetic properties of Sr-ferrite
(addition after calcination.)

Table 23a

Effect of additive on magnetic properties of sintered Sr-ferrite (addition after calcination)

Sintering conditions : 1100°C/2 hrs

Pellet No.	Sodium %	B_r (G)	$_bH_c$ (Oe)	$_iH_c$ (Oe)	$(BH)_{max}$	$4\pi M_s$	Density gm/cm^3
E-11	0.0	1800	1500	4600	0.67	2650	3.73
E-21	0.2	2200	1750	3550	1.10	3000	4.25
E-31	0.4	2250	1800	4050	1.10	2950	4.41
E-41	0.6	2400	1700	3200	1.13	2600	4.57
E-51	0.8	2350	1650	3300	1.06	2900	4.60
E-61	1.0	2300	1600	3250	1.06	3000	4.46

Table 23b

Effect of additive on magnetic properties of
sintered Sr-ferrite (addition after calcination)

Sintering conditions: 1130°C/2 hrs

Pellet No.	Sodium %	B_r (G)	$_bH_C$ (Oe)	$_iH_C$ (Oe)	$(BH)_{max}$	$4\pi M_s$	Density gm/cm^3
E-12	0.0	1700	1400	3850	0.60	2500	4.11
E-22	0.2	2100	1900	3650	1.10	2600	4.60
E-32	0.4	2400	1900	3600	1.25	2950	4.64
E-42	0.6	2450	1500	2700	1.04	3000	4.59
E-52	0.8	2300	1400	2700	0.94	3000	4.55
E-62	1.0	2150	1350	2900	0.81	2800	4.52

Table 23c

Effect of additive on magnetic properties of
sintered Sr-ferrite (addition after calcination)

Sintering conditions: 1160°C/ 2 hrs

Pellet No.	Sodium %	B_r (G)	$_bH_c$ (Oe)	$_iH_c$ (Oe)	$(BH)_{max}$	$4\pi M_s$	Density gm/cm^3
E-3	0.0	2100	1600	3300	0.94	2900	4.40
E-13	0.2	2300	1700	3000	1.08	2850	4.71
E-23	0.4	2000	1600	3500	0.88	2500	4.58
E-33	0.6	1700	1200	2550	0.54	2250	4.66
E-43	0.8	2100	1550	3100	0.97	2600	4.00
E-53	1.0	2100	1500	3100	0.92	2750	4.00

166

thereafter decrease. The graphical presentation indicates that optimum properties are obtained for the samples sintered at 1130°C.

In view of these results, the magnetic properties of samples sintered at 1130°C are evaluated in more detail. Magnetic properties of sample with additive are compared with that of virgin sample to understand changes in magnetic performance parameters with additive incorporation. Following are some important observations of the study (Table 23b):

a)   The remanence increases from 1700 G to 2450 G as the percentage of sodium increased from 0.0 to 0.4% and drop down to 2150 G with increasing sodium concentration to 1.0%.

b)   The changes in other magnetic properties like energy product $(BH)_{max}$, saturation magnetization $(4\pi M_s)$ and sintered density (ς) as a function of additive concentration also show similar trend as that of remanence (B_r).

c)   The $_bH_c$ initially increases up to additive concentration 0.4 wt% but decreases thereafter.

d)   The intrinsic coercivity is found to decrease continuously with increase in additive concentration. This decrease is small up to 0.4% of sodium (from 3850 Oe to 3600 Oe). When this limit is exceeded, sharp drop in $_iH_c$ is noticed for 0.6% and 0.8% of additive (from 3850 Oe to 2700 Oe).

167

To find out whether there is any orientation due to additive incorporation, the XRD pattern of sample without additive (virgin sample) and with additive are analysed. The XRD pattern of sintered sample with additive is not showing any preferential increase in intensity of lines parallel to c-axis {(006), (008) etc.} [85]. This indicates that there is no change in degree of orientation due to mixing of additive. Other important factors which affect remanent induction is saturation magnetization ($4\pi M_s$) and sintered density (ρ). The increase or decrease in remanence goes hand in hand with saturation magnetization and density. So change in remanence with additive of sodium ion is ascribed to changes in saturation magnetization and sintered density.

SEM Studies

The morphology of the sintered compacts is studied from scanning electron micrographs of the factured sintered samples. The microstructure of samples are shown in Fig. 24. The average grain size for sample without additive (Fig.24a) and with 0.4% additive (Fig.24b) is 1-2 μm. On further increase in the concentration of the additive ($\geq$ 0.6%), the average grain size increases to 2-4 um (Fig.24-c&d). With increase in particle size contribution of single domain size particle decreases leading to deterioration in intrinsic coercivity value.
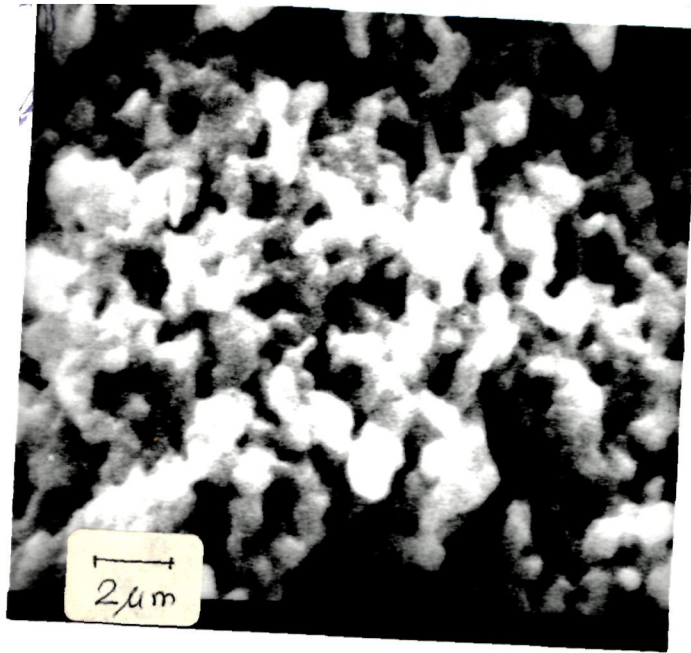
(a)
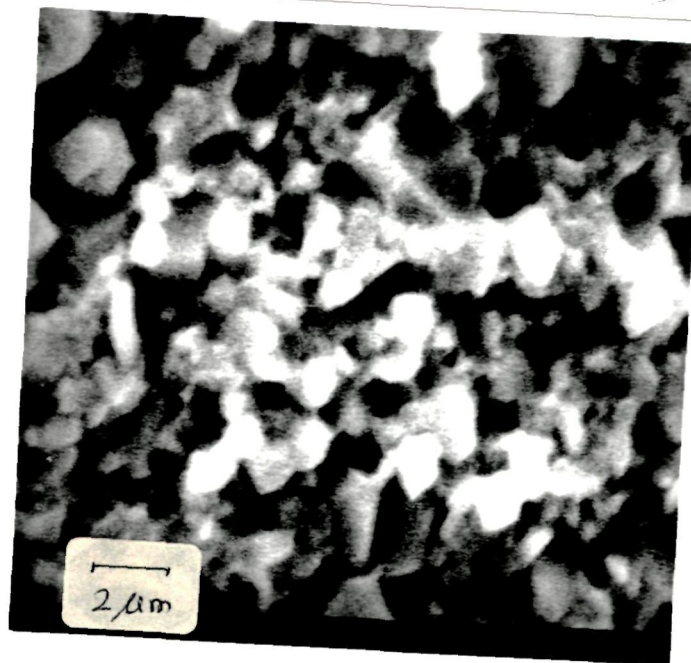
(b)

Fig 24 a-b : Scanning electron micrographs of sintered
samples (a) E-12 (b) E-32
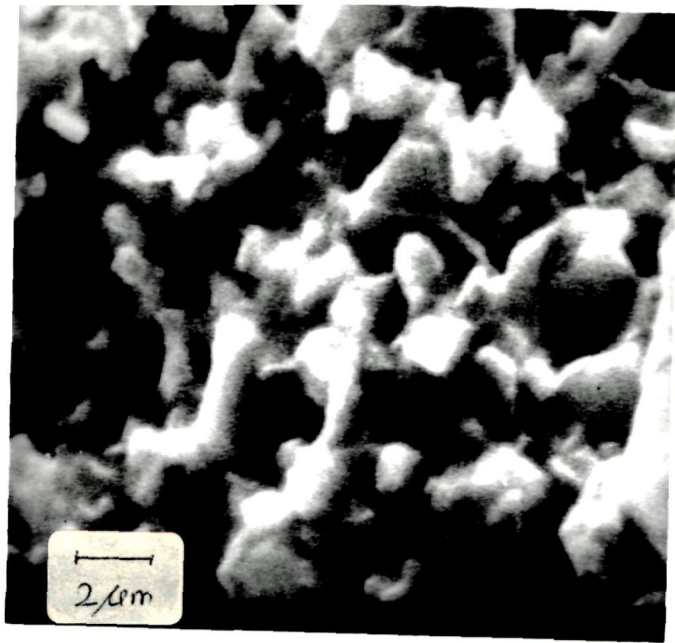
(c)
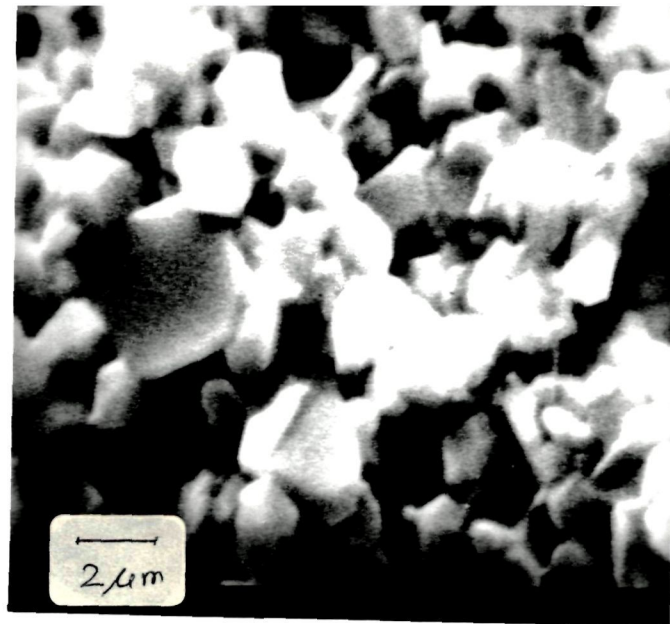
(d)

Fig 24 c-d : Scanning electron micrographs of sintered
samples (c) E-52 (d) E-62

3.3 SUMMARY

Magnetic materials comprise of a large variety of materials such as ferromagnetic metals, alloys, ferrimagnetic oxides etc. Of these, ferrites have notable technological utility because of their combined properties of a magnetic material and an electrical insulator. Extensive work has been done on ferrites with a view to determine their electrical, magnetic and microstructural properties and to tailor-make them for suitable applications. Apart from their chemical composition, the microstructural approach to ferrites has helped in many ways in improving their properties and suitability. The importance of microstructure control in dictating the electrical and magnetic properties has been thoroughly understood and established.

In SrO-Fe_2O_3 system, $SrFe_{12}O_{19}$ is known to be permanent magnetic material. The coprecipitation technique is used for synthesis. To obtain powder of desired quality, it is essential to control various processing parameters of coprecipitation method. In the present work, effect of following parameters have been studied:

(1) Mode of washing,

(2) Temperature of calcination,

(3) Effect of crystallinity of coprecipitated precursor,

(4) Effect of sodium ion incorporation.

Following are the observations:

It is observed that the mode of washing affect the crystallinity of coprecipitate. When coprecipitate is washed with centrifugal mode, it results into formation of amorphous coprecipitate while decantation mode gives crystalline coprecipitate. The DTA/DTG/TG studies showed that amorphous coprecipitate undergo ferritisation reaction exothermically around temperature ~ 700°C (Sample A & C-1). On the other hand, crystalline coprecipitate does not show any exothermic change when analysed by DTA/DTG/TG (Sample B & C-2). The structural analysis and magnetic property measurements reveal that both types of (amorphous and crystalline) samples show initiation of Sr-hexaferrite formation around 650°C in air. This temperature is much lower than the temperature required for conventional ceramic method. The XRD studies also showed that amorphous precursor undergoes ferrite formation with higher rate and without formation of intermediate phase. Whereas rate of ferrite formation for crystalline precursor is relatively low and presence of intermediate spinel phase is observed. The results indicate crystallinity of precursor sample affect the kinetics and mechanism of ferrite formation reaction.

In the study of optimisation of calcination temperature, both the types of precursors (A & B) were calcined at 750°C, 850°C & 925°C. The calcined powders thus obtained were pressed into pellets and subsequently sintered

in the temperature range 1100°C to 1250°C. The magnetic properties of sintered compacts were measured using hysteresis loop. It is observed that magnetic properties of samples having 750°C calcination temperature are superior. Hence this temperature is selected as optimum calcination in further studies.

To understand the effect of sodium ion additive, the precursor sample was mixed with predetermined quantity of additive. The effect of additive is found out by comparing the magnetic properties of samples containing additive with virgin sample (sample without additive). The results of magnetic property measurement showed that with additive concentration the values of B_r, $_bH_c$, $(BH)_{max}$ increase, reach to maxima and then decrease with further increase in additive concentration. The $_iH_c$ increases for low additive concentration. The results of magnetic properties are analysed in the light of changes in density, microstructure, and saturation magnetisation. It is found that increase in B_r and $(BH)_{max}$ is due to increase in saturation magnetisation (M_s) and sintered density (ρ) with incorporation of additive up to 0.7% Na. For higher concentration of additive, values of saturation magnetisation and sintered density decrease. This results into lowering of remanence and energy product. The increase in $_iH_c$ with additive incorporation is attributed to decrease in particle size and uniform microstructure. The addition of additive after calcination also shows similar results.

171

The EPMA analysis of selective samples was carried out to find out the role of additive. The results of EPMA analysis indicate that additive is not present on grain surface but segregates in intergranular spaces and voids. This helps in controlling the microstructure. It is also responsible for higher density without increase in grain size.

REFERENCES

1. G. Aminoff, Goel. Foren. Stockholm, Forth, 47 (1925) 283.

2. V. Alelskold, Arkiv. Kemi Mineral Geol., 12-A (1938) 1.

3. H. Kojma, Ferromagnetic Material, Edited by E. P. Wohlforth, North Holland Publishing company Vol. 3 (1982) 305.

4. X. Obradors, A. Collomb, M. Pernet, D. Samaras & J.C. Joubert, J. Solid State Chemistry, 56 (1985) 171.

5. X. Obradors, X. Solans, A. Collomb, D. Samaras, J. Rodriguez, M. Pernel & M. Font-Altaba, J. Solid State Chemistry, 72 (1988) 218.

6. L. Neel, Ann. Phys. (Paris), 3 (1948) 137.

7. P.W. Anderson, Phys. Rev., 79 (1950) 350.

8. A. Grill and F. Haberey, Appl. Phys. 3 (1974) 131.

9. E.W. Gorter, Proc. IEEE 104:B (1957) 225.

10. B.T. Shirk, W.R. Buessem, J. Appl. Phys. 40:3 (1969) 1294.

11. A.P.B. Sinha in : Solid State Chemistry, edited by C.N.R. Rao (1974), Marcel Dekker, Inc., New York.

12. A.J. Dekker, Solid State Physics, (1952), Macmillan & Co. Ltd., London.

13. D.C. Heck, Magnetic Materials and Their Applications (1974), Butterworth & Co. Ltd.

14. T.Nomura, K. Okutani, T. Ochiai in Advanced Ceramics (1987) Edited by S. Saito, Oxford University Press.

15. J.M. Haspers in: Modern Materials Vol.3 (1962) 259, edited by Henrey H. Hausner, Academic Press, New York & London.

16. H.B. Von Basel, IEEE Trans. Mag., 17 (1981) 2654.

17. K. Haneda, C. Miyakawa & H. Kojima, J. Am. Ceramic Soc., 57 (1974) 354.

18. H. Taguchi, F. Hirota, T. Takeishi & T. Mori, Ferrites: Proc. Sixth Int. Conf. Japan, (1992) 1118.

19. F.C. Stoner & E.P. Wohlforth, Phil. Trans. Roy. Soc. London Ser.A 240 (1948) 599.

20. Shailaja Kulkarni, Jyotsna Shrotri, C.E. Deshpande & S.K. Date, J. Mat. Sci., 24 (1989) 3739.

21. R. Chandrashekhar, S.W. Charles, K. O'Grady, S. Morup & J. Van Wonterghem, Adv. Ceramic Materials, 2 (1987) 65.

22. W.A. Kaczmarek, B.W. Ninham & A. Calka, J. Appl. Phys., 70 (1991) 5909.

23. N.K. Ghosh, A.R. Das & K.N. Rai, Trans. of Indian Ceramic Soc., 43 (1984) 89.

24. P. Brahma, D. Chakravorty, K. Singh & D. Bahadur, J. Mat. Sci. Lett., 9 (1990) 1438.

25. K. Oda, T. Yoshio, K.O. Oka & F. Kanamarel, J. Mat. Sci. Lett., 3 (1984) 1007.

26. K. Haneda, C. Miyakawa & K. Goto, IEEE Trans. Mag., 23 (1987) 3134.

27. S.K. Date, C.E. Deshpande, S.D. Kulkarni & J.J. Shrotri, Advances in Ferrites, Proc. Fifth Int. Conf. on Ferrites, Ind. Vol.1 (1989) 55.

28. K. Friess, Z. Angew. Phys., 21 (1966) 90.

29. F. Kools, J. de Physique Coll., 46 (1985) C-349.

30. NMAB Report on Magnetic Materials, Mar. 1985, National Research Council, U.S.A.

31. J.J. Went, G.W. Rathenau, E.W. Gorter and G.W. Van Oosterhout, Philips Techn. Rev., 13 (1951-52) 194.

32. H. Fahlenbrach & W. Heister, Arch. Eisenhüttenw, 29 (1953) 523.

33. A.L. Stuijts, Trans. Brit. Ceram. Soc., 55: (1956) 57.

34. J. Smit and H.P.J. Wijn, Ferrites (Philips Technical Library, Eindhoven), (1959).

35. H.P.J. Wijn in: Landolt-Bornstein Numerical Data & Functional Relationship in Science & Technology, New Series III/4b Ed. K.H. Hellewege (Springer, Berlin), (1970) p.552.

36. Y. Goto & T. Takada, J. Amer. Ceram. Soc., 43 (1960) 150.

37. Y. Goto, M. Hgashimoto & K. Takahashi, J. Japan Soc. Powder & Powder Metallurgy, 21 (1974) 21.

38. A. Cochardt, J. Appl. Phys. 37, 3 (1966) 1112.

39. K. Haneda & H. Kojima, Jap. J. Appl. Phys., 12:3 (1973) 355.

40. Y. Kato & T. Takei, U.S. Patents 1,976,230 & 1,997,193.

41. H. Harada, Ferrites: Proc. of Sixth Int. Conf., Japan (1992) 1112.

42. D.W. Johnson, Jr. and B.B. Ghate, Advance in Ceramics (Forth Int. Conf. on Ferrites), 15 (1986) 27.

43. H.B. Ries, Adv. in Ferrites: Proc. of Fifth Int. Conf., India 1 (1989) 155.

44. S. Jey-Ho, K. Jeong-Joo, L. Byang-Kyo & C. Sang-Hee, Ferrites: Proc. of Sixth Int. Conf., Japan (1992) 180.

45. K. Haneda & H. Kojima, J. Amer. Ceram. Soc., 57 (1974) 68.

46. Ph.D. Thesis, S.D. Kulkarni, Poona University (1990).

47. A. Srivastava, P. Singh & M.P. Gupta, J. Mat. Sci., 22 (1987) 1489.

48. D. Barb, L. Diamandescu, A. Rusi, D. Tarbasa, M. Morariu & V. Teodorescu, J. Mater. Sci., 21 (1986) 1118.

49. H. Taguchi, F. Hirata, T. Takeishi and T. Mori, Ferrites: Proceedings of Sixth Int. Conf., Japan (1992) 1118.

50. S. Garcia & E. Alteshuler, Phy. Stat. Sol.(a), 89 (1985) 427.

51. G.C. Bye & C.R. Howard, J. Appl. Chem. Biotechnol., 21 (1971) 319.

52. K. Melzer & A. Martin, Phys. Stat. Sol.(a), 107 (1988) K 163.

53. W. Roos, J. Am. Ceram. Soc., 683 (1980) 601.

54. A. Srivastava, P. Singh, V.G. Gunjikar & A.P.B. Sinha, Thermochimica Acta, 86 (1985) 77.

55. F. Chow, X. Feng, J.L. & Y. Liu, J. Appl. Phys., 61 (1987) 3881.

56. K. Higuchi, S. Naka & S. Hirano, Adv. Ceram. Mat., 1 (1986) 104.

57. F. Kools, Science of Sintering, 17 (1985) 49.

58. F.J.A. Den Broeder & P.E.C. Franker, in: Adv. in Ceramics, Vol.1 (1981) 494.

59. H. Harada, Ferrites: Proc. of the Int. Conf. (1980) Japan, p.354.

60. K.K. Laroia & A.P.B. Sinha, Ind. J. Pure & Appl. Phys., 2 (1964) 48.

61. E. Lucchini, S. Meriani & G. Slokar, J. Mat. Sci., 18 (1983) 1331.

62. R.H. Arendt, J. Appl. Phys., 44 (1973) 3300.

63. J.S. Van Wieringen, Philips Tech. Rev., 28 (1967) 33.

64. B.J. Evans, F. Garndjean, A.P. Lilot, R.H. Vogel & A. Gerard, J. Magn. & Mag. Mat., 67 (1987) 123.

65. E. Krober & U. Gonser, Appl. Phys., 1 (1973) 339.

66. Q.A. Pankhurst, D.H. Jones, A.M. Morrish, X.Y. Zhou and A.R. Corradi, Advances in Ferrites: Proc. Fifth Int. Conf. on Ferrites, India, (1989) 323.

67. G. Turill, F. Licci, S.Rinaidi & A. Deriu, J. Magn. Mag. Mat., 59 (1986) 127.

68. P.M. Rao, A. Gerard & F. Grandjean, Phys. Stat. Sol.(a), 54 (1979) 529.

69. X. Obradors, A. Isalgue, A. Collomb, M. Pernet, J. Panntier, J. Rodriguez, J. Tejada & J.C. Joabert, IEEE Trans. mag., 20 (1984) 1636.

70. S.D. Kulkarni, C.E. Deshpande, J.J. Shrotri, V.G. Gunjikar and S.K. Date, Thermochimica Acta, 153 91989) 47.

71. A.G. Bagul, C.E. Deshpande, J.J. Shrotri, S.D. Kulkarni, Ila Nigam and S.K. Date, Ind. J. Chem. 31A

(1992) 661.

72. ASTM File No. 5 - 0418.

73. R.D. Goodenough and V.A. Stenger, Comprehensive Inorganic Chemistry, Vol.1, edited by J.G. Bailor, H.J. Emeleus, R. Nyholam and A.E. Trotmum-Dickenson (Pergamon Press, NY) 1973, p.591.

74. ASTM File No. 1 - 1053.

75. ASTM File No. 33 - 1340.

76. Kaelble, Handbook of X-ray.

77. C.Duval, Inorganic Thermogravimetric Analysis, 2nd Edn. A Wiley-Interscience Publications, John Wiley & Sons New York. (1963) P.440

78. W.D.Kingery, H.K.Bowen & D.R.Vhlmann, Introduction to ceramics 2nd Edn. A Wiley-Interscience Publications, John Wiley & Sons, New York.

79. J.Beretka & M.J.Ridge, J.Chem.Soc(A) (1968) 2463.

80. K.H.Yoon, D.H.Lee, H.J.Jung & S.O.Yoon, J.Mat.Sci. 27 (1992) 2941.

81. JCPDS File No. (i) 32-1100 (ii) 13-521.

Chapter 4

Nickel Zinc Ferrite

4.1 INTRODUCTION

In the group of mixed magnetic oxides, ferrites are extensively studied. In ferrites, there is a combination of useful ferrimagnetic properties and high electrical resistivity. Soft ferrites are ferrimagnetic oxides with spinel structure. They constitute largest and most established group of ferrites. Their technical importance lies primarily in their applications in various fields such as high frequency transformer cores, antenna rods, fly-back transformers for TV sets, computer memory cores, telecommunication applications and recording heads, etc. The present chapter is devoted to the study of spinel ferrites. Section-1 deals with crystal and magnetic structure of spinel ferrites which is followed by a discussion on important magnetic properties and factors governing magnetic properties. In the next section, literature survey is presented covering various aspects of soft ferrites. The results of effect of different additives on magnetic properties of Ni-Zn ferrite synthesised by ceramic technique is discussed in the section-3.

4.1.1 Crystal Structure of Spinel Ferrite

Spinel is a generic name for a class of compounds, isostructural with the mineral, magnesium aluminate i.e.

$MgAl_2O_4$. In 1915 Bragg [1] studied the structure of this mineral and found it to be cubic and comparable to the structure of diamond, with each carbon atom replaced by a molecule of the spinel. Spinel can be represented by a general formula AB_2O_4 where A is a bivalent and B is a trivalent ion. Ferrite, magnetite, aluminates, cromites etc. are few of the well known members of spinel family.

Spinel ferrite, also known as soft ferrite, has a general chemical formula $MeFe_2O_4$ where Me is a bivalent metal ion such as, Mg, Mn, Fe, Co, Ni, Cu, Zn and Cd etc. Combination of these ions is also possible 'forming solid solution of the ferrites i.e. mixed ferrites. The unit cell of spinel ferrite, as shown in Fig.1, is a face centered cubic structure with a ~ 8.3-8.5°A. The cubic unit cell of spinel contains eight molecules of $MeFe_2O_4$. Hence unit cell formula becomes $Me_8Fe_{16}O_{32}$. In the unit cell 32 oxygen ions are arranged in a closed-packed manner forming two types of interstitials - (i) tetrahedral site is situated at one-fourth of cube diagonal, where each metal atom is surrounded by or coordinated with four nearest oxygen ions forming tetrahydron and this site is denoted as A site. (ii) Octahedral site is present at the center of the oxygen cube and in the middle of cube edge where such metal ion is surrounded by or coordinated with six neighbouring oxygen ions forming octahedron. This site is denoted as B site. There are total 96 interstitial sites in a unit cell, out of which 64 are tetrahedral and 32 are octahedral. Out of
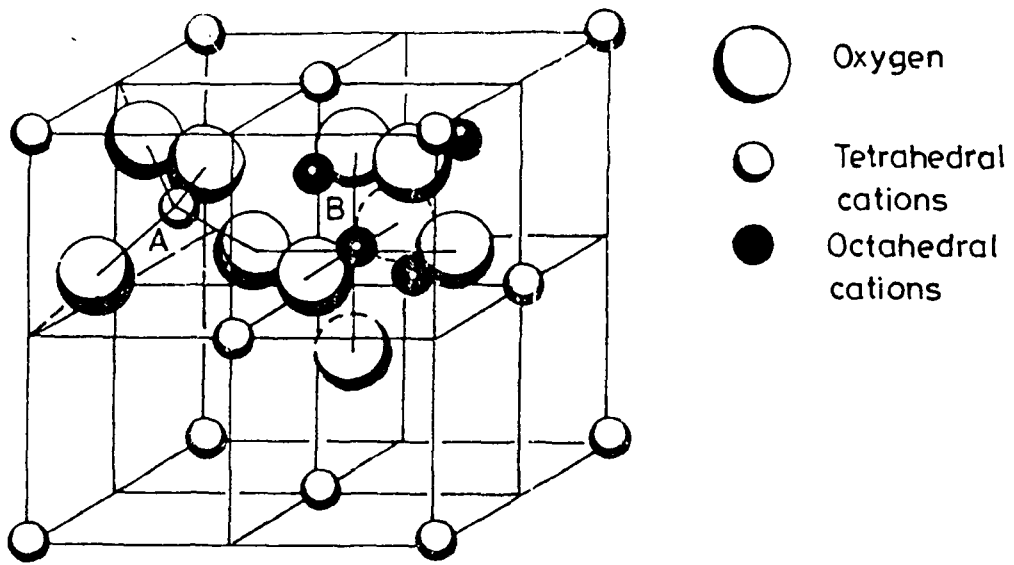
Fig 1a : Unit cell of spinel
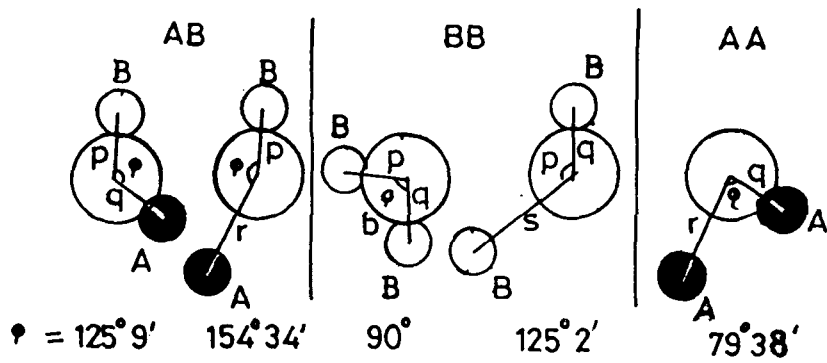
Fig 1b : Important interctions in spinel ferrites

these, only 8 tetrahedral and 16 octahedral sites are occupied.

Different ions prefer these two types of lattice sites according to the (i) ionic charge, (ii) ionic radii, (iii) temperature and (iv) the orbital preference for specific coordination.

Classification of Spinels on the Basis of Cation Distribution

On the basis of cation distribution, spinels are classified into three groups. Barth and Posnjak [2] introduced the names a) Normal, b) Inverse, and c) Random, to the following three types of distribution of cations:

a)   Normal spinel - 8 divalent ions occupy 8 tetrahedral sites. 16 trivalent ions occupy 16 octahedral sites e.g., $ZnFe_2O_4$, $CdFe_2O_4$.

b)   Inverse spinel - 8 trivalent ions occupy 8 tetrahedral sites. 8 divalent ions and remaining 8 trivalent ions occupy 16 octahedral sites e.g., $NiFe_2O_4$, $CoFe_2O_4$.

c)   Random spinel - 8 divalent and 16 trivalent cations are distributed randomly among 8 tetrahedral and 16 octahedral sites e.g., $Ni_xZn_{1-x}Fe_2O_4$, $Mn_xZn_{1-x}Fe_2O_4$.

This cation distribution play a very significant role

in electrical and magnetic properties of the spinel ferrite [3-5]. The cation distribution cannot be easily detected by X-ray diffraction method as most of the A & B ions have similar X-ray scattering power; whereas determination of resultant magnetic moment has proved to.be a useful method for analysing the cation distribution. Verwey [6] investigated the cation distribution in spinels and gave the following site preference for various ions:

a) Zn^{2+}, Cd^{2+}, Ca^{2+}, In^{2+}, Ge^{4+} prefer tetrahedral site.

b) Ni^{2+}, Cr^{3+}, Ti^{4+}, Sn^{4+} prefer octahedral site.

c) Mg^{2+}, Fe^{2+}, Co^{2+}, Mn^{2+}, Fe^{3+} are indifferent ions (random sites).

4.1.2 Magnetic Structure of Spinel Ferrite

The spinel ferrites represent a classical example of a magnetic order called ferrimagnetism. In fact, spinel ferrites were the first materials where existence of such magnetic ordering was found. Before the discovery of ferrimagnetism, magnetic spinels were grouped under a class called Ferromagnetic materials. However, it was difficult to explain low magnetic moment of spinel ferrites on the basis of ferromagnetism. Neel [7] extended molecular field approximations to propose the theory of ferrimagnetism, which satisfactorily explained magnetic properties of spinel ferrites.

In ferrites, the metallic ions occupy two

crystallographically different sites i.e. octahedral (B) and tetrahedral (A) sites. These cations are mutually separated by bigger anion (oxygen ion) making direct exchange very weak. The presence of oxygen ion, as bridges between metal ions in ferrites, indicates that the exchange interaction between transition-metal ions in ferrites cannot be as simple as in the case of pure metals. The exchange mechanism is indirect via the intervening oxygen ions. Anderson named such interaction as superexchange interaction [8].

The magnitude of the interaction energy between two magnetic ions, M^I and M^{II} depends upon,

a)   The distance of these ions from the oxygen ion through which interaction occurs. The magnitude of superexchange interaction decreases rapidly with increasing distance.

b)   *The angle M-O-M* - Antiferromagnetic interaction is strongest when this angle approaches 180° and weakest when this angle becomes 90°. Fig.2 shows the interatomic distances and the angles between the ions for different types of interactions. For cubic spinel, the B-O-B angles are 90° and 125°, (when the angle is 125°, one of the B-O distances is larger), while A-O-A angle is about 80°. Due to unfavourable angle and distance, these interactions are weak. The A-O-B angles are about 125° and 154°. The best combination of distances and angles are found in A-B interactions. Therefore, the interaction between moments of A & B site is strongest. The A-B interaction orients the

magnetic moments of these ions antiparallel.

Individual A site interacts with a single B site, but each A site is linked to four such units and each B site is linked to six such units. All octahedrally coordinated cations form one sublattice only (B) and similarly the tetrahedral sites compose the other sublattice (A). These sublattices are coupled antiparallel. These sublattices are crystallographically inequivalent and if both of them contain paramagnetic ions in sufficient concentrations, the ferrimagnetism may occur. The value of magnetisation for B lattice (M_B) is greater than sublattice magnetisation for A lattice (M_A), the net magnetisation $M = M_A + M_B$.

4.1.3 Factors Governing Magnetic Properties of Spinel Ferrites

For applications of soft ferrites, following magnetic performance parameters and their temperature dependence are technically important:

i) Saturation magnetisation

ii) Permeability

iii) Magnetic losses.

The magnetic properties depend upon combination of,

1) intrinsic properties such as chemical composition, cation distribution, curie temperature, anisotropy, magnetostriction etc. and,

2) extrinsic factors such as quality of powder,

calcination and sintering conditions, impurity inclusion, microstructure etc.

For commercial purpose, the optimisation of properties is decided by the type of application. In practice, it is not possible to optimise all the parameters relevant to various applications simultaneously. Hence compromise have to be made and processing conditions are optimised in such a way that tailor-made ferrite product has the best performance parameters needed for a particular application. In order to achieve ferrite product with desired quality, it is essential to have a sound knowledge of the inter-relation of magnetic performance parameters with extrinsic and intrinsic properties of soft ferrite.

i)   <u>Saturation magnetisation</u>:

When a ferromagnetic or ferrimagnetic substance is placed in magnetic field of strength H, an additional magnetisation flux, $4\pi M$ occurs resulting in a total induction,

$$B = H + 4\pi M$$

when H is increased, $4\pi M$ also increases, and as all electronic cation spins are oriented parallel, the material is saturated showing a saturation magnetisation $4\pi M_s$. In the case of ferrimagnetic material, due to antiferromagnetic interactions, total moment partly cancels itself. Ferrite being a ferrimagnetic material, its saturation magnetisation

is low as compared to ferromagnetic metals. The saturation magnetisation of a ferrimagnetic compound is decided by its composition and the distribution of ions over various lattice sites. The saturation magnetisation of ferrites is directly proportional to the net magnetic moment per formula unit. In the case of spinel ferrite, superexchange interactions align the moments of the ions on A sites antiparallel to those on B sites. If ions on B sites are denoted by square brackets, an inverse spinel would be,

$$Fe^{III} \downarrow [Me^{II} \uparrow Fe^{III}\uparrow] \quad O_4.$$
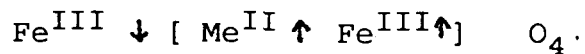
The net moment per formula unit is equal to moment of the Me^{II} ions. In the case of Normal spinel eg., (Zn or Cd) Fe_2O_4, the A sites are occupied by dimagnetic Zn or Cd ions. Hence A-A and A-B interactions do not exist. Negative B-B interaction orient spins of Fe^{III} ions nearly antiparallel resulting in $ZnFe_2O_4/CdFe_2O_4$ to be antiferromagnetic. The substitution of Zn in inverse spinel ferrite increases the saturation magnetization Zn or Cd.

ii) Permeability

The magnetic permeability is one of the important properties which is useful for deciding the application of soft magnetic material. The permeability is the ratio of induction, B, to the magnetizing field, H. When magnetizing field is very low approaching to zero, the ratio will be called as initial permeability (μ_i) and is given by the

equation [10]

$$\mu_i = \frac{1}{\mu_o} \lim_{H \to O} \frac{B}{H}$$

where μ_o is permeability of vacuum.

Initial permeability cannot be measured directly. It is found by extrapolating measurements made at finite field strength to zero. The permeability increases with field and reaches a maximum value called as μ_{max}. Both μ_i and μ_{max} are temperature dependent. As temperature increases, permeability value increases and maxima occurs near Curie temperature. For soft magnetic metals, the ratio μ_{max}/μ_i is usually about 10 while for ferrite it is between 2 to 4 [11].

The initial permeabilities of most of the ferrites are lower than metallic magnets. In the case of ferrites, the value of permeability depends upon the domain rotation and the mobility of the Bloch walls. The permeability caused by domain rotation and domain wall movement are related to $(M_s)^2$ [12]. Naturally, to obtain high permeability, it is essential to increase saturation magnetisation (M_s). In addition to saturation magnetisation, low values of anisotropy and magnetostriction also help to increase permeability value. When these intrinsic properties are coupled with good extrinsic factors such as dense

microstructure with big grains and clear grain boundary, high permeability value can be obtained. There are three important factors which govern the value of initial permeability viz., a) composition, b) additives and c) microstructure.

a) Composition: One of the most important advantages of ferrites is their very high degree of compositional variability. Most of the commercially important ferrites are mixed ferrites and consist of solid solutions of various ferrites. A judicious combination of the individual ferrites in a proper ratio is helpful to optimise the different properties according to the requirement of the final application. For example, the zinc ion substitution for other divalent ion in $MnFe_2O_4$ or $NiFe_2O_4$ increases effective magnetic moment and saturation magnetization. The zinc addition also lowers magnetostriction and anisotropy [13]. The cumulative effect of this increases μ_i of Mn-Zn and Ni-Zn ferrite with an increase in zinc concentration.

Cobalt is frequently used in Ni and NiZn ferrite to compensate the negative anisotropies of these ferrites. The permeability (μ_i) is found to increase with cobalt addition in NiZn and MnZn ferrite upto 0.05 mole% and thereafter for higher concentration it decreases [12]. For Mn or Mn-Zn ferrites where high permeability is usually desired, certain amount of excess Fe_2O_3 is added which on firing reduces to Fe_3O_4. Ferrous ferrite is the only ferrite that has positive

magnetostriction. Therefore its presence in composition is useful to minimise the net magnetostriction by compensating negative values of Mn-Zn ferrites.

b) Additives: The addition of some elements in low concentration and small amount can sometimes increase the quality of the ferrite to a large extent. Guillaud [15] showed that there is an initial increase in permeability of MnZn and NiZn ferrites with addition of small quantity of alkali and alkaline earth impurity. Akashi [16] showed that when SiO_2 and CaO are added together in ferrite, they form $CaSiO_3$. At low concentration it substantially improved the properties of MnZn ferrite but at higher concentrations it deteriorates the properties.

c) Microstructure: Guillaud & Paulus [17] studied the relation between permeability and grain size for MnZn ferrite. Heister [18] reported that μ_i increased from 1000 to 4000 as grain size increased from 3.5 to 30 um. If pores can be suppressed or located at grain boundaries, the permeability shows linear dependence on grain size [19]. When exaggerated grain growth occurs, some grains grow rapidly and they trap pores. These pores can limit the permeability by pinning domain walls. The ferrite sample with exaggerated grain growth and included porosity had a permeability of 2000. As against it, the ferrite with nearly same grain size that has grown normally had a permeability

of 40,000 [20].

iii) <u>Magnetic losses</u>:

When an alternating magnetic field is applied across a magnetic material, a certain amount of the magnetic energy is absorbed by the material and dissipated as heat. This portion of energy is termed as loss energy.

If magnetic material is subjected to an alternating field H, say $H = H_o e^{i\omega t}$, then the induction B can be represented as,

$$B = B_o e^{i(\omega t + \delta)}$$

so that,

$$\mu = \frac{B}{H} = \frac{B_o}{H_o} (\cos \delta + i \sin \delta)$$

$$= \mu' + i \mu'',$$

where μ' represents the component of B in phase with H while μ'' refers to that of B which is out of phase by 90° with the applied field H. The former therefore represents the magnetic energy stored in the circuit while the latter describes the energy dissipated in the circuit.

The ratio μ''/μ' is known as loss factor.

$$\frac{\mu''}{\mu'} = \tan \delta \text{ (the loss factor)}.$$

190

The inverse of the loss factor represents the quality factor 'Q' also known as circuit magnification factor. The loss factor can be decreased by the introduction of an air gap in the magnetic circuit. Therefore it follows that, tan ε/μ is a correct representative of the losses; or μQ is regarded as figure of merit of a magnetic core material irrespective of its shape, form and air gap [11]. The core losses are divided into three broad categories depending on their origin, viz., a) eddy current losses, b) hysteresis losses and c) residual losses.

a)   Eddy current losses:

When a material is magnetized by an A.C. current, a voltage is induced in the material in the opposite direction to the voltage producing the alternating magnetic field. The induced voltage sets up circular current in the material which produce magnetic field opposite to the original magnetic field. This induced current is known as eddy current which causes heating and power loss. The induced voltage is a function of the rate of change of induction with time, i.e. dB/dt. At higher frequency, the induced voltage is greater and hence greater the eddy current losses. Eddy current losses occur in all types of materials but will be greater in magnetic materials because of the higher permeability.

The relationship between eddy current loss and factors governing it is given by the equation, [13]

$$P_e = KB^2_m \; f^2d^2/\varrho$$

where,

K = Proportionality constant

B_m = Maximum induction

f = Frequency

d = Smallest dimension transverse to flux

ϱ = Resistivity

In ferrites, the eddy current loss is usually negligible because of the high resistivity (ϱ) which is about 10^{12} times that of metal. Only MnZn ferrites containing ferrous ions has lower resistivity and hence losses are higher for this ferrite in high frequency (10^6c/sec) range. The eddy current loss in these ferrites can be reduced effectively by a uniform and fine grain microstructure. Another way is to increase resistivity of grain boundary by addition of dopant. TiO_2 and SnO_2 are known to increase the electrical resistivity [20,21].

b)   **Hysteresis loss**:

Hysteresis is caused by the fact that the magnetisation is not a single-valued function of the field intensity. The energy dE required to change the magnetisation I to I+dI at a field H is given by dE = HdI. Thus the total energy absorbed for a complete hysteresis cycle is,

$$W = \oint HdI$$

which is equal to the area under this hysteresis loop. When

permeability of material is high or it has low coercivity, area under loop will be small and hence smaller will be the loss.

In ferrites, hysteresis losses are caused by irreversible wall-displacements. The domain walls get firmly bound to certain equilibrium position in the presence of large internal stresses and non-magnetic impurities. Hence such impurities should be avoided.

The hysteresis loss can be minimised by lowering anisotropy and magnetostriction. All the spinel ferrites, except $CoFe_2O_4$, have negative magnetocrystalline anisotropy. So the anisotropy of ferrite material is lowered by incorporating optimum amount of cobalt ion. The magnetostriction is lowered by taking excess iron oxide in composition, which during processing at higher temperature gets converted into ferrous ferrite. The presence of Fe_3O_4 in optimum amount reduces the magnetostriction near to zero.

c)   Residual losses:

The residual losses are the losses left over after allowing for both the eddy-current and the hysteresis losses. The magnetic moments due to electron spins are oriented by the internal anisotropic field H_A. If external magnetic field H_i is applied in a direction perpendicular to H_A, the spin starts to precess with a frequency f_r given by,

$$2\pi f_r = \gamma \, H_A$$

where γ is gyromagnetic constant. If the applied field is alternating, one of matching frequency f_r, then there will be resonant absorption of energy due to spin precession and therefore an energy loss. A low anisotropic field as explained earlier, contributes to a high permeability and by the above analysis the spin-precession frequency is proportional to the anisotropy field [22].

$$H_A = - \frac{4K}{3I_s}$$

If only rotational processes are important then,

$$\mu-1 = 2\pi \frac{I_s^2}{K} \quad \text{or} \quad f_r = \frac{4\gamma I_s}{3(\mu-1)}$$

It follows therefore that the conditions which favours a high permeability also favours low precession frequency. In other words, the frequency at which the energy losses become appreciable in a ferrite core is lower for the higher permeability material. Residual losses can also occur due to a) relaxation processes involving a rearrangement of Fe^{2+} and Fe^{3+} ion in the lattice by interchange of valency electrons. b) Due to domain wall resonance.

4.1.4 Literature Survey

Ferrites are magnetic oxides containing iron as major metallic component. During last forty years, soft

ferrites have remained the largest class in terms of weight of the total industrial production of ferrites. Soft ferrites have general formula $MeO.Fe_2O_3$ where Me is a divalent metal ion such as Mn, Mg, Ni, Co, Zn, Fe etc. Hilpert [23] synthesised soft ferrites for the first time in 1909. After a decade, Snoek [24] and his co-workers carried out intensive studies on preparation of ferrites and their magnetic properties. Further, Vervey [4] showed that ferrite with inverted spinel structure are magnetic while those with normal spinel structure are nonmagnetic. In 1948, Neel [7] gave his famous theory of ferrimagnetism which dealt with spin-spin interactions in these materials. A more detailed examination of basic interactions was further made by Anderson [8]. Gorter [25] and Guillaud [26] gave the direct experimental proof of Néel's modified theory. Yafet and Kittle [27] put forth the theory of 'Triangular" arrangement of spins.

Soft ferrites have been extensively studied as they exhibit interesting structural, electrical and magnetic properties. With the rapid expansion of technology, the applications of soft ferrites have been established in many branches. Hoshino's 'application tree' [28] shows twenty-five application groups belonging to the six branches of electronics viz., telecommunications, radio and televisions, microwave, computers, magnetic recording and miscellaneous uses. Right from the beginning, soft ferrites are exclusively related to electronics. The electronics shapes .

the areas of soft ferrite use and their production volume. MnZn and NiZn ferrites are the two representative classes of soft ferrites. In practice, most of the soft ferrite applications are covered by these two mixed ferrites. MnZn ferrites have a much higher permeability and having lower resistivity. Use of MnZn ferrite is restricted upto 2 MHz only because of lower resonance frequency and higher eddy current losses. In contrast, NiZn ferrite have lower permeability but much higher resistivity. They can be used in the range of 2 MHz-70 MHz.

The electrical and magnetic properties of soft ferrites depend upon chemical composition, site distribution of ions among the tetrahedral and octahedral sites. In addition to this, properties of ferrites also depend upon microstructure. Hence, ferrites are extremely process sensitive [29]. Preparation of ferrites is the fundamental step in processing of ferrites. It occupies key position in the processing since characteristics of the calcined powder will strongly affect the quality of the product after sintering. Some of the important methods are listed below:

1)   Ceramic method [21]

2)   Coprecipitation [30,31]

3)   Hydrothermal oxidation [32]

4)   Fused salt method [33]

5)   Hydrolysis of organometallic precursor [34]

6)   Citrate method [35]

7)   Combustion of solid solution precursor [36-38].

The ferrite powder obtained after calcination is processed further to obtain the product having desired properties. Substantial efforts have been taken in the various laboratories to improve the properties of ferrites. Various magnetic properties are found to be improved with addition of small amount of different magnetic and nonmagnetic oxides. The use of such additives play crucial role in tailor-making of ferrites for particular application. Guillaud [39] made the earliest attempt to use CaO as additive in Mn-Zn ferrite to lower eddy current losses. Akashi [40] achieved lower losses using a combination of CaO and SiO_2 in MnZn ferrites. On the basis of role of additives, they are categorised into three types. The additives from the first group alter the magnetic properties by substituting cation from crystal lattice of ferrite. Additives which normally segregate at grain boundaries are grouped in the second type. The additives from this group have a marked effect on microstructure. Thus selection of adequate additives is very important. The additives from the third group are useful for liquid phase sintering. Table-1 gives representative examples of additives from each group and their effects on performance parameters of the sintering products.

After 1980, switch-mode power supply market have grown rapidly. This created a need for a ferrite material

Table-1

Effect of different additives/dopants on properties of soft ferrites

Ferrite composition	Additive Type I	Effect of Additive	Ref.
$Mn_{0.58}Zn_{0.37}Fe_{0.05}Fe_2O_4$	Cr, Al, In	Lattice constant is decreased with an increase in the amount of Cr and Al dopant. On the other hand, with indium addition the lattice constant increases, and magnetisation decreases linearly with dopant content. μ_i and T_C are also found to decrease with increasing concentration of dopant Cr^{3+} and In^{3+}.	[41]
$Ni_{0.75}Zn_{0.25}Fe_2O_4$	Ti^{4+}	Saturation magnetisation and T_C show linear fall with titanium content.	[42]
$Ni_{0.35}Zn_{0.65}Fe_{1.98}O_4$	Sb^{5+}	M_s decreases with increasing amount of dopant. Some trend is observed in the case of T_C, n_B and D_m.	[43]

Ferrite composition	Additive Type II	Effect of Additive	Ref.
$(MnZn)Fe_2O_4$	CaO	Ca rich phase segregate at grain boundaries. Ca-rich liquid phase is observed at high sintering temperature.	[44]
NiZn ferrite	Bi_2O_3	Bi_2O_3 addition increases rate of densification and grain size during sintering. It also increases uQ product. Bi_2O_3 tends to segregate at grain boundaries.	[45-47]
$Mn_{0.54}Zn_{0.374}Fe_{2.06}O_4$	SiO_2	The u_i and density increases for lower concentration of SiO_2. Sample containing silica shows discontinuous grain growth at higher silica content.	[48]
$Ni_{0.58}Zn_{0.40}Fe_{2.04}O_4$	GeO_2	Small addition of GeO_2 increases density, initial permeability and reduce the core losses. At higher GeO_2 concentrations, the sintered density decreases.	[49]
$NiZnCoFe_2O_4$		Additive increases the density and help in obtaining uniform microstructure with small grain size and low magnetic losses at high frequency.	[50]
	Additive Type III		
$MnZnFe_2O_4$	MoO_3	MoO_3 cause a liquid phase sintering of the ferrite at a lower temperature. It helps to obtain better microstructure and better magnetic properties.	[51]

199

operating at a much higher flux level. With these advances the operating frequencies also increased to hundreds of kHz. Power supplies operating at 1 MHz and above are commercially available. There is a great demand for power ferrites due to their applications in areas like computers, microprocessors and VCRs [52].

4.2 RESULTS AND DISCUSSION

In the forthcoming years the applications and demand of power ferrites will go on increasing. To satisfy the need, ferrites having high cut-off frequency with high saturation magnetisation, uniform microstructure, low magnetic losses over the working range of frequencies and very high resistivity should be synthesised. Since economy is crucial factor as far as large scale production is concerned, the improvement in performance must be cost effective to users [53]. Considering these requirements we have chosen NiZn ferrite for our study. Its properties are modified with the help of different additives and optimisation of sintering conditions.

4.2.1 Synthesis of Ni-Zn Ferrite

For the preparation of ferrites which can be used at frequencies $\geq$ 30 MHz, the Ni-Zn ferrite having chemical composition $Ni_{0.8}Zn_{0.2}Fe_2O_4$ was chosen. The ferrite was

synthesized by two different methods viz.,

a)   Ceramic method and

b)   Liquid mix technique.

In ceramic method of preparation, the oxides NiO, ZnO and Fe_2O_3 were mixed in the required proportion. The mixture was divided into four parts and was calcined at various temperatures in the range 850°C to 1150°C for 3 hrs. The X-ray diffractograms of the calcined samples were scanned for detection of various phases at different stages of preparation. Fig.2 depicts the changes in XRD patterns of reactants at different temperatures. The XRD pattern of sample calcined at 850°C shows peaks corresponding to NiZn ferrite along with the peaks of αFe_2O_3, (Fig. 2 a). With an increase in calcination temperature, intensity of peaks belonging to Ni-Zn ferrite increases with single phase formation at the temperature 1150°C.

4.2.2   **Effect of Additives**

Additives are found to alter the magnetic properties in various ways. They play a vital role in tailor-making of ferrite product. We tried to study the effect of five different additives viz., (1) BaO, (2) BaO-B_2O_3 on magnetic properties of $Ni_{0.8}Zn_{0.2}Fe_2O_4$.

During the study of additive effect on magnetic
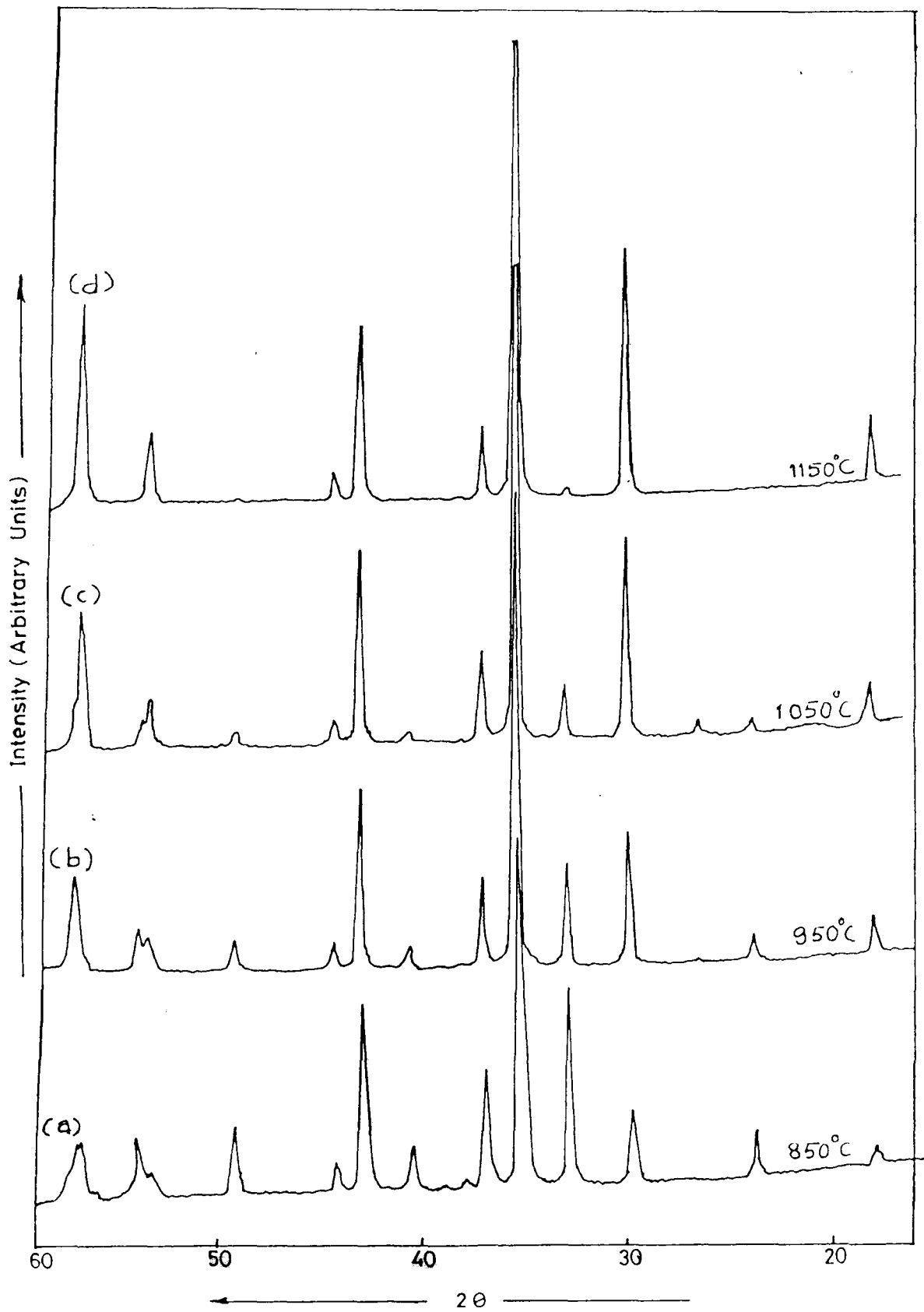
Fig 2 : X-ray diffraction patterns of NiZn ferrite samples

properties, different samples were derived using the calcined powder from the same batch. For this study, $Ni_{0.8}Zn_{0.2}Fe_2O_4$ was synthesised using ceramic method of preparation. The calcination was done at 950°C/3 hr in air [47]. The powder thus obtained was ball milled for 24 hours. The ground calcined material was divided into six parts. One part of the same was processed without additive and the green toroids subsequently prepared using this part were labelled as C721 to C725. These samples without additive (virgin samples) were used as reference samples during further studies. The remaining five parts were further subdivided and each part was mixed with predetermined quantity of one of the additives mentioned above. The homogenization was carried out by wet mixing in pestle and mortar. The wet mixed powders were dried under IR lamp. The dried powders were mixed with PVA binder and pressed into toroids. The toroids were sintered at different temperatures in the range 1100-1250°C for 4 hours in air. The sintered samples were characterised with the help of Q meter, VSM, SEM etc.

Measurement of permeability:

The complex initial permeability, $\mu_o = \mu' - i\mu''$, was measured on toroids in the frequency range 4 to 50 MHz with a Q meter using a 3-5 turn winding. The instrument was set at the required frequency and the capacitance was adjusted till the resonance point was obtained. The value of Q and

capacitance were recorded. The inductance was calculated
using the following formula [10]:

$$L = \frac{1}{{}^2 \times C}$$

where, $= 2\pi f$

C = capacitance

$$\text{and } \mu_i = \frac{L \times 10^9}{4.6 \times N^2 \times T \times \log \frac{O.D.}{I.D.}}$$

μ'' values were obtained from μ' and Q values using the
relation $Q = \mu'/\mu''$. Such measurements were taken at various
frequencies for all the samples and μ', μ'' values were
found out. The Q value increases with frequency and reaches
maxima then decreases with further increase in frequency.
The frequency at which Q becomes half of its maximum value
is considered as cut off frequency i.e. maximum limit of
operating frequency. We have limited our measurements upto
cut off frequency of the sample. The density and
magnetisation value was also measured for sintered samples.

The measurement of performance parameters of sintered
samples showed that samples sintered at 1100°C possess low
density and low permeability. As against this, samples
sintered at 1220°C show higher density and permeability but
lower cut-off frequency. The comparative study shows that
the samples sintered at 1140°C and 1180°C show optimum
values of performance parameters. Therefore the samples

sintered at these temperatures were selected for detailed analysis.

To find out the effect of additive incorporation, the magnetic properties of samples with additive are compared with magnetic properties of virgin sample (i.e., sample without additive) processed under the same conditions. The comparative study is carried out by plotting magnetic performance parameters, namely, Q, μ', $\mu'Q$ and μ'' as a function of frequency for doped and virgin samples. The graphical representation is shown in the figure nos. 3 to 6. The results are tabulated in the tables 2 and 3. This study is also helpful for optimisation of additive concentration. Following are the observations of the study of additive incorporation on different magnetic properties.

The magnetic properties of undoped (virgin) sample sintered at 1140°C/4 hrs:

The results of measurements are given in table 2a. The permeability (μ') is found to be in the range of 26 to 30 when measurements are carried out in the frequency range of 4 MHz to 46 MHz. This result indicates that variation in μ' hardly varies with frequency. For the same frequency range, imaginary part of the permeability i.e. μ'' value varies between 0.23 to 0.73. The measurement of quality factor Q as a function of frequency showed that upto 18 MHz Q value increases when frequency reaches a maxima of 115. In the

frequency range 18 to 22 MHz, it remains steady and decreases with further increase in frequency (Fig.3c). The figure of merit of a magnetic core is μQ product. Its variation with frequency has the same trend (Fig.3d). The saturation magnetisation ($4\pi M_s$) of the sample measured by VSM is 2660G. The microstructural analysis of fractured sintered sample shows that average particle size is 1-2 μm. Agglomerates of 3-4 um size are also observed. Presence of small and big voids is also observed (Fig.7a). The presence of voids (porosity) is also reflected in sintered density value which is equal to 3.64 gm/cm^3 i.e. about 68% of the theoretical density of Ni-Zn ferrite.

The magnetic properties of undoped (virgin) sample sintered at 1180°C/4 hrs (C-723):

The results of measurements are given in table 3a. The permeability of the sample C-723 lies between 35 to 40 when measured in the frequency range 4 MHz to 40 MHz indicating little variation in permeability. In the same frequency region μ'' varies between 0.29 to 1.12. The quality factor Q is found to increase with frequency and reaches 122 at the frequency 18 MHz. The cut off frequency for the sample is about 34 MHz. The μQ product of sample increases when frequency attains maximum value at frequency 18 MHz and thereafter decreases showing trend similar to that of quality factor. The saturation magnetisation ($4\pi M_s$) of the sample is 3821G and sintered density is 4.58 gm/cm^3.

The magnetic properties of sintered Ni-Zn ferrite having composition $Ni_{0.8}Zn_{0.2}Fe_2O_4$ (which is same as that of sample under study) are reported by Smit & Wijn [54]. The permeability of this sample is about 45 and remains fairly constant upto 20 MHz frequency. Then it rises slightly upto 50 and falls rapidly above 50 MHz. For the same sample, imaginary component μ'' remains steady for lower frequency range showing value about 0.3 at and below 5 MHz. It rises slowly upto 20 MHz and reaches upto 1.0 when it increases abruptly. The computed quality factor i.e. μ'/μ'' is maximum with value of ~ 150 around 5 MHz. 'Q' drops slowly with increasing frequency reaches to 45 at 20 MHz.

The observed permeability μ' and quality factor Q are lower for samples C-722 and C-723 than that of reported in literature [54]. The observed low value of μ' for these samples is attributable to lower density, smaller grain size and low saturation magnetisation.

Effect of BaO Addition: The samples with BaO additive were sintered at various temperatures. The properties of samples sintered at 1140°C and 1180°C are analysed in details. The results of measurements of BaO doped samples are compiled in tables 2b to 2e and 3b to 3e.

A) The magnetic properties of doped samples sintered at 1140°C are compared with properties of virgin sample C-722. For the comparative evaluation, the performance parameters

206

such as Q, μ', μ'' and μQ are plotted as a function of frequency for undoped and doped samples. Fig.3 illustrates the effect of BaO additive in comparison with reference sample.

i) Effect of permeability (μ' & μ''): Fig.3a illustrates the graphs of μ Vs freq. for virgin sample and samples with varying concentration of BaO additive. It is seen from the figures that with addition of small amount of BaO (0.1%) permeability is found to decrease. The μ' value ranges from 23 to 26 for sample with 0.1% additive indicating lowering in μ' value by about 12 to 16 percent as compared to the virgin (reference) sample. The samples with additive 0.2% and above show higher permeability value than the reference sample. The observed increase in permeability of sample with 0.2% BaO is 2 to 3%. For higher concentrations of BaO the increase in μ' is about 8 to 12%.

Effect of quality factor Q: The nature of plots of Q Vs F for all the doped samples have similar nature as that for virgin sample (Fig.3c). As seen from figure upto frequency 20 MHz, Q value for doped samples is slightly lower than reference sample. In contrast to this, above 20 MHz frequency the value of Q is higher than the reference sample. The higher Q value for the doped samples indicate that losses are decreased with addition of BaO. Table 4 includes the saturation magnetisation, sintered density and cut-off frequency measured for the doped and virgin samples.
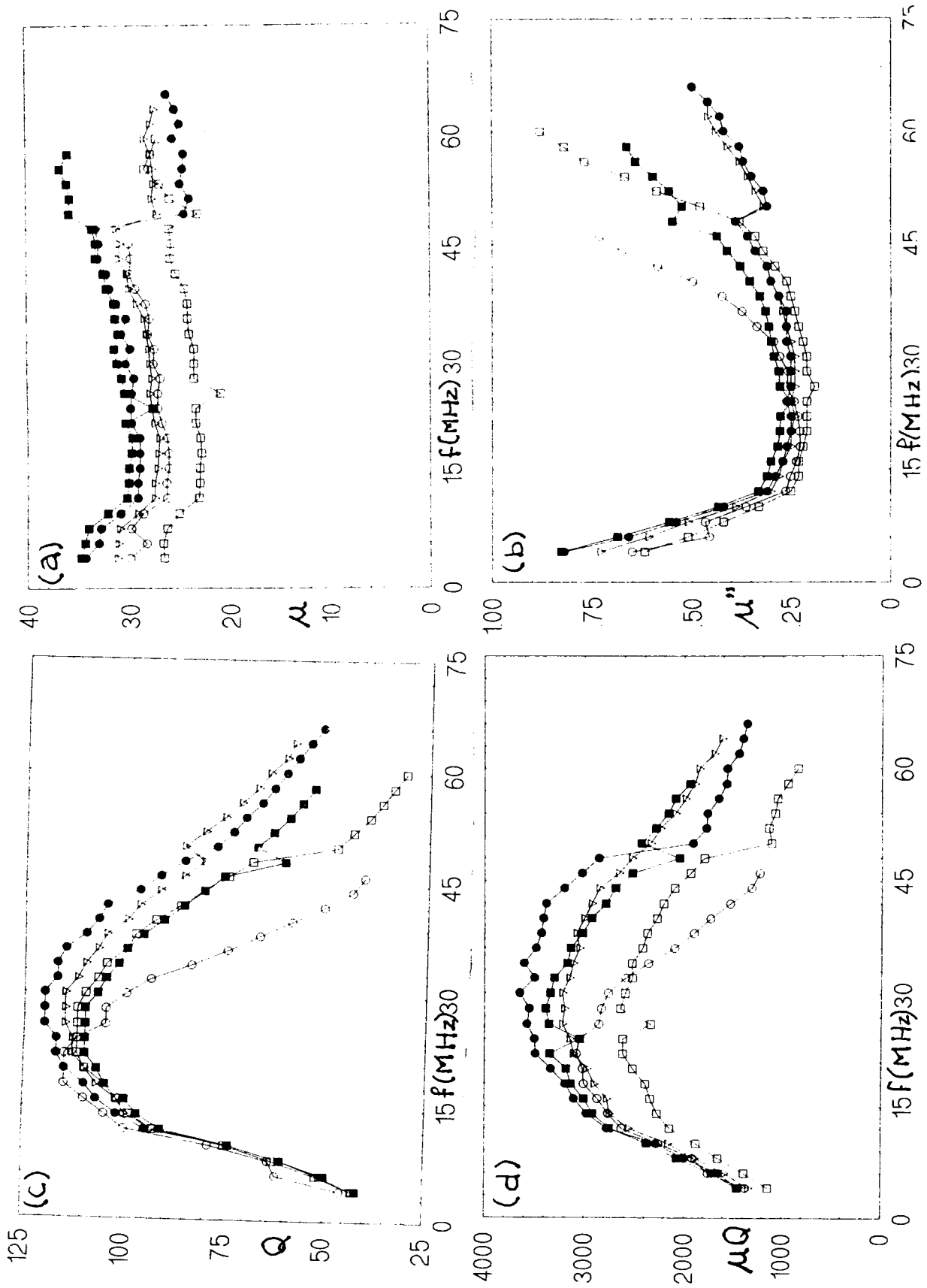
Fig. 3 : Effect of BaO addition on magnetic properties
of Nizn ferrite (Sintering condition 1140°c/4hr)
(i) o—o   Virgin   (ii) □—□   0.1·% BaO
(iii) ▽—▽   0.2 % BaO (iv) ●—●   0.3 % BaO
(v) ■—■   0.4 % BaO

Steady increase of 20 to 40% in magnetisation is observed for the samples with addition of BaO additive as compared to virgin sample. The sintered density of doped samples is found to be higher by 5 to 16% as compared to corresponding reference sample.

The microstructure of two representative samples C-746 and C-756 was analysed with the help of Scanning electron microscope. The photomicrographs of fractured sintered samples show that average particle size is 1 μm with few big particles. Microphotographs show presence of small voids only. The result implies that BaO additive acts as grain-growth inhibitor and helps to obtain uniform microstructure. Besenicar et al. [50] also observed similar effect of BaO addition on microstructure of sintered compacts of NiZnCo ferrite. The above mentioned observed changes in properties of NiZn ferrite sample due to BaO incorporation are analysed in the light of saturation magnetisation, sintered density and microstructure studies of these samples.

According to Went & Wijn [55], the initial permeability of sintered polycrystalline spinel is predominantly due to spin rotation and is given by,

$$(\mu_O - 1)/4\pi = \frac{2}{3} (M^2/K_1)$$

where M_s is saturation magnetisation and K_1 is the anisotropy constant. The higher initial permeability is

favoured by large grain size, high saturation magnetisation, low porosity, low crystal anisotropy, and low magnetostriction [55].

The chemical composition of reference sample and sample with additive is same i.e. $Ni_{0.8}Zn_{0.2}Fe_2O_4$ and all the samples are processed under identical conditions. It is reasonable to presume that factors such as crystal anisotropy, magnetostriction are identical. Therefore, changes in permeability can be correlated to saturation magnetisation and particle size. The saturation magnetisation and density increase with incorporation of additive whereas the particle size decreases. With 0.1% BaO addition μ' gets reduced. The lowering in μ' value may be due to reduction in particle size. Though there is increase in magnetisation and density of the sample, it may not be sufficient to compensate the lowering of permeability with particle size reduction. With increasing concentration of additive in permeability the magnetisation and sintered density are observed. Though BaO addition reduces particle size the combined effect of increase in $4\pi M_s$ and density is responsible for increase in μ' value as compared to the reference sample.

The higher value of quality factor Q at higher frequency range and lower μ'' value for doped samples imply that with addition of BaO losses are reduced. The cut-off frequency is found to be higher for doped samples. These

changes are attributed to reduction in particle size and uniform microstructure with incorporation of BaO as an additive [53].

B) The magnetic properties of BaO doped samples sintered at 1180°C are compared with properties of virgin sample C-723. The plots of magnetic properties as a function of frequency are given in Fig.4.

Effect on μ' & μ'': The permeability (μ') of sample containing additive is higher than the reference virgin sample. The doped samples also show fast rise in permeability after 20 MHz (Fig.4a). Such sudden rise in permeability is abnormal. The imaginary component of the complex permeability (μ'') is found to increase for doped samples. The rise is more conspicuous above frequency 20 MHz (Fig.4b).

Effect on **Q**: The **Fig.**4c shows the effect of BaO addition, on quality factor as compared to reference sample. The figure clearly shows that Q values for all doped samples are less than that of reference virgin sample. With increase in amount of BaO the Q factor is found to decrease.

The results of saturation magnetisation, density and cut-off frequency measurement for the samples sintered at 1180°C are compiled in the Table 5. The increase in saturation magnetisation for sample containing additive 0.1% and 0.2% is very low. For higher concentration of additive the increase in magnetisation is about 5 to 7% as compared
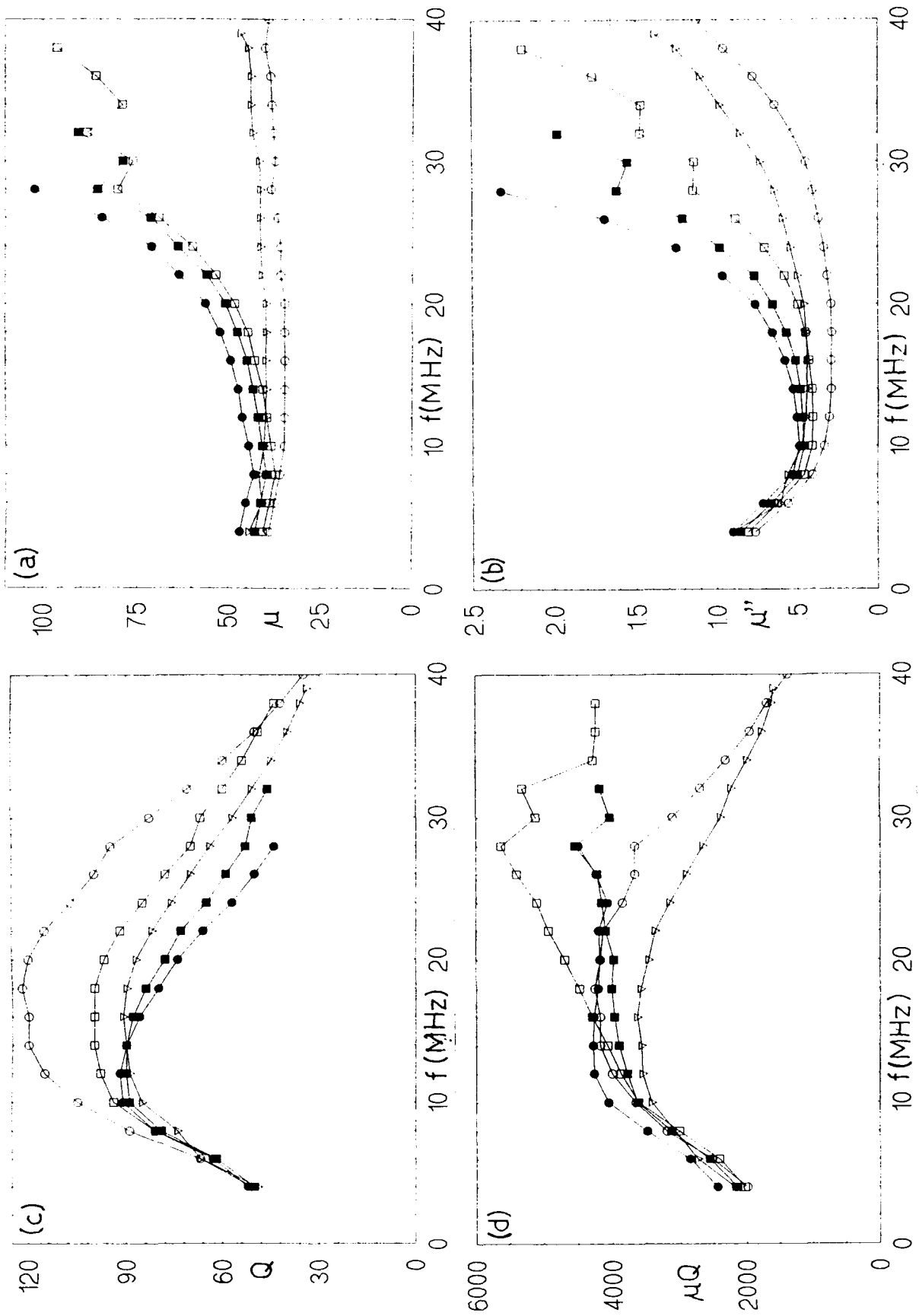
Fig. 4 : Effect of BaO addition on magnetic properties of Nizn
ferrite (Sintering conditions 1180°C/4 hr).
(i)O-O   Virgin   (ii)□-□   0.1% BaO
(iii)▽-▽   0.2 % BaO (iv)●-●   0.3% BaO
(v)■-■   0.4 % BaO

to reference sample. It is observed that the density value increases with additive concentration it reaches maximum for sample containing 0.3% BaO and then further decreases. The sintered density for samples containing 0.3 and 0.4% additive is higher than the reference sample. The addition of BaO upto 0.2% has no effect on cut-off frequency but for higher concentration of BaO cut-off frequency is lowered down.

The changes in the magnetic properties with BaO addition can be explained as follows. The higher value of permeability for doped samples may be due to higher saturation magnetisation and higher density value.

C) Effect of BaO-B₂O₃ additive on properties of Ni-Zn ferrite:

We have studied effect of $BaO-B_2O_3$ on NiZn ferrite. The amount of $BaO-B_2O_3$ added is in the range of 0.1 to 0.4% by weight. The molar ratio of BaO : B_2O_3 is 1 : 0.66. The samples with and without additive were sintered at different temperatures in the range 1100°C to 1220°C. The properties of samples sintered at 1140°C and 1180°C are studied in details. In the present section, results of $BaO-B_2O_3$ addition are discussed. The effects of additive are discussed by comparing the properties of doped samples with virgin sample processed under identical conditions. The results of property measurements of samples sintered at 1140°C and 1180°C are presented in the tables 2c to 2i and 3f to 3i respectively.

The magnetic properties of $BaO-B_2O_3$ doped samples sintered at 1140°C/4hrs are compared with properties of virgin sample C-722. The comparative study is carried out by plotting graphs of performance parameters like μ', μ'', Q and $\mu'Q$ as a function of frequency.

i) <u>Effect of permeability (μ' and μ'')</u> : The Fig.5a depicts the changes in μ' with addition of $BaO-B_2O_3$. The μ' value for doped samples is higher than virgin sample. The initial permeability (μ') increases upto additive concentration 0.3%. For 0.4% additive it is lowered. From the plots it is evident that initial permeability (μ') for reference sample is almost constant throughout the studied frequency range. Upto 20 MHz, rise in permeability is slow for doped samples. Above this frequency μ' rises fast. The Fig.5b shows that complex permeability μ'' which represents magnetic loss factor. μ'' value remained constant upto a certain frequency and then increased steeply for doped samples. This indicates that the magnetic losses are low at lower frequencies and increases with increasing frequency.

ii) <u>Effect on quality factor Q</u>: The quality factor (Q) of samples with additive is higher than the virgin sample upto 10 MHz (Fig.5c). In the frequency range 10-50 MHz the sample with 0.1% ($BaO-B_2O_3$) has higher Q value. In contrast to this, Q value of other samples containing higher concentration of additive is lower as compared to the virgin

Fig 5 : Effect of BaO-B$_2$O$_3$ addition on Magnetic properties of
Ni-Zn Ferrite (Sintering Condition 1140° C/4hr)

(i)O–O Vergin   (ii)□–□ 0.1% BaO-B$_2$O$_3$

(iii)▽–▽ 0.2 % BaO.B$_2$O$_3$ (iv)●–● 0.3 % BaO-B2O3

(V)■–■ 0.4 % BaO.B$_2$O$_3$

sample. The μQ value which is the figure of merit is considerably higher for samples containing additive than that of reference sample.

The results of magnetic property measurements are compiled in the Table-4. The measurement of saturation magnetisation shows that value of $4\pi M_s$ is higher for all the samples containing $BaO-B_2O_3$ additive. As concentration of additive increases $4\pi M_s$ also increases. The maximum value is obtained for the sample having 0.3% of additive. The improvement in saturation magnetisation is about 30-40% due to incorporation of additive.

The sintered density is also found to increase by addition of $BaO-B_2O_3$ in Ni-Zn ferrite. For sample containing 0.1% additive, the increase in density is low, about 7%. But for higher concentration of additive 20-25% rise in density is observed.

Effect on microstructure

Microstructure of two representative samples containing 0.2% and 0.4% of $BaO-B_2O_3$ additive and sintered at 1140°C are analysed with the help of SEM (Figs 7d&e). The particles are showing cubic shape with sharp edges and average size of 1-2 um. Some big particles of 3-4 um are also found to be present. The doped samples show less number of voids with more compact arrangement of particles.

It is clear from above experimental results that addition of BaO-B$_2$O$_3$ as an additive increases density, saturation magnetisation, permeability, uQ product. It also helps to get a compact microstructure. The higher value of u' for doped sample as compared to virgin sample is ascribed to better density and higher value of saturation magnetisation. Takada [56] reported that MnZn ferrite of high density and uniform grain size obtained by addition of BaO.B$_2$O$_3$ in small amount. Our results are comparable with his observations.

D) The magnetic properties of samples doped with BaO-B$_2$O$_3$ sintered at 1180°C/4 hr are compared with reference virgin sample C-723.

Effect on permeability (μ' & μ''): The changes in μ' with BaO-B$_2$O$_3$ additive is shown in Fig.6a. As compared to virgin sample the permeability μ' is found to increase with additive concentration upto 0.3% showing 60-70% rise in permeability. The permeability lowers down for additive concentration 0.4%. The imaginary part of complex permeability μ'' for virgin sample and sample containing 0.1% BaO-B$_2$O$_3$ additive show little variation throughout the studied frequency range. As against this, the value of μ'' increases fast for other doped samples (Fig.6b).

Effect on Q: The plots of quality factor Q Vs F are given in Fig.6c. It is clearly seen from the figure that with an increase in the amount of additive, there is marked decrease
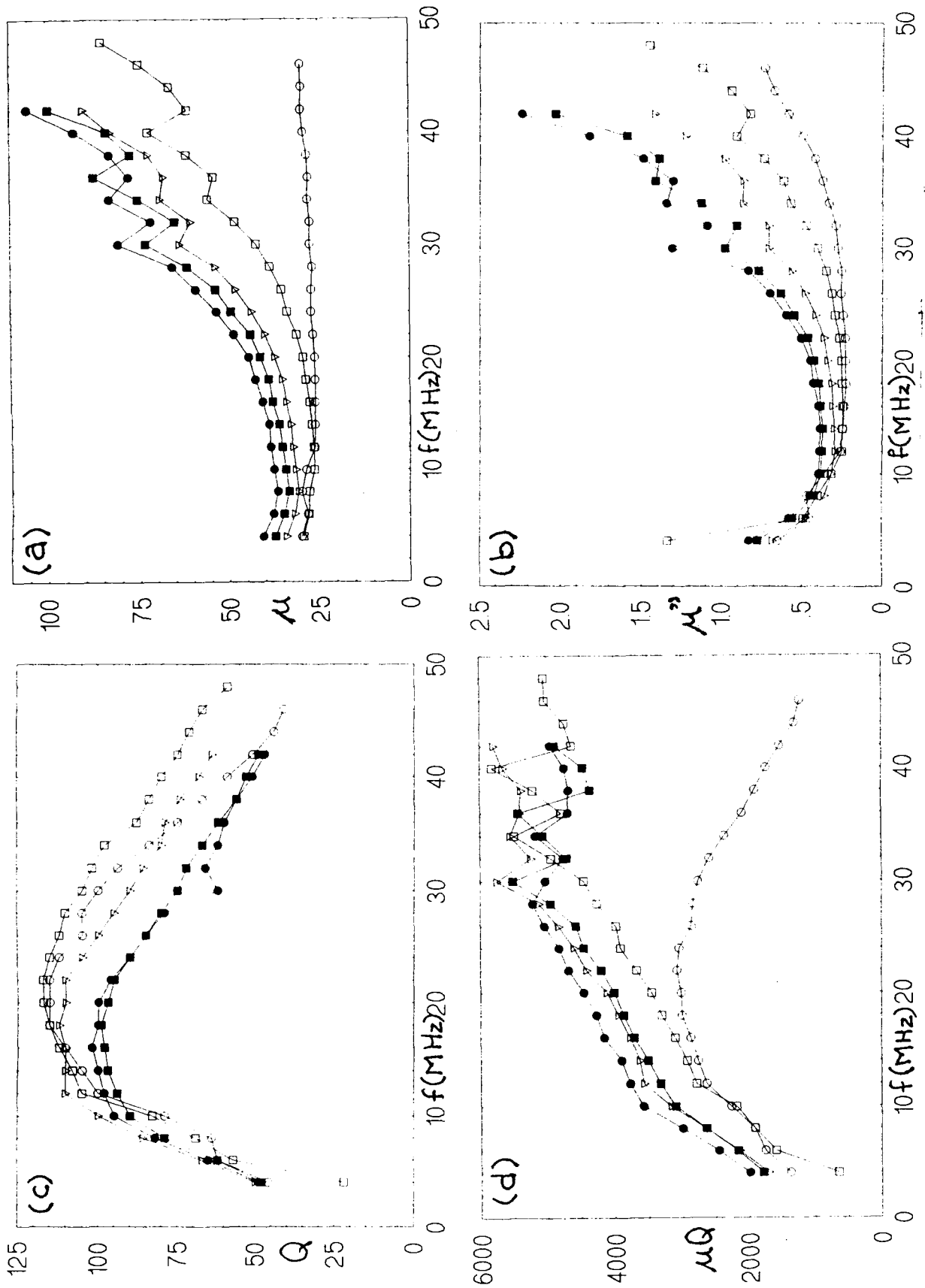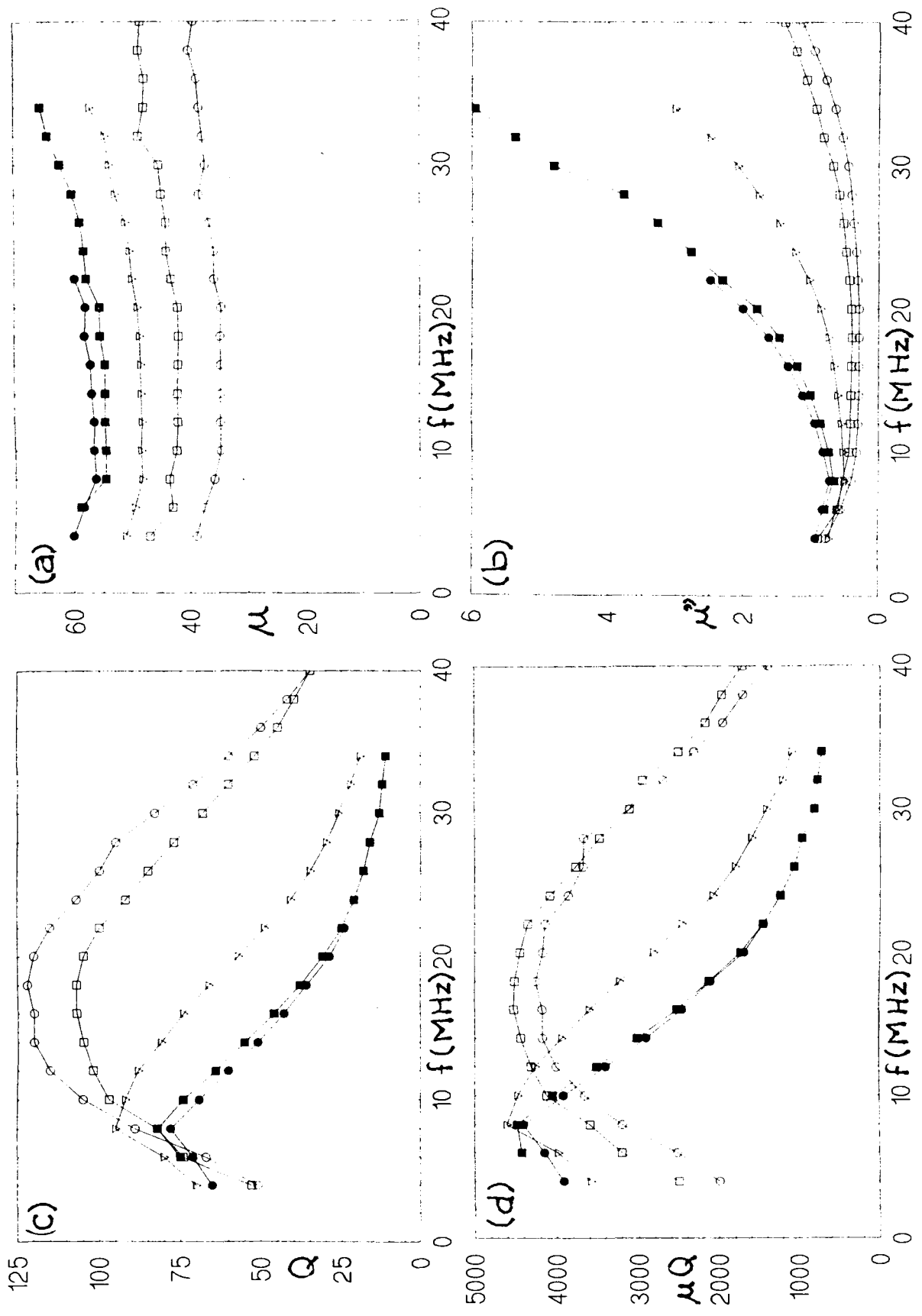
Fig 6 : Effect of BaO.B$_2$O$_3$ addition on Magnetic properties
of NiZn ferrite (Sintering condition 1180°C/4hrs)
(i) O—O   Virgin   (ii) □—□   0.1 % BaO.B$_2$O$_3$
(iii) ▽—▽   0.2 % BaO.B$_2$O$_3$ (iv) ●—●   0.3 % BaO.B$_2$O$_3$
(v) ■—■   0.4 % BaO.B$_2$O$_3$

in Q value.

Effect on μQ: In the studied frequency range the μQ product of the sample with 0.1% BaO-B_2O_3 additive is 5-10% higher than the corresponding virgin sample (C-723). The μQ product of samples with higher concentration of additive reaches maximum limit at 8 MHz and then sharply decreases. Up to 10 MHz μQ product of these samples is higher than virgin sample.

The results of saturation magnetisation measurement, cut-off frequency and density for doped samples are tabulated in the Table 5. The doped samples show increase in density by 2 to 9% as compared to the density of virgin sample. The rise of 5-14% in $4\pi M_s$ value is observed with addition of dopant. Addition of BaO-B_2O_3 additive to 0.2% or above has found to decrease cut-off frequency.

From above results it is clear that increase in permeability (μ') with additive incorporation is due to increase in saturation magnetisation and sintered density. The results of BaO-B_2O_3 addition shows that addition of small amount of these additives increases rate of densification, saturation magnetisation and also helps to obtain uniform microstructure. These changes in turn are responsible to increase the initial permeability (μ') and μQ product.

EHT=10.00 kV   WD=   9 mm   Mag= 5.00 K X
1μ   Photo No.=23   Detector= SE1
30-May-1995   SIL/SRS   C722
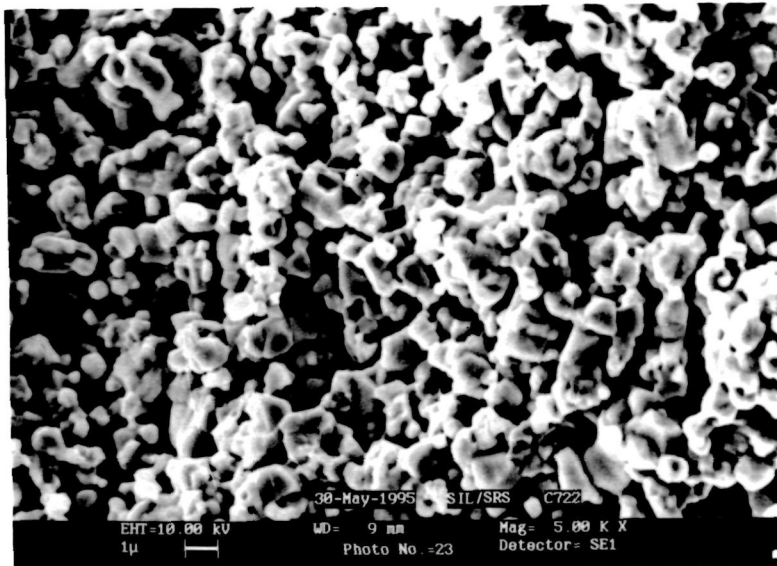
(a)

Fig 7a : Scanning Electron micrograph of sintered NiZn
         ferrite sample without additive (Virgin sample)
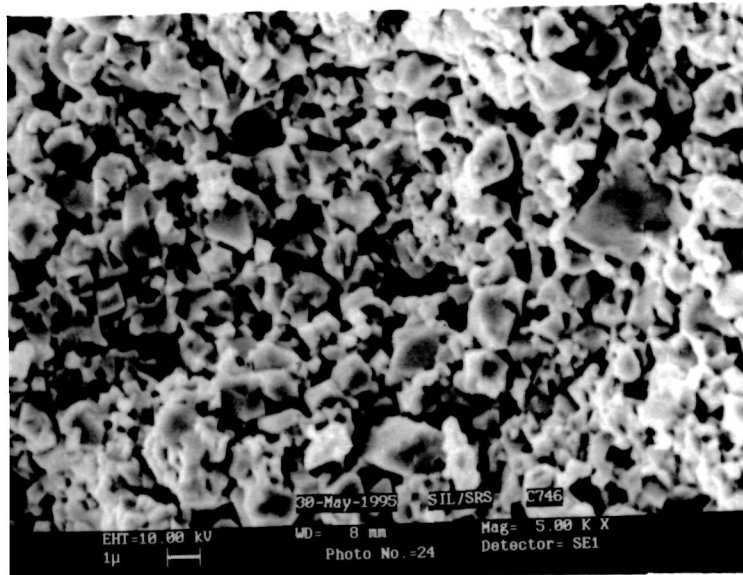
(b)
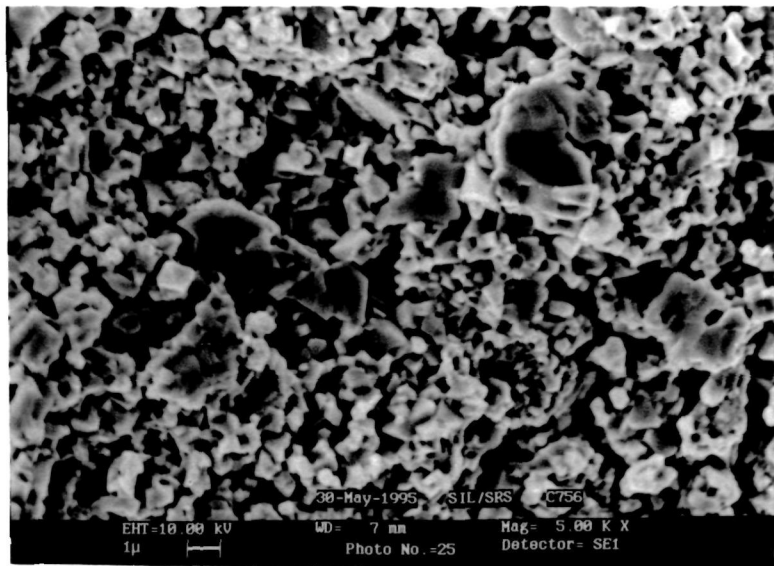
(c)

Fig 7 b-c : Scanning electron micrographs of sintered NiZn
ferrite sample with BaO additive
b) 0.2 % BaO c) 0.4 % BaO
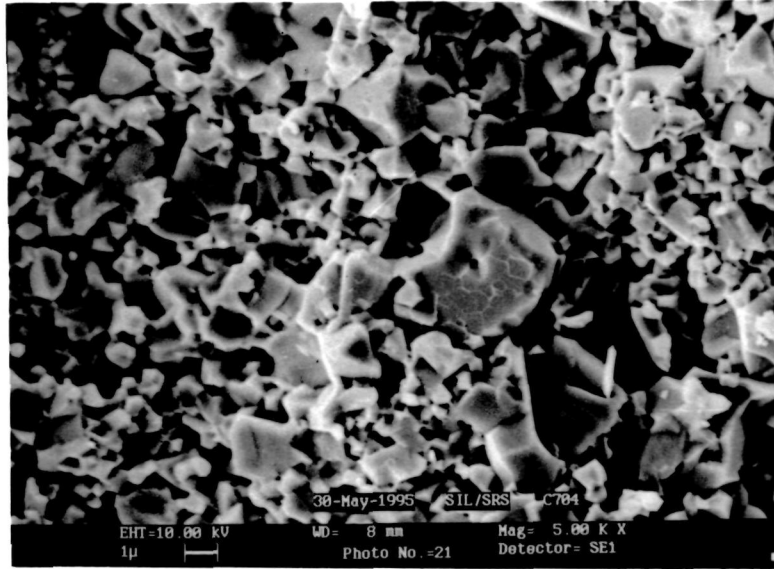
(d)
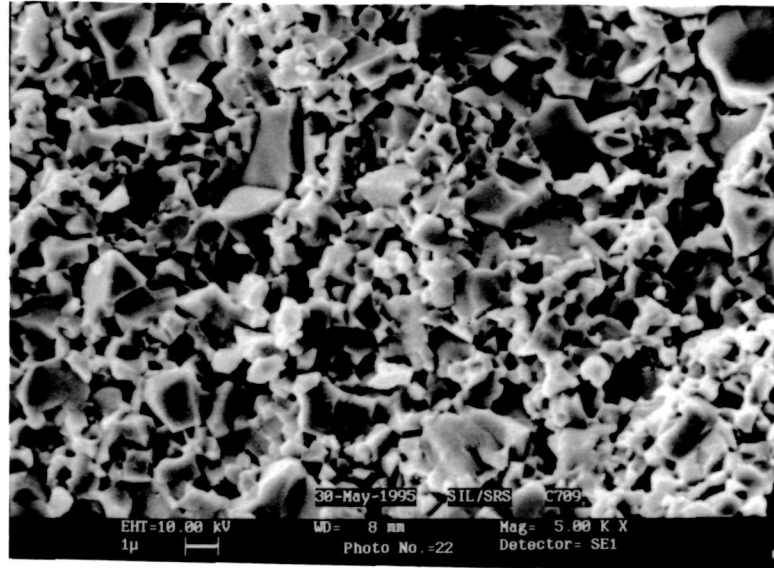
(e)

Fig 7 d-e : Scanning electron micrographs of sintered NiZn
ferrite sample with $BaO-B_2O_3$ additive
d) 0.2% $BaO-B_2O_3$ e) 0.4% $BaO-B_2O_3$

Table - 2

Magnetic properties of undoped and doped NiZn ferrite samples
Sintering condition - 1140°C/4 hrs

Table - 2a

Sample name : C-722
(Virgin sample)

Freq MHz	Q	μ'	$\mu' * Q$	μ''
4	46	29.9	1375.4	0.65
6	62	28.3	1754.6	0.46
8	64	29.9	1913.6	0.47
10	79	28.7	2267.3	0.36
12	100	26.3	2630.0	0.26
14	105	26.3	2761.5	0.25
16	110	26.1	2871.0	0.24
18	115	26.1	3001.5	0.23
20	115	26.2	3013.0	0.23
22	115	26.8	3082.0	0.23
24	112	27.2	3046.4	0.24
26	105	27.2	2856.0	0.26
28	105	27.0	2835.0	0.26
30	100	27.7	2770.0	0.28
32	94	27.5	2585.0	0.29
34	84	28.2	2368.8	0.34
36	75	28.0	2100.0	0.37
38	67	28.4	1902.8	0.42
40	59	29.4	1734.6	0.50
42	51	30.0	1530.0	0.59
44	44	29.8	1311.2	0.68
46	41	30.0	1230.0	0.73

	Table - 2b				**Table - 2c**	

Sample name : C-741   Sample name : C-746

(0.1% BaO)   (0.2 % BaO)

Freq MHz	Q	μ'	$\mu' * Q$	μ''	Freq MHz	Q	μ'	$\mu' * Q$	μ''
4	43	26.6	1143.8	0.62	4	43	31.2	1341.6	0.73
6	52	26.7	1388.4	0.51	6	51	31.1	1586.1	0.61
8	63	26.3	1656.9	0.42	8	61	31.0	1891.0	0.51
10	75	25.1	1882.5	0.33	10	74	29.2	2160.8	0.39
12	93	23.1	2148.3	0.25	12	93	27.5	2557.5	0.30
14	99	23.0	2277.0	0.23	14	100	27.5	2750.0	0.28
16	102	23.0	2346.0	0.23	16	102	27.2	2774.4	0.27
18	105	22.8	2394.0	0.22	18	107	27.1	2899.7	0.25
20	110	22.9	2519.0	0.21	20	110	27.0	2970.0	0.25
22	112	23.4	2620.8	0.21	22	113	27.5	3107.5	0.24
24	112	23.4	2620.8	0.21	24	113	27.8	3141.4	0.25
26	112	20.9	2340.8	0.19	26	115	28.0	3220.0	0.24
28	112	23.6	2643.2	0.21	28	115	27.8	3197.0	0.24
30	110	23.6	2596.0	0.21	30	115	28.0	3220.0	0.24
32	107	23.6	2525.2	0.22	32	112	28.1	3147.2	0.25
34	105	24.1	2530.5	0.23	34	110	28.3	3113.0	0.26
36	100	24.2	2420.0	0.24	36	107	28.5	3049.5	0.27
38	98	24.2	2371.6	0.25	38	105	29.3	3076.5	0.28
40	93	24.5	2278.5	0.26	40	100	30.0	3000.0	0.30
42	87	25.4	2209.8	0.29	42	97	30.2	2929.4	0.31
44	81	25.9	2097.9	0.32	44	92	31.0	2852.0	0.34
46	75	25.8	1935.0	0.34	46	86	30.9	2657.4	0.36
48	69	26.0	1794.0	0.38	48	81	31.2	2527.2	0.39
49	64	26.1	1670.4	0.41	50	86	27.2	2339.2	0.32
50	48	23.1	1108.8	0.48	52	81	27.7	2243.7	0.34
52	44	25.9	1139.6	0.59	54	76	27.5	2090.0	0.36
54	40	26.9	1076.0	0.67	56	72	27.6	1987.2	0.38
56	37	28.4	1050.8	0.77	58	68	27.8	1890.4	0.41
58	34	27.8	945.2	0.82	60	65	28.4	1846.0	0.44
60	31	27.2	843.2	0.88	62	61	27.8	1695.8	0.46
					64	59	27.4	1616.6	0.46

	Table - 2d					Table - 2e			

Sample name : C-751   Sample name : C-756

(0.3 % BaO)   (0.4% BaO)

Freq MHz	Q	μ'	$\mu' * Q$	μ''	Freq MHz	Q	μ'	$\mu' * Q$	μ''
4	42	34.3	1440.6	0.82	4	42	34.8	1461.6	0.83
6	50	33.0	1650.0	0.66	6	50	34.3	1715.0	0.69
8	61	32.8	2000.8	0.54	8	61	34.0	2074.0	0.56
10	74	30.9	2286.6	0.42	10	74	32.1	2375.4	0.43
12	95	29.2	2774.0	0.31	12	91	30.2	2748.2	0.33
14	102	29.2	2978.4	0.29	14	97	30.1	2919.7	0.31
16	107	29.0	3103.0	0.27	16	100	30.0	3000.0	0.30
18	110	29.0	3190.0	0.26	18	105	29.8	3129.0	0.28
20	115	29.0	3335.0	0.25	20	107	29.7	3177.9	0.28
22	117	29.8	3486.6	0.25	22	110	30.4	3344.0	0.28
24	117	29.9	3498.3	0.26	24	110	27.7	3047.0	0.25
26	120	29.8	3576.0	0.25	26	110	30.5	3355.0	0.28
28	120	29.6	3552.0	0.25	28	110	30.8	3388.0	0.28
30	120	30.4	3648.0	0.25	30	107	31.2	3338.4	0.29
32	117	29.9	3498.3	0.26	32	105	31.4	3297.0	0.30
34	117	30.8	3603.6	0.26	34	102	31.1	3172.2	0.30
36	115	30.3	3484.5	0.26	36	100	31.4	3140.0	0.31
38	110	31.2	3432.0	0.28	38	96	31.5	3024.0˙	0.33
40	107	31.9	3413.3	0.30	40	91	32.2	2930.2	0.35
42	105	32.2	3381.0	0.31	42	86	32.5	2795.0	0.38
44	97	33.0	3201.0	0.34	44	81	33.3	2697.3	0.41
46	92	32.9	3026.8	0.36	46	76	33.2	2523.2	0.44
48	86	33.2	2855.2	0.39	48	61	33.5	2043.5	0.55
50	78	24.5	1911.0	0.31	50	68	35.8	2434.4	0.53
52	74	24.0	1776.0	0.32	52	64	35.7	2284.8	0.56
54	71	24.9	1767.9	0.35	54	60	36.0	2160.0	0.60
56	67	24.6	1648.2	0.37	56	57	36.7	2091.9	0.64
58	64	24.5	1568.0	0.38	58	54	35.9	1938.6	0.66
60	61	25.6	1561.6	0.42					
62	58	24.9	1444.2	0.43					
64	55	25.4	1397.0	0.46					
66	52	26.2	1362.4	0.50					

	Table - 2f					Table - 2g			

Sample name : C-726
(0.1 % (BaO B2O3))

Sample name : C-704
(0.2 % (BaO B2O3))

Freq MHz	Q	μ'	$\mu' * Q$	μ''	Freq MHz	Q	μ'	$\mu' * Q$	μ''
4	22	29.5	649.0	1.34	4	50	34.2	1710.0	0.68
6	57	28.0	1596.0	0.49	6	67	32.0	2144.0	0.48
8	69	27.7	1911.3	0.40	8	86	30.8	2648.8	0.36
10	83	26.4	2191.2	0.32	10	100	31.6	3160.0	0.32
12	105	26.5	2782.5	0.25	12	110	32.4	3564.0	0.29
14	108	27.1	2926.8	0.25	14	110	33.1	3641.0	0.30
16	112	27.7	3102.4	0.25	16	110	34.3	3773.0	0.31
18	115	28.7	3300.5	0.25	18	112	35.2	3942.4	0.31
20	117	29.6	3463.2	0.25	20	110	37.5	4125.0	0.34
22	117	31.4	3673.8	0.27	22	110	40.2	4422.0	0.37
24	115	34.0	3910.0	0.30	24	105	43.8	4599.0	0.42
26	112	35.5	3976.0	0.32	26	100	48.4	4840.0	0.48
28	110	38.8	4268.0	0.35	28	·95	54.0	5130.0	0.57
30	105	42.4	4452.0	0.40	30	90	63.9	5751.0	0.71
32	102	48.5	4947.0	0.48	32	86	61.0	5246.0	0.71
34	98	56.0	5488.0	0.57	34	80	69.4	5552.0	0.87
36	88	54.4	4787.2	0.62	36	79	68.5	5411.5	0.87
38	84	62.0	5208.0	0.74	38	74	72.8	5387.2	0.98
40	80	72.7	5816.0	0.91	40	68	83.2	5657.6	1.22
42	75	61.7	4627.5	0.82	42	64	90.6	5798.4	1.42
44	71	66.8	4742.8	0.94					
46	67	75.2	5038.4	1.12					
48	59	85.5	5044.5	1.45					

Table - 2h					Table - 2i				

Sample name : C-732   Sample name : C-709
(0.3 % (BaO B2O3))   (0.4 % (BaO B2O3))

Freq MHz	Q	μ'	$\mu' * Q$	μ''	Freq MHz	Q	μ'	$\mu' * Q$	μ''
4	49	40.6	1989.4	0.83	4	48	37.2	1785.6	0.78
6	65	37.8	2457.0	0.58	6	62	34.8	2157.6	0.56
8	82	36.5	2993.0	0.45	8	79	33.4	2638.6	0.42
10	95	37.6	3572.0	0.40	10	90	34.4	3096.0	0.38
12	98	38.4	3763.2	0.39	12	94	35.3	3318.2	0.38
14	100	39.0	3900.0	0.39	14	97	36.2	3511.4	0.37
16	102	40.7	4151.4	0.40	16	98	37.9	3714.2	0.39
18	100	42.7	4270.0	0.43	18	99	39.1	3870.9	0.39
20	100	44.6	4460.0	0.45	20	97	41.3	4006.1	0.43
22	96	48.8	4684.8	0.51	22	95	44.2	4199.0	0.47
24	90	53.6	4824.0	0.60	24	90	49.5	4455.0	0.55
26	85	59.4	5049.0	0.70	26	85	53.8	4573.0	0.63
28	79	66.1	5221.9	0.84	28	80	61.9	4952.0	0.77
30	62	81.1	5028.2	1.31	30	75	73.5	5512.5	0.98
32	66	72.1	4758.6	1.09	32	72	65.3	4701.6	0.91
34	62	83.5	5177.0	1.35	34	67	75.7	5071.9	1.13
36	60	78.2	4692.0	1.30	36	62	87.7	5437.4	1.41
38	56	83.5	4676.0	1.49	38	56	77.8	4356.8	1.39
40	51	92.9	4737.9	1.82	40	53	84.2	4462.6	1.59
42	47	105.3	4949.1	2.24	42	49	99.6	4880.4	2.03

Table - 3

Magnetic properties of undoped and doped NiZn ferrite sample
Sintering condition - 1180 C/4 hrs

Table - 3a

Sample name : C-723 (Virgin sample)

Freq MHz	Q	μ'	$\mu' * Q$	μ''
4	51	39.0	1989.0	0.76
6	67	37.5	2512.5	0.56
8	89	35.9	3195.1	0.40
10	105	34.8	3654.0	0.33
12	115	34.8	4002.0	0.30
14	120	34.8	4176.0	0.29
16	120	34.8	4176.0	0.29
18	122	34.9	4257.8	0.29
20	120	34.7	4164.0	0.29
22	115	36.0	4140.0	0.31
24	107	36.0	3852.0	0.34
26	100	36.7	3670.0	0.37
28	95	38.6	3667.0	0.41
30	83	37.4	3104.2	0.45
32	71	37.9	2690.9	0.53
34	60	38.5	2310.0	0.64
36	50	38.9	1945.0	0.78
38	42	40.3	1692.6	0.96
40	35	39.4	1379.0	1.13

Table - 3b

Sample name : C-742

(0.1 % BaO)

Freq MHz	Q	μ'	$\mu' \star Q$	μ''
4	50	40.6	2030.0	0.81
6	62	38.9	2411.8	0.63
8	81	37.1	3005.1	0.46
10	94	38.4	3609.6	0.41
12	98	39.5	3871.0	0.40
14	100	40.7	4070.0	0.41
16	100	42.9	4290.0	0.43
18	100	44.8	4480.0	0.45
20	97	48.4	4694.8	0.50
22	92	53.5	4922.0	0.58
24	85	60.0	5100.0	0.71
26	78	69.3	5405.4	0.89
28	70	80.5	5635.0	1.15
30	67	76.4	5118.8	1.14
32	60	88.6	5316.0	1.48
34	54	79.3	4282.2	1.47
36	49	86.4	4233.6	1.76
38	44	96.3	4237.2	2.19

Table - 3c

Sample name : C-747

(0.2 % BaO)

Freq MHz	Q	μ'	$\mu' \star Q$	μ''
4	49	44.4	2175.6	0.91
6	67	40.8	2733.6	0.61
8	74	41.5	3071.0	0.56
10	85	40.2	3417.0	0.47
12	89	39.9	3551.1	0.45
14	90	39.7	3573.0	0.44
16	91	39.9	3630.9	0.44
18	90	39.8	3582.0	0.44
20	87	39.7	3453.9	0.46
22	82	41.1	3370.2	0.50
24	76	41.4	3146.4	0.54
26	70	41.5	2905.0	0.59
28	64	41.5	2656.0	0.65
30	57	41.8	2382.6	0.73
32	51	43.7	2228.7	0.86
34	45	44.2	1989.0	0.98
36	40	44.2	1768.0	1.11
38	36	45.0	1620.0	1.25
39	34	47.0	1598.0	1.38

	Table - 3d					Table - 3e			

Table - 3d | **Table - 3e**

Sample name : C-752 | Sample name : C-757

(0.3 % BaO) | (0.4 % BaO)

Freq MHz	Q	μ'	$\mu'*Q$	μ''	Freq MHz	Q	μ'	$\mu'*Q$	μ''
4	52	47.0	2444.0	0.90	4	50	42.8	2140.0	0.86
6	63	45.3	2853.9	0.72	6	62	41.2	2554.4	0.66
8	81	43.0	3483.0	0.53	8	79	39.5	3120.5	0.50
10	91	44.5	4049.5	0.49	10	89	40.7	3622.3	0.46
12	92	46.4	4268.8	0.50	12	90	42.0	3780.0	0.47
14	90	47.5	4275.0	0.53	14	90	43.4	3906.0	0.48
16	86	49.7	4274.2	0.58	16	88	45.1	3968.8	0.51
18	80	52.6	4208.0	0.66	18	84	47.8	4015.2	0.57
20	74	56.4	4173.6	0.76	20	78	50.9	3970.2	0.65
22	66	63.7	4204.2	0.97	22	73	56.1	4095.3	0.77
24	57	71.3	4064.1	1.25	24	65	64.0	4160.0	0.98
26	50	84.6	4230.0	1.69	26	59	71.5	4218.5	1.21
28	44	102.2	4496.8	2.32	28	53	85.8	4547.4	1.62
					30	51	79.0	4029.0	1.55
					32	46	90.8	4176.8	1.97

	Table - 3f				Table - 3g			

Sample name : C-728

Sample name : C-703

(0.1 % BaO·B2O3)

(0.2 % (BaO·B2O3))

Freq MHz	Q	μ'	$\mu' * Q$	μ''	Freq MHz	Q	μ'	$\mu' * Q$	μ''
4	53	47.1	2496.3	0.89	4	70	51.2	3584.0	0.73
6	74	43.2	3196.8	0.58	6	80	49.7	3976.0	0.62
8	82	43.8	3591.6	0.53	8	95	48.5	4607.5	0.51
10	97	42.4	4112.8	0.44	10	92	48.6	4471.2	0.53
12	102	42.3	4314.6	0.41	12	88	48.5	4268.0	0.55
14	105	42.3	4441.5	0.40	14	81	48.6	3936.6	0.60
16	107	42.3	4526.1	0.40	16	74	48.7	3603.8	0.66
18	107	42.2	4515.4	0.39	18	66	48.9	3227.4	0.74
20	105	42.3	4441.5	0.40	20	57	49.3	2810.1	0.86
22	100	43.5	4350.0	0.44	22	49	50.2	2459.8	1.02
24	92	44.3	4075.6	0.48	24	41	50.6	2074.6	1.23
26	85	44.3	3765.5	0.52	26	35	51.4	1799.0	1.47
28	77	45.2	3480.4	0.59	28	30	53.2	1596.0	1.77
30	68	45.5	3094.0	0.67	30	26	54.0	1404.0	2.08
32	60	49.1	2946.0	0.82	32	22	54.8	1205.6	2.49
34	52	48.1	2501.2	0.93	34	19	57.4	1090.6	3.02
36	45	48.1	2164.5	1.07					
38	40	49.0	1960.0	1.23					
40	35	48.7	1704.5	1.39					

Table - 3h						Table - 3i				

Sample name : C-733 (0.3 % (BaO·B2O3))   Sample name : C-708 (0.4 % (BaO·B2O3))

Freq MHz	Q	μ'	$\mu' * Q$	μ''	Freq MHz	Q	μ'	$\mu' * Q$	μ''
4	65	60.1	3906.5	0.92	4	67	57.6	3859.2	0.85
6	71	58.4	4146.4	0.82	6	75	58.9	4417.5	0.79
8	78	56.4	4399.2	0.72	8	82	54.7	4485.4	0.67
10	69	56.7	3912.3	0.82	10	74	54.7	4047.8	0.74
12	60	56.7	3402.0	0.95	12	64	54.8	3507.2	0.86
14	51	57.0	2907.0	1.12	14	55	54.8	3014.0	1.00
16	43	57.2	2459.6	1.33	16	46	54.8	2520.8	1.19
18	36	58.2	2095.2	1.62	18	38	55.7	2116.6	1.47
20	29	58.1	1684.9	2.00	20	31	55.7	1726.7	1.80
22	24	60.0	1440.0	2.50	22	25	58.0	1450.0	2.32
					24	21	58.5	1228.5	2.79
					26	18	59.0	1062.0	3.28
					28	16	60.4	966.4	3.78
					30	13	62.4	811.2	4.80
					32	12	64.3	771.6	5.36
					34	11	65.5	720.5	5.95

Table 4

Properties of NiZn ferrite samples sintered at 1140°C/4 hr

Sample name	Additive and its percentage		$4\pi M_s$ G	D gm/cm^3	Cut-off freq. MHz	Q_{max}
C-722	Virgin sample		2660	3.64	40	115
C-741	BaO	0.1	3246	3.84	.49	112
C-746	BaO	0.2	3514	4.11	64	115
C-751	BaO	0.3	3640	4.14	60	120
C-756	BaO	0.4	3733	4.23	56	110
C-726	$BaO.B_2O_3$	0.1	3469	3.90	48	117
C-704	$BaO.B_2O_3$	0.2	3529	4.38	44	112
C-732	$BaO.B_2O_3$	0.3	3736	4.54	40	102
C-709	$BaO.B_2O_3$	0.4	3700	4.48	4	97

Table 5

Properties of NiZn ferrite samples sintered at 1180°C/4 hr

Sample name	Additive and its percentage		$4\pi M_s$ G	D gm/cm^3	Cut-off freq. MHz	Q_{max}
C-723	Virgin sample		3821	4.58	34	122
C-742	BaO	0.1	3871	4.40	35	100
C-747	BaO	0.2	3828	4.54	34	90
C-752	BaO	0.3	4032	4.69	27	92
C-757	BaO	0.4	4085	4.59	32	90
C-728	$BaO.B_2O_3$	0.1	4019	4.65	34	107
C-703	$BaO.B_2O_3$	0.2	3920	4.85	22	95
C-733	$BaO.B_2O_3$	0.3	4221	4.96	17	78
C-708	$BaO.B_2O_3$	0.4	4345	4.98	17	82

4.2.3 Properties of NiZn Ferrite Prepared by Liquid Mix Technique

The $Ni_{0.8}Zn_{0.2}Fe_2O_4$ was synthesized by using Liquid mix technique or citrate route. The glassy precursor obtained was calcined at different temperatures. The precursor and calcined powders were analysed with the help of powder XRD. Fig.8 depicts the results of X-ray analysis. The XRD patterns of glassy precursor is X-ray amorphous (Fig.8a). When the precursor was calcined at 450°C, single phase formation of spinel ferrite took place. This temperature is much lower than the temperature required for single phase formation by ceramic method. The particle size and its distribution is studied by using Scanning electron microscope. Fig.9 shows SEM picture of calcined material. It shows that particle size of NiZn ferrite are $\leq$ 0.5 μm with uniform particle size distribution. The result implies that synthesis of spinel ferrite by LMT method leads to the formation of submicron size particles at considerably low temperature.

The calcined powder was subsequently mixed with binder and pressed into toroids. The green toroids were sintered at different temperatures in the range from 1140 to 1220°C for 4 hours in air. The samples sintered at 1140°C and 1180°C are analysed in details. The changes in performance parameters namely, Q, μ', μQ and μ'' at different frequencies are studied by their graphs as a function of
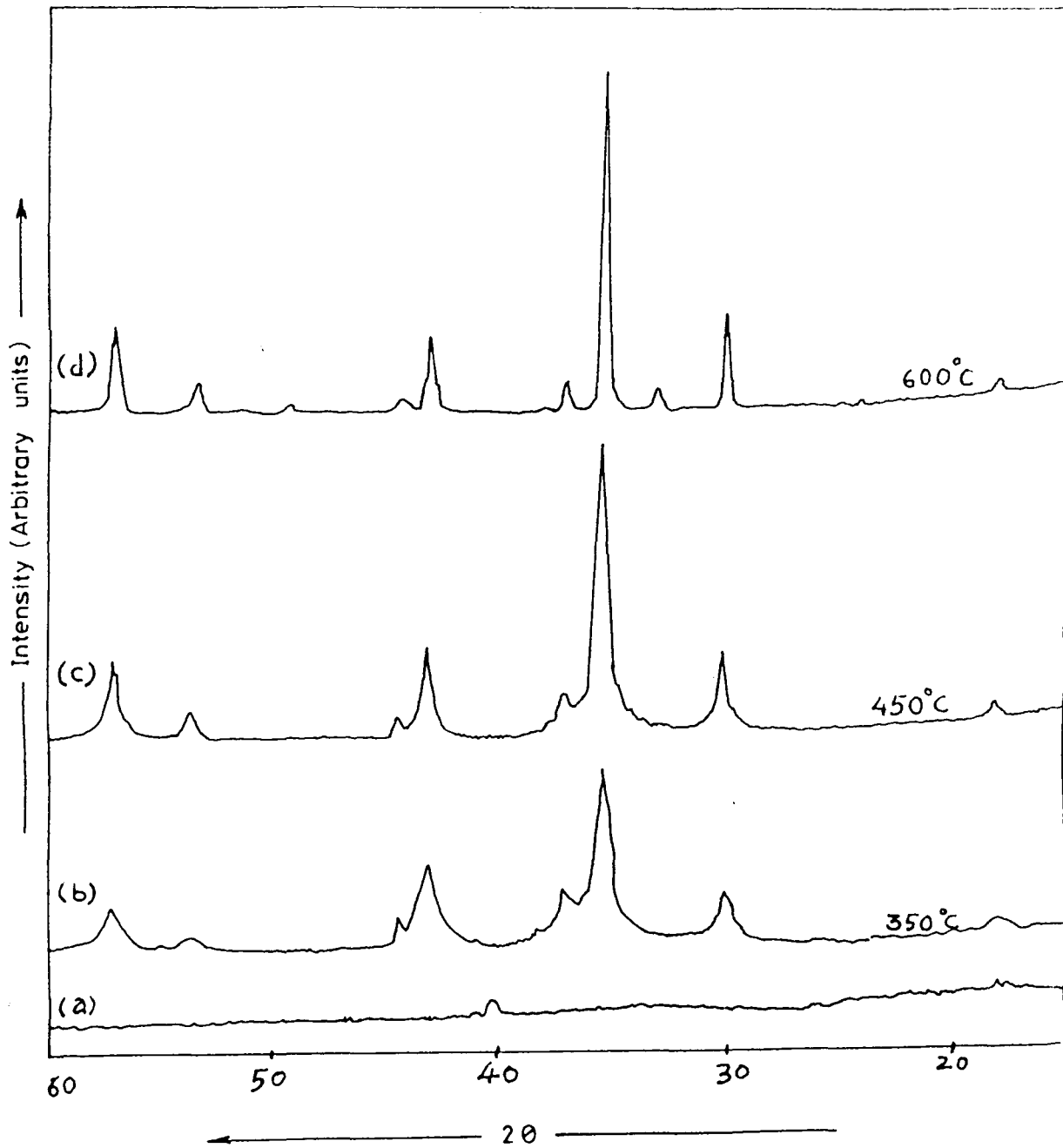
Fig. 8 : X-ray differaction pattern of NiZn ferrite
prepared by Liquid Mix Technique
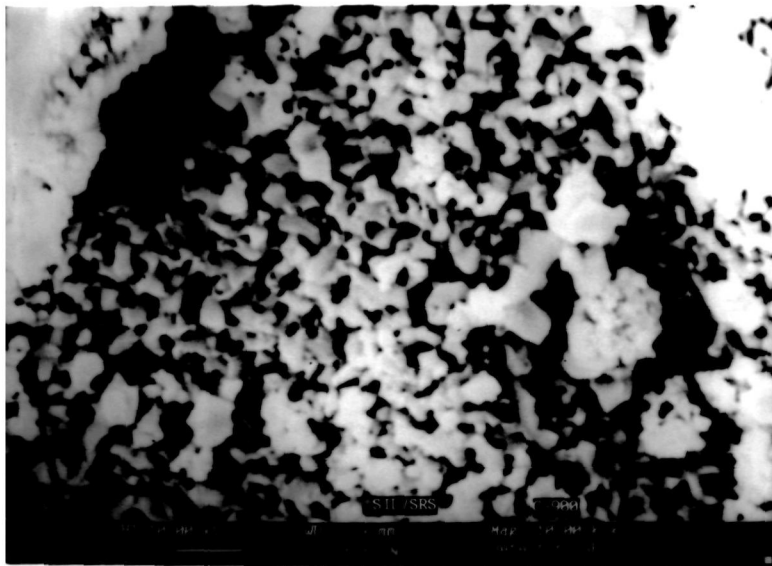
(a)

Fig. 9a : Scanning electron microgrpgh of calcined powder
        prepared by LMT
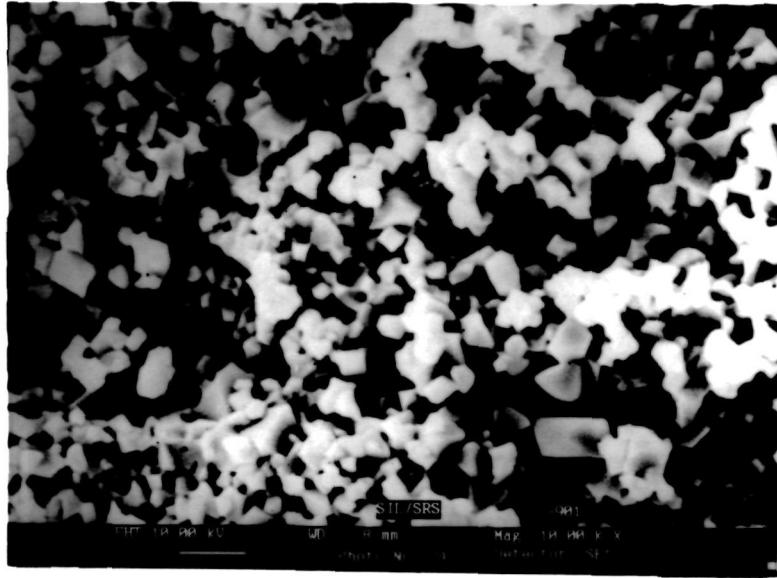
(b)
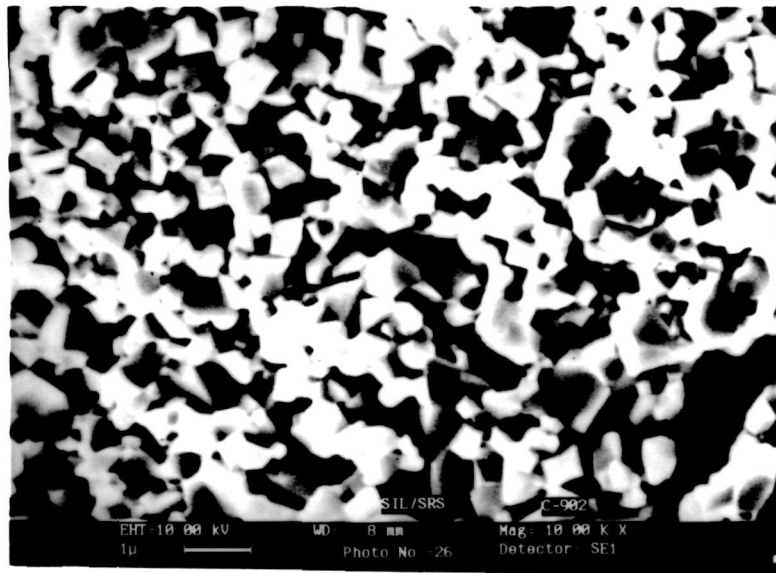
(c)

Fig. 9 : b-c Scanning electron micrograph of sintered Ni-Zn
         Ferrite Samples

frequency. The results of magnetic property measurements are given in the Table 4. The microstructure of sintered sample is studied by scanning the photomicrographs of fractured sintered samples. The microstructure of sample sintered at 1140°C (C-901) shows uniform microstructure with particle size of 1-2 um. The sample also shows presence of many voids. The microstructure of sample sintered at 1180°C shows increase in particle size with less number of voids. This change in microstructure is reflected in sintered density which is found to increase with increase in sintering temperature (Fig.9).

Table - 4

Magnetic properties of NiZn ferrite synthesised by LMT method

Table - 4a		Table - 4b	

Sample name : C-901
Sintering cond.- 1140 C/4 hrs

Sample name : C-902
Sintering cond. - 1180 C/4 hrs

Freq MHz	Q	μ'	$\mu' * Q$	μ''	Freq MHz	Q	μ'	$\mu' * Q$	μ''
4	44	27.4	1205.6	0.62	4	53	34.6	1833.8	0.65
6	53	27.1	1436.3	0.51	6	68	33.4	2271.2	0.49
8	64	27.0	1728.0	0.42	8	89	32.0	2848.0	0.36
10	75	25.8	1935.0	0.34	10	105	31.2	3276.0	0.30
12	93	24.3	2259.9	0.26	12	105	31.0	3255.0	0.30
14	98	24.2	2371.6	0.25	14	105	30.9	3244.5	0.29
16	102	24.2	2468.4	0.24	16	99	30.9	3059.1	0.31
18	102	24.1	2458.2	0.24	18	93	31.0	2883.0	0.33
20	102	24.0	2448.0	0.24	20	85	30.8	2618.0	0.36
22	100	24.6	2460.0	0.25	22	77	32.0	2464.0	0.42
24	97	24.7	2395.9	0.25	24	69	31.8	2194.2	0.46
26	94	24.8	2331.2	0.26	26	63	32.2	2028.6	0.51
28	90	24.7	2223.0	0.27	28	56	32.3	1808.8	0.58
30	85	24.9	2116.5	0.29	30	50	32.3	1615.0	0.65
32	81	25.2	2041.2	0.31	32	45	32.4	1458.0	0.72
34	76	25.6	1945.6	0.34	34	40	32.6	1304.0	0.82
36	70	25.6	1792.0	0.37	36	35	33.6	1176.0	0.96
38	65	25.4	1651.0	0.39	38	31	34.5	1069.5	1.11
40	60	25.6	1536.0	0.43	40	27	34.9	942.3	1.29
42	56	26.3	1472.8	0.47					
44	52	26.6	1383.2	0.51					
46	47	27.4	1287.8	0.58					
48	44	27.5	1210.0	0.63					
50	40	27.8	1112.0	0.70					

230

4.3 SUMMARY

In recent years electronic ceramics have been gaining increasing importance because of wide applications and uses which they can be put as components in various electronic circuits. The properties of electronic ceramics are found to be very sensitive to their microstructure particularly fine grain size, type and concentration of additive etc. Soft ferrites is one of the important classes of electronic ceramics. Mn-Zn ferrite and Ni-Zn ferrite are the two representative examples of soft ferrites. In addition to composition dependent, ferrites are process sensitive. Important properties of ferrites have been made through close control of processing and inovations in processing.

In the present work, ceramic method and liquid Mix Technique (LMT) have been used to synthesis NiZn ferrite ($Ni_{0.8}$ $Zn_{0.2}$ Fe_2O_4) which can be used at high frequency. The effect of two different additives namely (i) BaO and (ii) $BaO.B_2O_3$ on NiZn ferrite have been studied. The toroids with and without addities are sintered at various temperatures between 1100° C to 1250° C to find out optimum sintering temperature. The sintered product is characterised by the magnetic properties such as u, Q, uQ, Ms, density, microstructure etc. The properties of toroids sintered at 1140° C and 1180° C are discussed in detail. The effect of additive is studied by compairing the magnetic properties of

doped samples with the virgin (undoped) sample process under same conditions. The comparative study reveals that incorporation of BaO or BaO-B_2O_3 upto 0.2 wt% helps to improve magnetic properties of sintered NiZn ferrite.

The liquid mix technique offers the preparation of finely subdivided powders at comparatively low temperature.

REFERENCES

1. W.H. Bragg, Nature 95 (1951) 561; Phil. Mag., 30 (1915) 305.

2. T.F.W. Barth and E. Posnjak, Z. Krist, 82 (1932) 325.

3. H. Forestier, C.R. Acad. Sci. Paris, 192 (1931) 842.

4. E.J.W. Verwey, P.W. Haayman and F.C. Romeijn, J. Chem. Phys., 15 (1947) 181.

5. F. de Boer, J.H. Van Santen and E.S.W. Verwey, J. Chem. Phys., 15 (1947) 174.

6. E.J.W. Verwey and E.L. Heilmann, J. Chem. Phys., 15 (1947) 174.

7. L. Neel, Ann. Phys., 3 (1948) 798.

8. P.W. Anderson, Phys. Rev. 115 (1959) 2.

9. J. Smit and H.P.J. Wijn, Ferrites (1959), John Wiley & Sons, New York.

10. Ing. C. Heck, Magnetic Materials and Their Applications (1974), Butterworth & Co. (Publishers) Ltd.

11. J.M. Haspers, in Modern Materials, Vol.3 (1962) 259, ed. by H.H. Hausner, Academic Press, New York and London.

12. S. Chikazumi, Physics of Magnetism (1964) p.263, John Wiley & Sons, New York.

13. A. Goldman, Modern Ferrite Technology. (1990), Van Nostrand Reinhold, New York.

14. S. Pyun, S.H. Chang, D.N. Yoon & Y.J. Shim, Am. Ceram. Soc. Bull., 64 (1985) 585.

15. C. Guillaud, Proc. IEEE Supp. No.5 (1957) 165.

16. T. Akashi, NEC R&D Reports 8 (1966) 89.

17. C. Guillaud and M. Paulus, Comptes Rendus 246 (1956) 2525.

18. W. Heister, J. Appl. Phys. 30 (1959) 225.

19. H. Igarashi and K. Okazaki, J. Am. Cer. Soc., 60 (1977) 51.

20. E. Roess, Ferrites, Proc. Int. Conf. Ferrites, Japan (1971) 187.

21. B.K. Das, Preparation and characterization of materials, ed. by C.N.R. Rao.

22. A.P.B. Sinha and P.G. Menon, in Solid State Chemistry, edited by C.N.R. Rao.

23. G. Hilpert, DR Patent No.226347 & 227767 (1909).

24. J.L. Snoek, Physica 3 (1936) 463.

25. E.W. Gorter, Nature, 165 (1950) 798.

26. C. Guilland, J. Phys. Radium, 12 (1951) 65.

27. Y. Yafet and C. Kittel, Phys. Rev., 87 (1952) 280.

28. Y. Hoshino, Ferrites, Proc. 3rd Int. Conf. on Ferrites, Kyoto 1980.

29. D.J. Craik, Magnetic Oxides; pt.1, p.63, John Wiley & Sons, New York, 1975.

30. K.J. Klabunde, Z.X. Tang, and C.M. Sorensen, J. Appl. Phys., 69 (1991) 5279.

31. E.B. Rigby, W.D. Kehr and C.B. Meldrum, IEEE Trans. Mag. 20 (1984) 1506.

32. T. Takada and M. Kiyama, Ferrites, Proc. Int. Conf. Japan (1970) 69.

33. T. Kimura, T. Takahashi and T. Yamagahi, Ferrites,

Proc. Int. Conf. Japan (1980) 27.

34. S. Hirano, I. Watanable and S. Naka, Adv. Ceram. 15 (1986) 151.

35. F.R. Sale, V.A. Roberts and R. Freer, Br. Ceram. Proc. 41 (1989) 33.

36. L. Patron, I. Illie and M. Brezeana, J. Mater. Sci. Lett., 6 (1987) 932.

37. R.T. Richardson, J. Mat. Sci., 15 (1980) 2569.

38. K.C. Patil and P. Ravindranathan, J. Am. Ceram. Soc. Bull., 66 (1987) 688.

39. C. Guillaud, Proc. IEEE, 104B (1957) 165.

40. T. Akashi, Trans. Jap. Inst. Metals, 2 (1961) 171.

41. K.H. Rao, N.K. Gaur, K. Aggarwal and R.G. Mendiratta, J. Appl. Phys. 52 (1982) 1122.

42. A.R. Das, V.S. Anathan and D.C. Khan, J. Appl. Phys. 57 (1985) 4189.

43. M. Purnanandam, T. Bhimasankaram and S.V. Suryanayana, J. Mat. Sci. (1991) 6131.

44. I. Nan Lin, R.K. Mishra and G. Thomas, IEEE Trans. Mag., Mag. 18 (1982) 295.

45. S. Gasiorek and J. Kulikowski, J. Mang. and Mag. Mat., 26 (1982) 295.

46. H.T. Kim and H.B. Im, IEEE Trans. Mag., Mag. 18 (1982) 1541.

47. S. Pyun and J. Baek, Am. Ceram. Soc. Bull., 64 (1985) 602.

48. G.C. Jain, B.K. Das and S. Kumari, J. Appl. Phys. 49 (1978) 2894.

49. G.C. Jain, B.K. Das and S. Kumari, IEEE Trans. Magn. Mag-16 (1980) 1428.

50. S. Besenicar and D. Hanzel, J. De Phys. 46 (1985) C-6-169.

51. J.C. Jain, B.K. Das and N.C. Goel, J. Am. Ceram. Soc. 62 (1979) 79.

52. A. Goldman, Adv. in Ferrites, Proc. Int. Conf. Ferrites, Ind. 1 (1989) 13.

53. E.A. Snelling, Advances in Ferrites, Proc. Int. Conf. Ferrites, Ind. 1 (1989) 579.

54. Smit & Wijn, Advances in Electronics & Electron Physics 6 (1954) 69.

55. J.J. Went and H.P.J. Wijn, Phys. Rev. 82 (1951) 269.

56. T. Takada, Ferrites, Proc. Int. Conf. Ferrites, Japan (1980) 3.

List of Research Publications

1. Chemical processing of hexagonal Sr-ferrite : Part II - Effect of mode of washing and filtration on the magnetic parameters. A.G.Bagul, C.E. Deshpande, J.J. Shrotri, S.D.Kulkarni, Ila Nigam, and S.K. Date Ind. J. of Chem Vol 31A (1992) p 661.

2. Optimization of chemical processing parameters in synthesis of active strontium ferrite powders A.G. Bagul, J.J. Shrotri, S.D. Kulkarni, C.E. Deshpande and S.K. Date. Proceedings of The Sixth International Conference on ferrites (ICF6), Tokyo Japan (1992) p. 109

3. Utilization of defferent grades of iron orides in the synthesis of power ferrites. J.J. Shrotri, A.G.Bagul, S.D. Kulkarni, C.E. Deshpande and S.K. Date. Proceedings of The Sixth International Conference on ferrites (ICF6), Tokyo, Japan (1992) p. 229

4. Chemical processing of hexagonal Sr.Ferrite : Part III. Effect of predetermined addition of sodium ions on performance parameters of strontium ferrite A.G. Bagul, C.E. Deshpande and S.K. Date. Ind J. of Chem vol 31 A (1994) p. 33

5. Chemical processing of sodium doped hexagonal Sr-Ferrite : Part IV - Microstructured and magnetic studies. A.G. Bagul, S.K. Date, C.E. Deshpande and H. Minoura. Indian J. of Chem. Vol. 34A (1995) p. 176.

ACKNOWLEDGEMENT

N.C.L.

Pune - 8

1 September 95

(A.G.Bagul)